

Investigations of Cross Section Model and Near Detector Choices

Jake Calcutt¹, Joshua Hignight¹, and Kendall Mahn¹

¹Michigan State University

1 Overview

The Deep Underground Neutrino Experiment (DUNE) is a next-generation Long Baseline neutrino experiment designed to search for CP violation and establish the mass hierarchy. It consists of both a Near and Far Detector separated by 1300km and uses a neutrino beam created at Fermilab.[1]. While the design of the Liquid Argon Far Detector has been finalized, there is still ongoing effort in deciding the configuration of the Near Detector. The main near detector design includes a Fine-Grained Tracker (FGT) with possible inclusion of additional detectors. Under consideration are a Liquid (LArTPC) or High Pressure Gaseous Argon TPC (GArTPC). DUNE's physics goals require systematic uncertainties in the interaction model to be below the 2% limit after a near-to-far extrapolation[2]. The focus of this document is to quantify how the neutrino interaction model could affect DUNE's goals. This work was done concurrent with the DUNE ND Taskforce (NDTF), and so the studies investigate possible weaknesses and limitations of the current parameterization of neutrino interaction uncertainties. The studies also explore how different interaction models - used as proxies for variations in a given model - couple to the different NDs and the FD.

Below is a list of the studies we have conducted for this work.

- Choice of parameterization.
 - The sufficiency of a pure- Q^2 parameterization in a Near to Far extrapolation.
 - * Are variations in CCQE and 2p2h models covered in this parameterization?
 - Does the Q^2 parameterization ignore additional physics as represented as variations in q_0 - q_3 ?
- The different abilities of the 3 ND configurations to reconstruct the neutrino energy.

- Variations in neutron multiplicities and neutron energy.
 - * Do the detectors need to be sensitive to neutrons?
- How do different ND configurations couple to model differences in
 - * Variations in proton & pion multiplicity and momentum.
 - * Variations in nucleon multiplicity & invariant hadronic mass.
- Difference from true neutrino energy.

2 Methods

2.1 Monte Carlo Generators

Neutrino interaction modelling is of great interest to current and future oscillation experiments. Currently, there are a few different neutrino interaction software packages, so called "generators". While it is not guaranteed that the physics of nature corresponds to any of these software packages, the different choices made by the generators can act as a proxy for possible variations in the neutrino interaction model. The models considered span a range of different 'vertex-level' interaction models (e.g. CCQE, 2p2h, Resonant) and Final State Interaction (FSI) models. These are given in Table ??

2.2 Generating Events

Sets of ν and $\bar{\nu}$ events with an Argon-40 target are produced with these generators according to the 2015 DUNE CDR fluxes, shown in Figure 1. (NEED TO FIND THE OSCILLATION PARAMETERS) Note that the ν_μ and $\bar{\nu}_\mu$ flux correspond to the Forward and Reverse Horn Current (FHC and RHC) modes respectively. No 'wrong-sign' studies, where the $\bar{\nu}_\mu$ flux is that within the primary ν_μ beam, are considered in this work. The various data sets are then passed through the NUISANCE[6] software to reduce the outputs to a common format, in turn saving all final state particle information for each event.

Generator	Version	Model
GENIE	2.10	RFG
NEUT	5.3.6	Nieves et. al RPA+2p2h/MEC ($M_A = 1.01$)
NuWro	11	LFG + RPA + Nieves et. al

Table 1: The various Monte Carlo event generators used for this work.

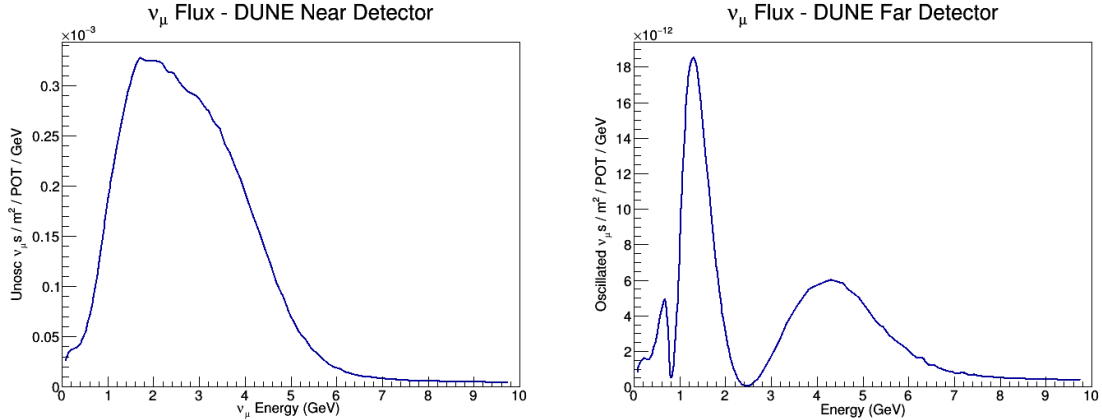


Figure 1: ν_μ flux at DUNE ND (Left) and FD (Right)

2.3 How We Study a Near to Far Extrapolation

The various studies regarding near to far extrapolations are explored using the following procedure. Ratios of either NEUT or NuWro to GENIE - referred to as 'single ratios' - separately at the ND and FD are taken. NEUT and NuWro are both normalized to GENIE to highlight shape differences rather than overall normalization effects. These offer insight into model variations in and how the dependence of ND configuration couple to variations. The effect of a near to far extrapolation is approximated by taking a 'double ratio' between the near and far single ratios. To be explicit and to avoid confusion, these are defined in Equations 2 and 3, where 'Other MC' refers to either NEUT or NuWro and 'Near' can be replaced by 'Far' in the single ratio. We note this is a crude approximation to give intuition about the problem for just a single reaction process; a fit to the ND spectrum will have multiple reactions in a given topology which can complicate the determination of physics effects for a single reaction.

$$\text{ND Single Ratio} = \frac{(\text{Other MC @ Near Detector})}{(\text{GENIE @ Near Detector})} \quad (1)$$

$$\text{Double Ratio} = \frac{(\text{ND Single Ratio})}{(\text{FD Single Ratio})} \quad (2)$$

2.4 Detector Configurations and Efficiencies

The studies highlight the effect of the different efficiencies of the various detectors. We first consider a 'perfect' ND and FD without any efficiencies applied, and then look what changes as we consider the 3 different configurations of the ND and a simple LAr efficiency in the FD. Efficiency information is included with the following procedure. Each particle is randomly accepted or rejected by throwing a random number and checking against the efficiency according to the particle's momentum. No angular efficiencies have yet been taken into account for this work. At time of this writing, only a full description of the FGT efficiency according to NDTF samples

is available, but other configurations will be added to subsequent versions of this note. An example of the efficiency for protons in the FGT is given in Figure 2, FGT efficiencies for other particles are included in Appendix ???. Simple thresholds for protons are applied for the GAr - 100 MeV/c - and LAr ND and FD - 200 MeV/c. Currently, we do not have the efficiencies for μ , $\pi^{+,-}$, and π^0 in the simple LAr and GAr descriptions, and so the detectors are assumed to be perfectly efficient (no rejections) to these particles. π^0 efficiency information is also currently missing in the all 3 configuration, and so none are rejected.

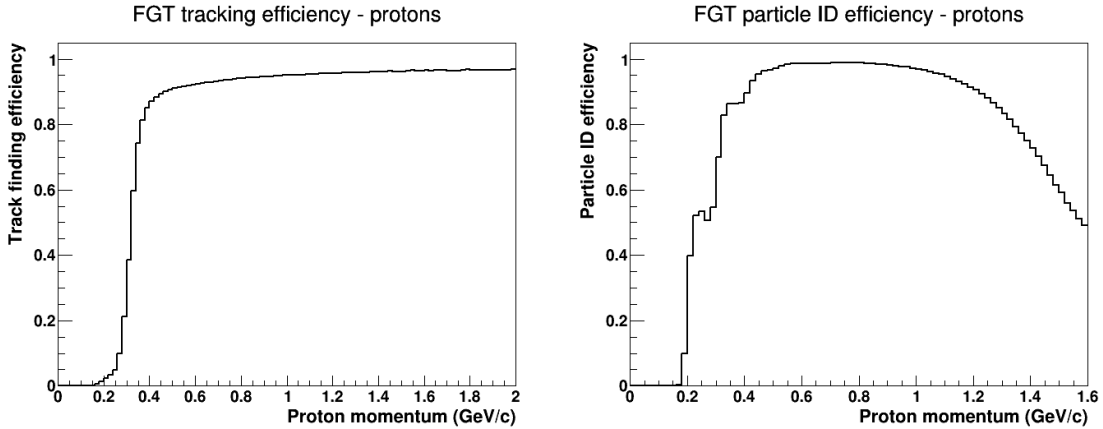


Figure 2: Left: Tracking efficiency for protons in FGT. Right: PID efficiency for protons in FGT. Total efficiency for a given proton momentum is given by the product of the two efficiencies.

3 Parameterization

The VALOR software package that has been used on multiple T2K oscillation analyses, and had recently been used to study the DUNE near detector configurations. (((The group uses MC templates to map between reconstructed and true information for various reactions.))) Uncertainties in interaction models are parameterized by model variations as a function of Q^2 . Currently, Q^2 parameterizations are defined for neutrinos and antineutrinos as:

- CCQE nm with Q^2 bins $\{0 - 0.20, 0.20 - 0.55, >0.55\}$ GeV 2
- CCQE nmb with Q^2 bins $\{0 - 0.20, 0.20 - 0.55, >0.55\}$ GeV 2
- 2p2h nm with 1 Q^2 bin
- 2p2h nmb with 1 Q^2 bin

This portion of the work seeks to determine if variations in CCQE and 2p2h models are well represented by these parameterizations in Q^2 . It also serves to highlight the behavior of the models as they couple to FSI and detector effects.

3.1 Q^2 Parameterization

The single and double ratio procedure described in Section ?? is conducted using events created by all three models at the ND and FD and distributed according to Q^2 . This is done separately with and without efficiencies, for both ν_μ and $\bar{\nu}_\mu$, and for true-CCQE and true-2p2h. Note that for distributions without efficiencies, the MC-level Q^2 quantity is used, giving us insight into the interaction model uncertainties. When including efficiencies, Q^2 becomes a reconstructed quantity. It is calculated from the final state particles that are accepted after efficiencies are applied. This is highlighted in Equations ?? - ?. However, though we call it 'reconstructed', it is calculated using the true energies and momentums without smearing applied, so it is not truly reconstructed in the usual sense of the word. Using the final state particles and the acceptances of the different detectors allows us to investigate FSI and detector effects.

$$Q^2 = |q_0^2 - q_3^2|, \quad (3)$$

$$q_0^2 = (E_{reco} - E_{lep})^2, \quad (4)$$

$$q_3^2 = (\vec{P}_{reco} - \vec{P}_{lep})^2 \quad (5)$$

$$E_{reco} = E_{lep} + \Sigma E_\pi + \Sigma (E_{prot} - M_{prot}) \quad (6)$$

Conclusions are drawn from the double ratios according to the following prescription. If the ratio is flat - i.e. if a horizontal line is within the statistical error bars - in a given bin of the parameterization, uncertainties can be considered sufficient.

For ν_μ CCQE events, both NEUT's and NuWro's models differ significantly from GENIE' model in Q^2 distributions, as seen in the single ratios in Figure 11. Despite this, the double ratios for both NEUT and NuWro to GENIE remain relatively flat and close to 1. For double ratios with FGT efficiencies applied to the ND and simple LAr efficiencies applied to the FD, shape variations are greater above around 1.25 GeV² as seen in Figure 12. This suggests an additional bin in the region .55 to 1.25 GeV² should be included. This motivates a focus on determining the origin of this variation as it seems to couple to the inclusion of FSI and detector effects. One possible source is the exclusion of low-momentum muons as efficiencies are included.

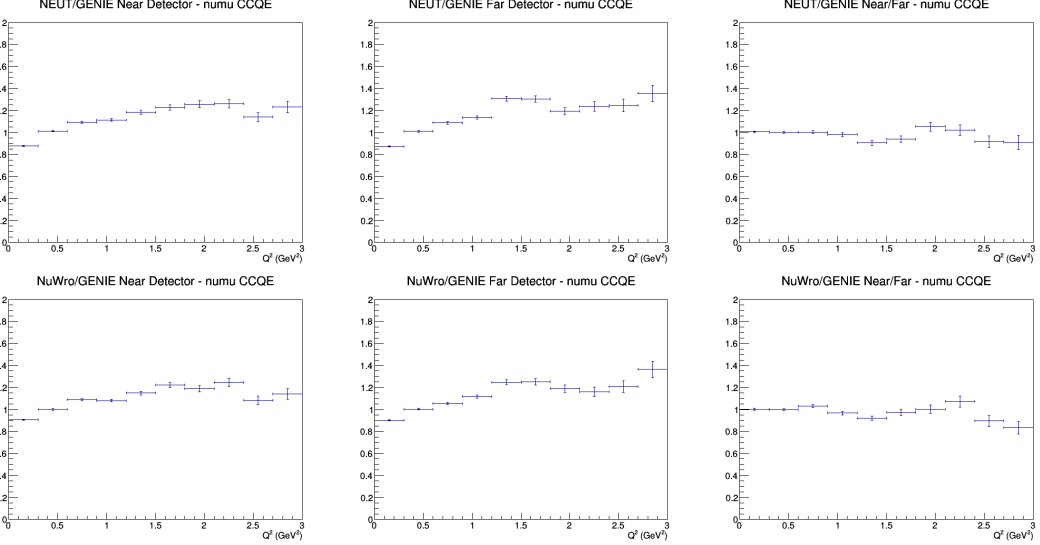


Figure 3: MC-level Q^2 distributed ν_μ events using DUNE flux, no efficiencies applied to ND or FD. Top: Ratios of NEUT to GENIE. Bottom: Ratios of NuWro to GENIE. Left to Right: Single ratio at ND, single ratio at FD, double ratio Near/Far. Of note is the relative flatness throughout the double ratio compared to the single ratio at the ND. Note that the VALOR binning is separated by lower bin edges of (0, 0.20, and 0.55) GeV^2

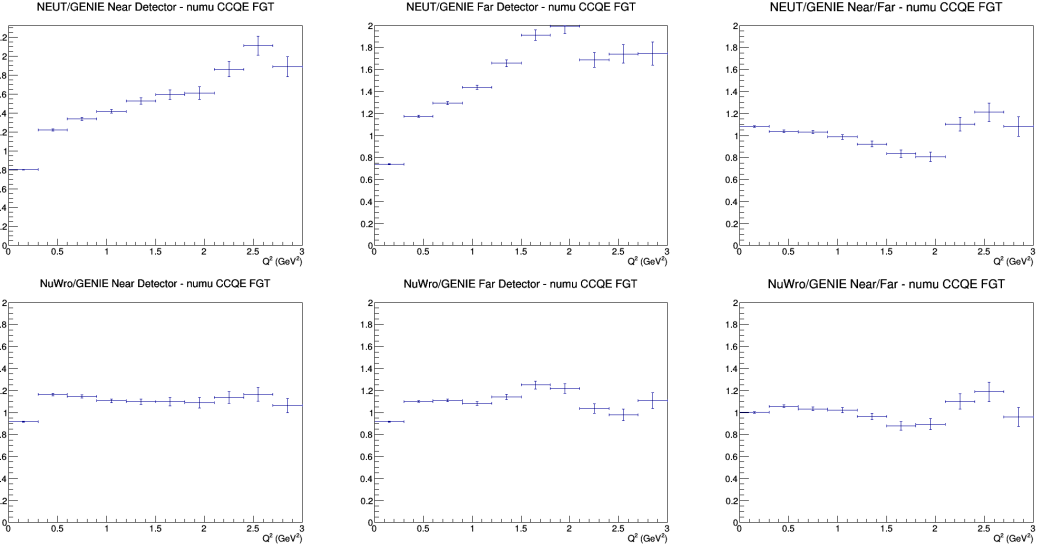


Figure 4: Reconstructed Q^2 distributed ν_μ events using DUNE flux, FGT efficiencies applied to ND and simple LAr efficiencies applied to FD. Top: Ratios of NEUT to GENIE. Bottom: Ratios of NuWro to GENIE. Left to Right: Single ratio at ND, single ratio at FD, double ratio Near/Far. More shape variations do arise above around 1.25 GeV^2 in the double ratios. This suggests another bin should encompass the region between $.55$ and 1.25 GeV^2 . Note that the current VALOR binning is separated by lower bin edges of (0, 0.20, and 0.55) GeV^2

However, for $\bar{\nu}_\mu$ CCQE events, we observe distortions in the Q^2 distribution even in the double ratios. This is true without efficiencies for both NEUT to GENIE and NuWro to GENIE ratios. This is displayed in Figure 13. The variations again arise above 1.5 GeV^2 for the double ratios, suggesting an additional bin to be added between $.55$ and 1.5 GeV^2 . This arises without efficiencies, and points to variations in the CCQE interaction model being responsible for this effect rather than FSI variations or detector effects.

We run into trouble extending the $\bar{\nu}_\mu$ CCQE study with efficiencies applied, as this leaves the high Q^2 region with very low statistics, preventing us from drawing any meaningful conclusions. These plots are included in Appendix D for completeness. The studies will be continued once we have higher statistics, and with more complete descriptions of the LAr and GAr as this information becomes available.

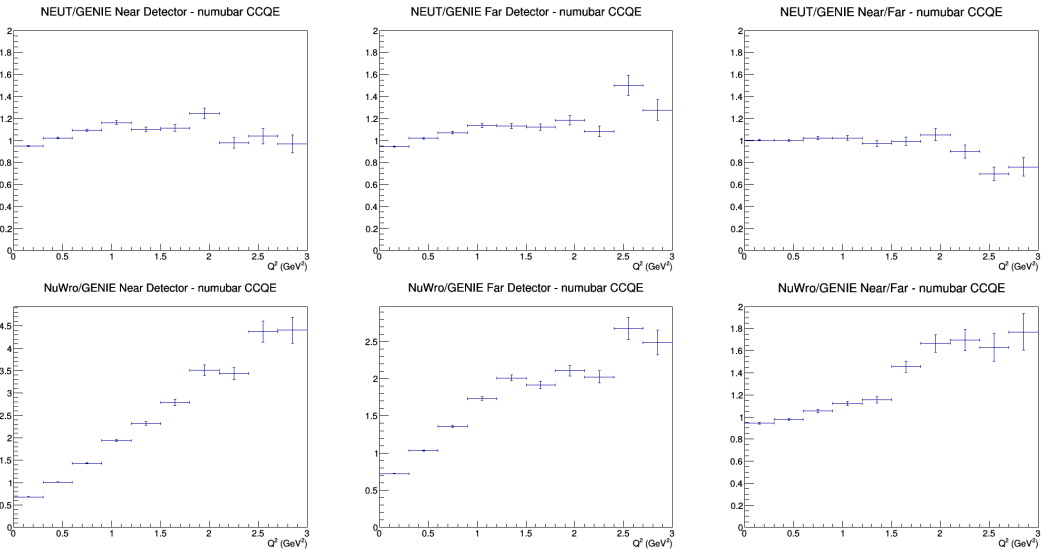


Figure 5: MC-level Q^2 distributed $\bar{\nu}_\mu$ CCQE events using DUNE flux. Top: Ratios of NEUT to GENIE. Bottom: Ratios of NuWro to GENIE. Left to Right: Single ratio at ND, single ratio at FD, double ratio Near/Far. Large amounts of variations in the region above 1.5 GeV^2 in both double ratios. This differs from ν_μ CCQE, where this arose in the ratios after efficiencies are added. Here, it exists without any efficiencies, pointing to variations in the CCQE model, rather than FSI or detector effects, not being covered by the parameterization. An additional bin between $.55$ and 1.5 GeV^2 is suggested. Note that the VALOR binning is separated by lower bin edges of $(0, 0.20, \text{ and } 0.55) \text{ GeV}^2$.

For 2p2h ν_μ and $\bar{\nu}_\mu$ events, the double ratios from both NEUT and NuWro remain centered close to or around 1 below about 1 GeV^2 without efficiencies applied, as seen in Figure ?? and ???. Above 1 GeV^2 , the statistics are again low. At this moment, the currently-proposed 1-bin normalization appears sufficient in the region below 1 GeV^2 . The low statistics prevent us from making conclusions in the high Q^2 region as well as drawing conclusions from applying efficiencies. These will be revisited in later iterations of this work.

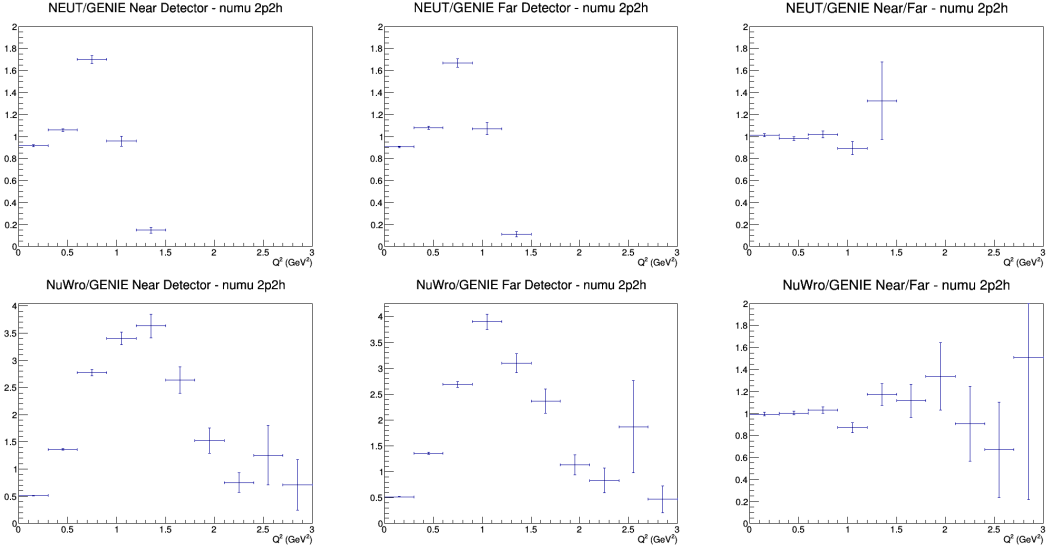


Figure 6: Q^2 distributed $\bar{\nu}_\mu$ 2p2h events using DUNE flux. Top: Ratios of NEUT to GENIE. Bottom: Ratios of NuWro to GENIE. Left to Right: Single ratio at ND, single ratio at FD, double ratio Near/Far. Large amounts of variations are present resulting from low statistics in the higher end of all distributions, but the lower end holds close to 1. Note that the VALOR binning is separated by lower bin edges of (0, 0.20, and 0.55) GeV^2 .

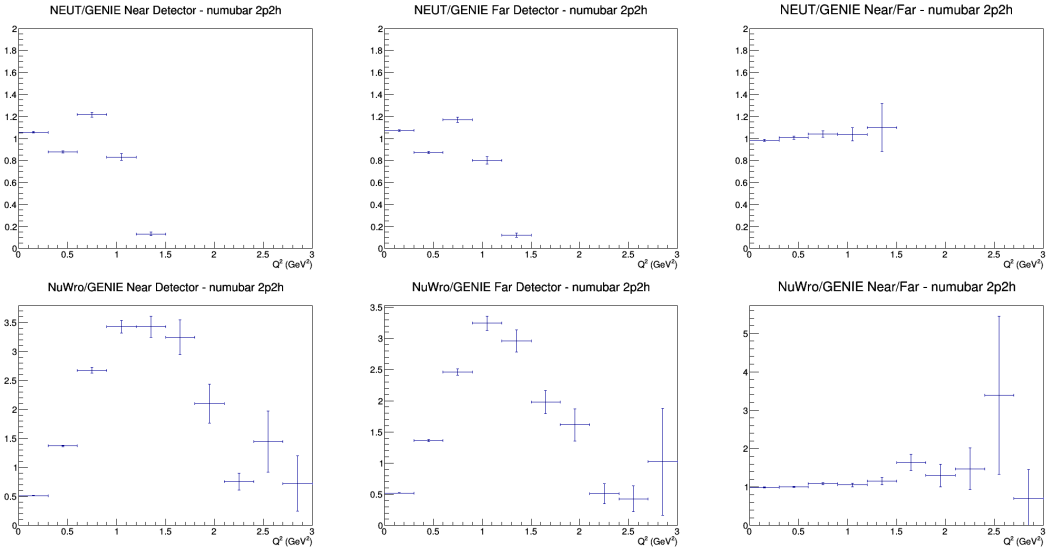


Figure 7: Q^2 distributed $\bar{\nu}_\mu$ 2p2h events using DUNE flux. Top: No efficiencies, Bottom: FGT efficiencies applied to ND, LAr efficiencies applied to FD. Left to right: NEUT to GENIE double ratio, NuWro to GENIE double ratio. Large amounts of deviations from 1 throughout distributions with efficiencies applied. Note that the VALOR binning is separated by lower bin edges of (0, 0.20, and 0.55) GeV^2 .

We currently find an additional bin in the region (.55, 1.25-1.5) will account for uncertainties in both ν_μ and $\bar{\nu}_\mu$ CCQE. For ν_μ and $\bar{\nu}_\mu$ 2p2h, the overall normalization appears sufficient at this moment. Investigations into the origin of the variation in the high Q^2 region of CCQE will be conducted as this work is furthered. Additional statistics and more complete efficiency descriptions for the LAr and GAr are required, and will be conducted at a later date.

3.2 q_0 vs. q_3 Variations

In addition to studying the Q^2 ratios, the ratios in q_0 - q_3 space were also investigated to explore possibilities that variations are highlighted when changing the parameterization from Q^2 to q_0 - q_3 . The Q^2 parameterization assumes the variations are purely functions of Q^2 . Under this assumption, the double ratios should be flat in q_0 - q_3 . If this is not the case, a pure- Q^2 parameterization cannot sufficiently account for CCQE and 2p2h variations.

These studies were done in the exact same way as those in the previous section, only with the events and ratios distributed in q_0 - q_3 bins. Note: to be symmetric about 1, the scale extends from 0 to 2, but the variations in those bins can actually be greater than 2. Again, the quantities are MC-level truth information in the distributions without efficiencies, but are reconstructed in those with efficiencies applied.

For ν_μ CCQE, the double ratios without efficiencies appear pretty flat for both NEUT and NuWro, as seen in Figure 16, though there is a bit of bin-to-bin variation in the upper right region, which is expected from the low statistics. When adding efficiencies, the phase space is smeared out and more bin-to-bin variation arises. The case for FGT efficiencies is shown in Figure 17. Though the individual bins do deviate from 1, there is no large-scale regional departure from flatness, and so these distributions do not show a need for a q_0 - q_0 parameterization.

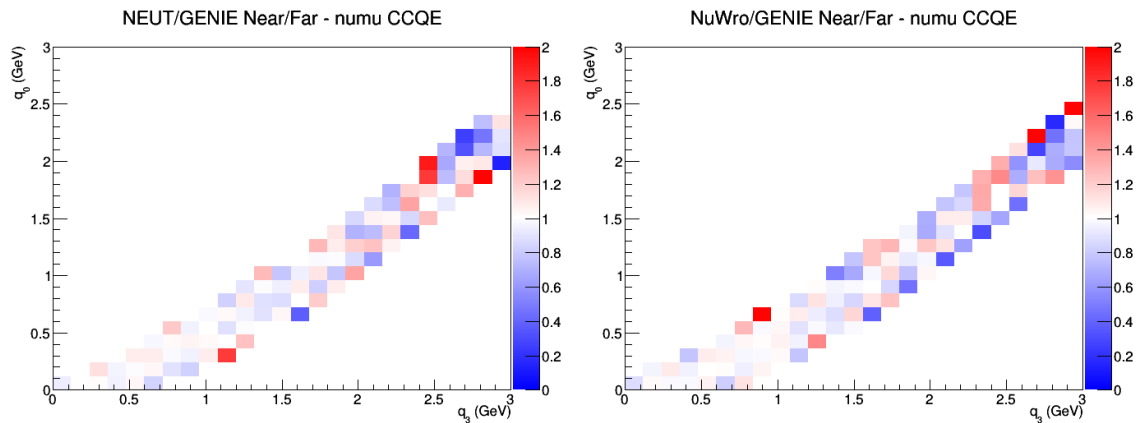


Figure 8: q_0 - q_3 distributed ν_μ CCQE events using DUNE flux without efficiencies applied. Left: Double ratio of NEUT to GENIE, Right: Double ratio of NuWro to GENIE. Relatively flat distributions, but with bin-to-bin variations arising from low statistics

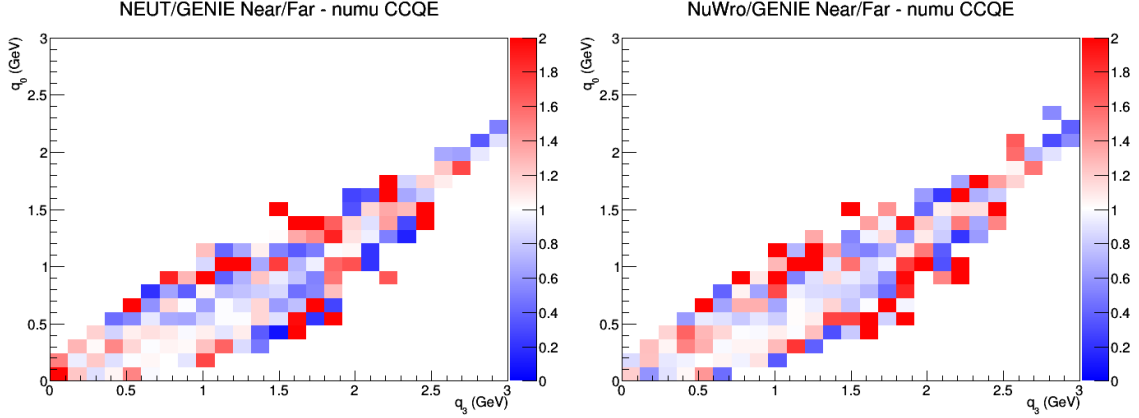


Figure 9: $q_0 - q_3$ distributed ν_μ CCQE events using DUNE flux, FGT efficiencies applied to ND and LAr efficiencies applied to FD. Left: Double ratio of NEUT to GENIE, Right: Double ratio of NuWro to GENIE. Distributions smeared out and variations between bins are higher than without efficiencies. Still appear relatively flat.

For $\bar{\nu}_\mu$ CCQE, however, there is a difference between NuWro and NEUT when looking at the ratios without efficiencies. Shown in Figure 18, it can be seen that the double ratio is consistently higher in the upper-right region of the NuWro/GENIE distribution as opposed to NEUT/GENIE, which is more similar to the corresponding ν_μ ratio. When adding efficiencies, much of the upper right region is cut out in GENIE and NEUT, shown in Figure 19, resulting in empty bins in both double ratios. Despite the distorted phase space, the NEUT/GENIE $\bar{\nu}_\mu$ CCQE double ratio appears to behave similarly to the corresponding ν_μ CCQE double ratio, while NuWro has ratios greater than 1 throughout the shared phase space, which is evident in Figure 20 which contains distributions with FGT ND and LAr FD efficiencies. Despite this deviation from 1 in NuWro, it suggests that an overall normalization rather than a different parameterization would be sufficient for $\bar{\nu}_\mu$ CCQE.

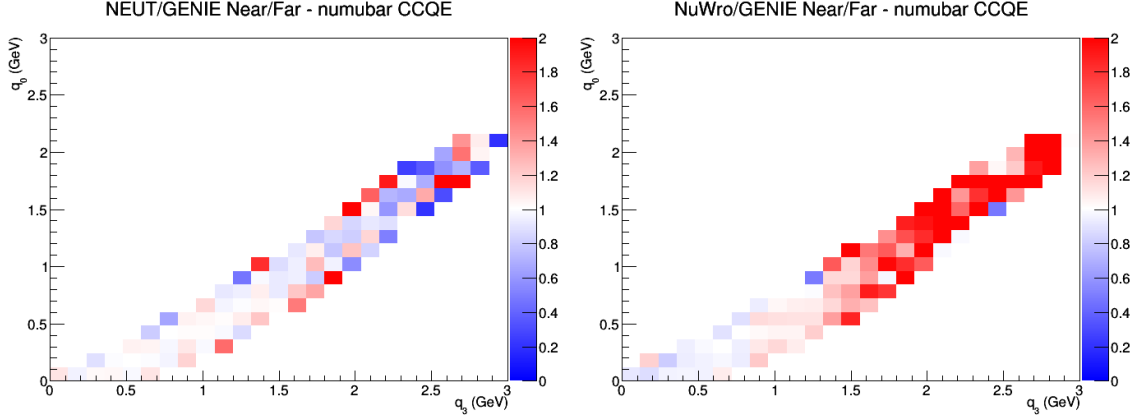


Figure 10: $q_0 - q_3$ distributed $\bar{\nu}_\mu$ CCQE events using DUNE flux without efficiencies applied. Left: Double ratio of NEUT to GENIE, Right: Double ratio of NuWro to GENIE. Relatively flat for NEUT/GENIE. NuWro/GENIE double ratio has heavy disagreement in upper-right region.

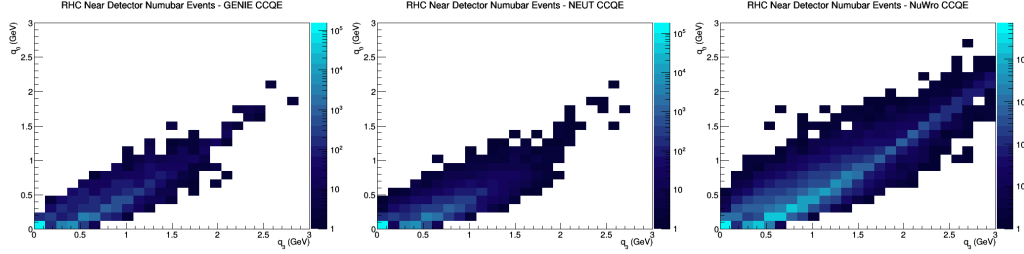


Figure 11: $q_0 - q_3$ distributed $\bar{\nu}_\mu$ CCQE events using DUNE flux, FGT efficiencies applied to ND and LAr efficiencies applied to FD. Right to Left: GENIE events distribution, NEUT events distribution, NuWro events distribution. Both GENIE and NEUT cut out the upper right region of phase space as opposed to NuWro.

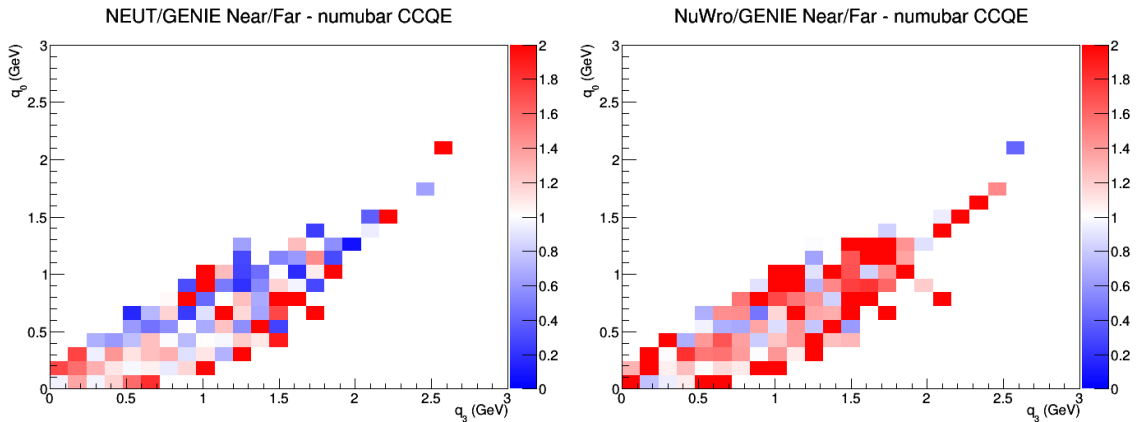


Figure 12: $q_0 - q_3 \bar{\nu}_\mu$ CCQE events using DUNE flux, FGT efficiencies applied to ND and LAr efficiencies applied to FD. Left: Double ratio of NEUT to GENIE, Right: Double ratio of NuWro to GENIE. NEUT to GENIE double ratio appears similar to the ν_μ double ratio, while NuWro to GENIE appears greater than 1 in shared bins.

Each of the three generators have very different behavior for 2p2h ν_μ and $\bar{\nu}_\mu$ events, as can be seen in the upper half of Figure 21 which contains 2p2h $\bar{\nu}_\mu$ events without efficiencies. This causes very restricted phase space in the double ratios. However, adding efficiencies and using reconstructed variables smears out the phase space, causing more bins to be shared between generators, though there are still variations in the shapes. See the bottom half of Figure 21. The double ratios seem to be mostly flat for both NEUT and NuWro in the FGT for ν_μ , seen in Figure 22. However for $\bar{\nu}_\mu$ 2p2h in the FGT, both NEUT to GENIE and NuWro to GENIE double ratios are generally greater than 1, seen in Figure 23. Similar to $\bar{\nu}_\mu$ CCQE events, an overall normalization correction should be able to sufficiently cover $\bar{\nu}_\mu$ 2p2h variations.

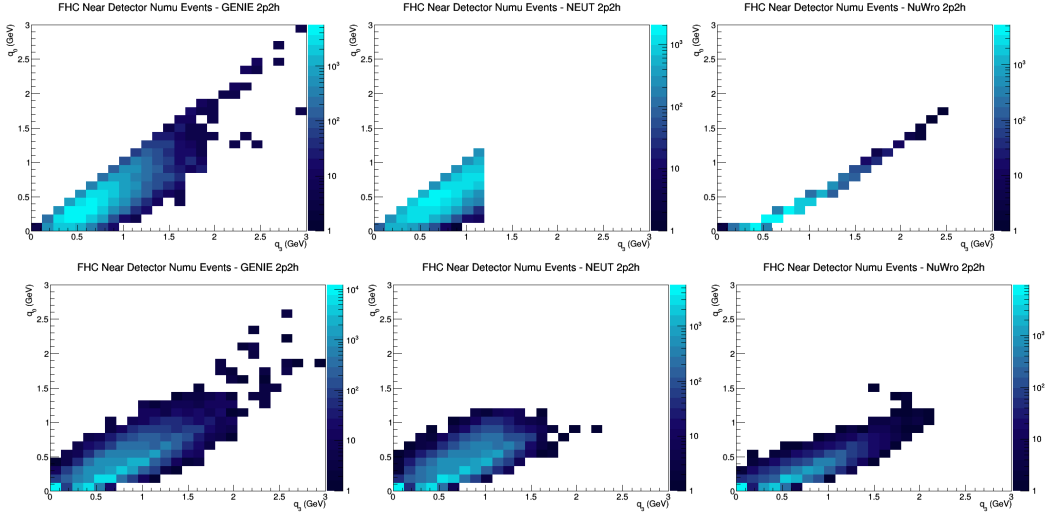


Figure 13: $q_0 - q_3$ distributed ν_μ 2p2h events using DUNE flux, Top Row: No Efficiencies applied, Bottom Row: FGT efficiencies applied to ND and LAr efficiencies applied to FD. Right to Left: GENIE events distribution, NEUT events distribution, NuWro events distribution. The phase spaces are very different without efficiencies, and restrict the coverage of the double ratios. With efficiencies applied, q_3 and q_0 are now quantities reconstructed from accepted particle kinematics, so more phase space is shared than in the true variables of the distributions without efficiencies.

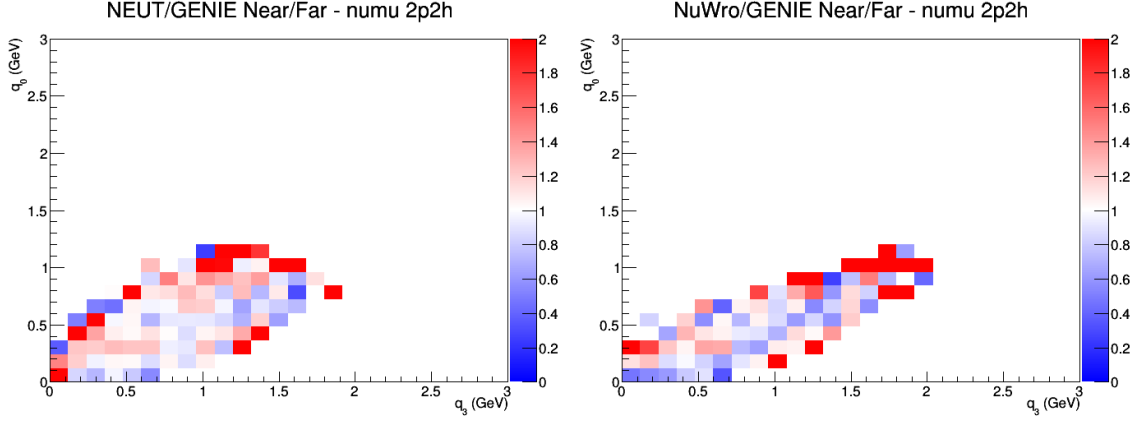


Figure 14: q_0 - q_3 distributed ν_μ 2p2h events using DUNE flux, FGT efficiencies applied to ND and LAr efficiencies applied to FD. Left: Double ratio of NEUT to GENIE, Right: Double ratio of NuWro to GENIE. Ratios appear mostly flat.

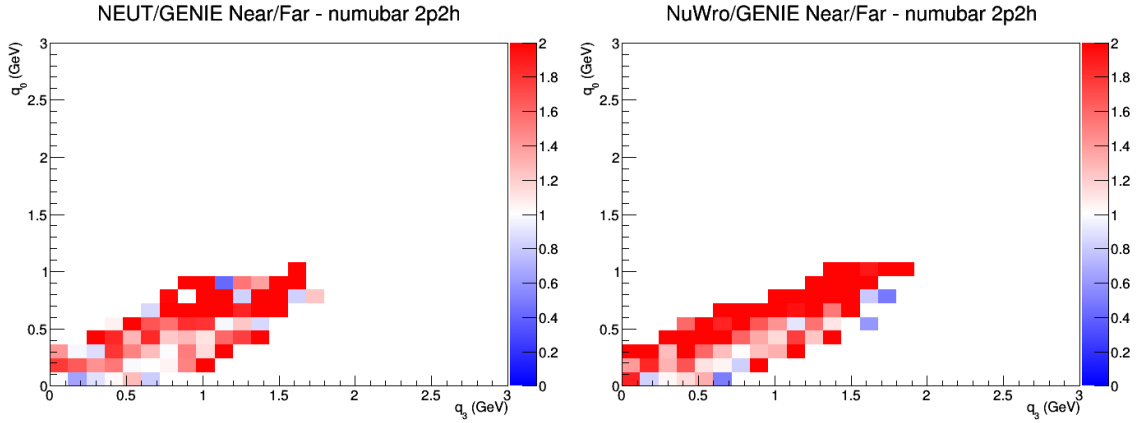


Figure 15: q_0 - q_3 distributed $\bar{\nu}_\mu$ 2p2h events using DUNE flux, FGT efficiencies applied to ND and LAr efficiencies applied to FD. Left: Double ratio of NEUT to GENIE, Right: Double ratio of NuWro to GENIE. Both double ratios consistently higher than 1.

3.3 Parameterization - Conclusions

It appears as though the pure- Q^2 parameterization and the binning developed by VALOR would cover model variations for ν_μ CCQE events. The near-to-far extrapolation plots - the double ratios - appear relatively flat in all reaction modes and in both the Q^2 and $q_0 - q_3$ distributions. However, the $\bar{\nu}_\mu$ CCQE events show that model variations are not covered in this extrapolation, at least when looking into the NuWro to GENIE double ratios, specifically in Q^2 . Additionally, though the distribution of ratios is generally flat in $q_0 - q_3$, a normalization correction appears needed. This is similarly true in 2p2h. With this, it is safe to assume that a pure- Q^2 distribution with different binnings and a normalization correction would be sufficient to cover CCQE and 2p2h model variations.

There is a degree of statistical limitation of the studies at this point, evident in the presence of bin-to-bin variations. To explore this point further, these studies can quickly and easily be extended to larger data sets to deal with statistics limitations. Additionally, the statistical uncertainties in the single and double ratios will also be investigated. With these, we can move on to quantify the degree to which the near-to-far extrapolation covers variations in the ν_μ case - or does not cover variations in the $\bar{\nu}_\mu$ case.

4 Reconstructed Energy

A framework for investigating variations in reconstructed energy calculations between different generators and ND configurations has been developed. Currently, the estimate for the incident neutrino energy is calculated by summing the total energy from final state leptons and pions (all charges) and the kinetic energy of final state protons after passing efficiencies through the data sets. All neutrons are assumed undetectable. This can be summed up in Equation 1: where E_{lep} is the energy of the outgoing lepton, E_π is the energy of the pion, and E_{prot} and M_{prot} are the energy and mass of the proton.

4.1 Difference from True Neutrino Energy

To investigate these variations, the difference between true and reconstructed neutrino energy from each generator - where NuWro and NEUT distributions have been normalized to GENIE - are plotted for each near detector configuration as well as the far detector, and for different reaction types. The reaction types considered are true-CCQE, true-2p2h, CC0 π , CC1 π , and CCOther. True-CCQE and true-2p2h are both defined as MC-level CCQE/2p2h interaction with 1 reconstructed lepton. CC0 π is defined as 0 π^\pm , 1 lepton, and any number of protons and π^0 after reconstruction. CC1 π is defined as 1 π^\pm , 1 lepton, and any number of protons and π^0 after reconstruction. Finally, CCOther is defined as any final state with 1 lepton and any number of hadrons reconstructed.

In ν_μ mode: for all reaction types except CCOther, all three generators seem to have similar differences in all detector configurations. This is evident in Figure 3 -

which includes CCQE and CCOther interactions in the ND with FGT efficiencies - and the figures in Appendix C. For CCOther, all three generators appear to have a long tail extending to high discrepancy regions - well past that of CCQE for example - though NuWro has a higher amount of events in the $\Delta E = 0.5$ GeV to 2 GeV region.

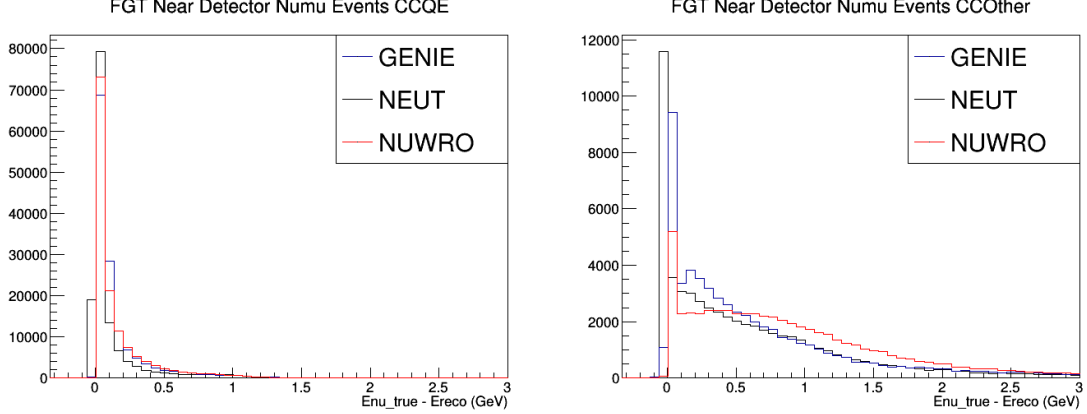


Figure 16: Difference between true and reconstructed Neutrino Energy in the FGT ND. CCQE events seem to have similar discrepancies, while CCOther mode has large tails in all three generators with NuWro having more events with higher discrepancy than the other two.

Meanwhile, for $\overline{\nu}_\mu$ CCQE, 2p2h, and CC0 π events NuWro consistently has ΔE closer to 0 than the other generators as shown in Figure 4. In CC1 π and CCOther NuWro again has more events where true neutrino energy is underestimated by reconstruction, shown in Figure 5. Additionally, there exists a large difference in the distribution of events from NEUT and NuWro between the FGT and LAr FD. This is slightly better in the LAr ND - as expected due to our naive LAr efficiencies. This can be seen in Figure 6.

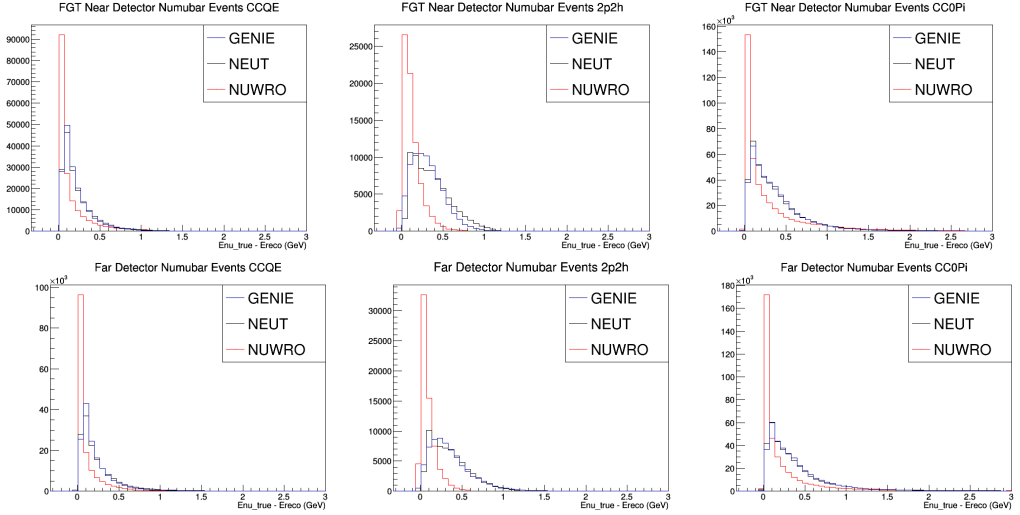


Figure 17: Difference between true and reconstructed E_{ν} . Top: At Near Detector with FGT efficiencies. Bottom: Far Detector with LAr efficiencies. Left to Right: CCQE, 2p2h, CC0 π . NuWro can be seen to have consistently less discrepancy in reconstructed energy than NEUT and GENIE in CCQE, 2p2h, and CC0 π .

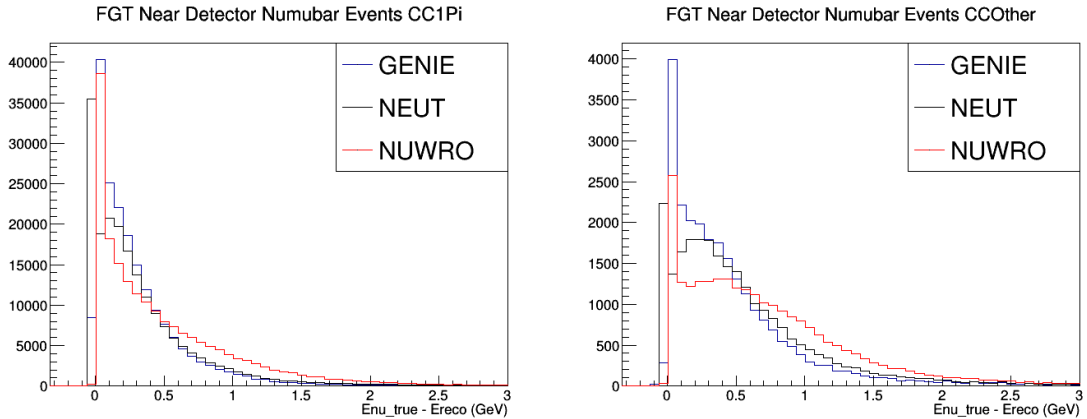


Figure 18: NuWro has higher discrepancy in reconstructed energy than NEUT and GENIE in both CC1 π and CCOther.

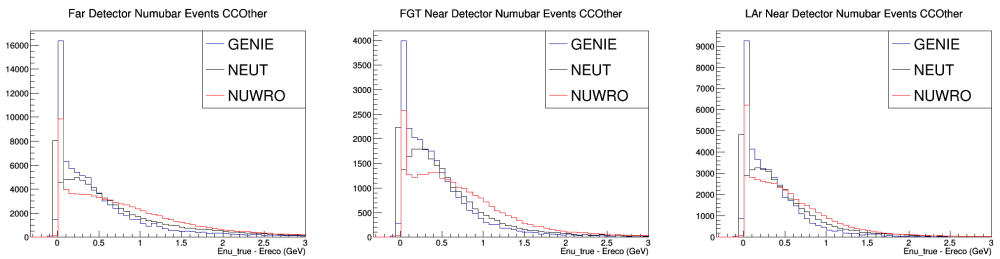


Figure 19: NuWro CCOther events have differences in shape between the Far Detector and LAr FD. The LAr ND matches more closely, though this is expected because of our current naive efficiency assumptions.

4.2 Neutron Multiplicities & Energy

Differences between models in the number of final state neutrons and the total energy into FS neutrons can largely affect reconstruction of neutrino energy. Large variations in reconstructed energy can arise due to missing energy caused by the inability to detect neutrons in the various models.

To investigate this, we have looked at GENIE, NEUT, and NUWRO to see if the different models showed a large difference in the neutron energy and multiplicity. This was done for CCQE-like, CC 1π , 2P2H, and everything else (“Other”) interactions and neutrinos as well as anti-neutrinos. In all cases, the generators agreed rather well with each other even though there were some differences in the neutron multiplicity. These differences only account for a small fraction of the events. Figure 7 shows an example of this for 2P2H neutrino events, while the other interaction modes can be found in Appendix A

Further more, the difference in the multiplicities between the generators becomes irrelevant after a ND to FD extraction, as can be seen in Figure 8. Here, the region where the most energy is lost agrees very well between the ND and FD for all generators and interaction types. The areas with low statistics do show a disagreement, but very few events fall into this area.

Care should still be taken when calculating the total neutrino of the event if only a calorimetric approach is used, as is the case in this document. This is because as much as 50% of the energy can be taken away by the neutron in CCQE-like events. Even for 2P2H events, as shown in Figure 9, it can be as much as 30%. The other interaction modes and anti-neutrino events can also be found in Appendix A and have a smaller fraction.

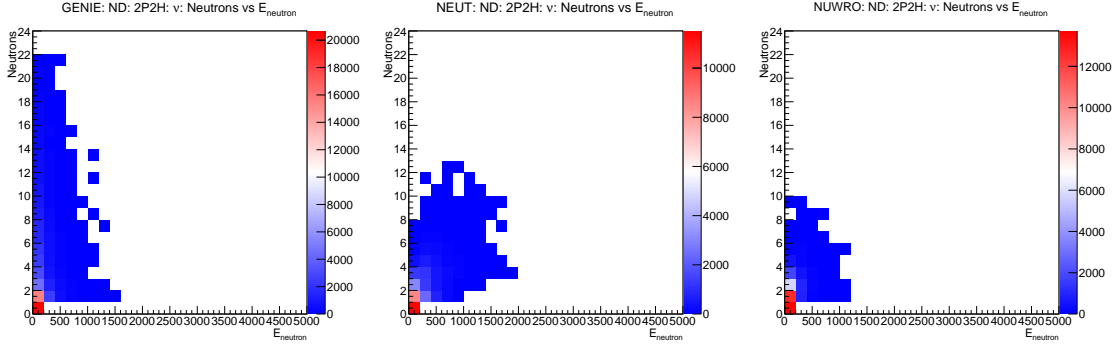


Figure 20: The neutron multiplicity vs total neutron energy for 2P2H interactions for GENIE, NEUT, and NUWRO, respectively. Even though they do show a different phase-space for the neutron multiplicity, they all agree where most of the energy lost to neutrons should be. This is similar for other interaction types as well.

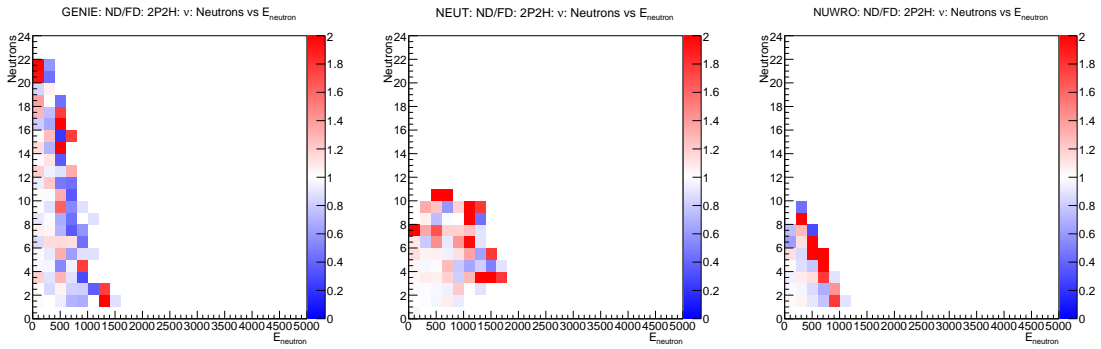


Figure 21: The ratio of the ND to the FD for neutron multiplicity vs total neutron energy for 2P2H interactions for GENIE, NEUT, and NUWRO, respectively. In the area where the largest amount of energy is lost to neutrons, low multiplicity and low energy, the agreement between the ND and FD is almost perfect.

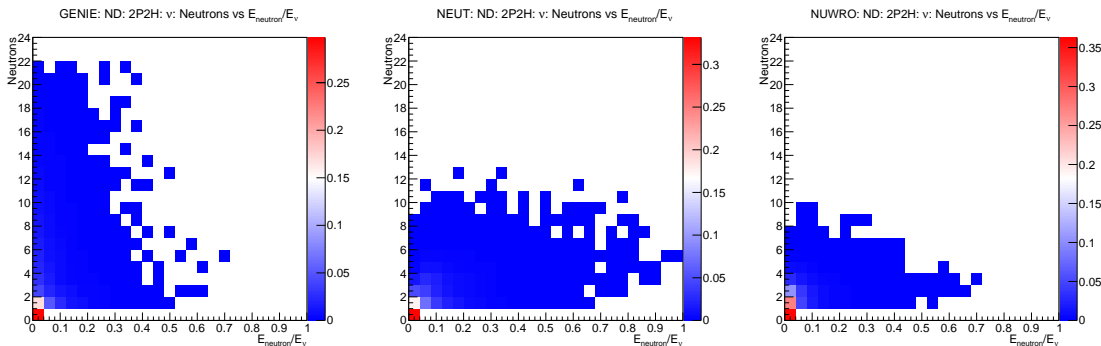


Figure 22: Neutron multiplicity vs total neutron energy divide by the neutrino energy for 2P2H interactions from GENIE, NEUT, and NUWRO, respectively. For low multiplicity, the neutron carries away a significant fraction of the neutrino energy.

Additionally, investigations in the ability for errors in GENIE to cover the differences between models have been started.

4.3 Proton/Pion Multiplicity and Momentum

Similar to the neutron multiplicity and energy studies, proton and pion mutliplicities and energies offer insight into the coupling of the detector configurations with variations in FSI models as well as the energy reconstruction capabilities of the different detector configurations. The total momentum of the particles gives us a proxy for the energy into the FS protons or pions as well as a direct link to detector efficiency effects. For these studies, the 3-momentum of the final state (after efficiencies) protons or charged pions are summed. The magnitude is then plotted against the multiplicity for the specific particle type. This was done for the FS particles in true-CCQE, true-2p2h, CC0 π , CC1 π , and CCOther, and with all 3 ND configuration efficiencies and the LAr FD efficiencies, as well as with no efficiencies applied. As the efficiencies for pions are currently unknown for the LAr and GAr, we will only consider the protons in the current iteration of this note. Note that the LAr and GAr are still only naive assumptions.

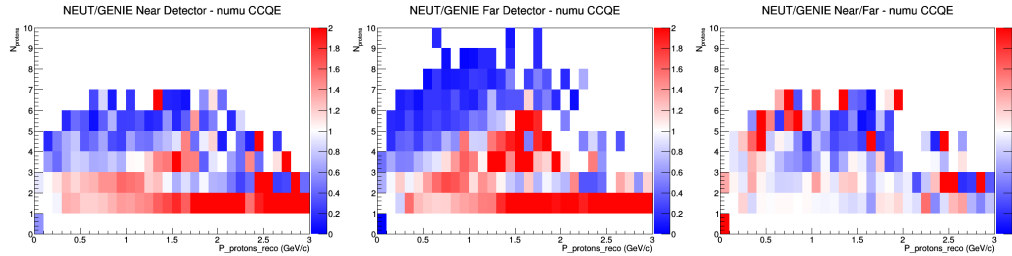


Figure 23: Nprotons vs. P protons distributed events using DUNE flux. Left: Ratio of NEUT to GENIE output at ND with FGT efficiencies, Mid: Ratio of NEUT to GENIE output at FD with LAr efficiencies, Right: Double ratio of NEUT to GENIE, Near to Far

4.4 Nucleon multiplicity vs. W

Differences in mapping from E_{reco} to true variables can arise from shape differences in nucleon multiplicities vs. W distributions. These distributions can also show where in the phase space most of the events shown in Section 3.2 and Section ?? exist. A first look of this is shown in this section.

4.4.1 Neutrons vs W

Apart from the difference in neutron multiplicity discussed in Section 3.2, the exact phase space of these event in the neutron/W plane is slightly different. This is most pronounced for 2P2H events, as can be seen in Figure ???. The width of NEUT's

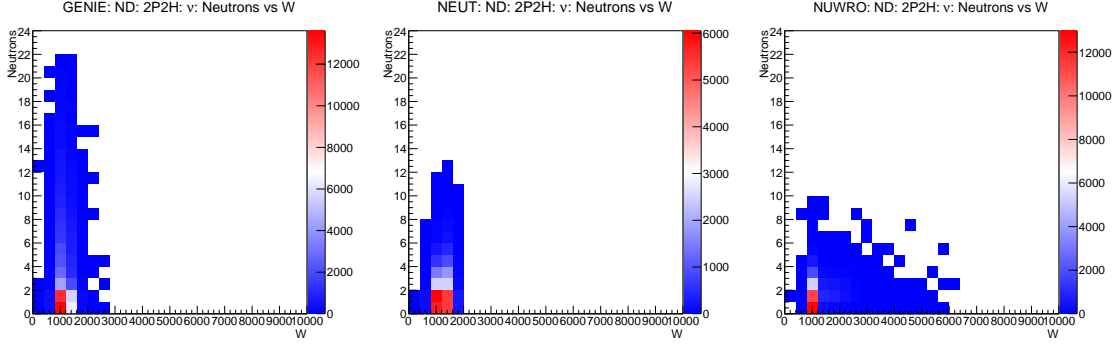


Figure 24: The neutron multiplicity vs W for 2P2H interactions from GENIE, NEUT, and NUWRO, respectively. It can be seen that all three event generators have the peak of the distribution at the same place, but NEUT’s peak is much broader while NUWRO allows for much higher W ’s.

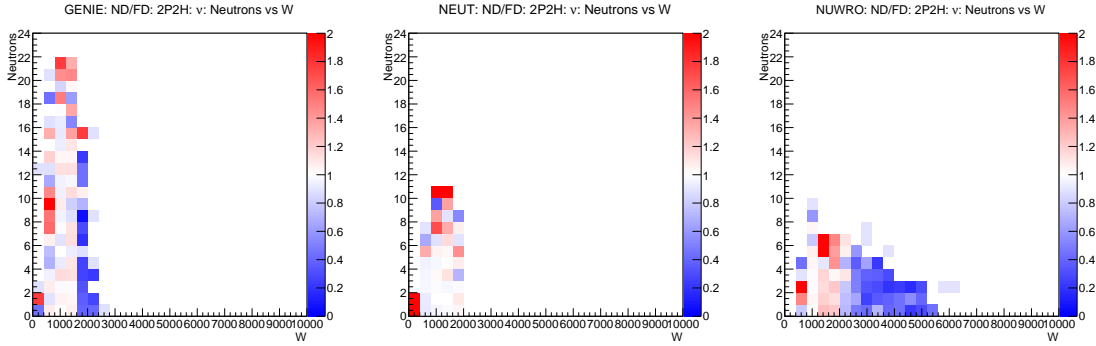


Figure 25: The ND/FD ratio of neutron multiplicity vs W for 2P2H interactions from GENIE, NEUT, and NUWRO, respectively. The effects of the different phase space seen in Figure 24 is not great if a ND ro FD extrapolation is used. This can be seen by the ratio being very close to one at the peak of Figure 24 distribution.

peak is broader than GENIE’s or NUWRO’s while NUWRO allows for much higher W ’s.

However, Figure 25 shows that the differences are not so important if a near to far extrapolation is used, as both the ND and FD have similar responses. To see if the different models could have a larger affect on the physics results, we have taken a double ratio of the ND/FD and the different generators to GENIE. Interestingly, Figure 26 indicates that there would not be large affect if a few percent difference between the models is acceptable.

These results are also true for protons and pions, though pions have a much lower multiplicity. Those results, along with other interactions can be found in Appendix B.

4.4.2 Protons vs W

In the last section we saw a difference in the phase space between the different generators. Now we will show an instance where the phase space is almost the same but

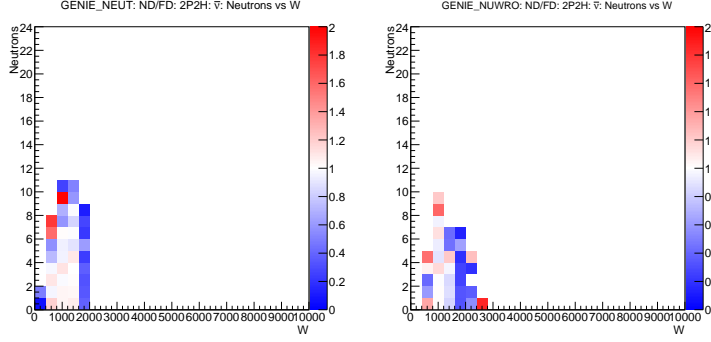


Figure 26: The double ratio of ND/FD and the event generators to GENIE of the neutron multiplicity vs W for 2P2H interactions. Despite the differences seen in the W distributions, the double ratio shows surprisingly good agreement between the generators, indicating that the different models should not have a large impact on the final results.

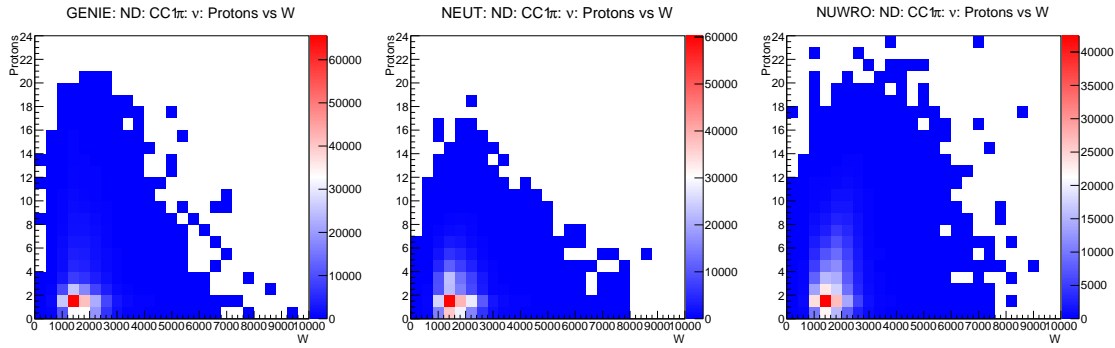


Figure 27: The proton multiplicity vs W for CC1 π interactions from GENIE, NEUT, and NUWRO, respectively. It can be seen that all three event generators have the peak of their distribution at the same place and are almost identical

there is a large difference between the ND and FD. Though here we are only showing the results for CC1 π via protons, the results are the same for CC-Other (anything not CCQE, CC1 π , or 2P2H), and neutrons along with pions. Figure 27 shows that GENIE, NEUT, and NUWRO have very similar distributions.

If a near to far detector extrapolation is used, however, there are much larger differences in region of most interest. Figure 28 shows that there is a difference between the two detectors between 20% and 40% at the peak of the distribution. There is also a clear difference in lower W values compared to higher W values.

We can again see if the different models could have a larger affect on the physics results, by taking the double ratio as we did before. Similar to before, Figure 29 indicates that there would not be large affect if a few percent difference between the models is acceptable. In the region of interest, the difference between GENIE and NEUT is negligible while it is small compared to NUWRO.

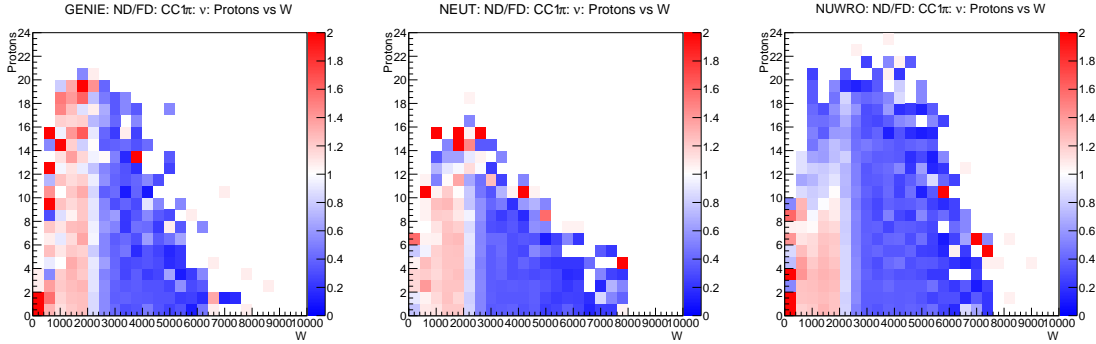


Figure 28: The ND/FD ratio of the proton multiplicity vs W for CC1 π interactions from GENIE, NEUT, and NUWRO, respectively. Unlike with 2P2H events shown for neutrons, there are clear differences between the ND and FD. At the peak of the distribution this is between 20% and 40%. Furthermore, there is a clear difference between W values below 2000 and ones above it.

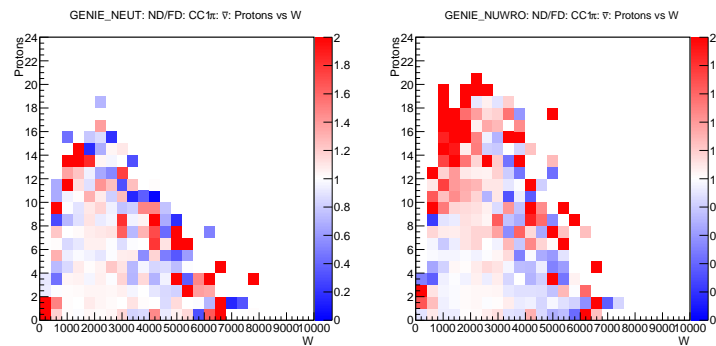


Figure 29: The double ratio of ND/FD and the event generators to GENIE of the proton multiplicity vs W for CC1 π interactions. Despite the differences seen in the single ratio, the double ratio shows surprisingly good agreement between the generators

5 Future Work

The above studies need to be furthered and expanded upon to successfully arrive at useful conclusions on ND configuration choice.

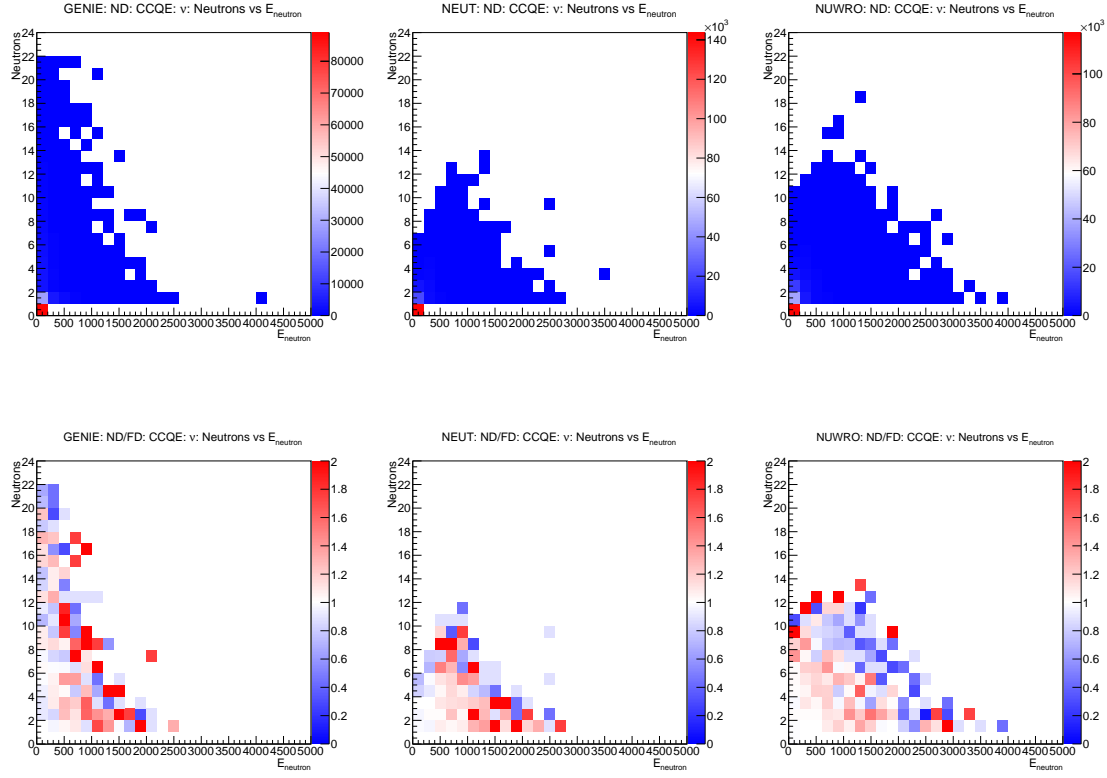
- Extend studies to include LAr and GAr efficiency and acceptance information when available.
- Include a mapping of E_{true} to E_{reco} along with y_{true} to y_{reco} and investigate differences between configurations.

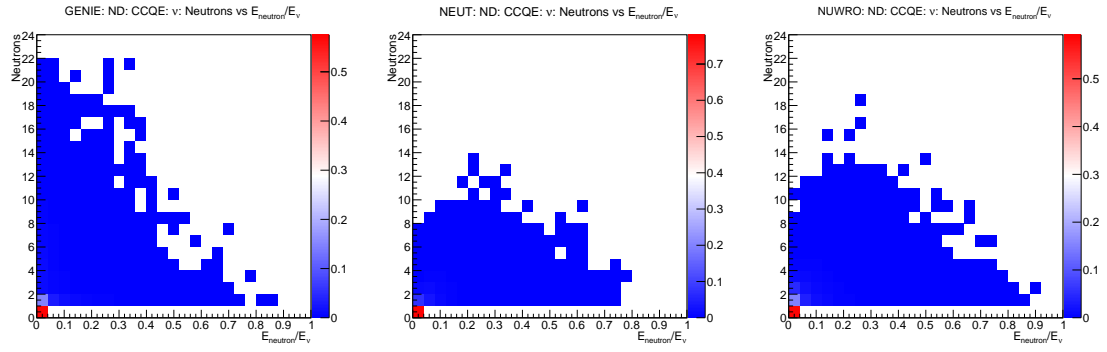
A Neutron Multiplicities & Energy

This appendix includes all the plots not shown in Section 3.2. For full description of the files, please make reference to that section. The plots will be put in the same order as before.

A.1 ν Plots

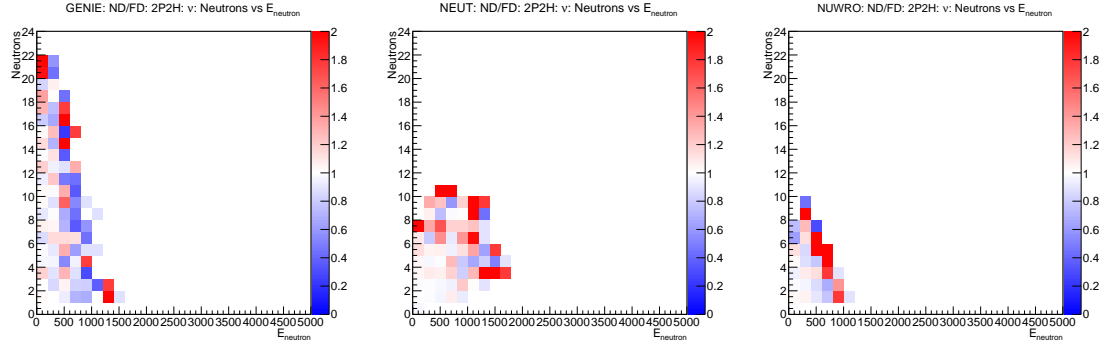
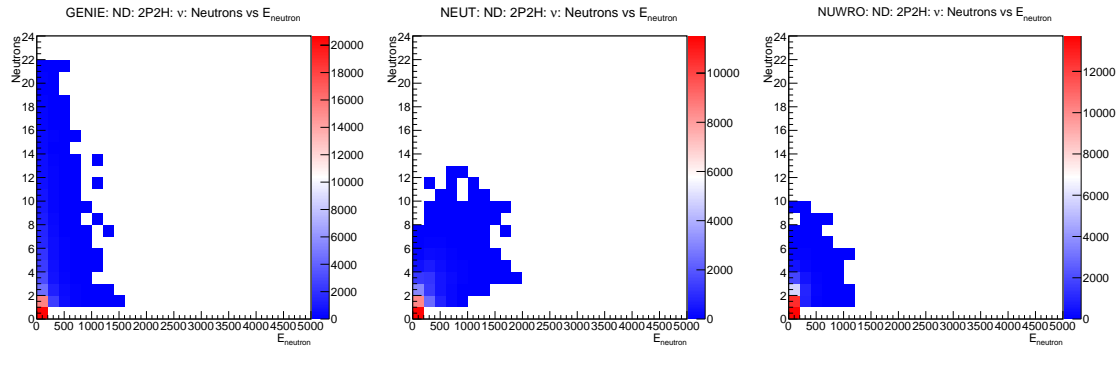
A.1.1 CCQE

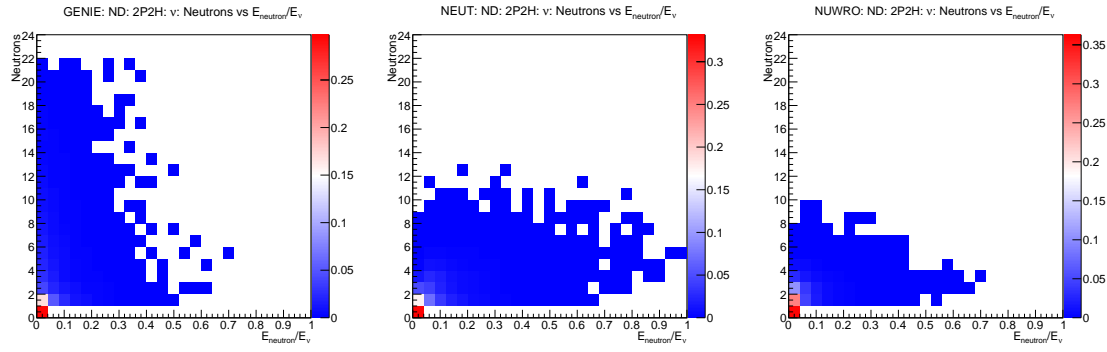




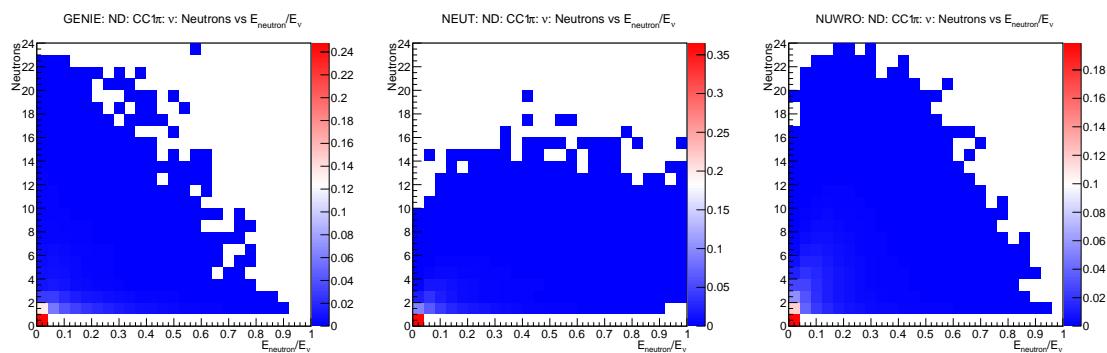
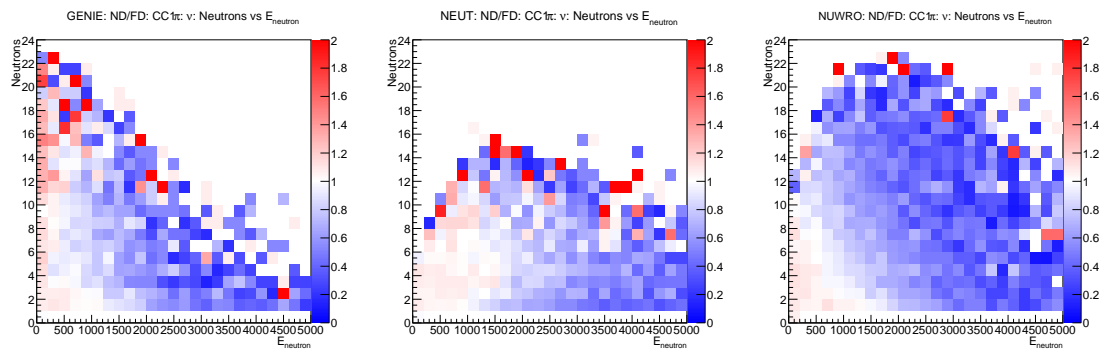
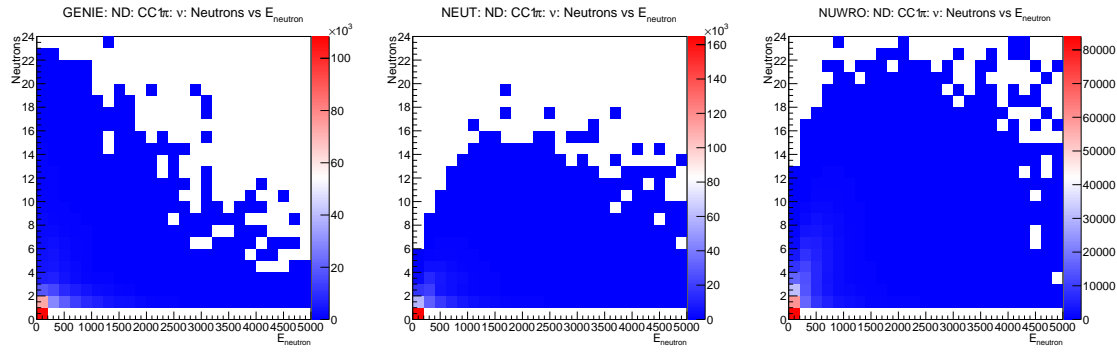
A.1.2 2P2H

These are the same as shown in Section 3.2.

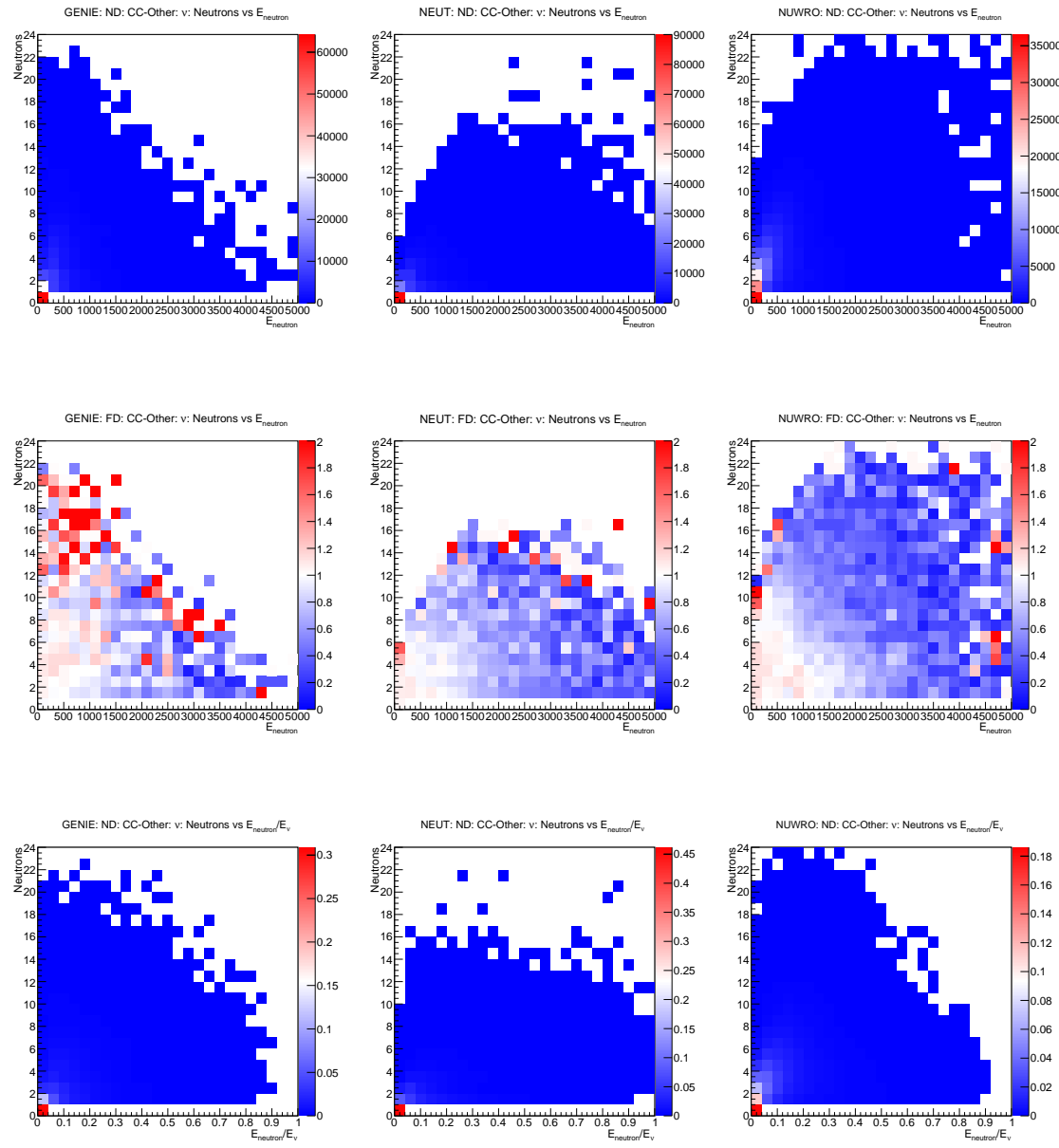




A.1.3 CC1 π

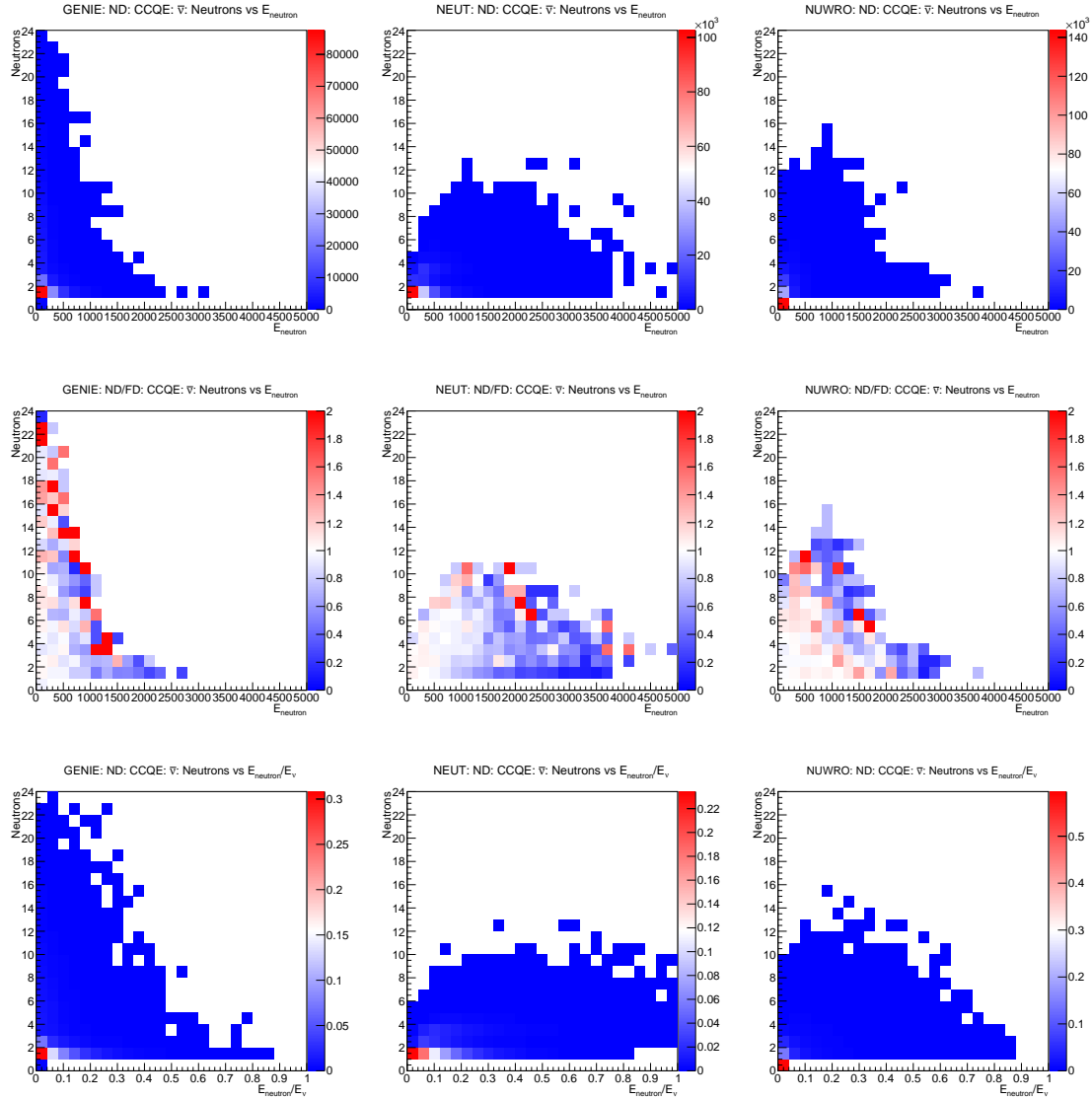


A.1.4 CC-Other



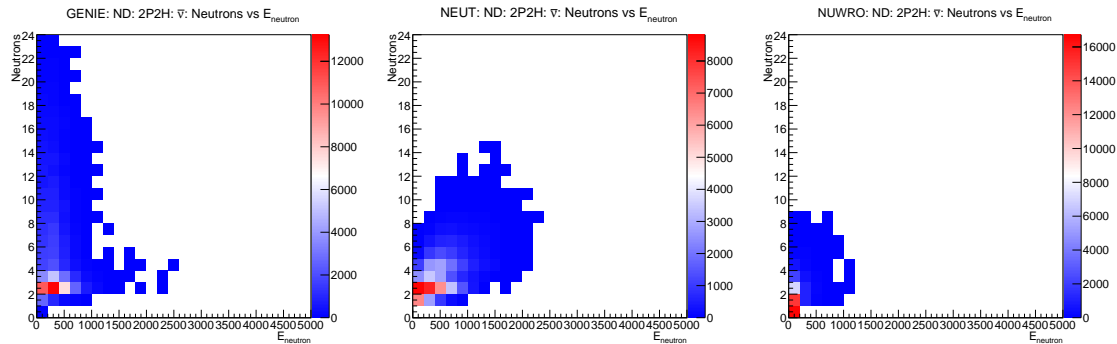
A.2 $\bar{\nu}$ Plots

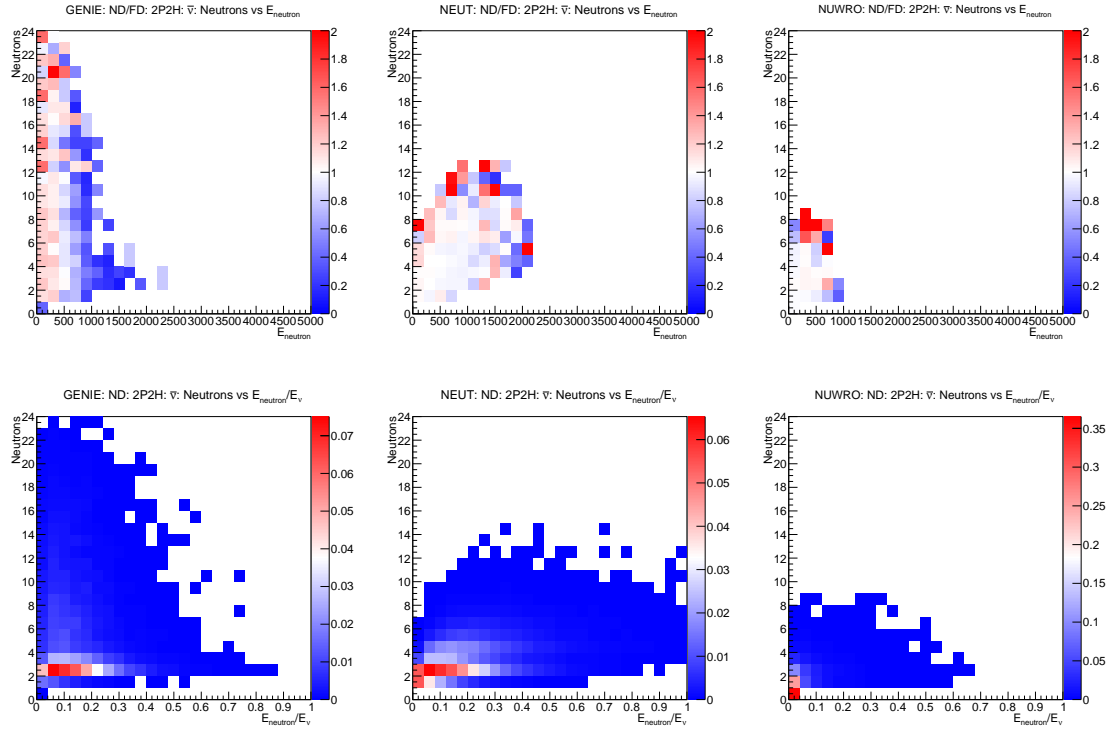
A.2.1 CCQE



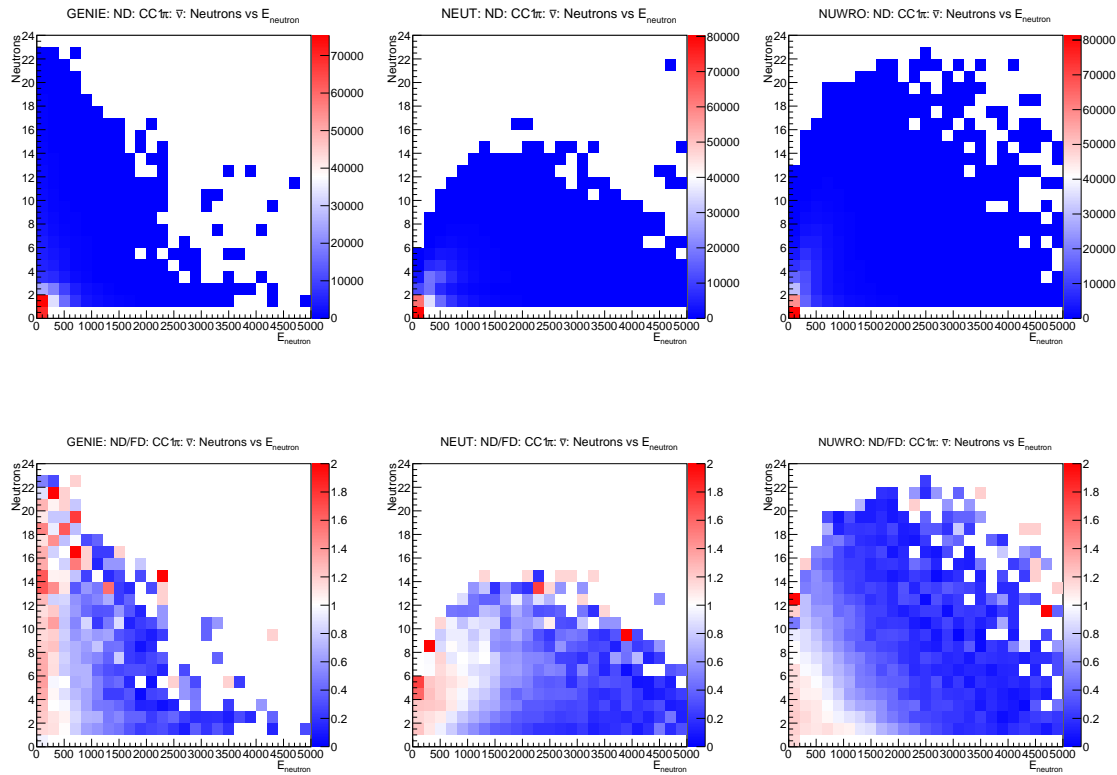
A.2.2 2P2H

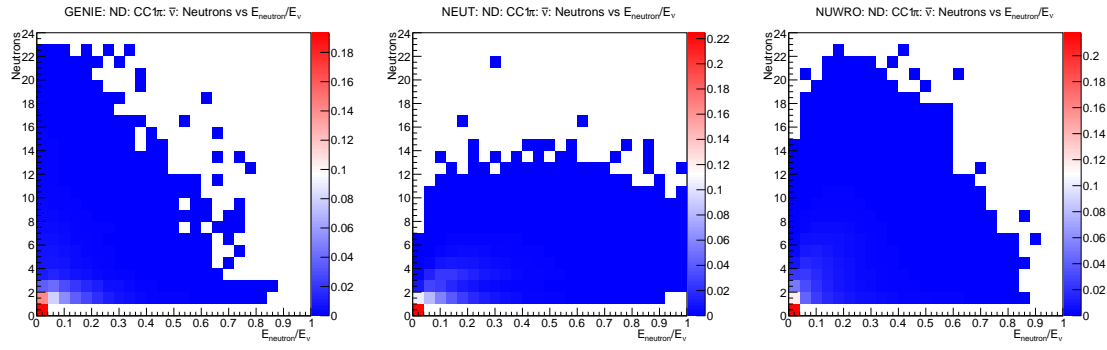
These are the same as shown in Section 3.2.



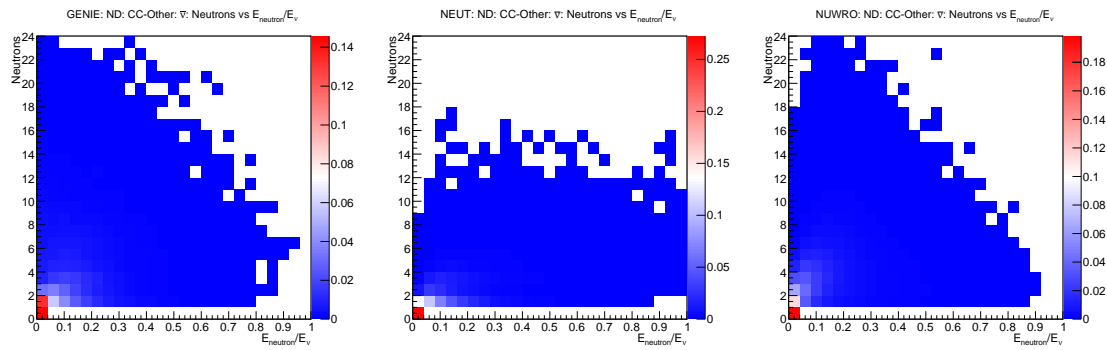
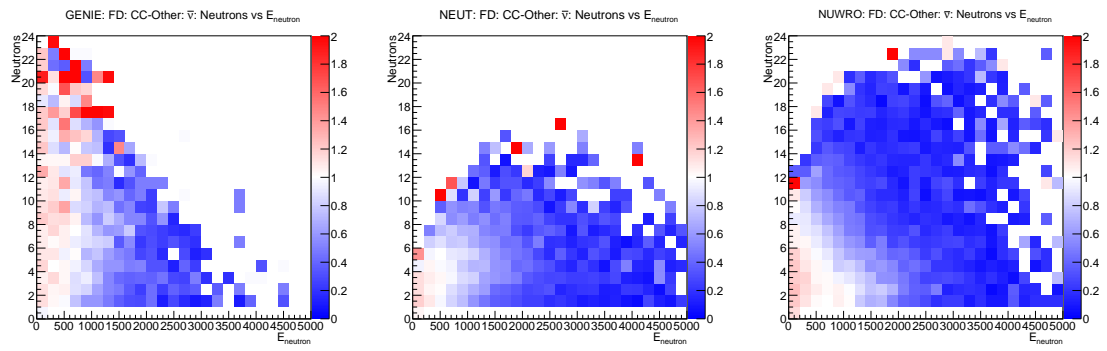
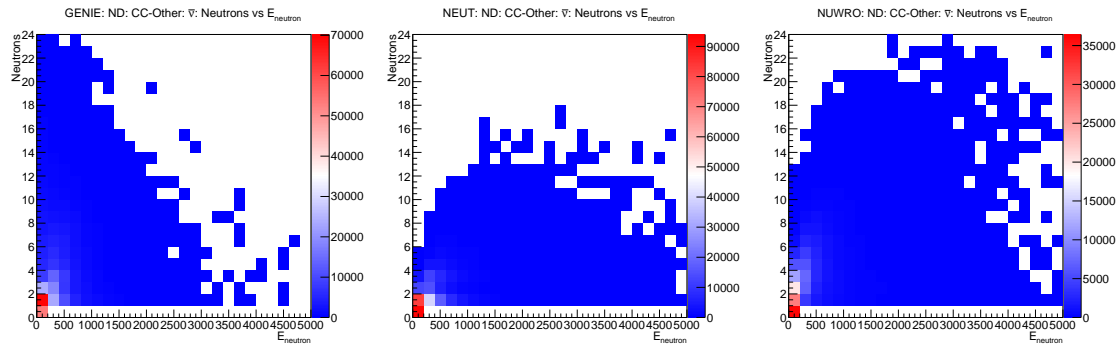


A.2.3 CC1 π





A.2.4 CC-Other

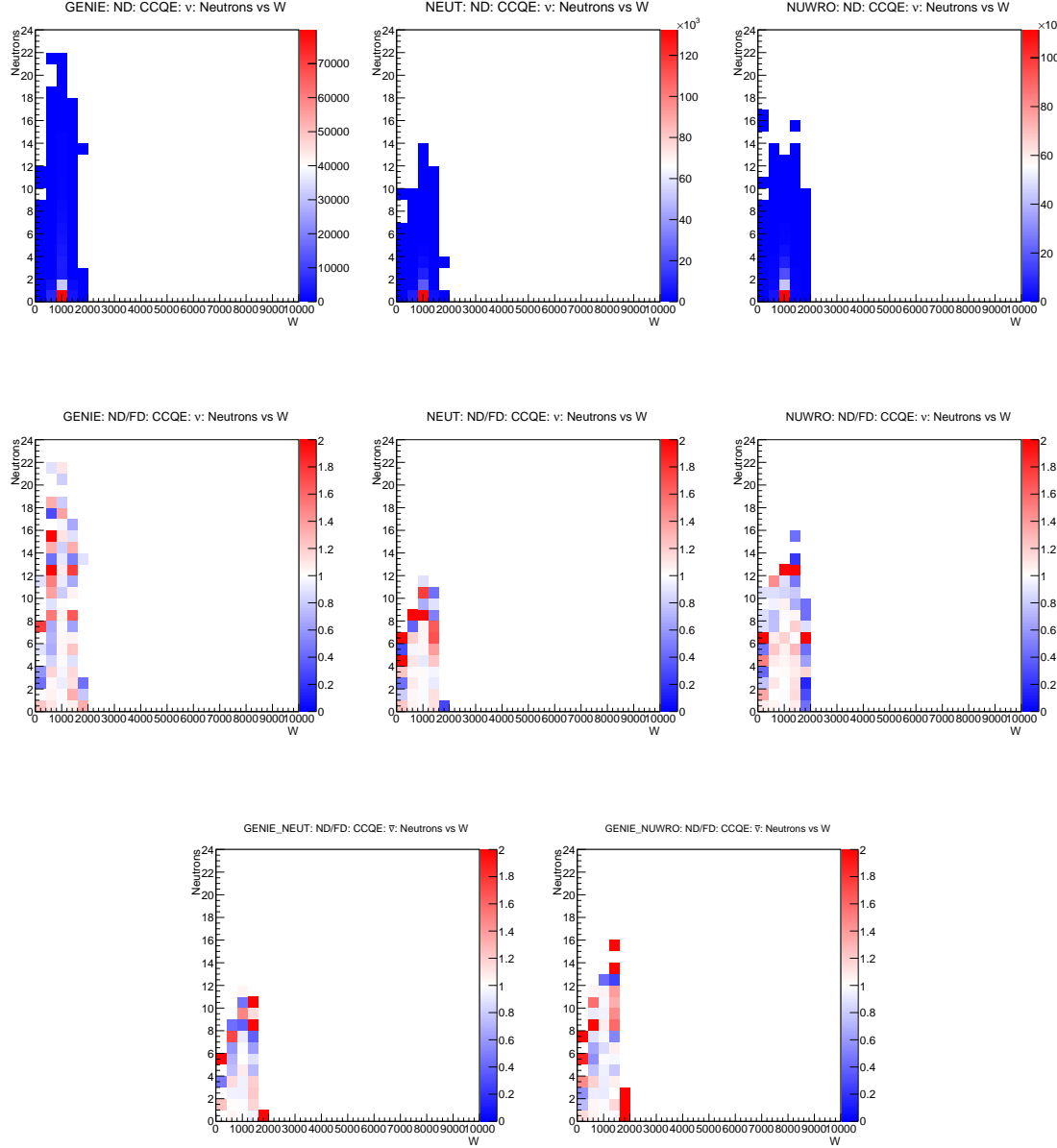


B Nucleon Multiplicity vs W

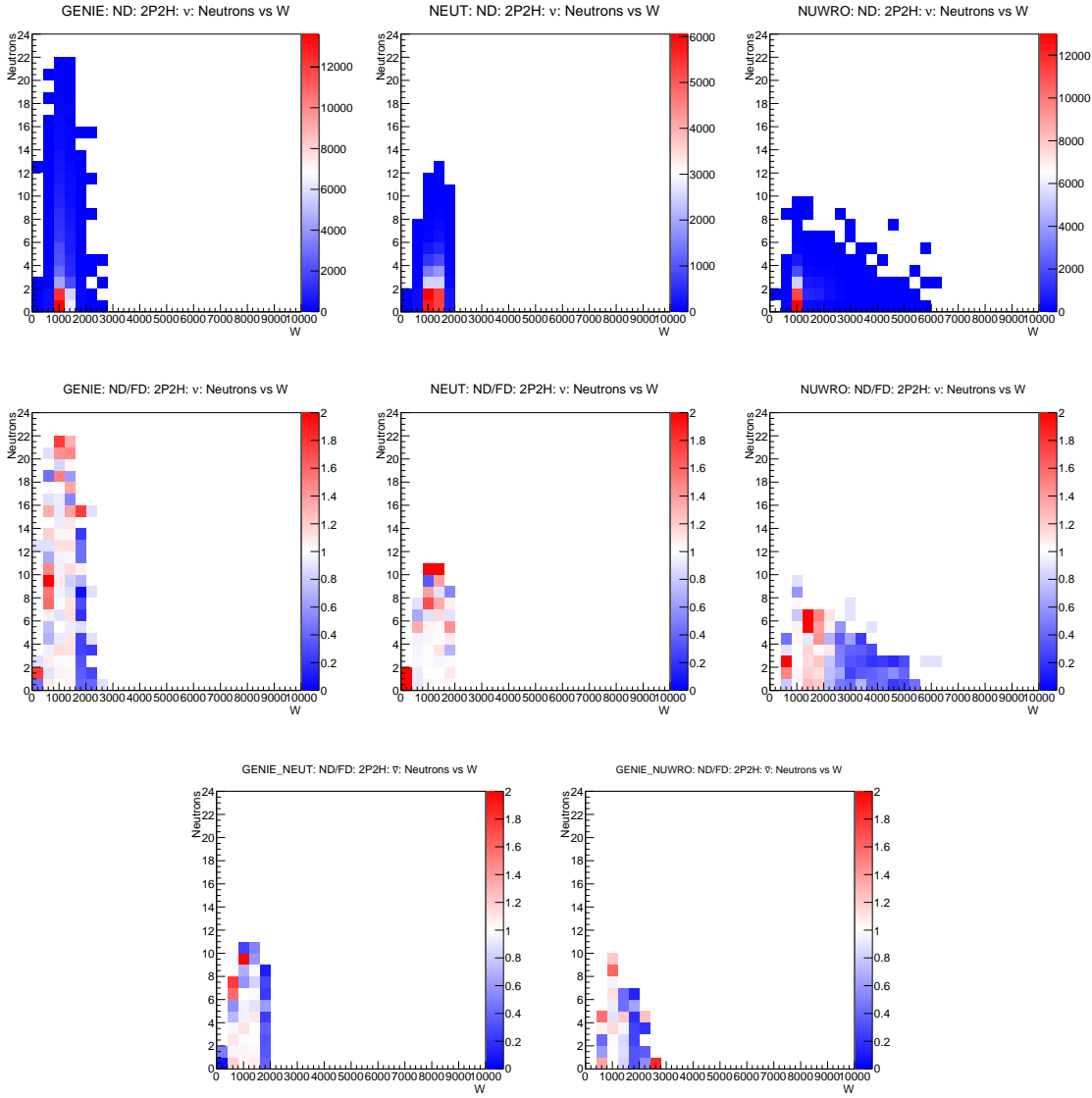
This appendix includes all the plots not shown in Section 4.4. For full description of the figures, please make reference to that section. The plots will be put in the same order as before.

B.1 Neutron Multiplicity vs W

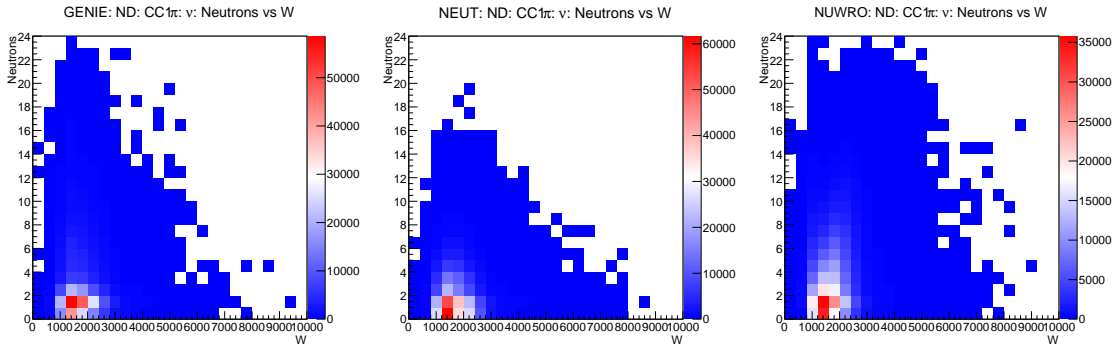
B.1.1 ν CCQE

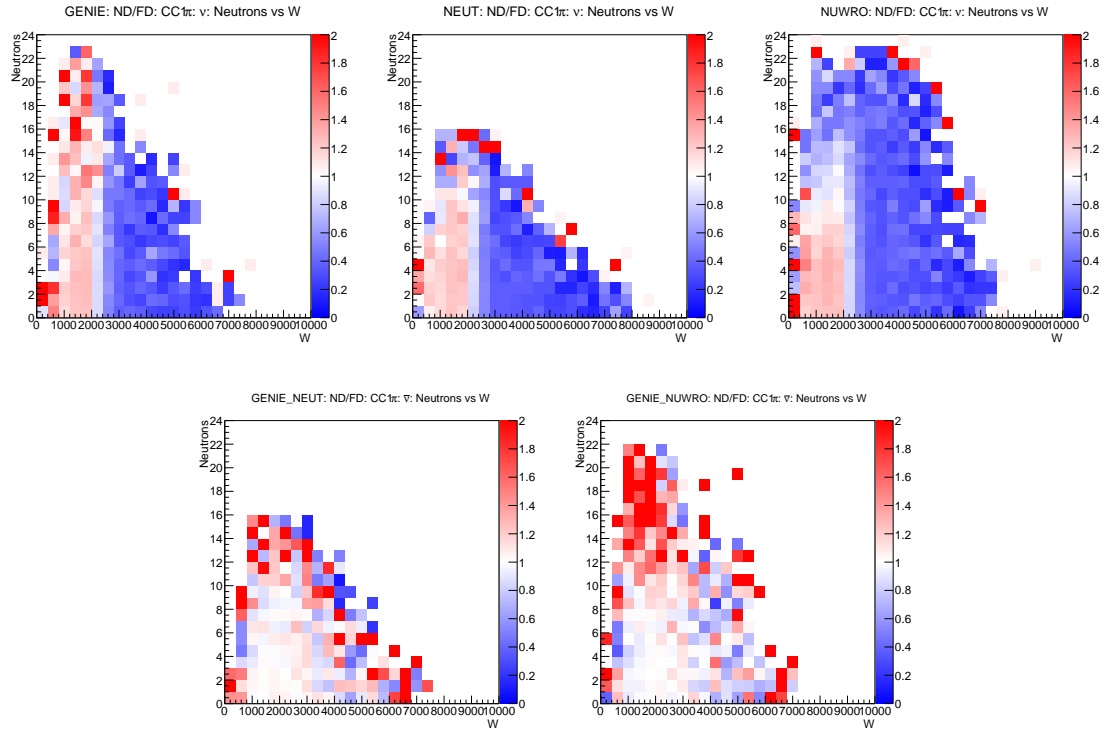


B.1.2 ν 2P2H

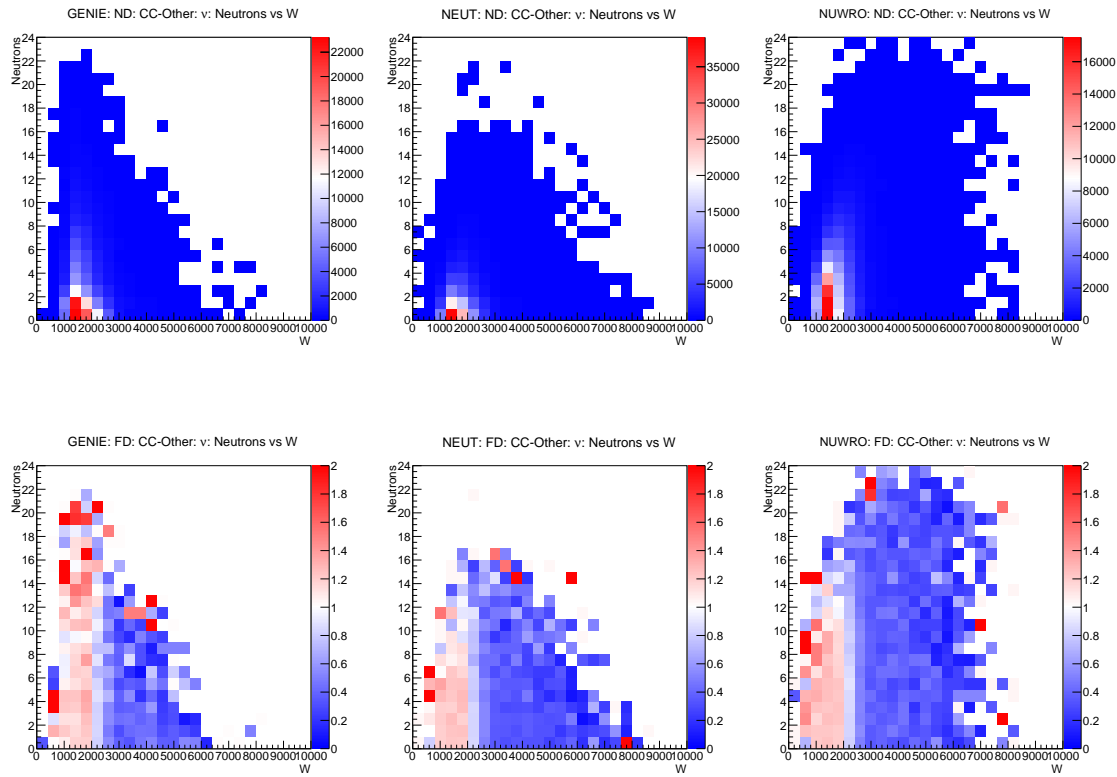


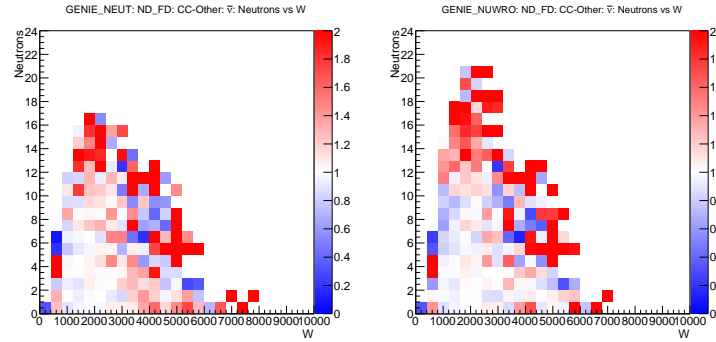
B.1.3 ν CC1 π



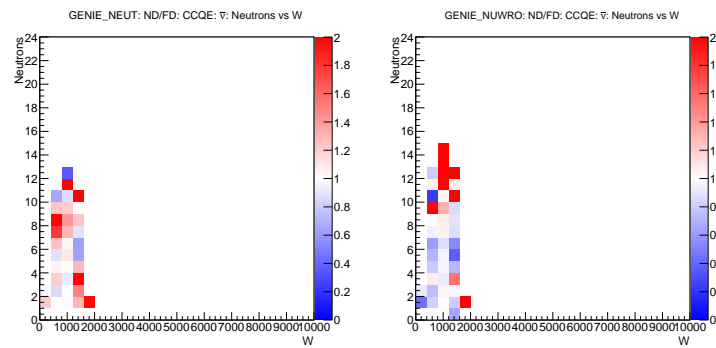
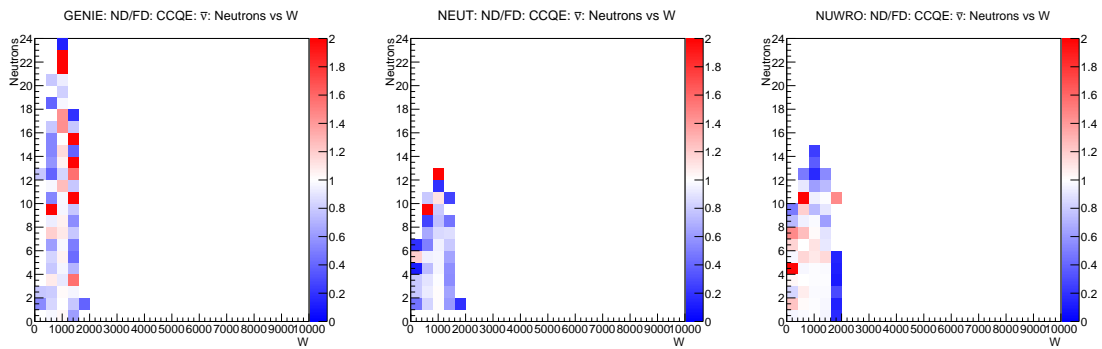
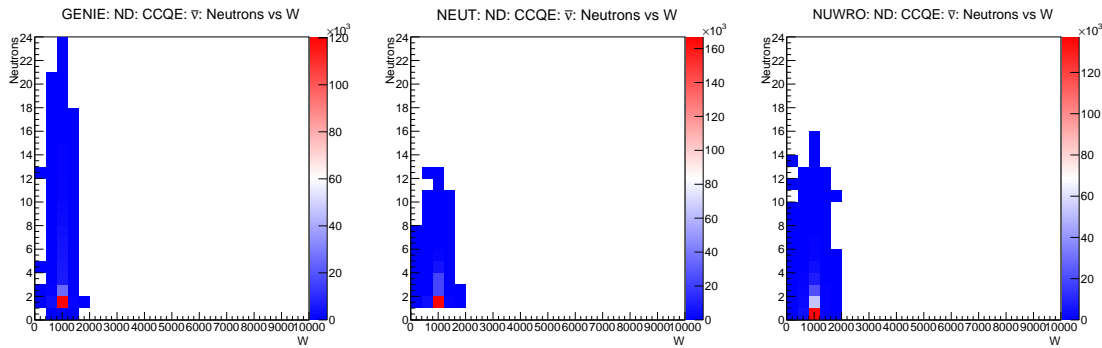


B.1.4 ν CC-Other

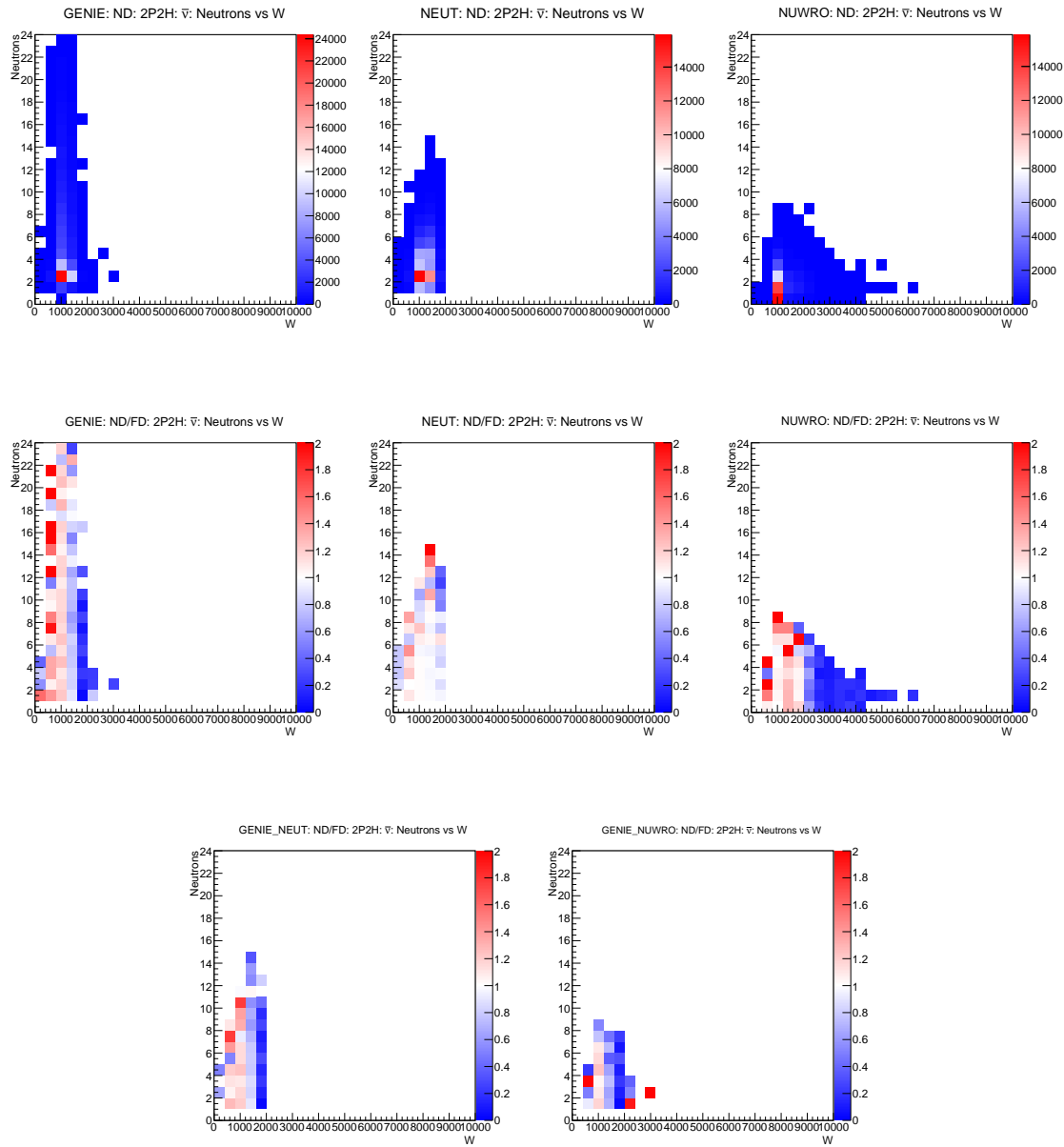




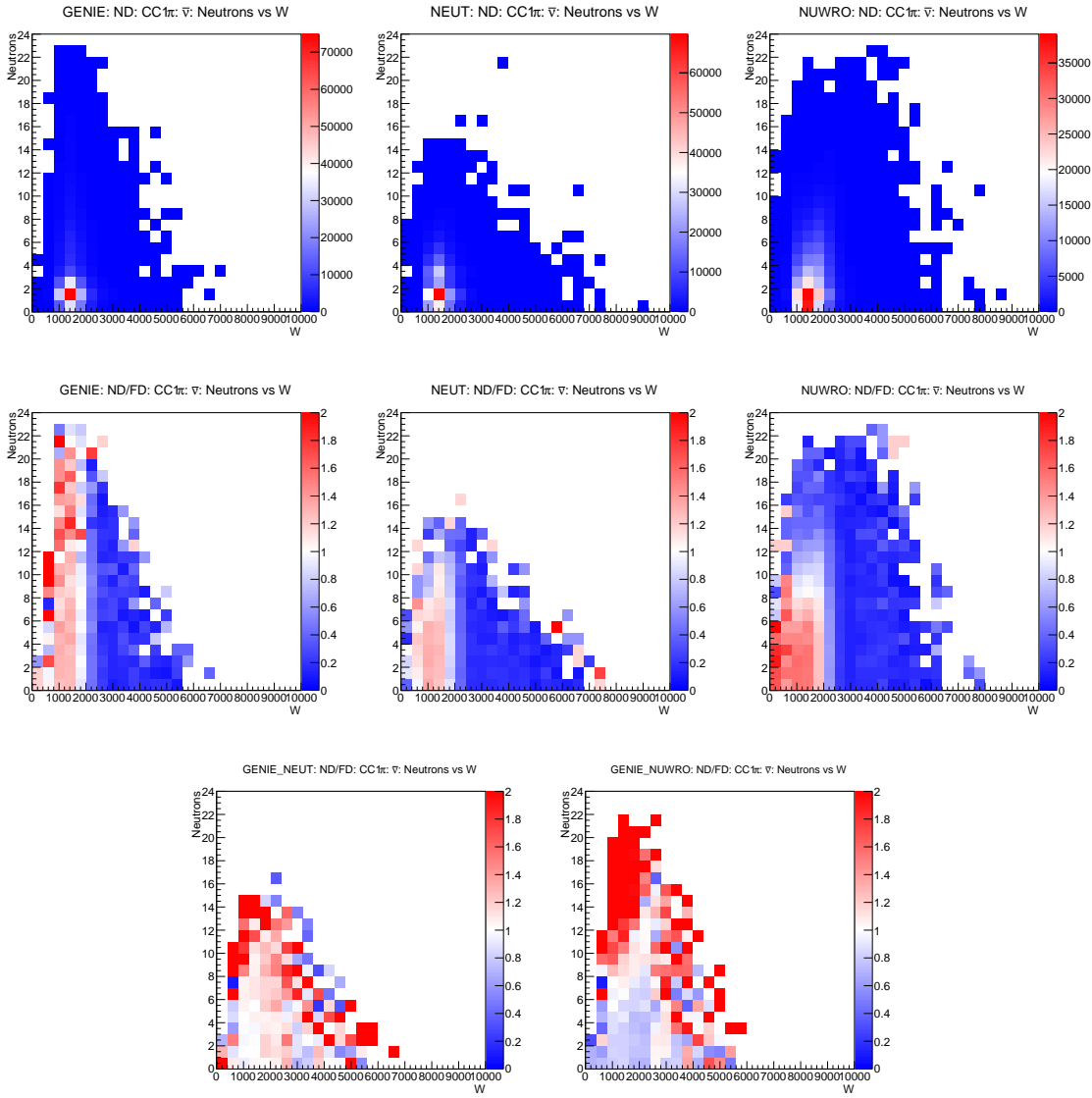
B.1.5 $\bar{\nu}$ CCQE



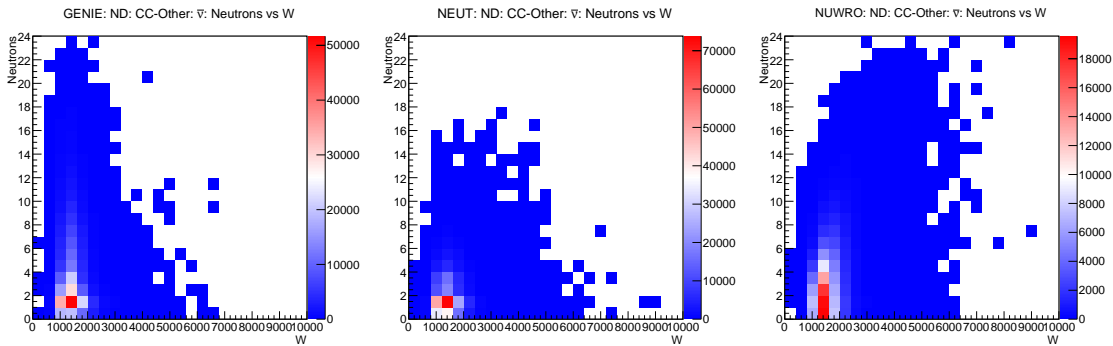
B.1.6 $\bar{\nu}$ 2P2H

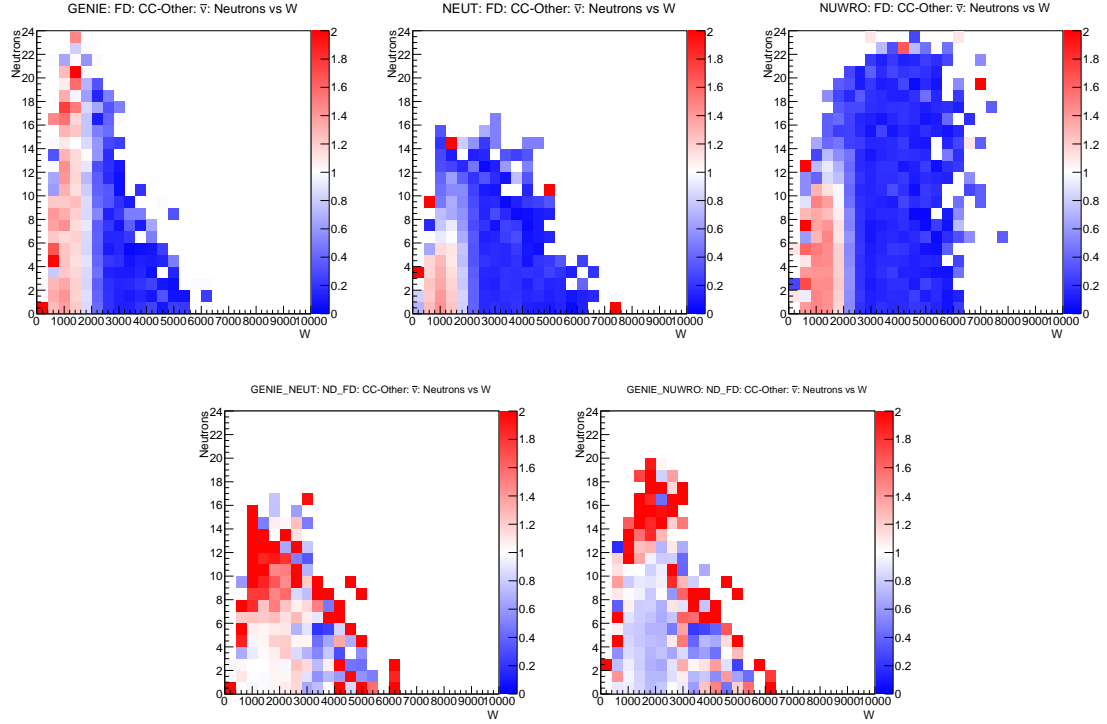


B.1.7 $\bar{\nu}$ CC1 π



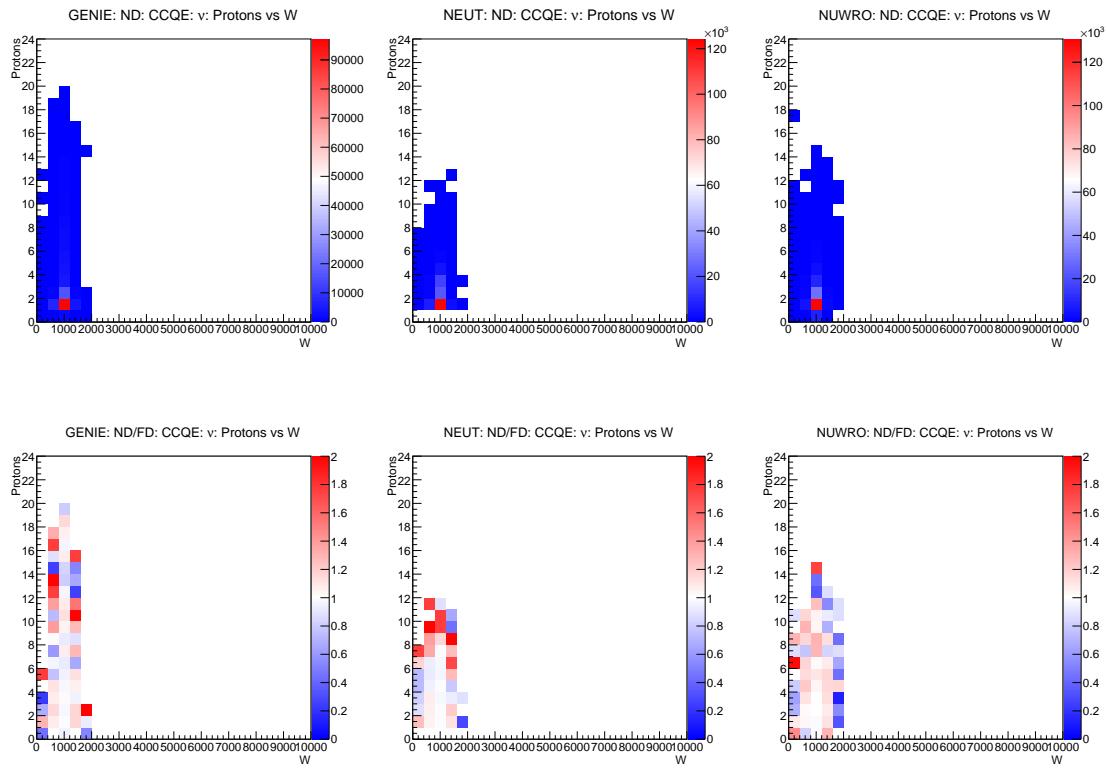
B.1.8 $\bar{\nu}$ CC-Other

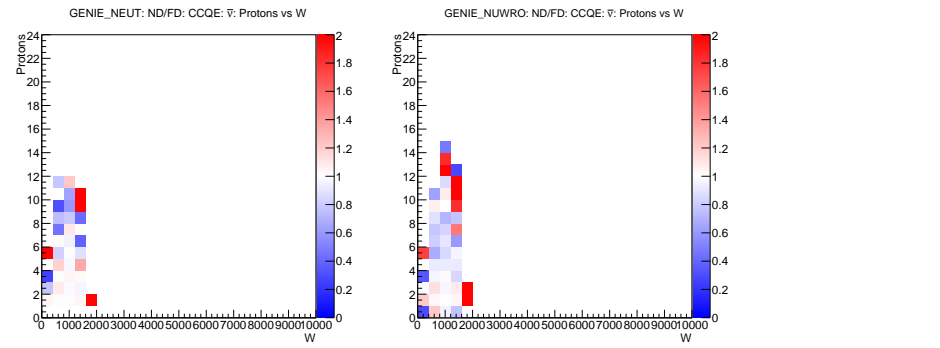




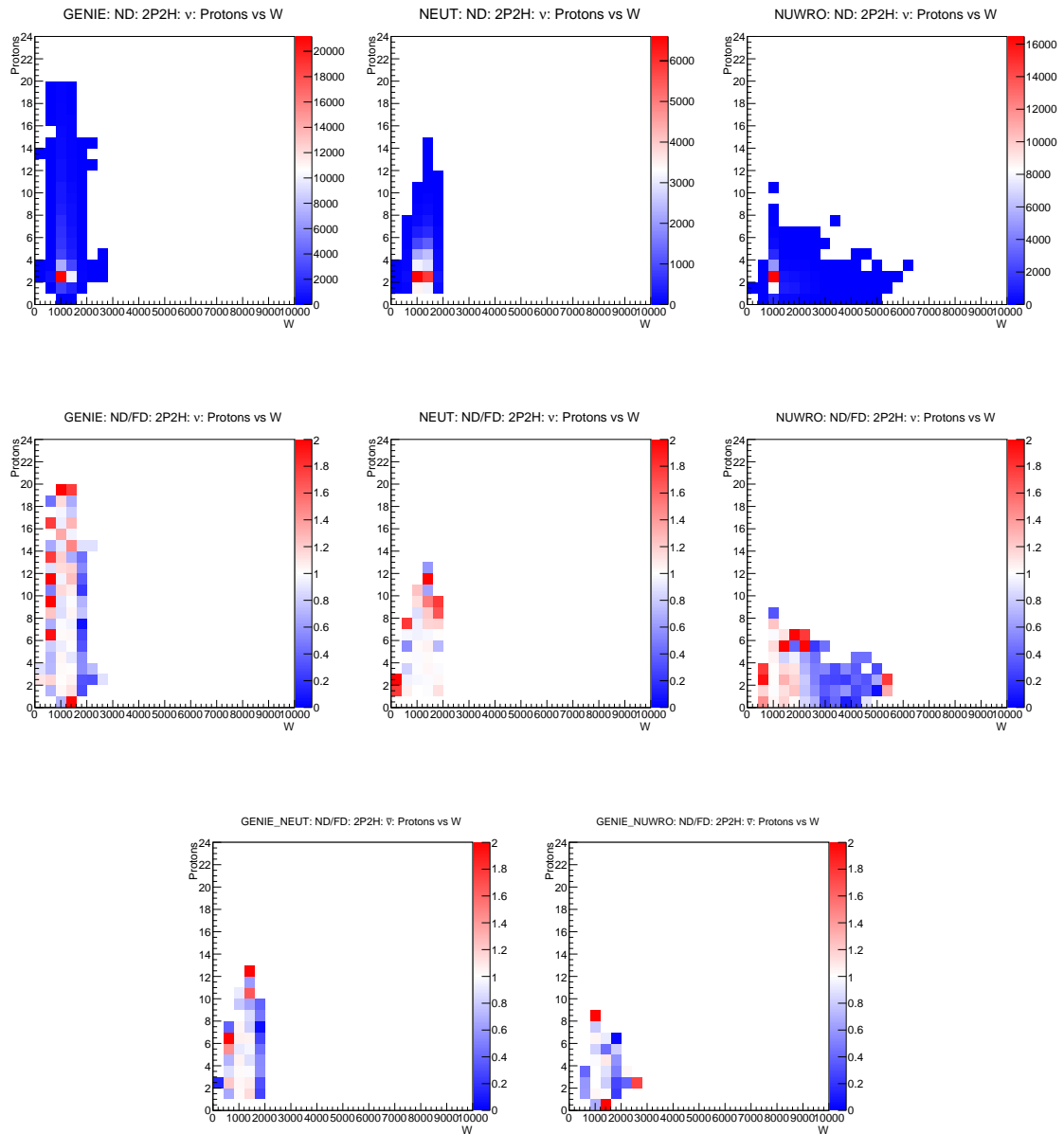
B.2 Proton Multiplicity vs W

B.2.1 ν CCQE

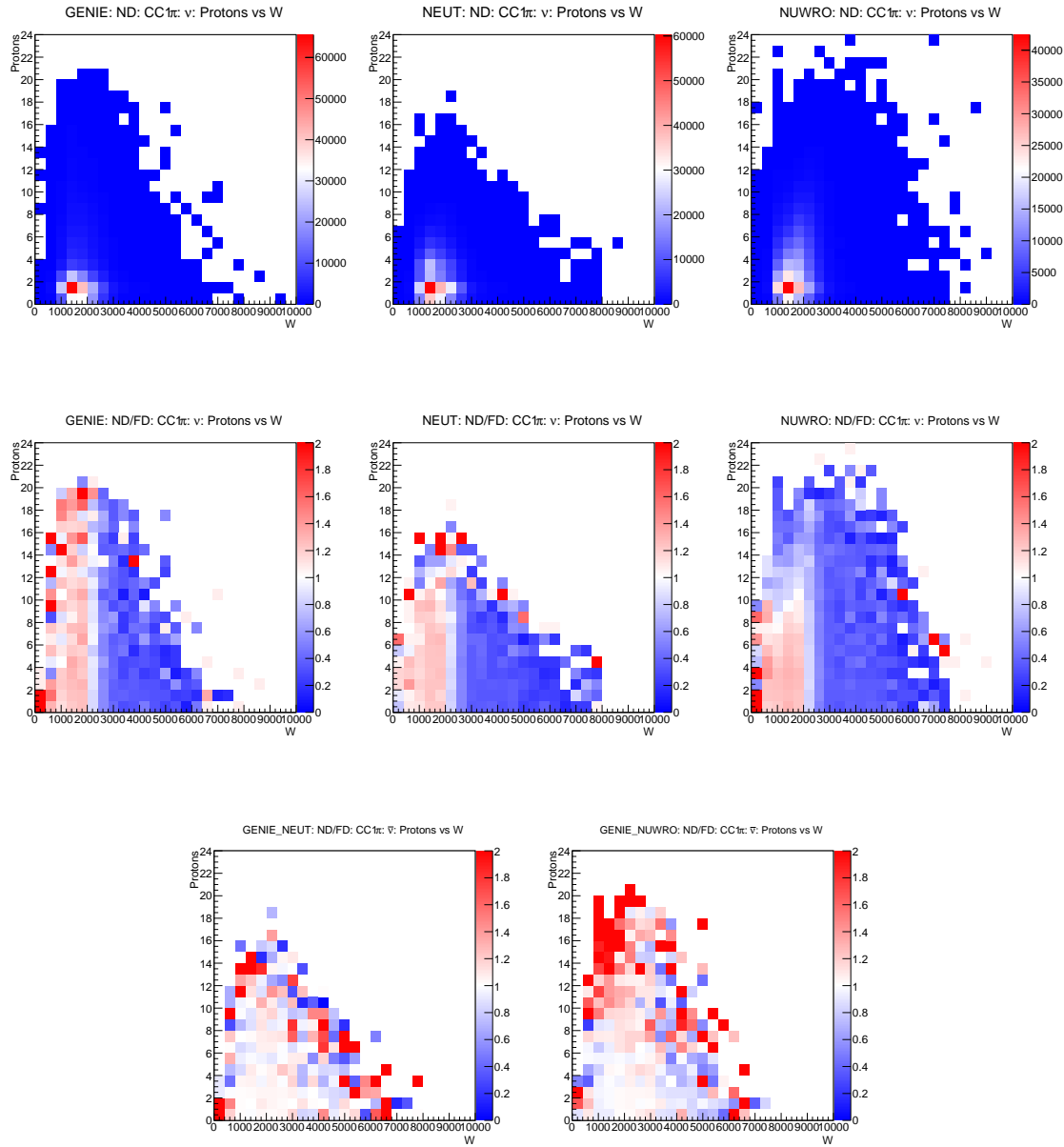




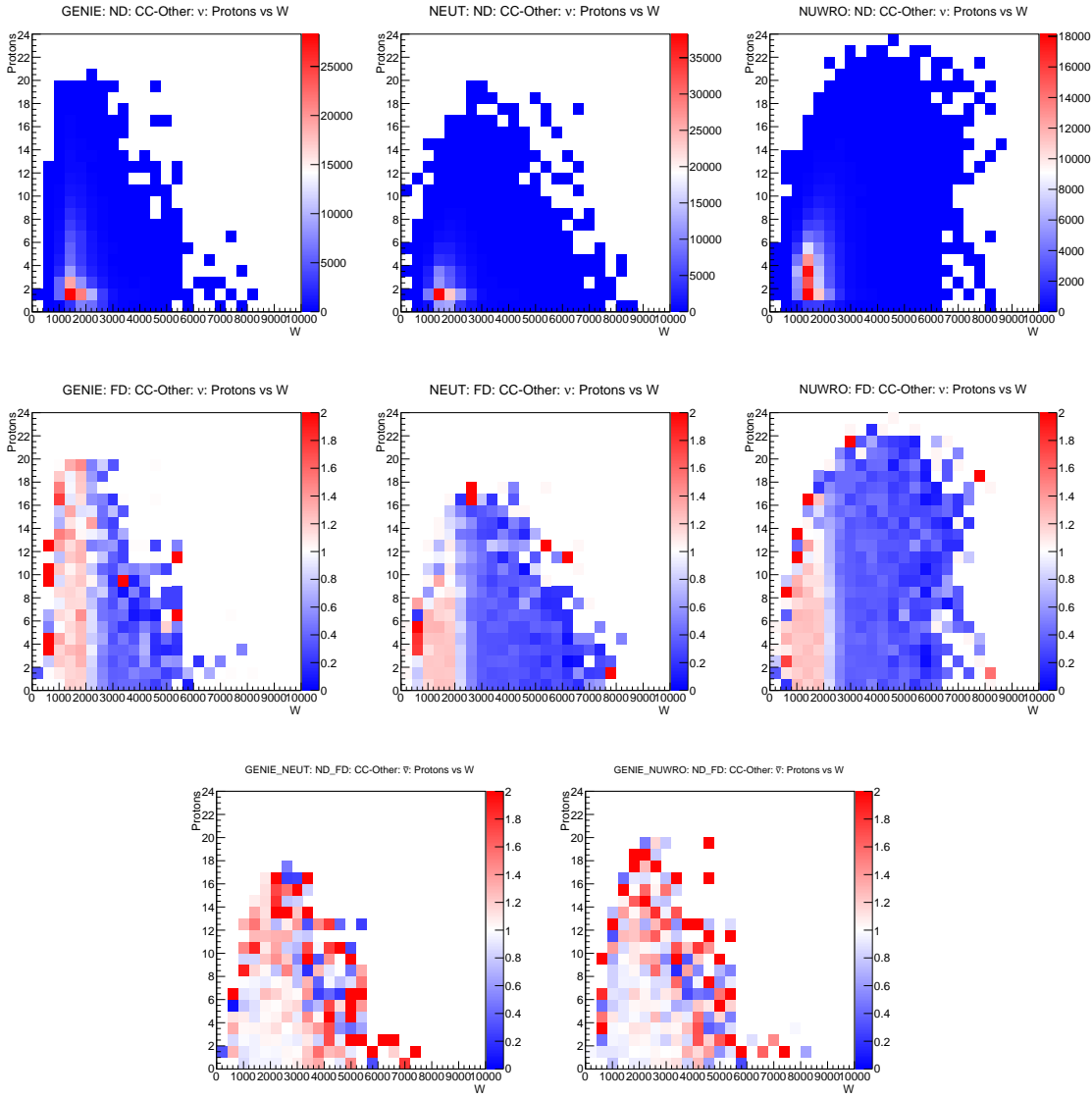
B.2.2 ν 2P2H



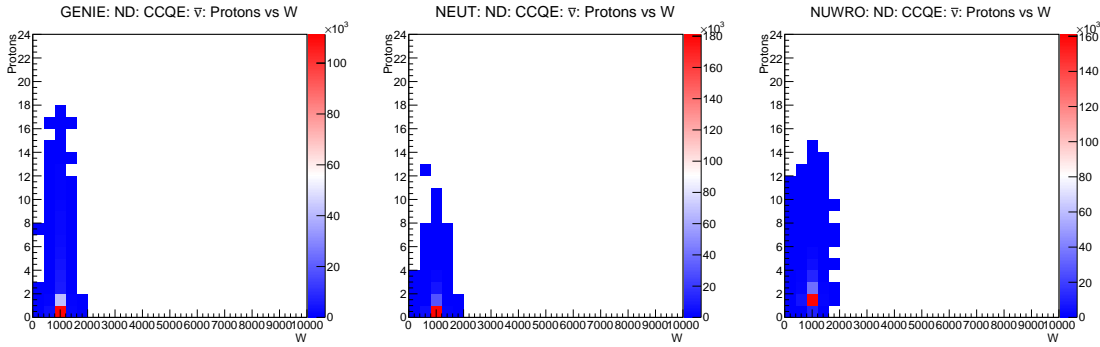
B.2.3 ν CC1 π

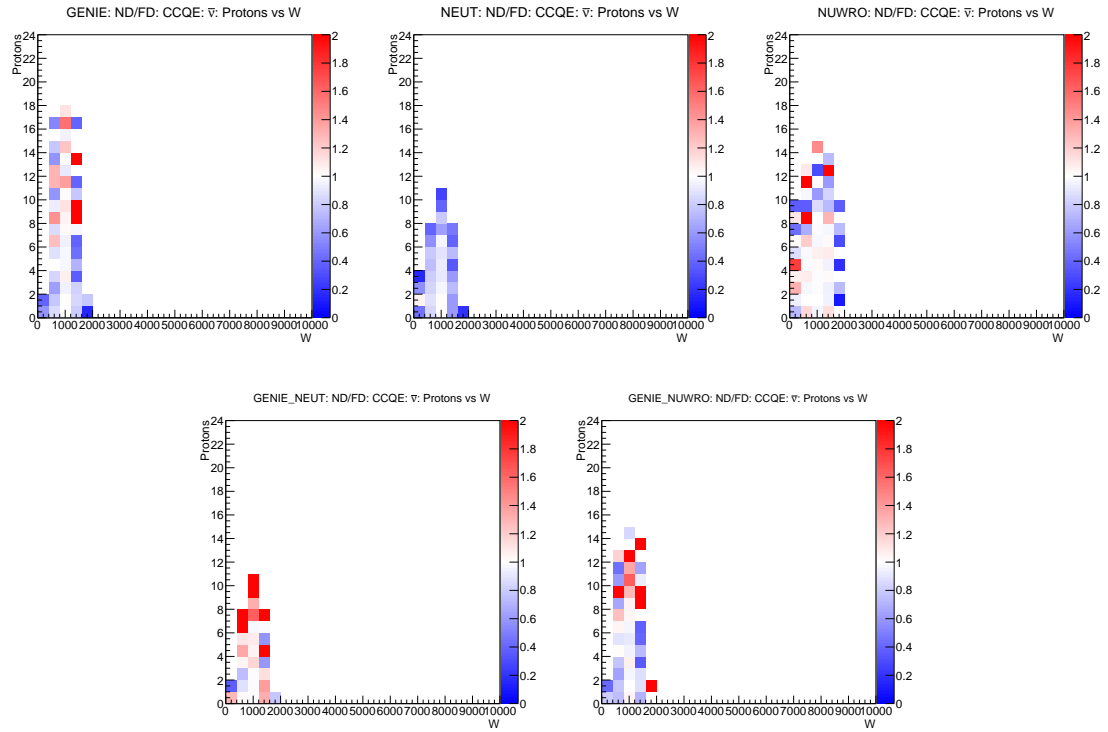


B.2.4 ν CC-Other

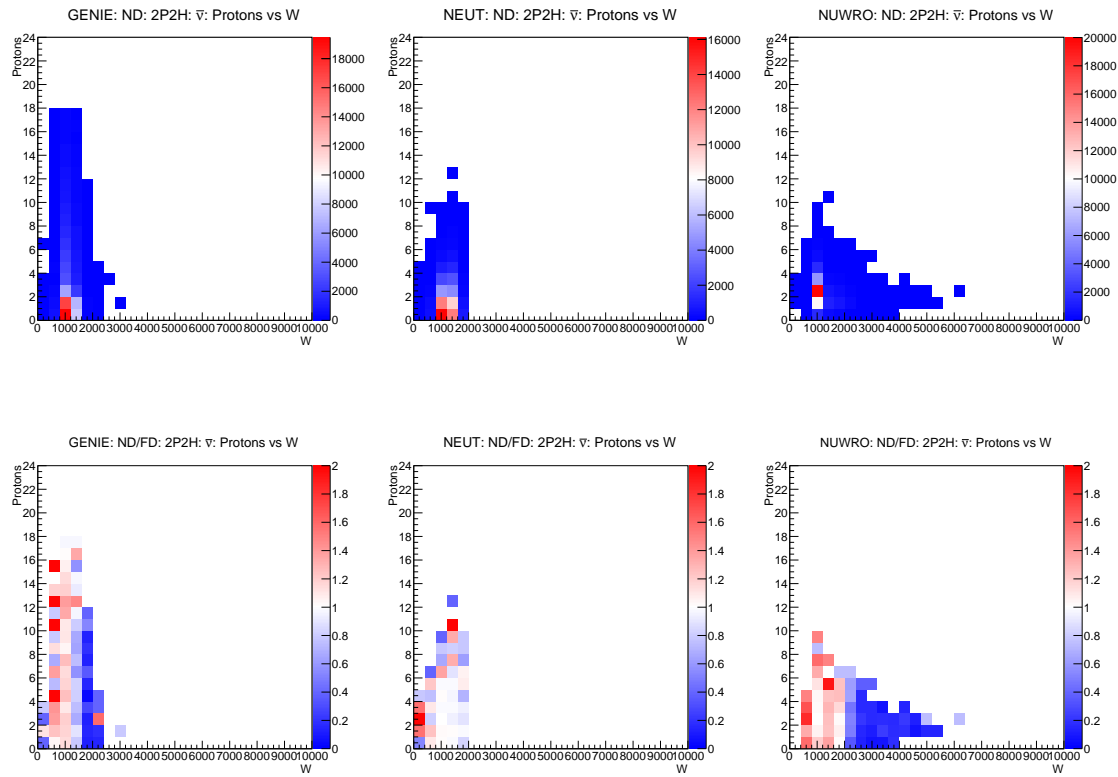


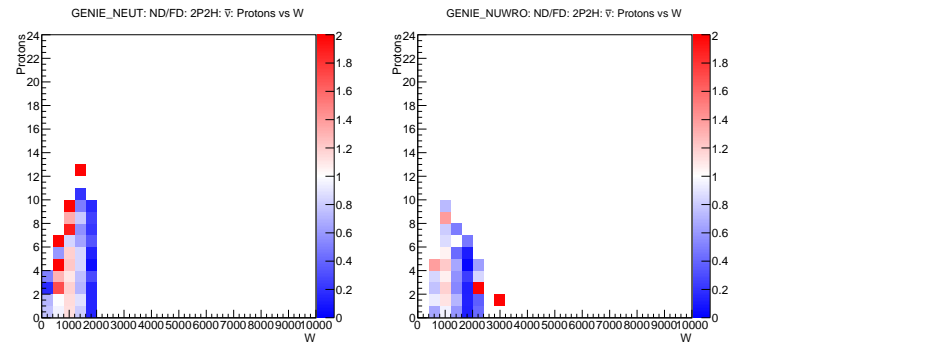
B.2.5 $\bar{\nu}$ CCQE



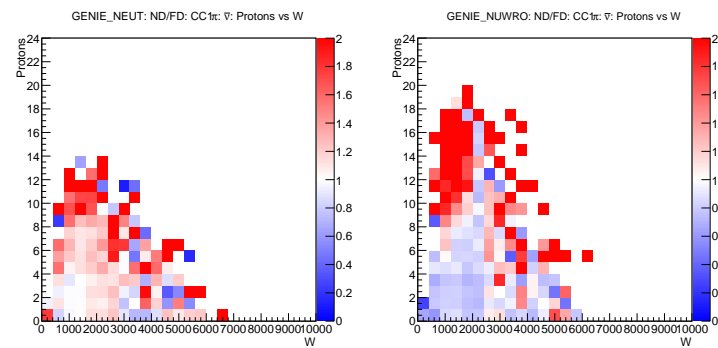
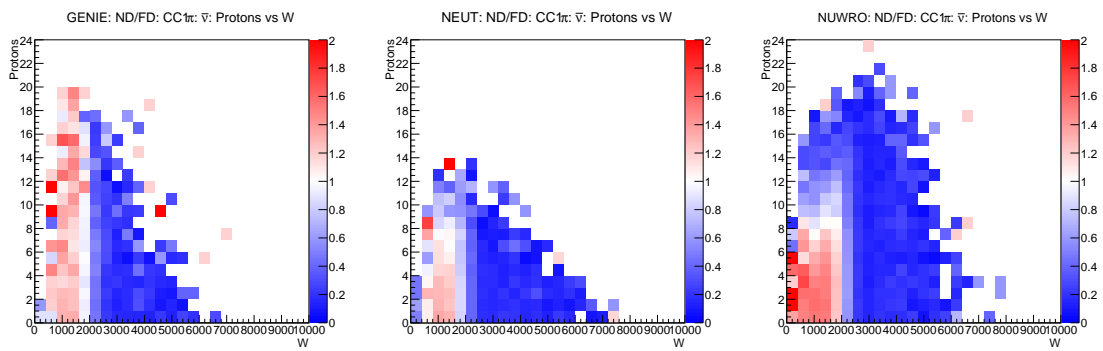
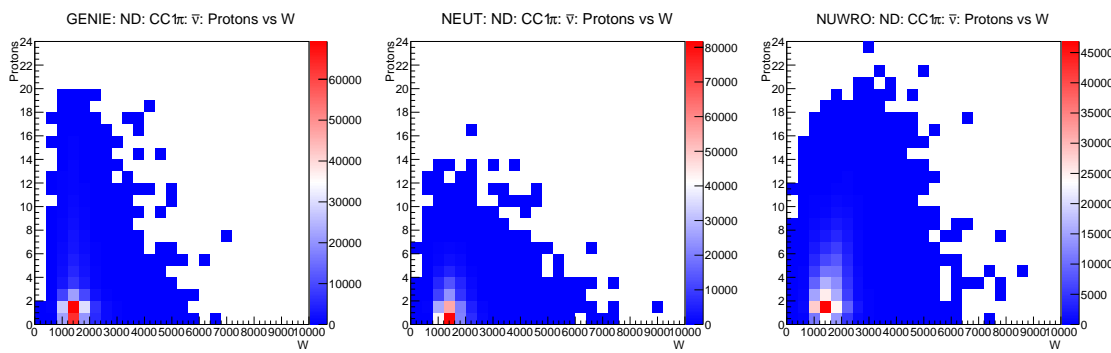


B.2.6 $\bar{\nu}$ 2P2H

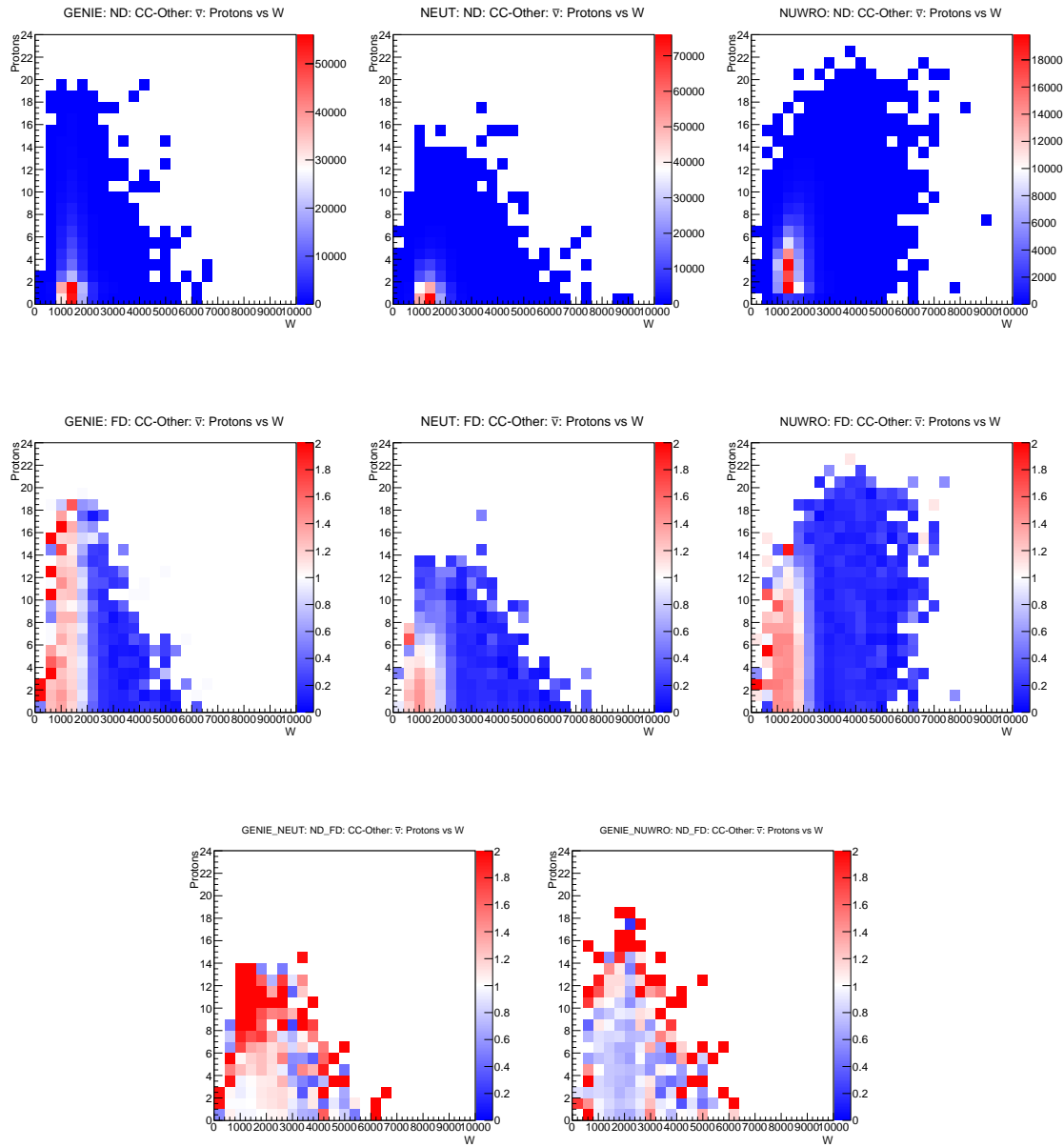




B.2.7 $\bar{\nu}$ CC1 π

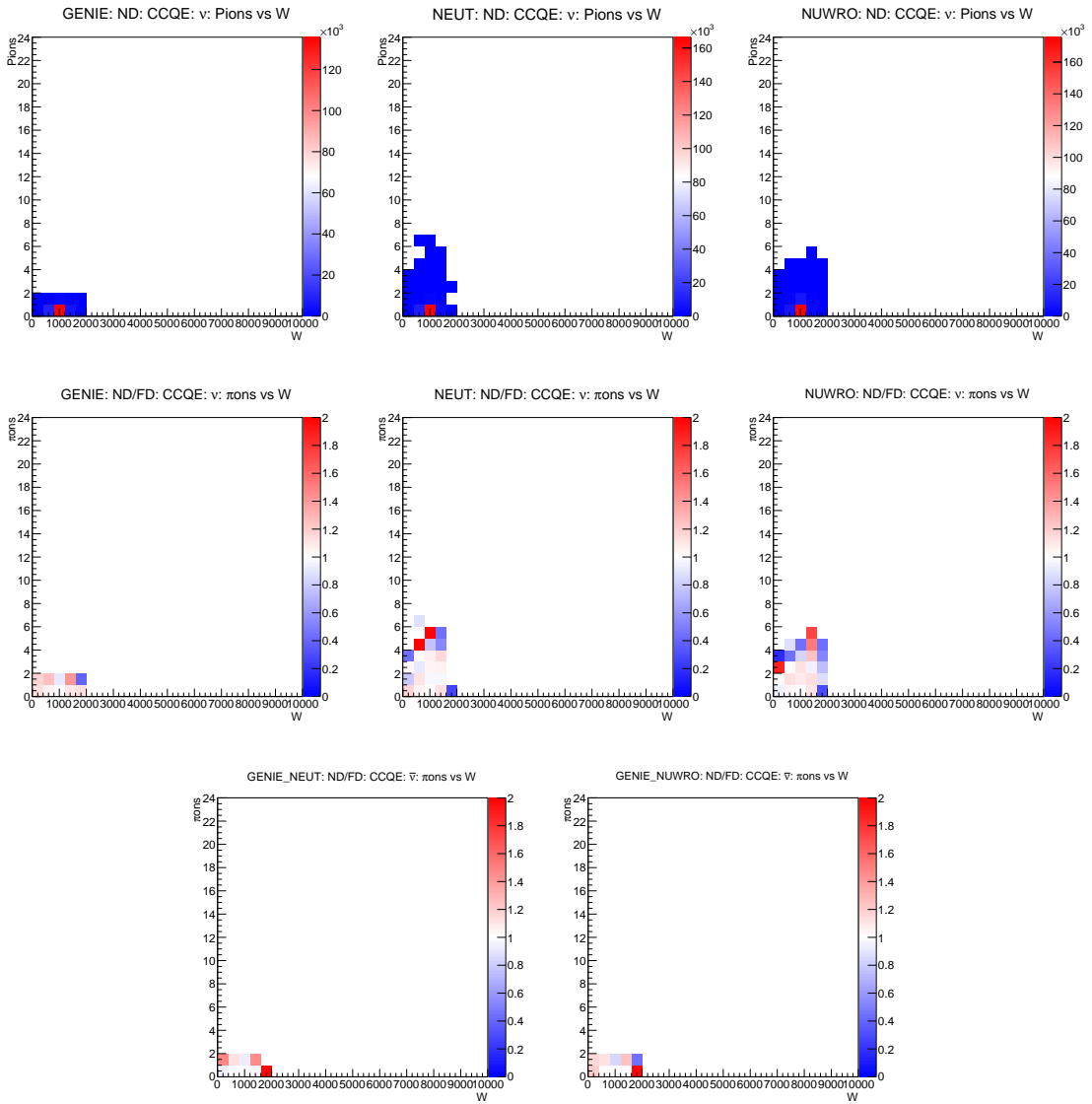


B.2.8 $\bar{\nu}$ CC-Other

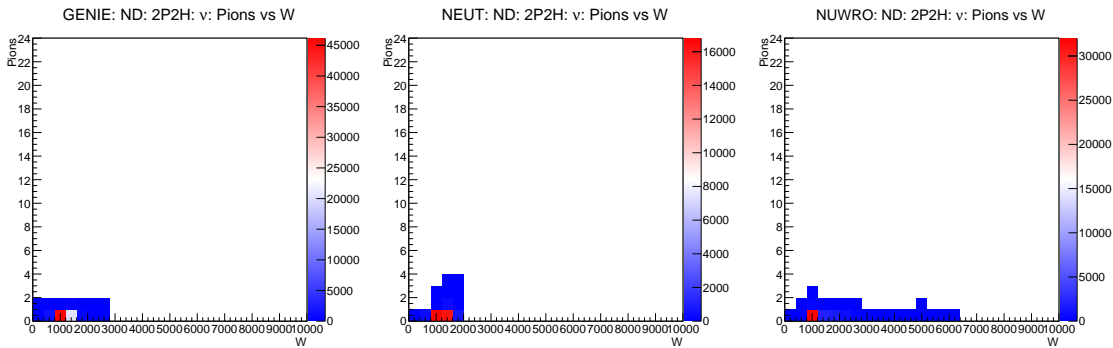


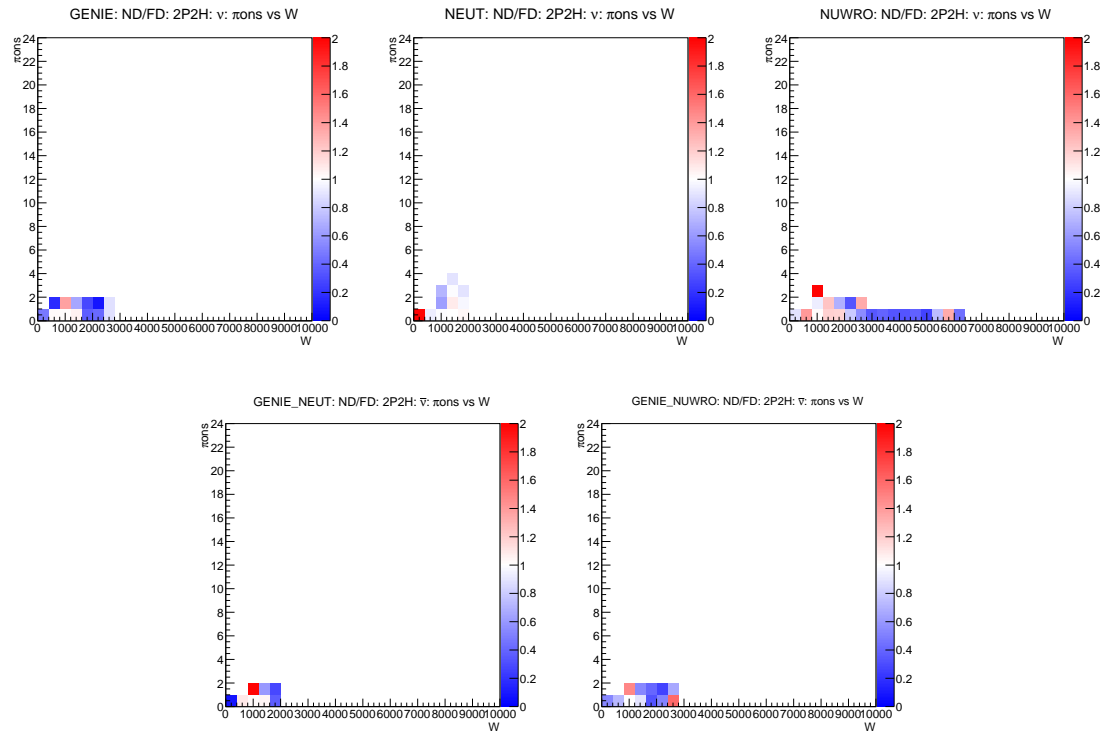
B.3 Pion Multiplicity vs W

B.3.1 ν CCQE

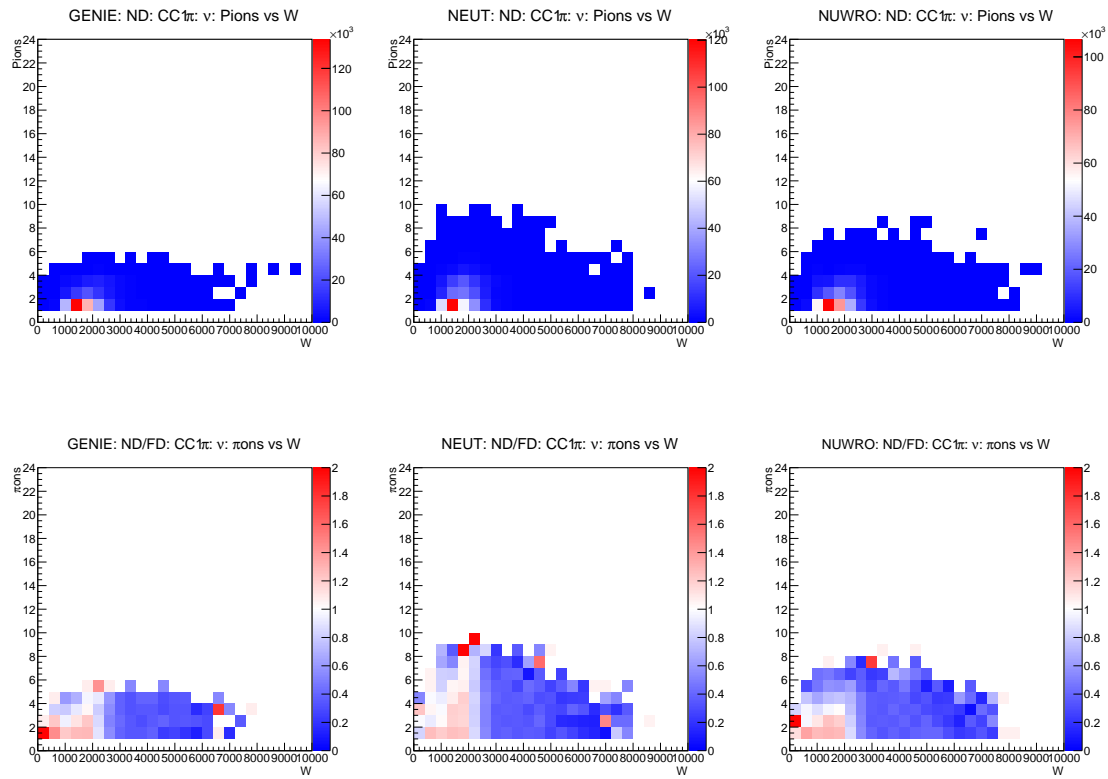


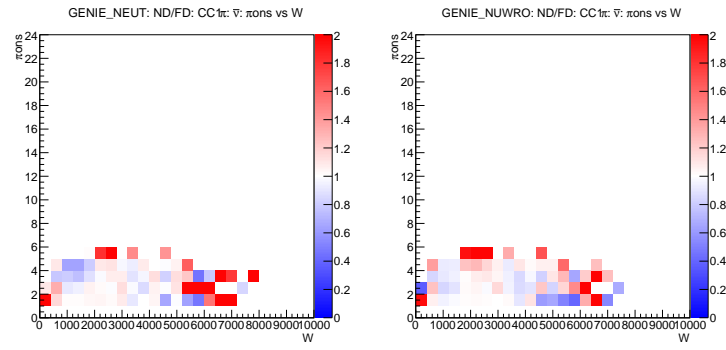
B.3.2 ν 2P2H



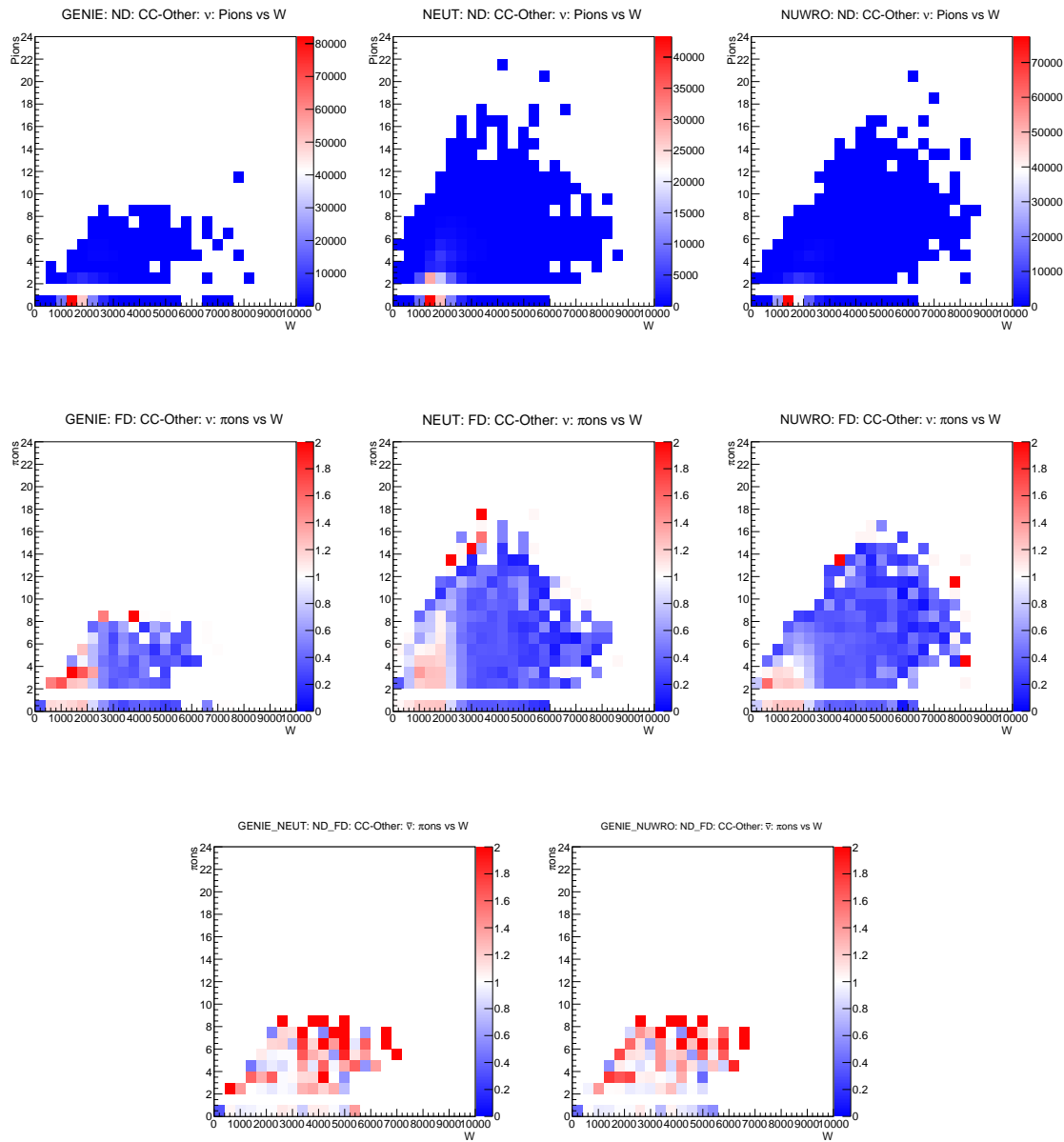


B.3.3 ν CC1 π

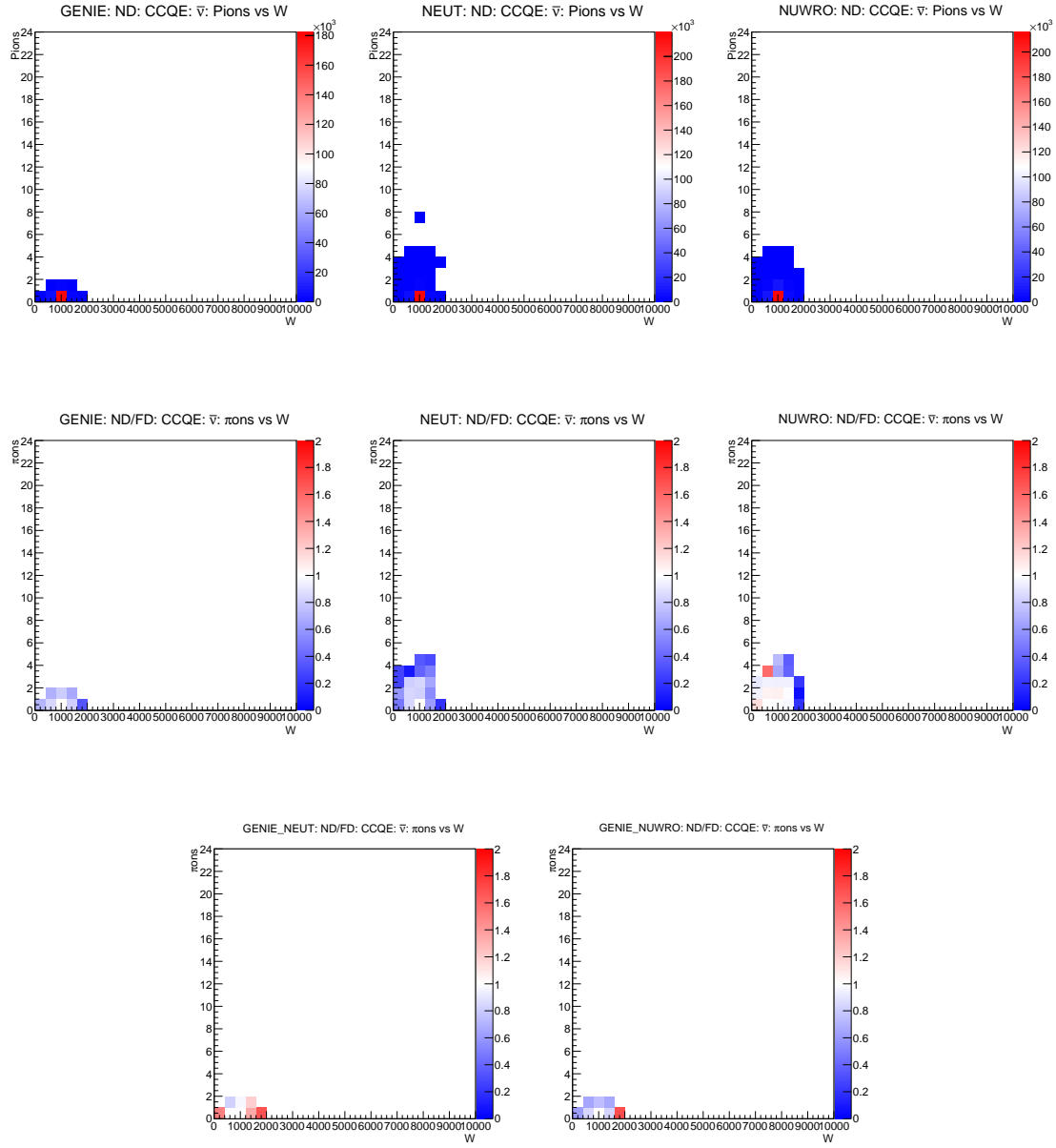




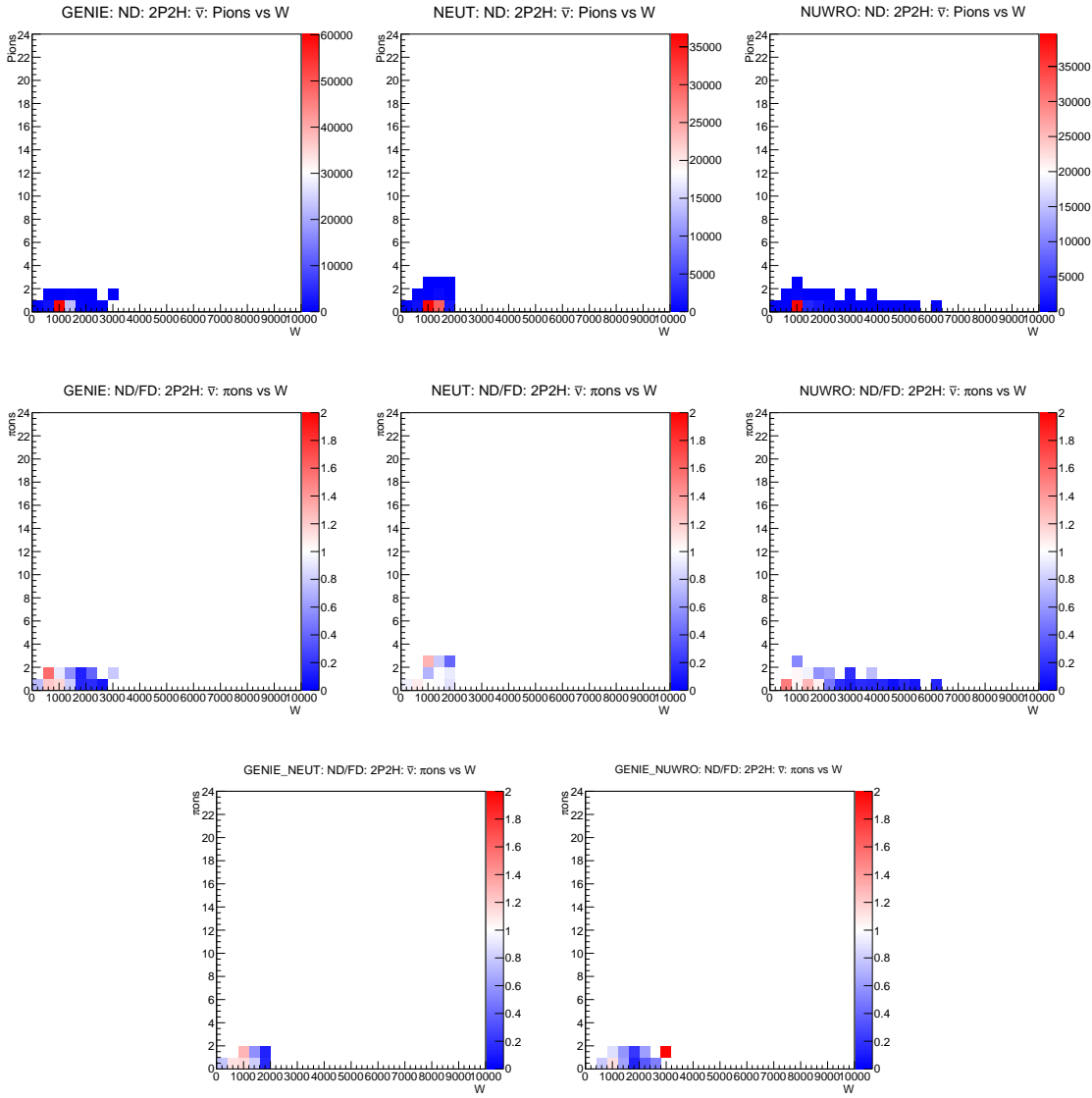
B.3.4 ν CC-Other



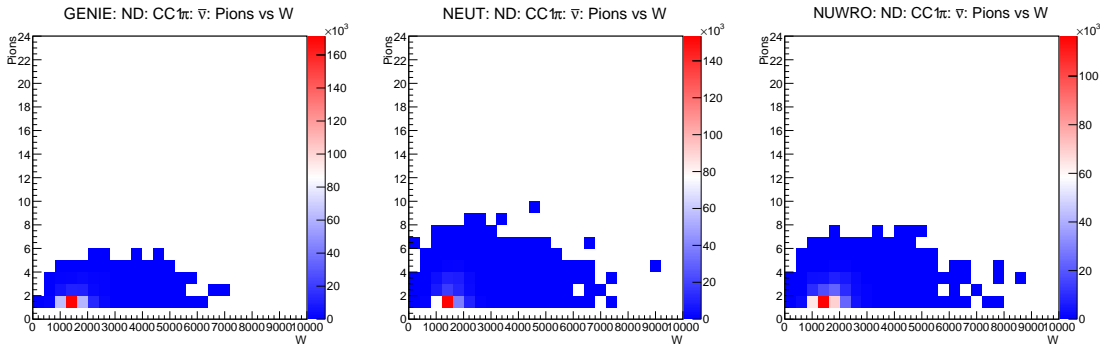
B.3.5 $\bar{\nu}$ CCQE

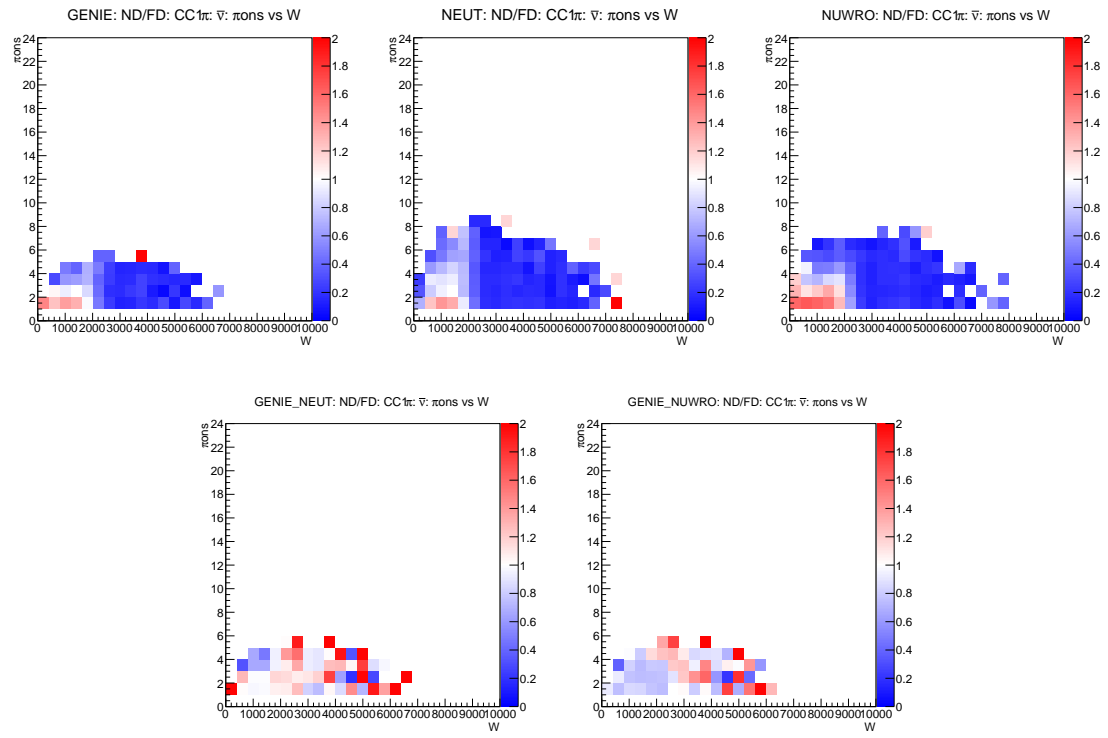


B.3.6 $\bar{\nu}$ 2P2H

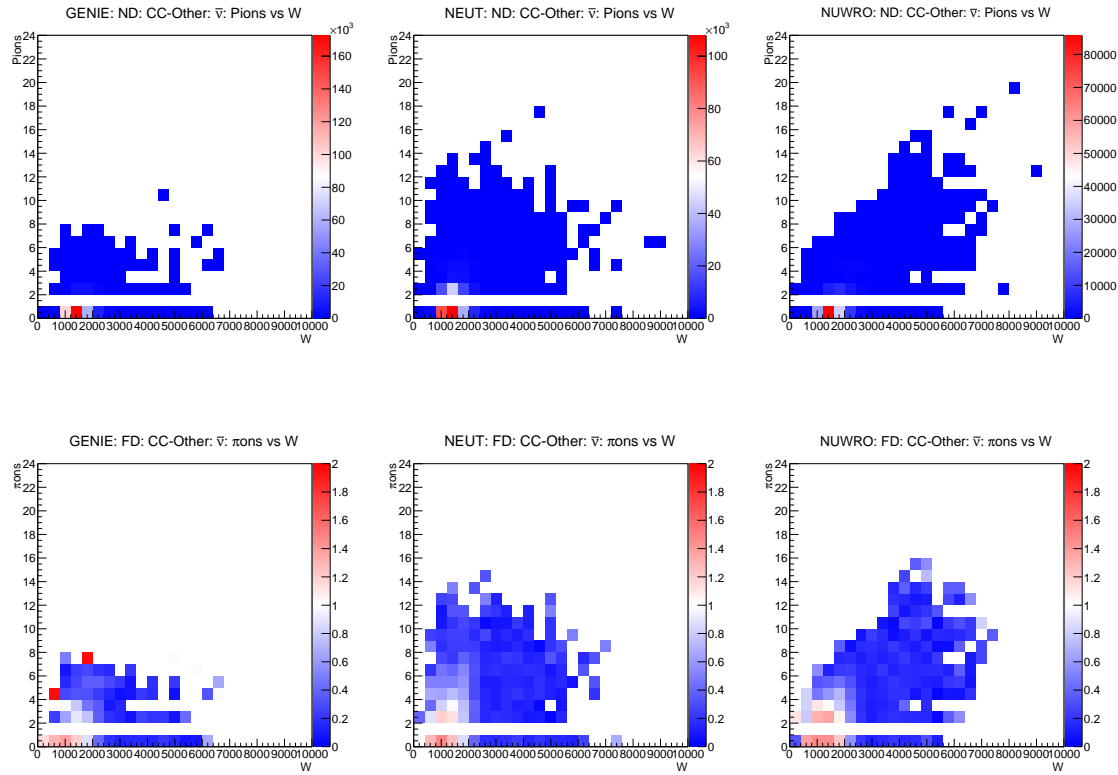


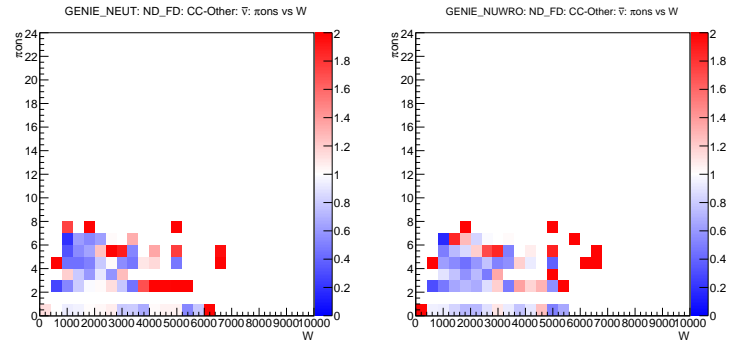
B.3.7 $\bar{\nu}$ CC1 π





B.3.8 $\bar{\nu}$ CC-Other

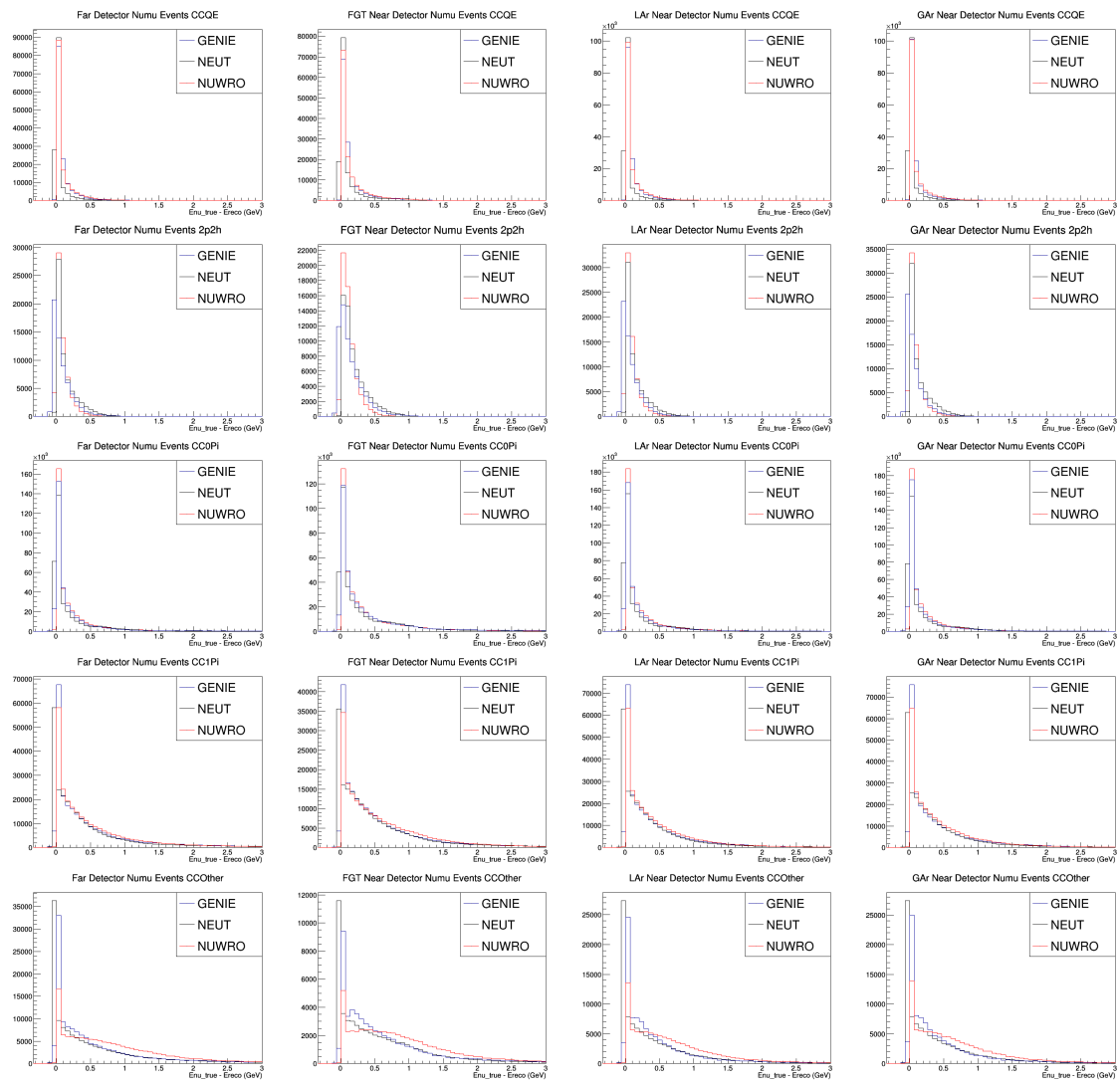




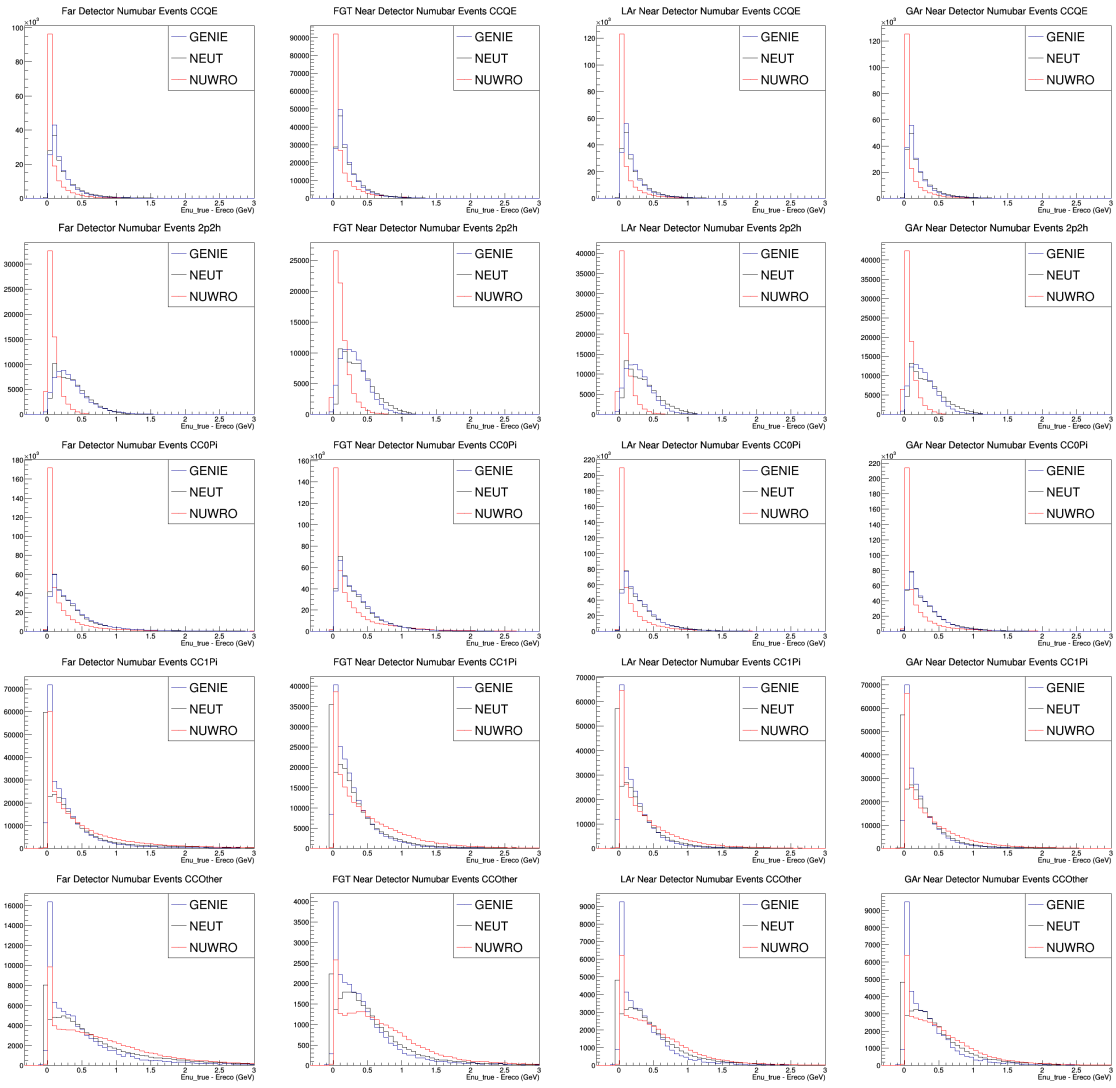
C Etrue - Ereco Plots

This appendix includes all the plots not shown in Section 3.1. For full description of the files, please make reference to that section. The plots will be put in the same order as before.

C.1 numu



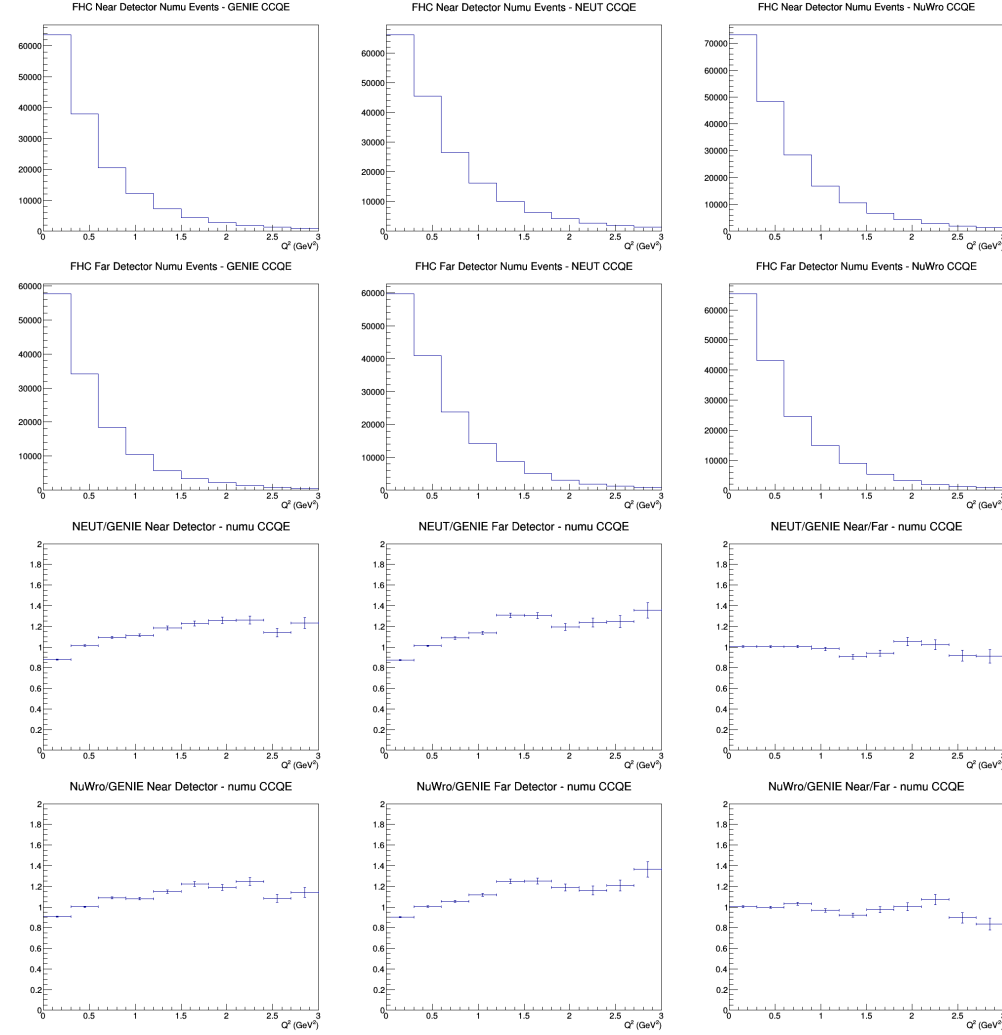
C.2 numubar



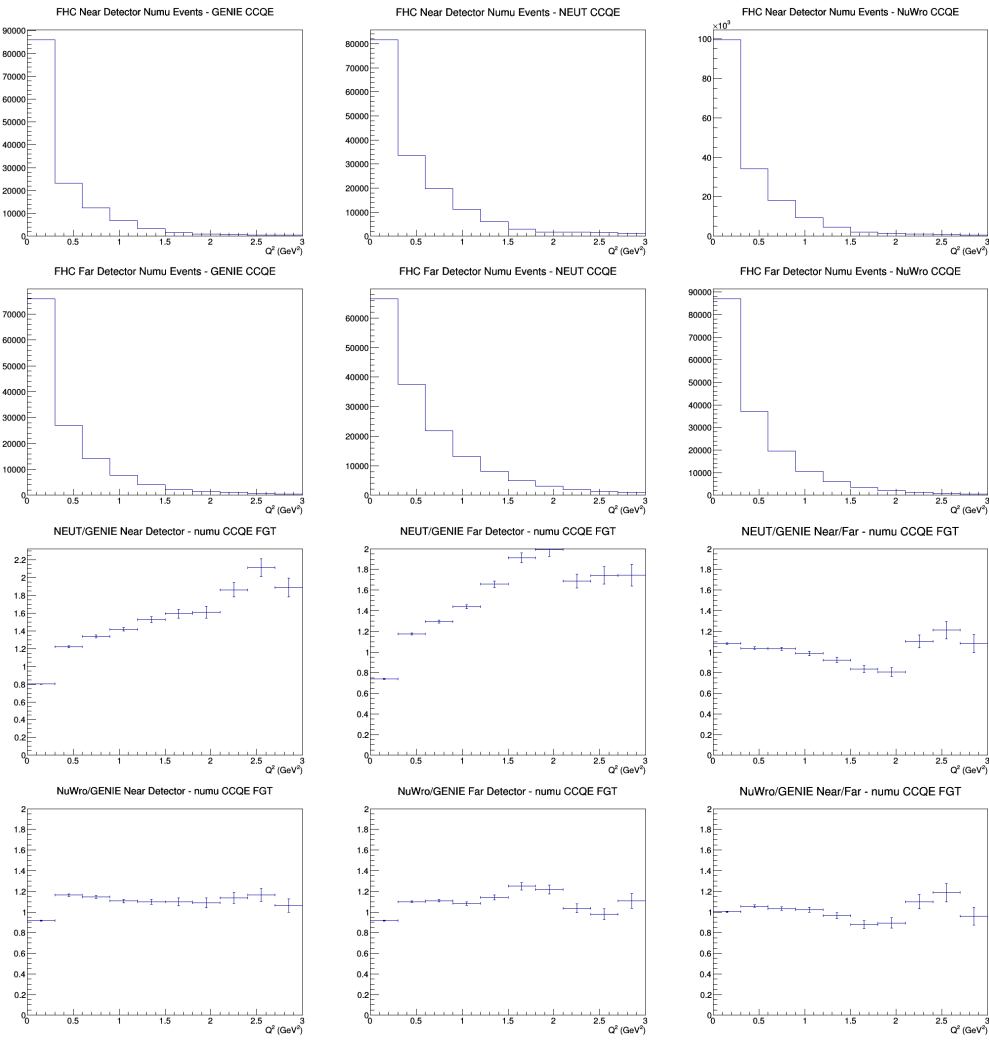
D Q^2 Plots

This appendix includes all the plots not show in Section 4.1. For full description of the files, please make reference to that section. The plots will be put in the same order as before.

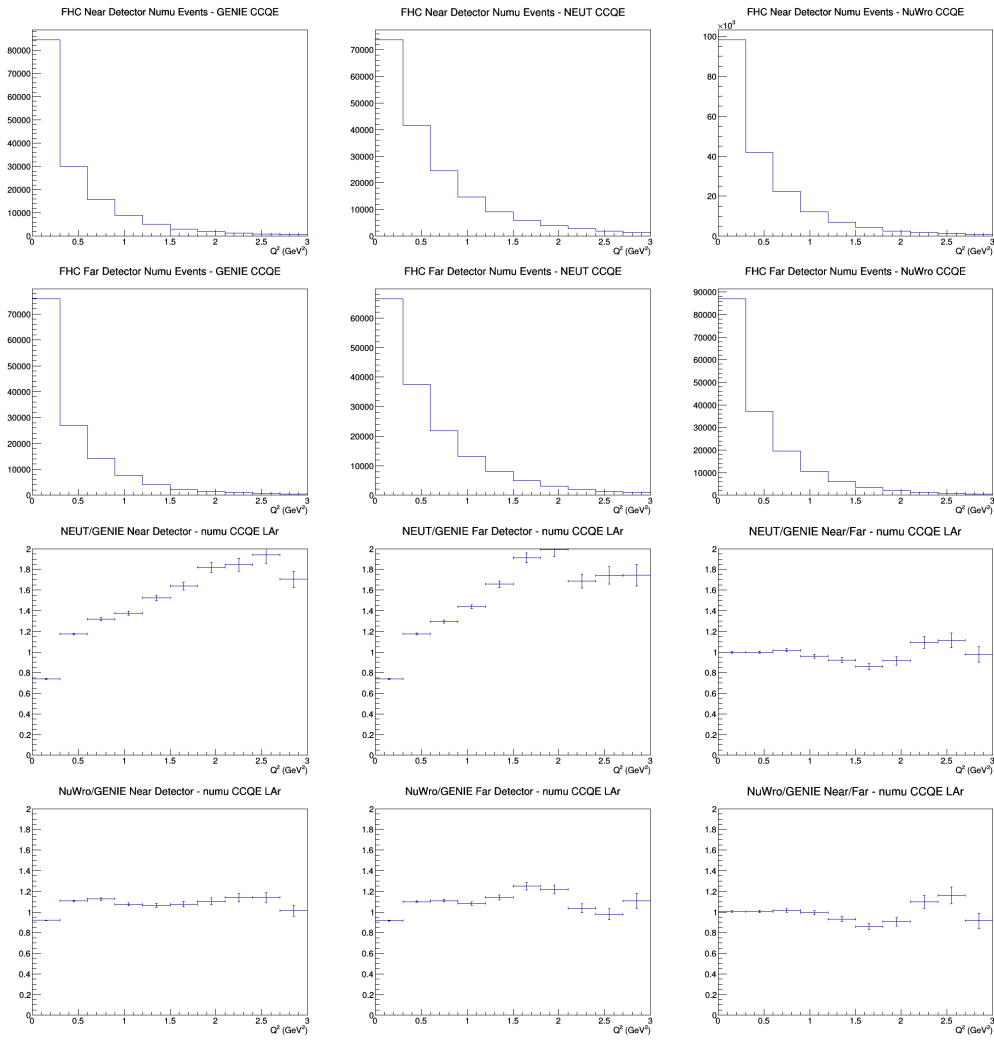
D.1 numu CCQE no efficiencies



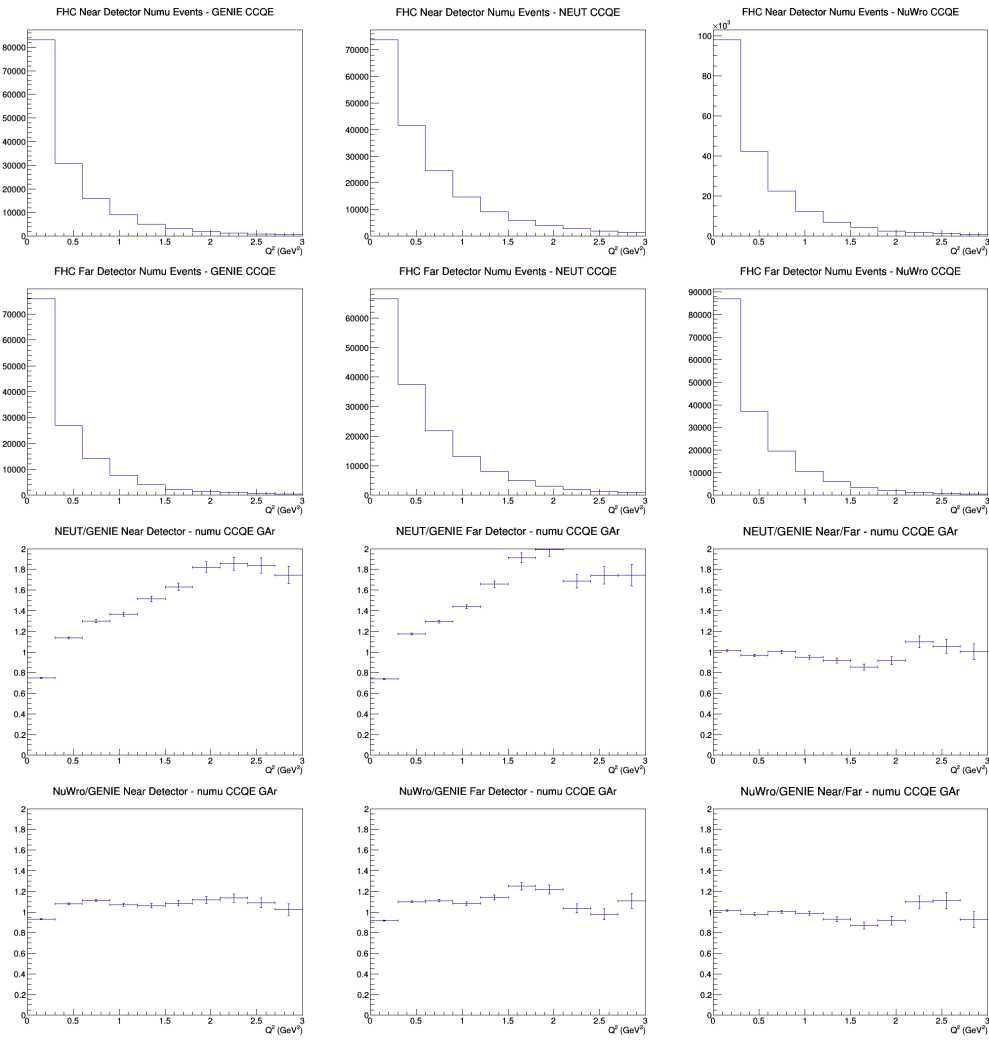
D.2 numu CCQE FGT efficiencies



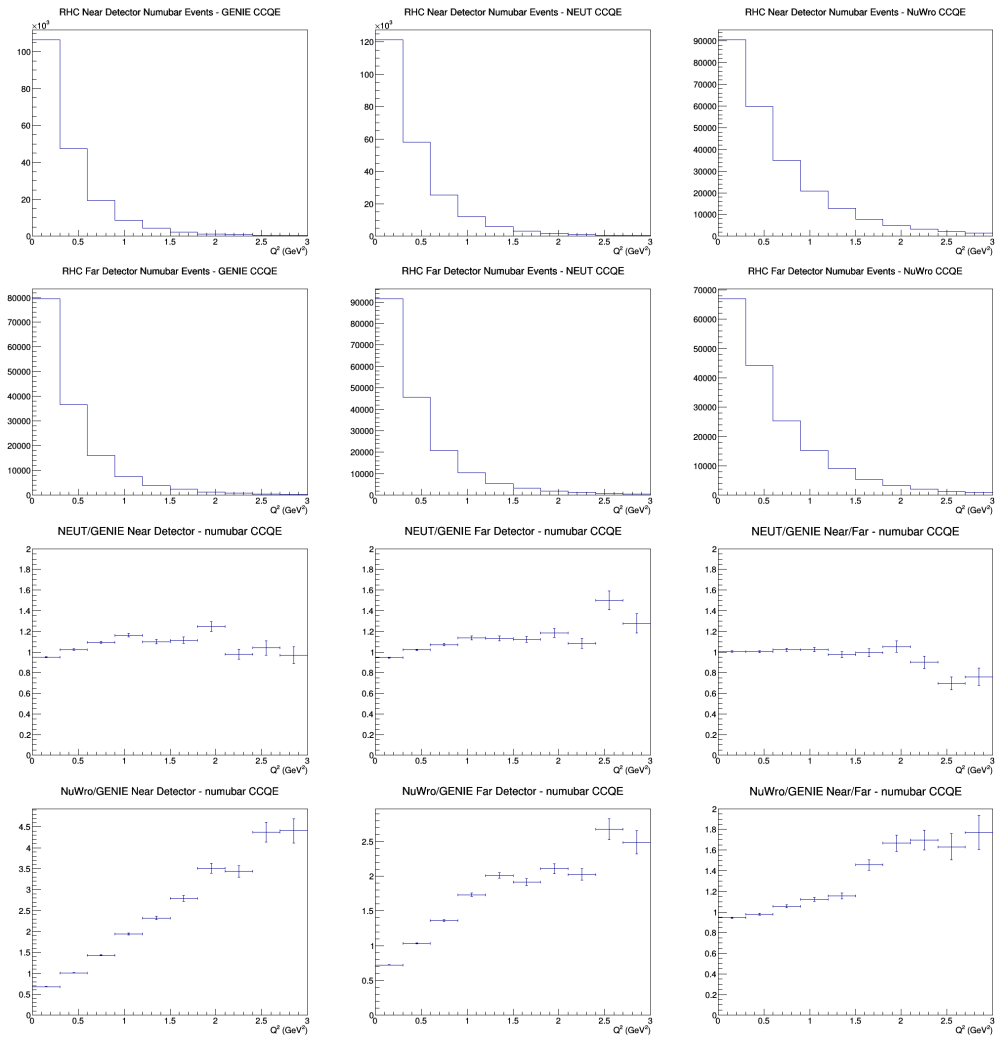
D.3 numu CCQE LAr efficiencies



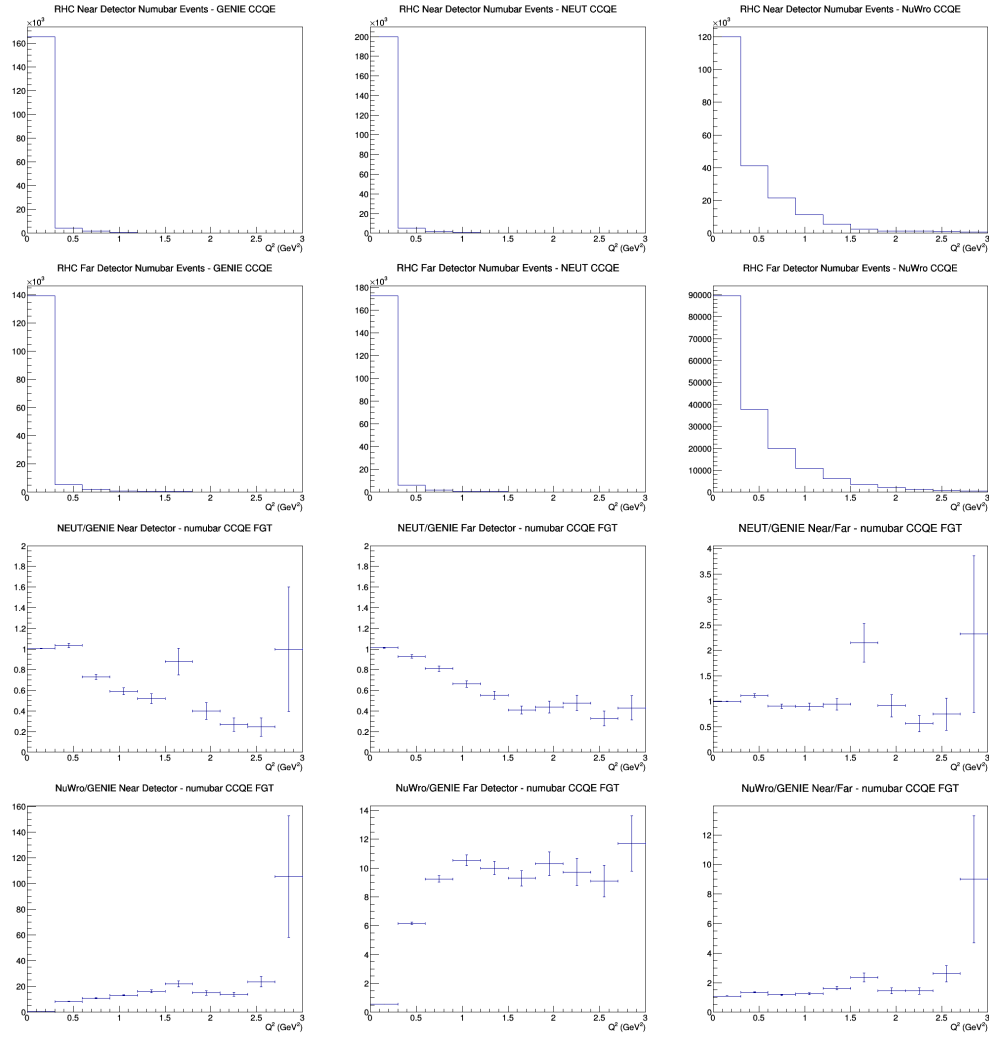
D.4 numu CCQE GAr efficiencies



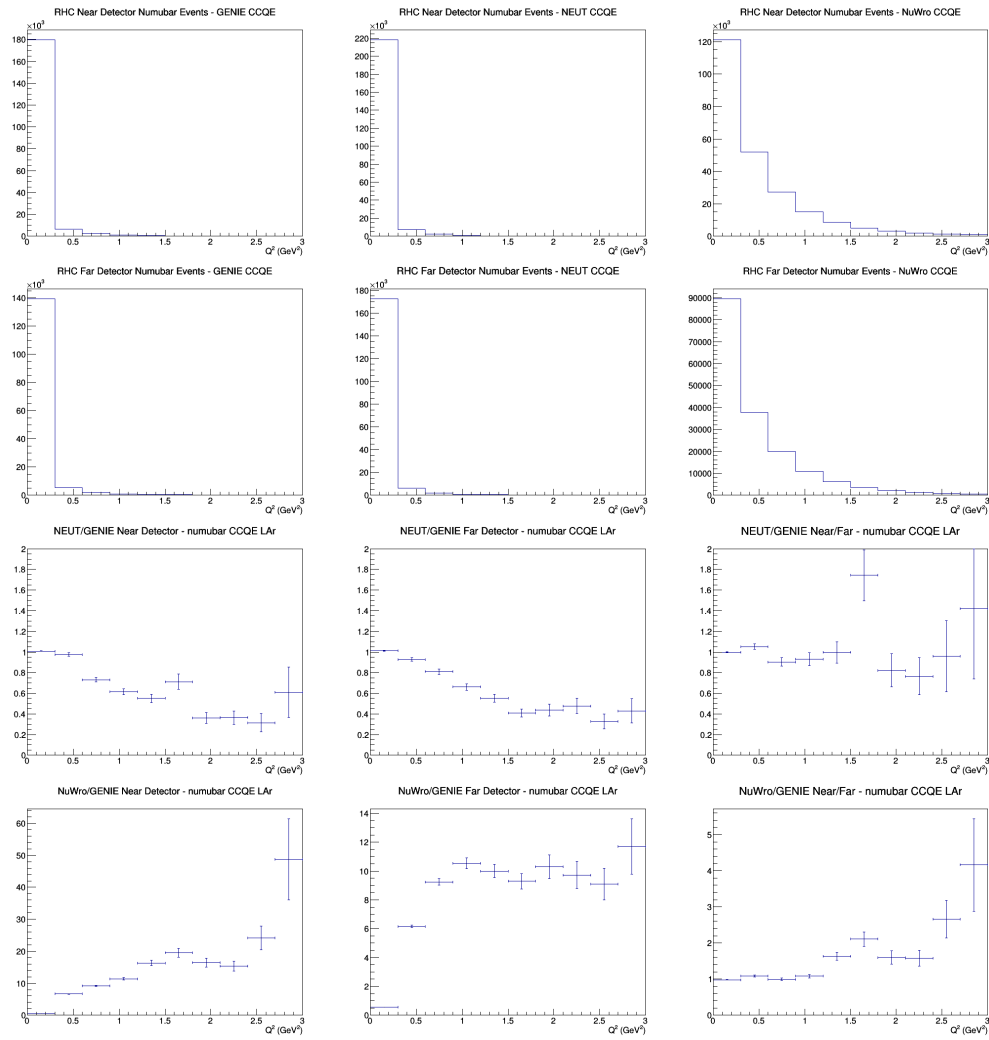
D.5 numubar CCQE no efficiencies



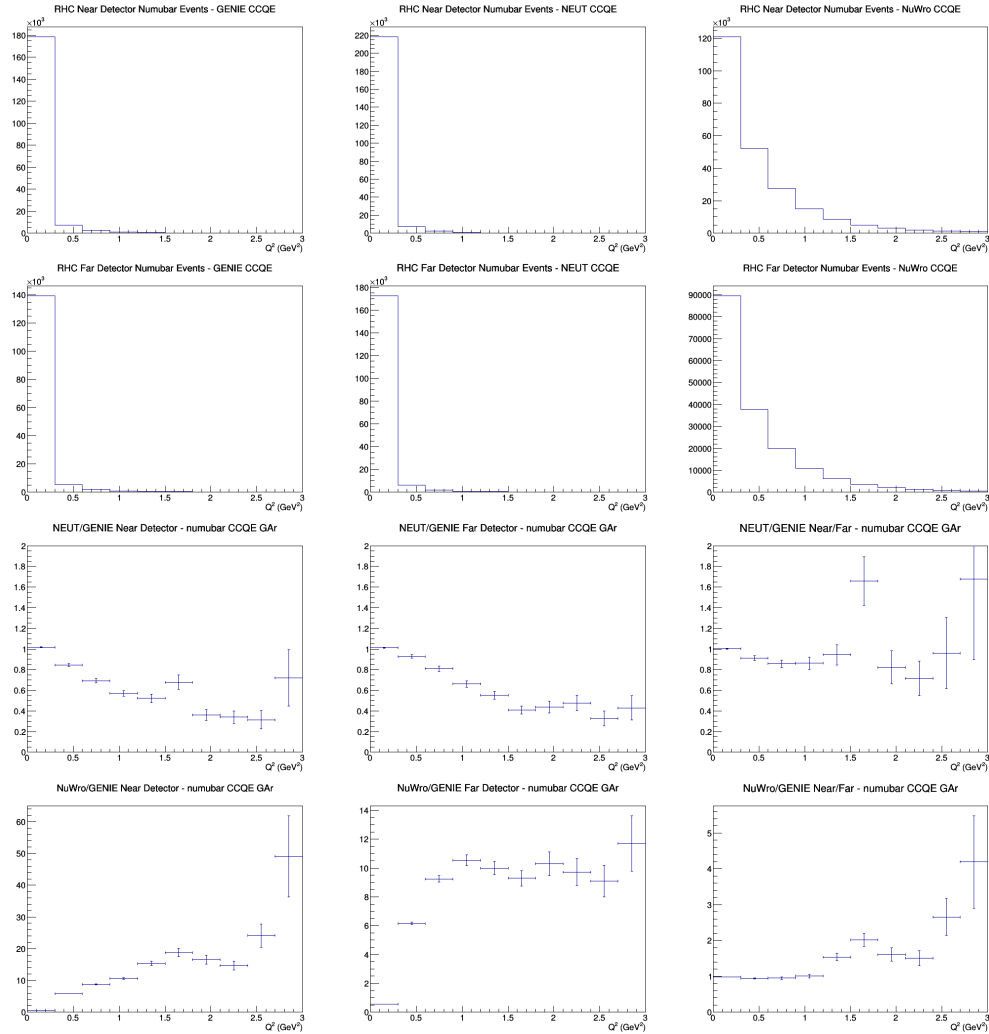
D.6 numubar CCQE FGT efficiencies



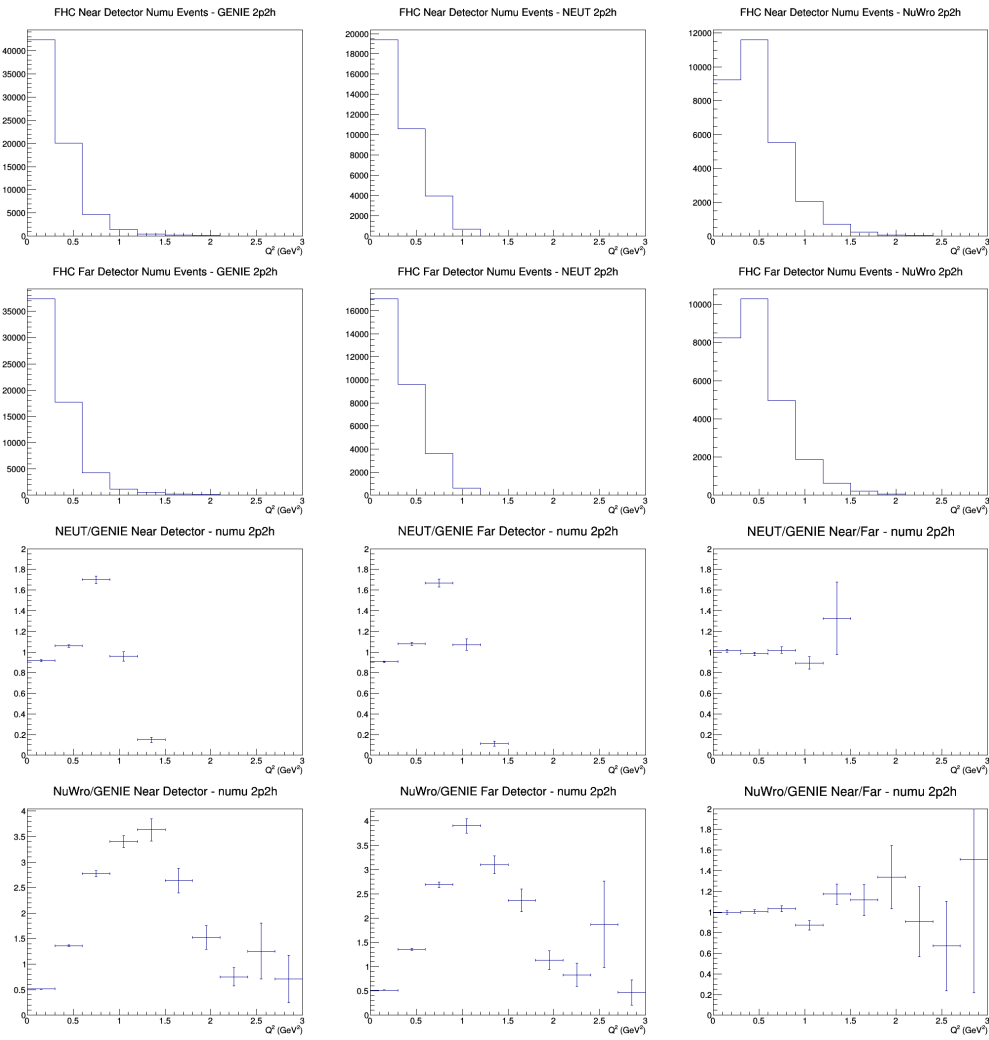
D.7 numubar CCQE LAr efficiencies



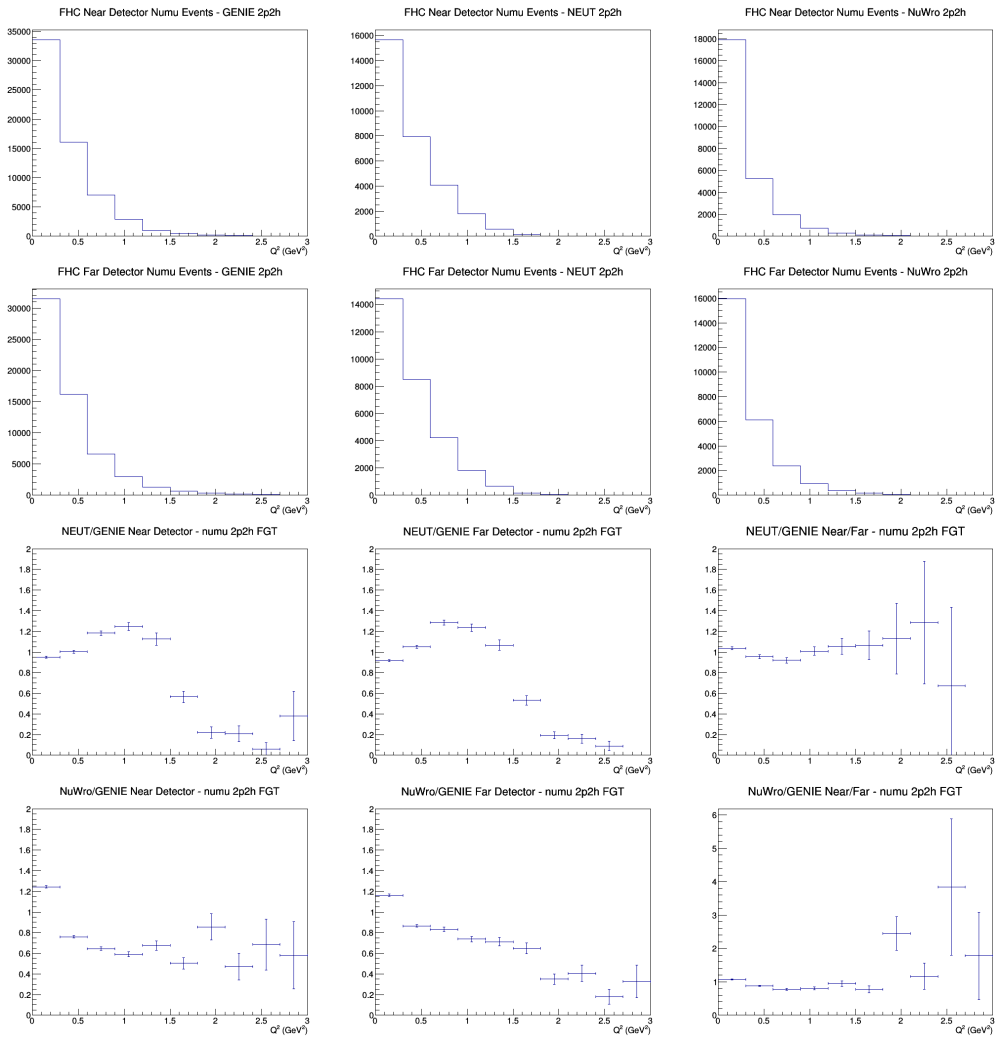
D.8 numubar CCQE GAr efficiencies



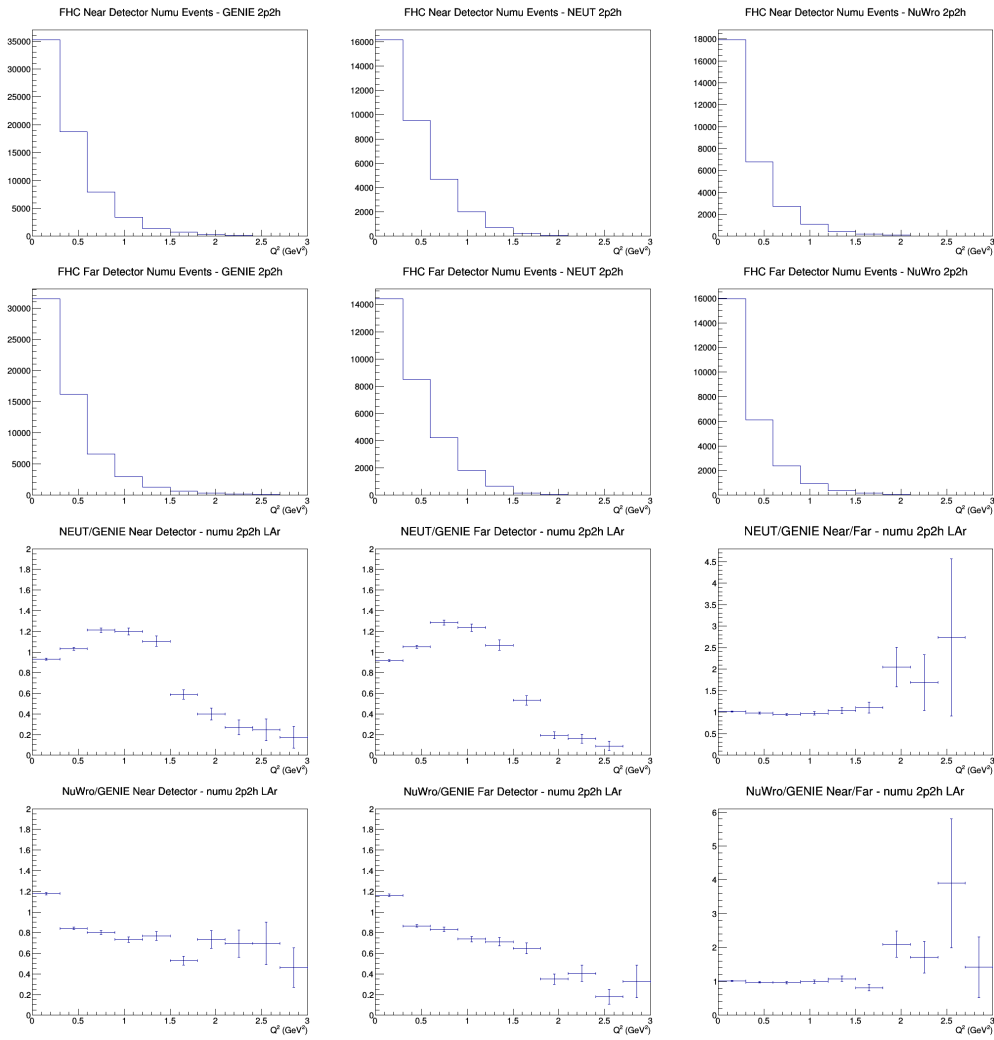
D.9 numu 2p2h no efficiencies



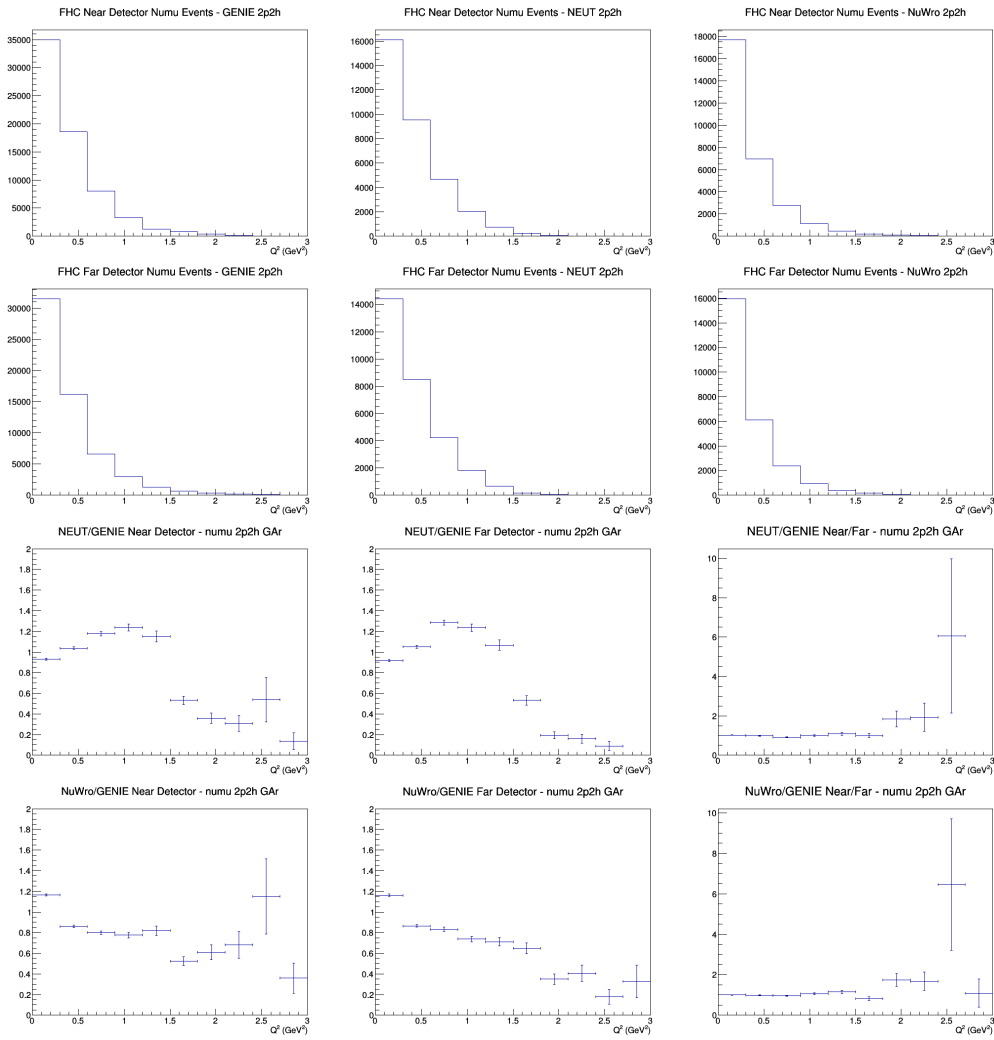
D.10 numu 2p2h FGT efficiencies



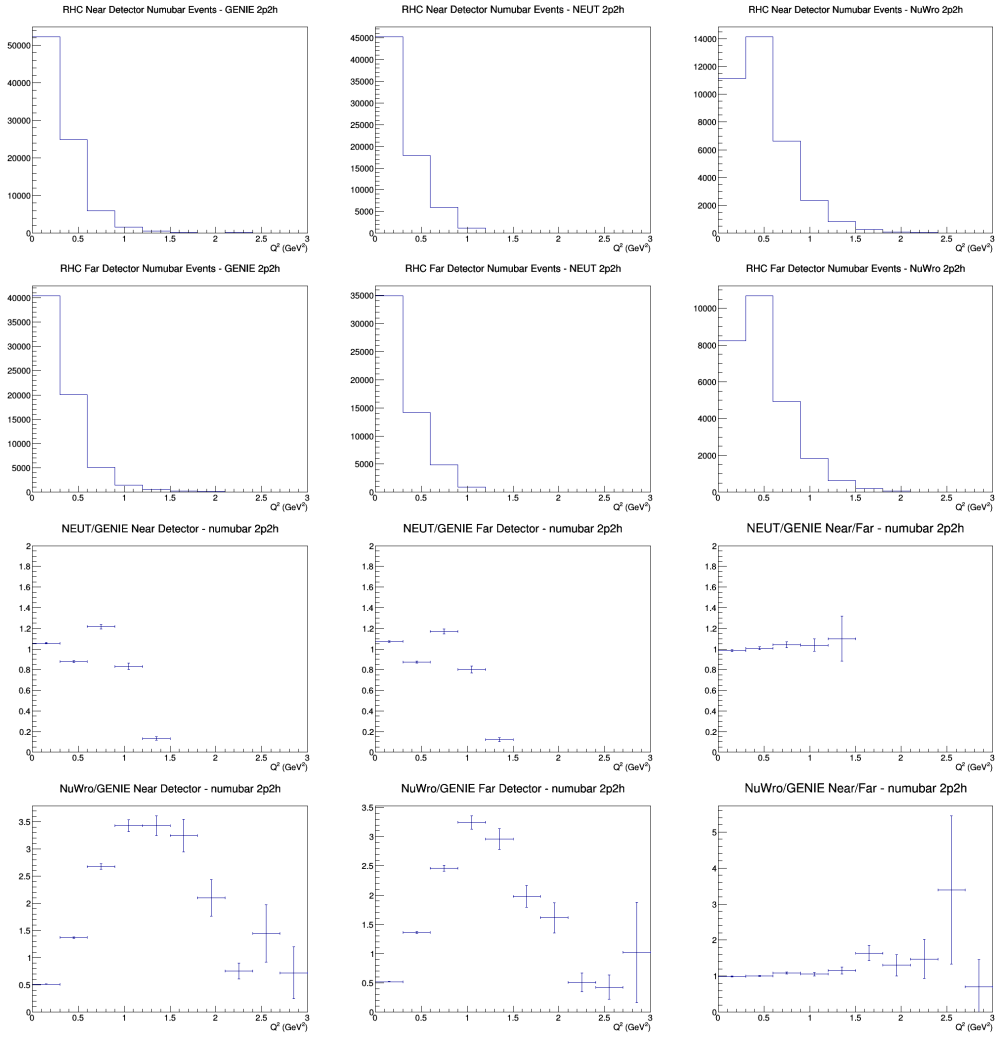
D.11 numu 2p2h LAr efficiencies



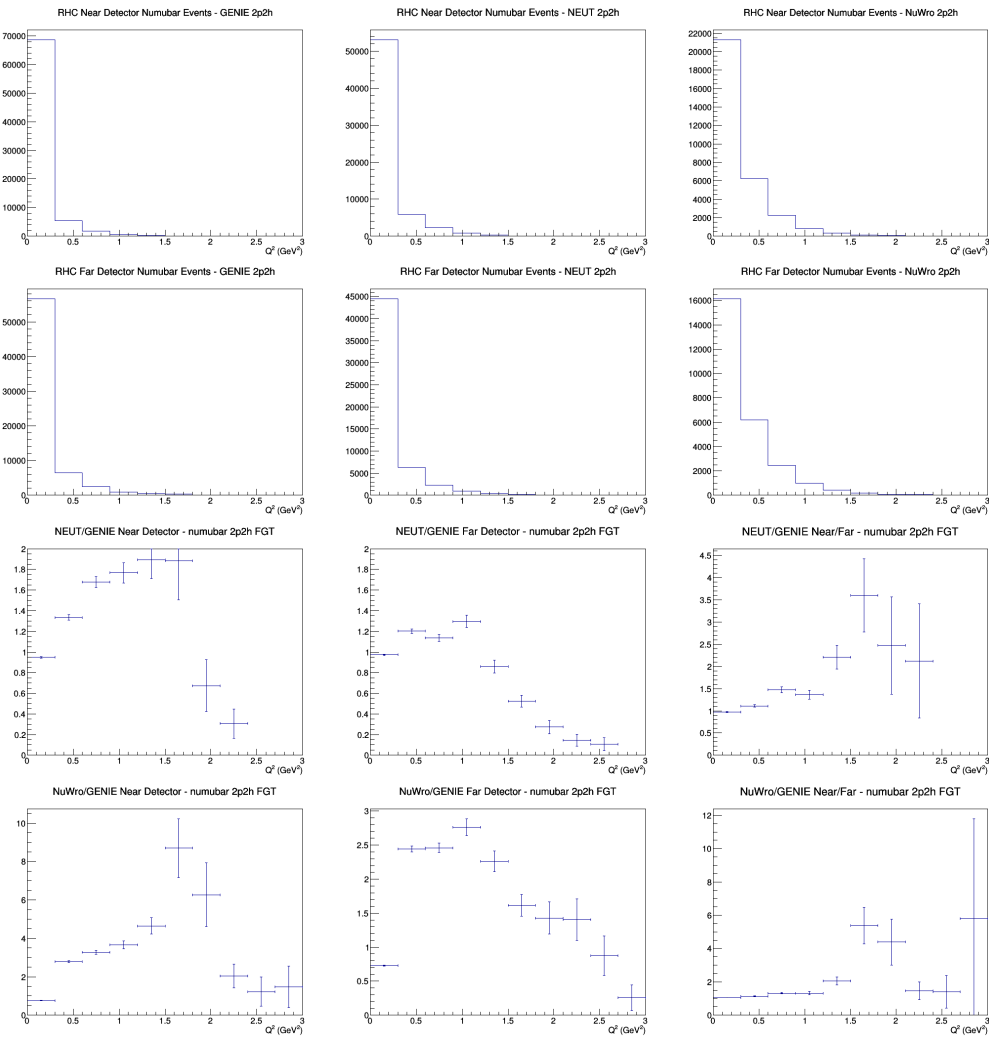
D.12 numu 2p2h GAr efficiencies



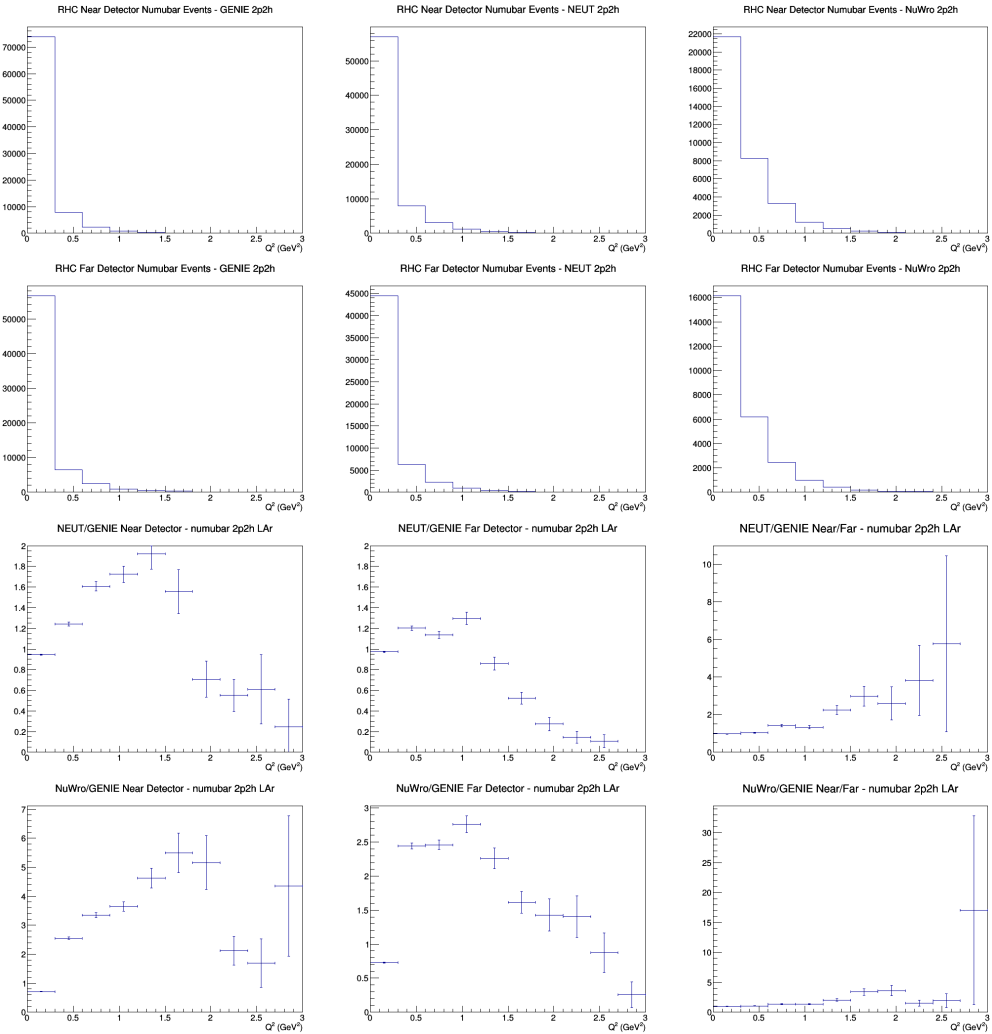
D.13 numubar 2p2h no efficiencies



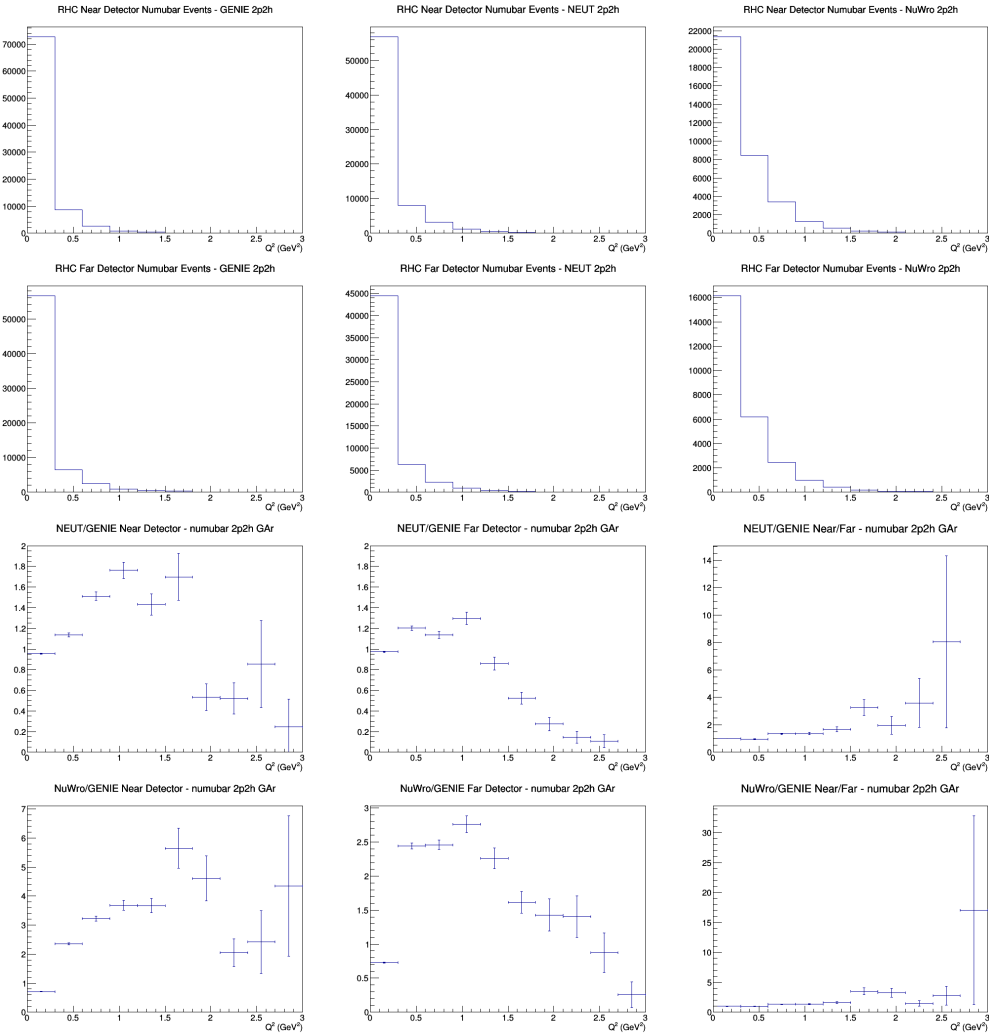
D.14 numubar 2p2h FGT efficiencies



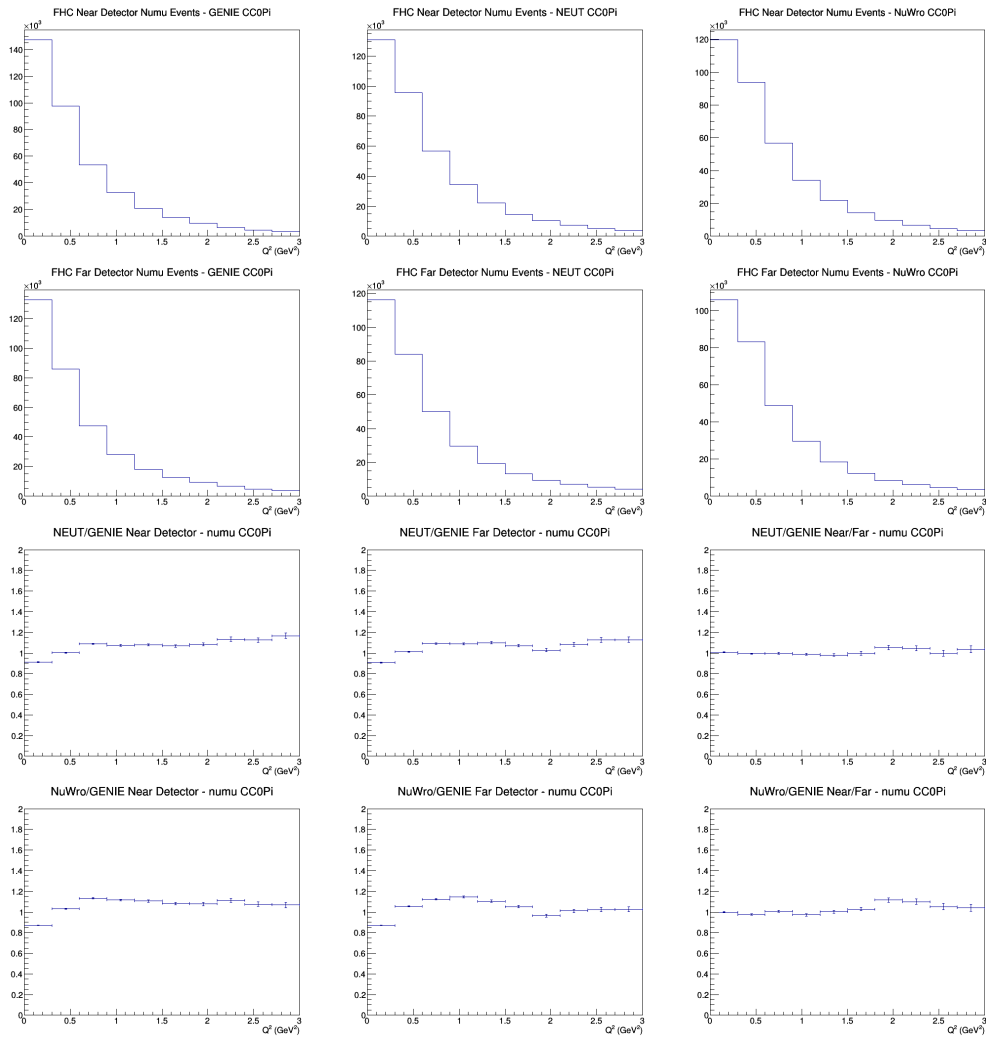
D.15 numubar 2p2h LAr efficiencies



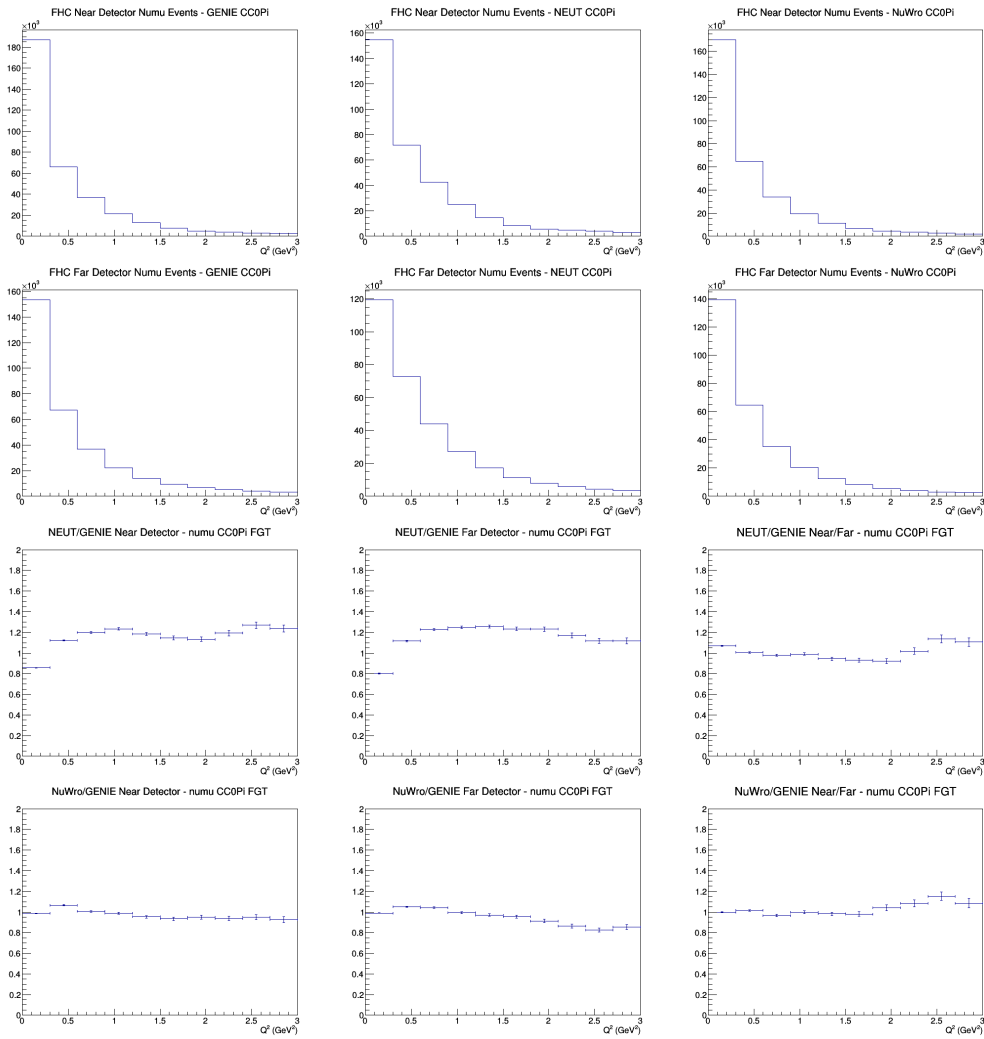
D.16 numubar 2p2h GAr efficiencies



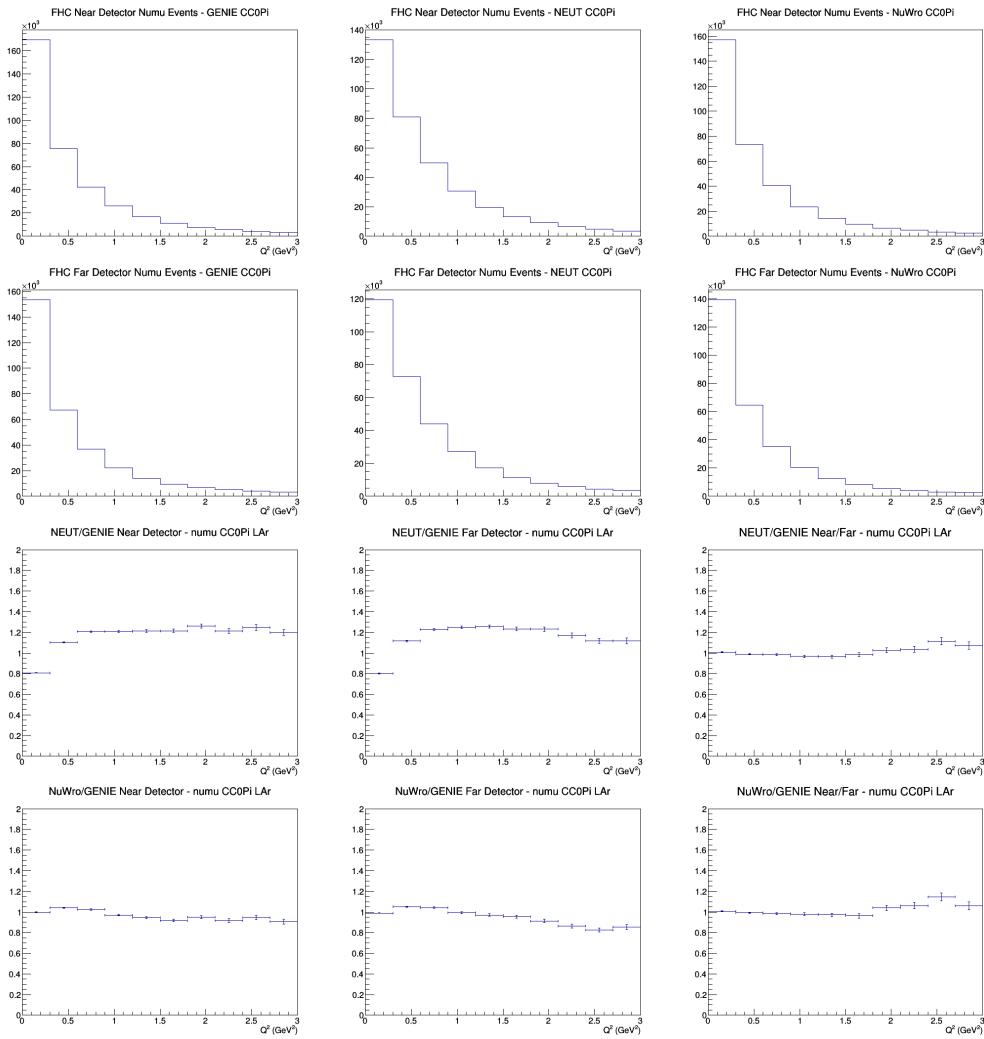
D.17 numu CC0Pi no efficiencies



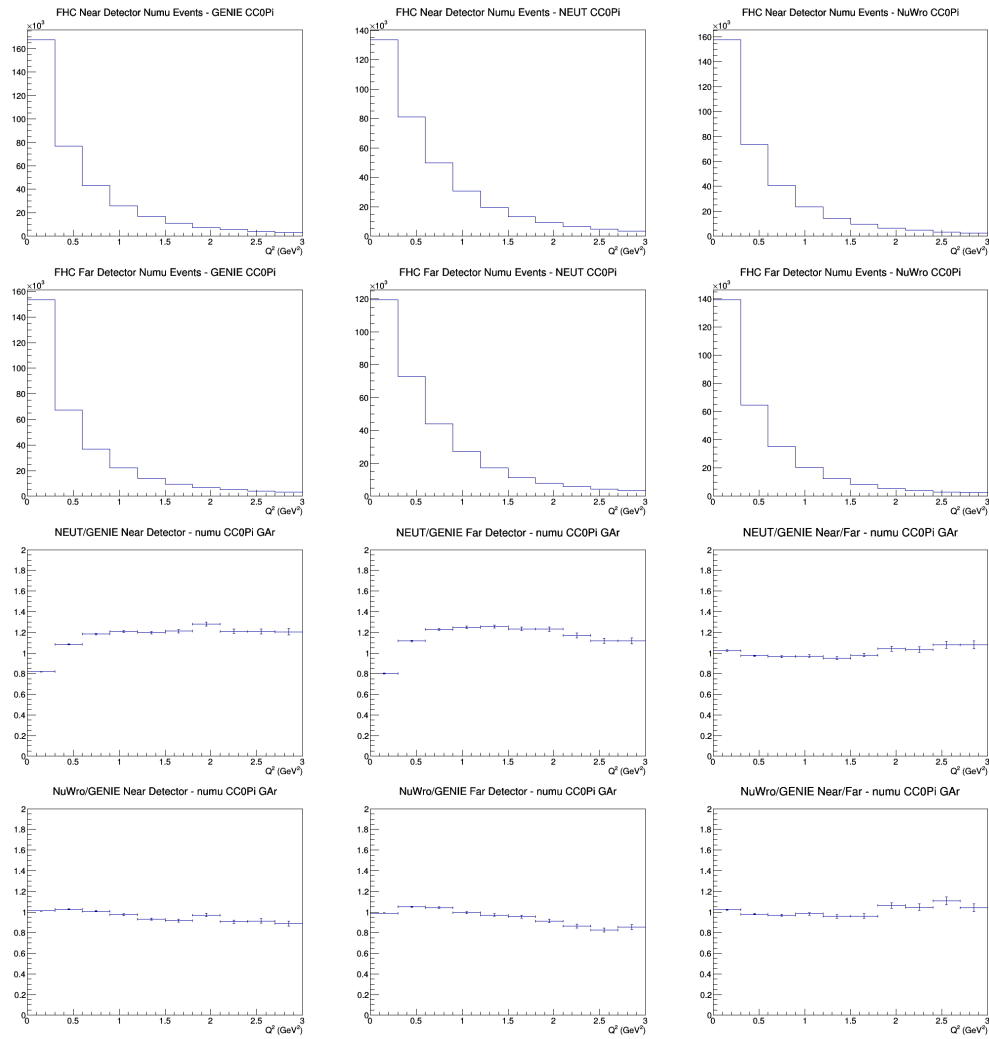
D.18 numu CC0Pi FGT efficiencies



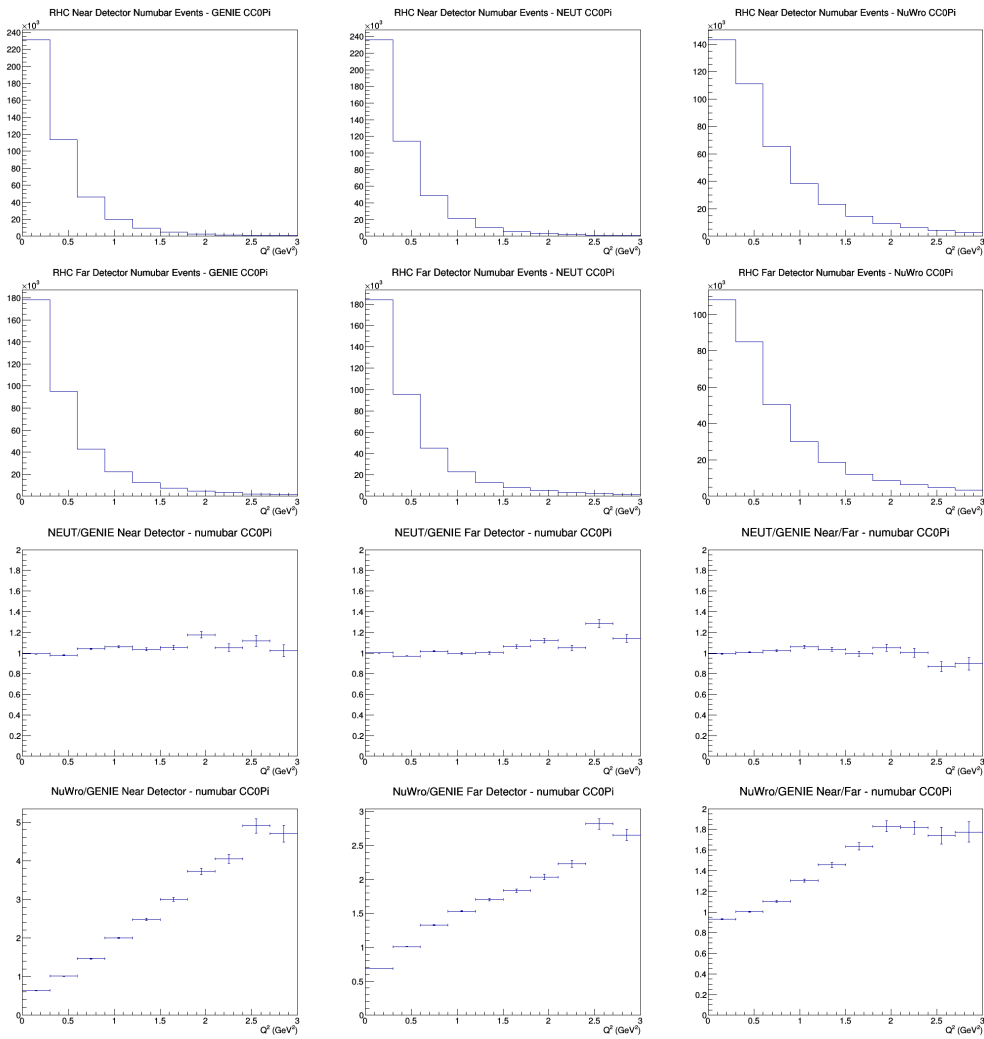
D.19 numu CC0Pi LAr efficiencies



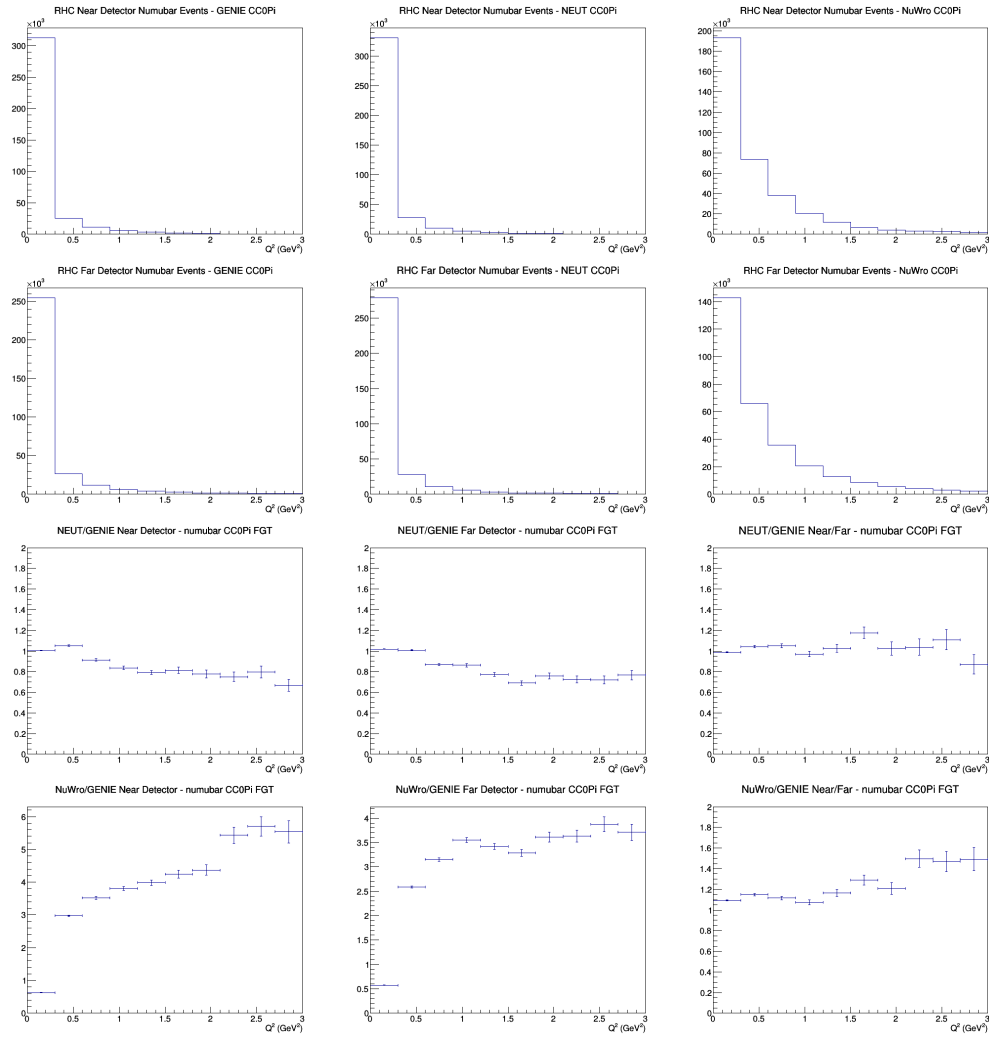
D.20 numu CC0Pi GAr efficiencies



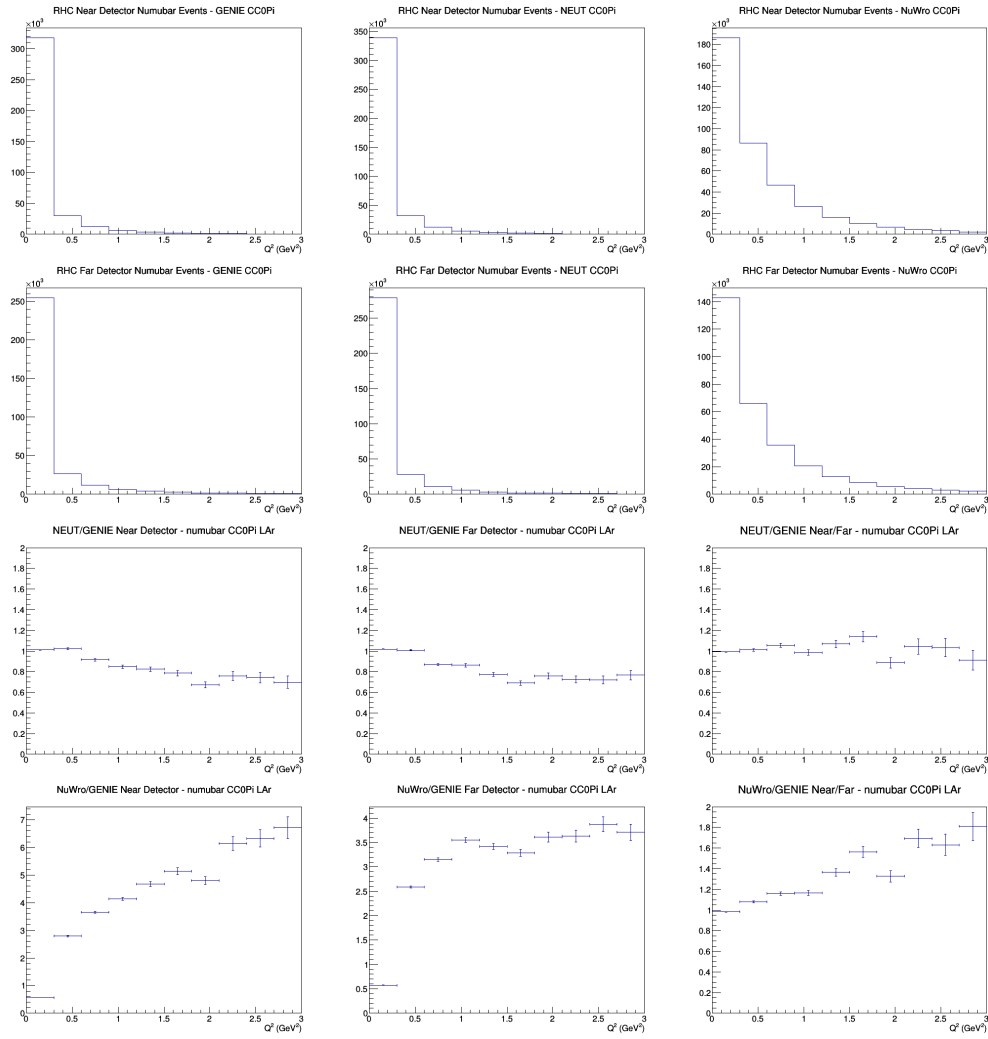
D.21 numubar CC0Pi no efficiencies



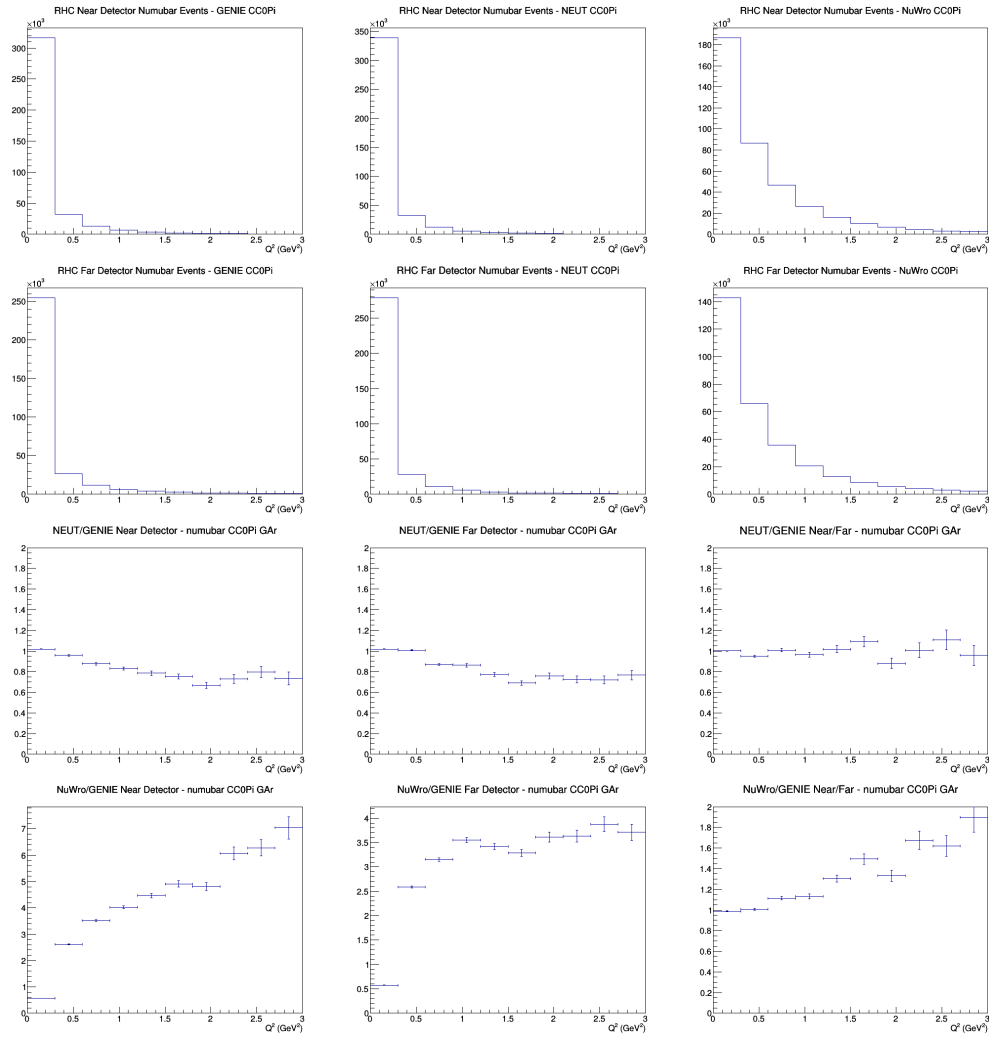
D.22 numubar CC0Pi FGT efficiencies



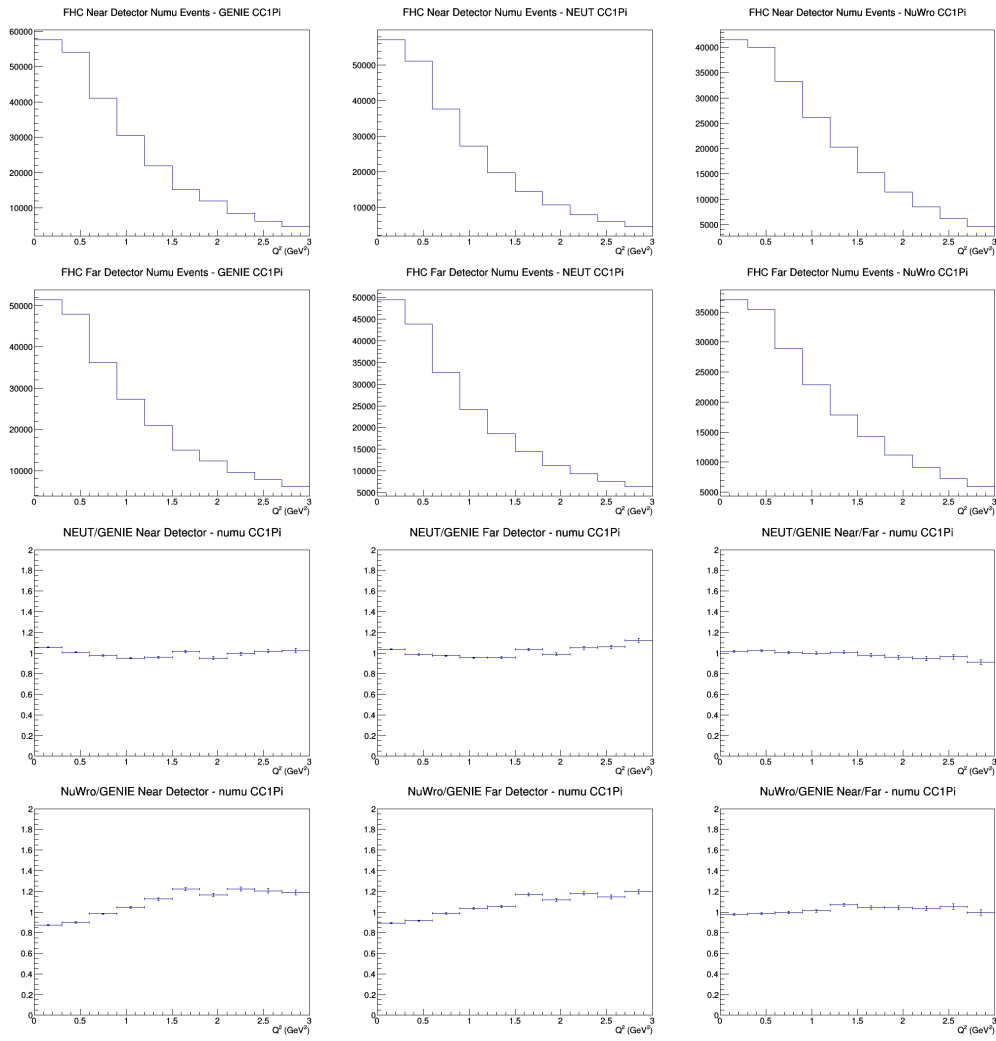
D.23 numubar CC0Pi LAr efficiencies



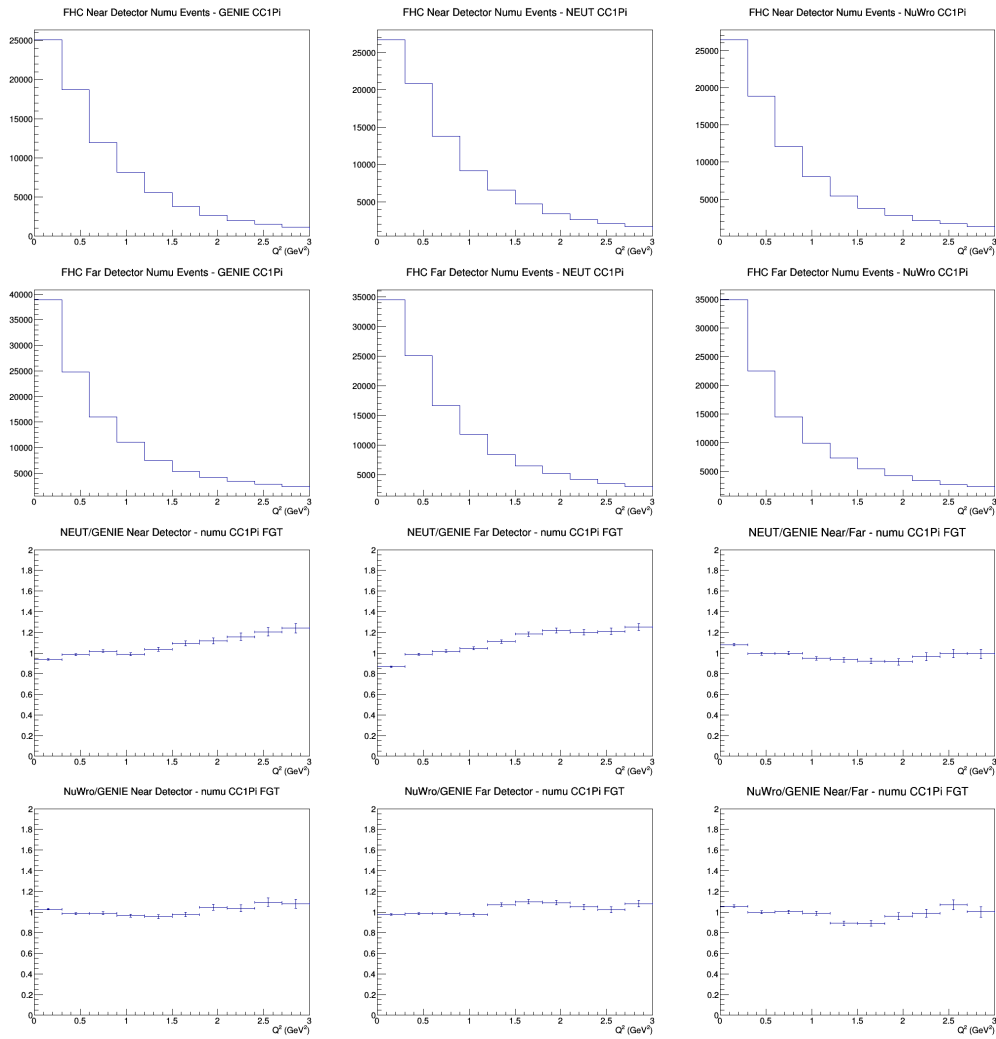
D.24 numubar CC0Pi GAr efficiencies



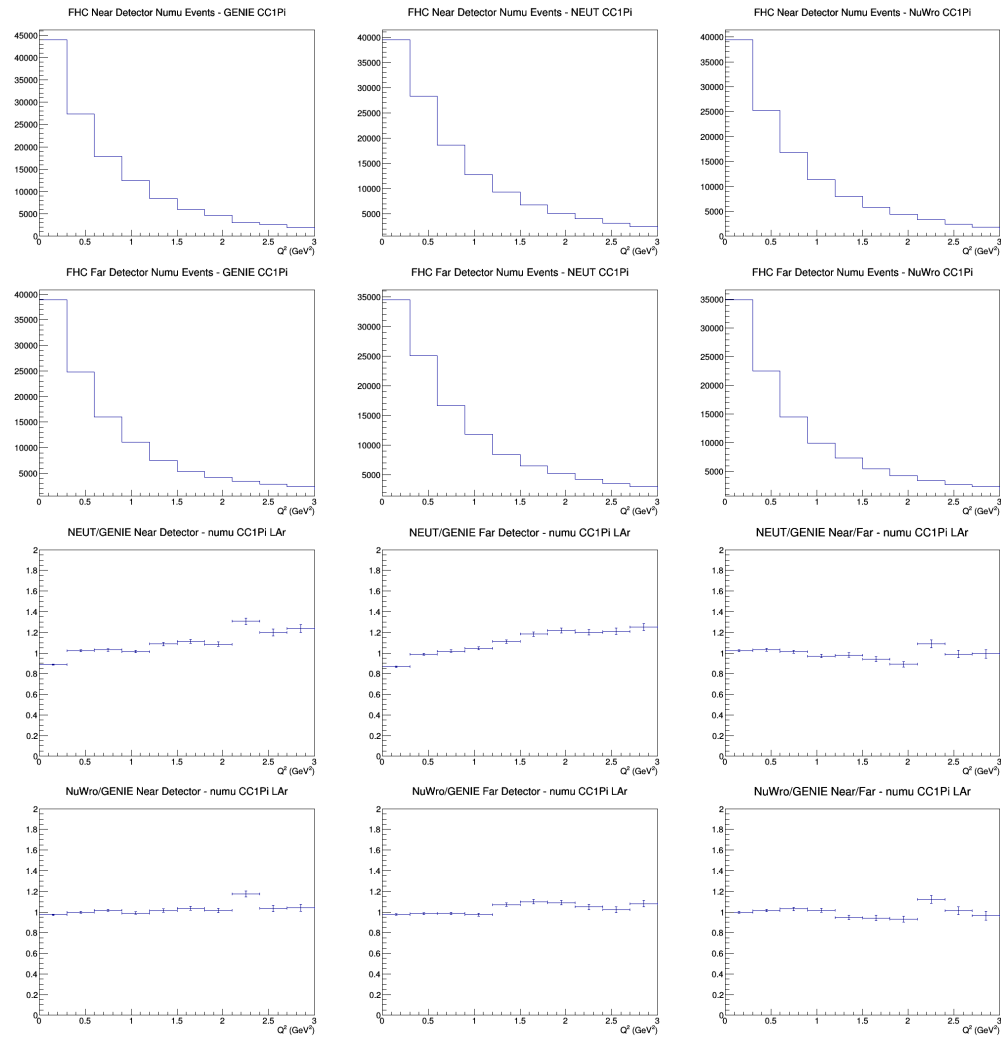
D.25 numu CC1Pi no efficiencies



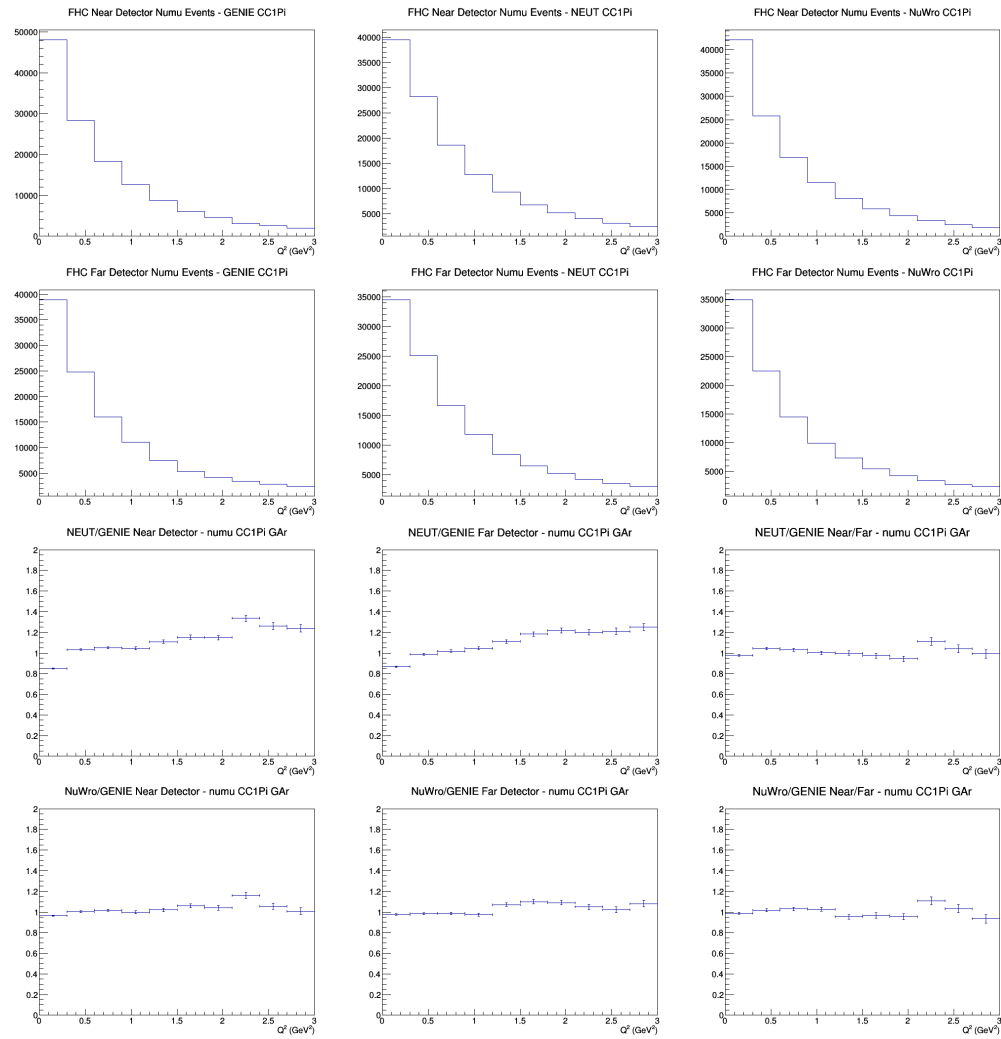
D.26 numu CC1Pi FGT efficiencies



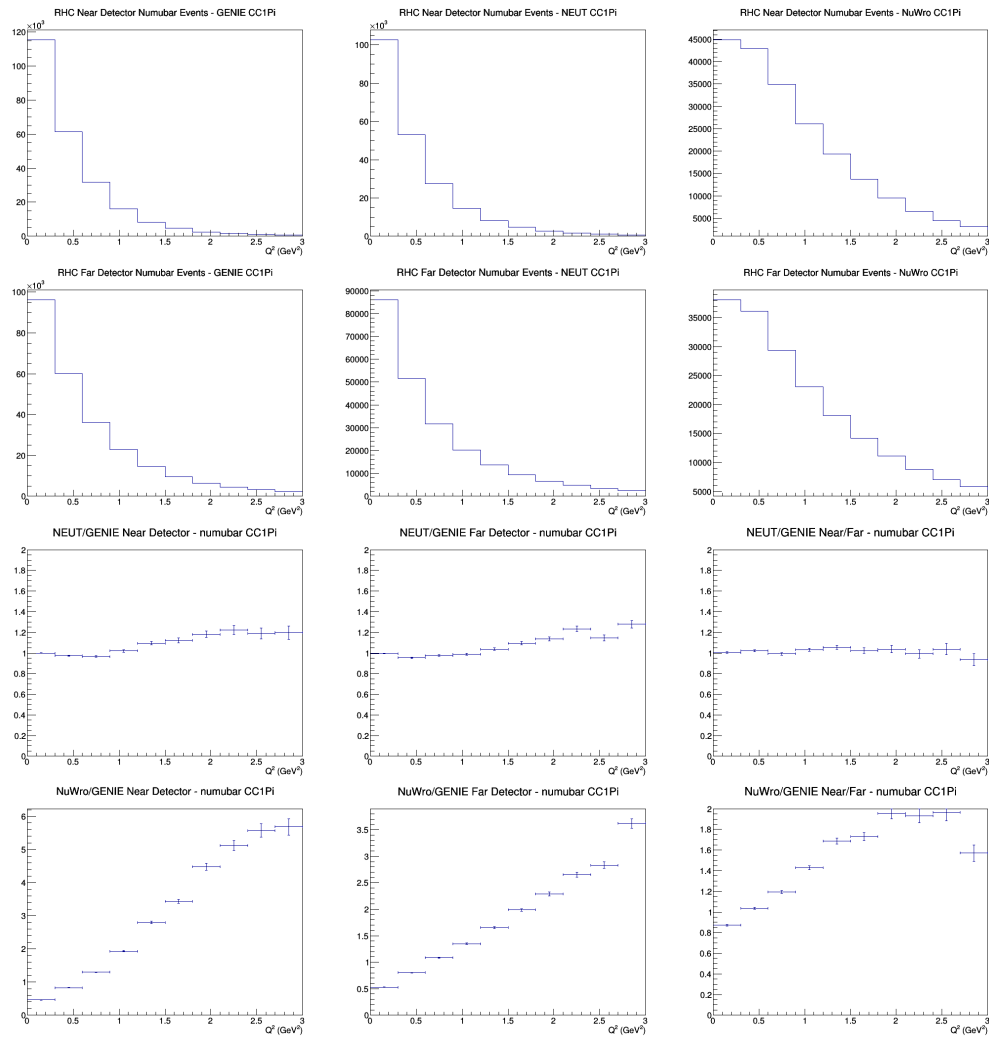
D.27 numu CC1Pi LAr efficiencies



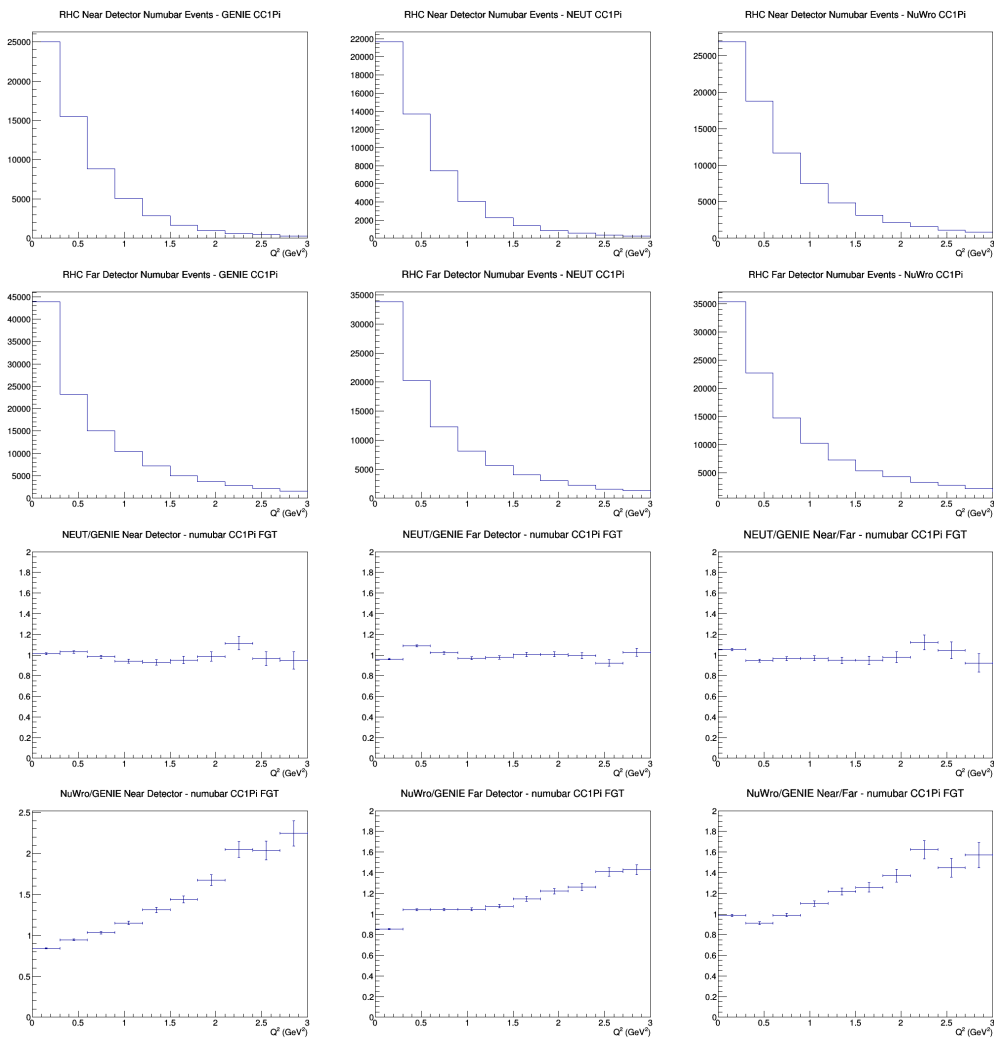
D.28 numu CC1Pi GAr efficiencies



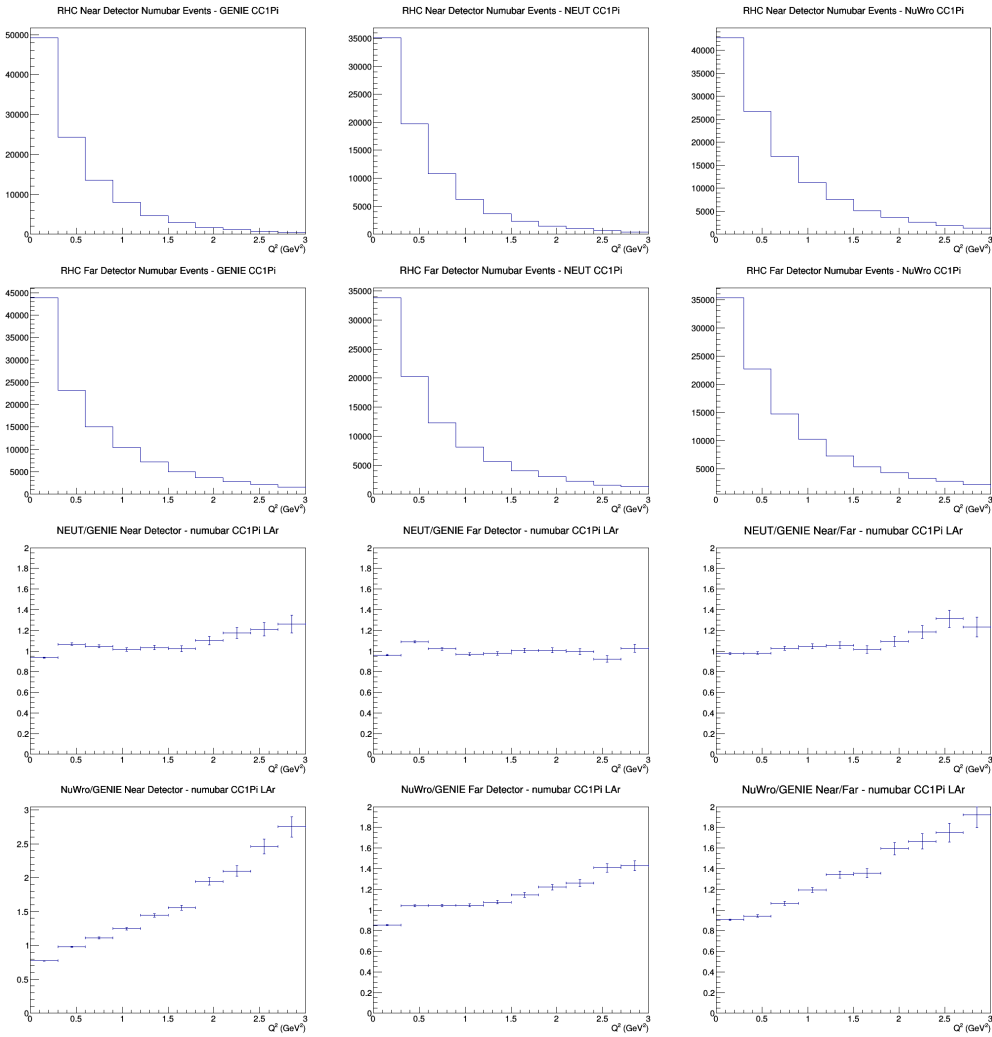
D.29 numubar CC1Pi no efficiencies



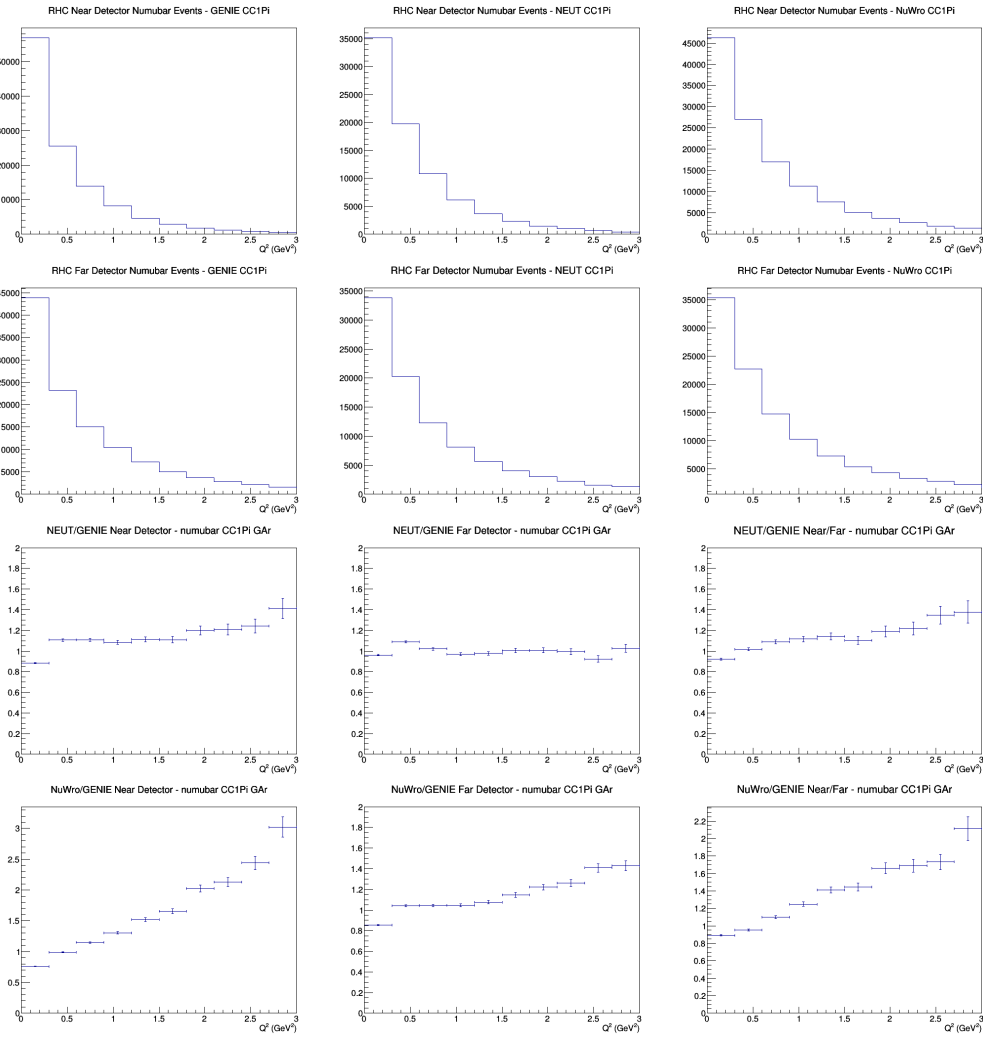
D.30 numubar CC1Pi FGT efficiencies



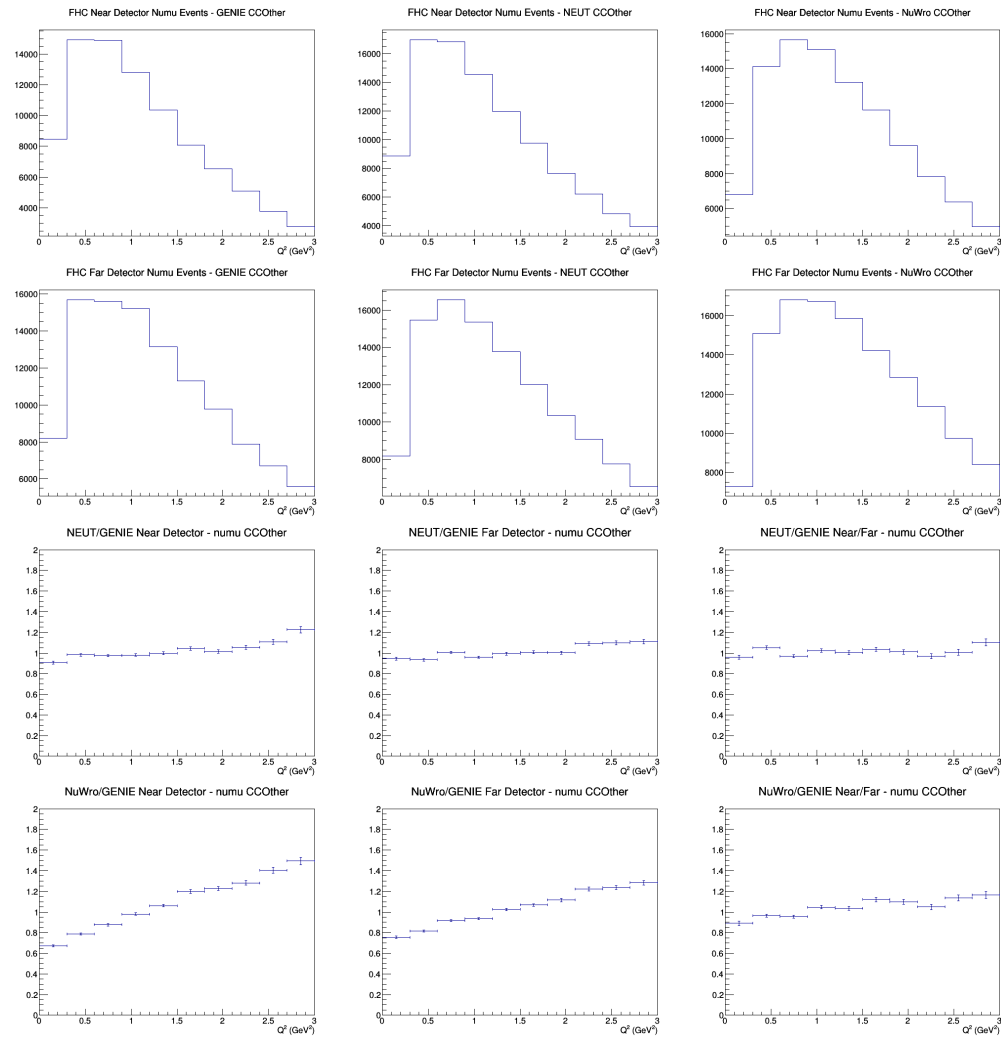
D.31 numubar CC1Pi LAr efficiencies



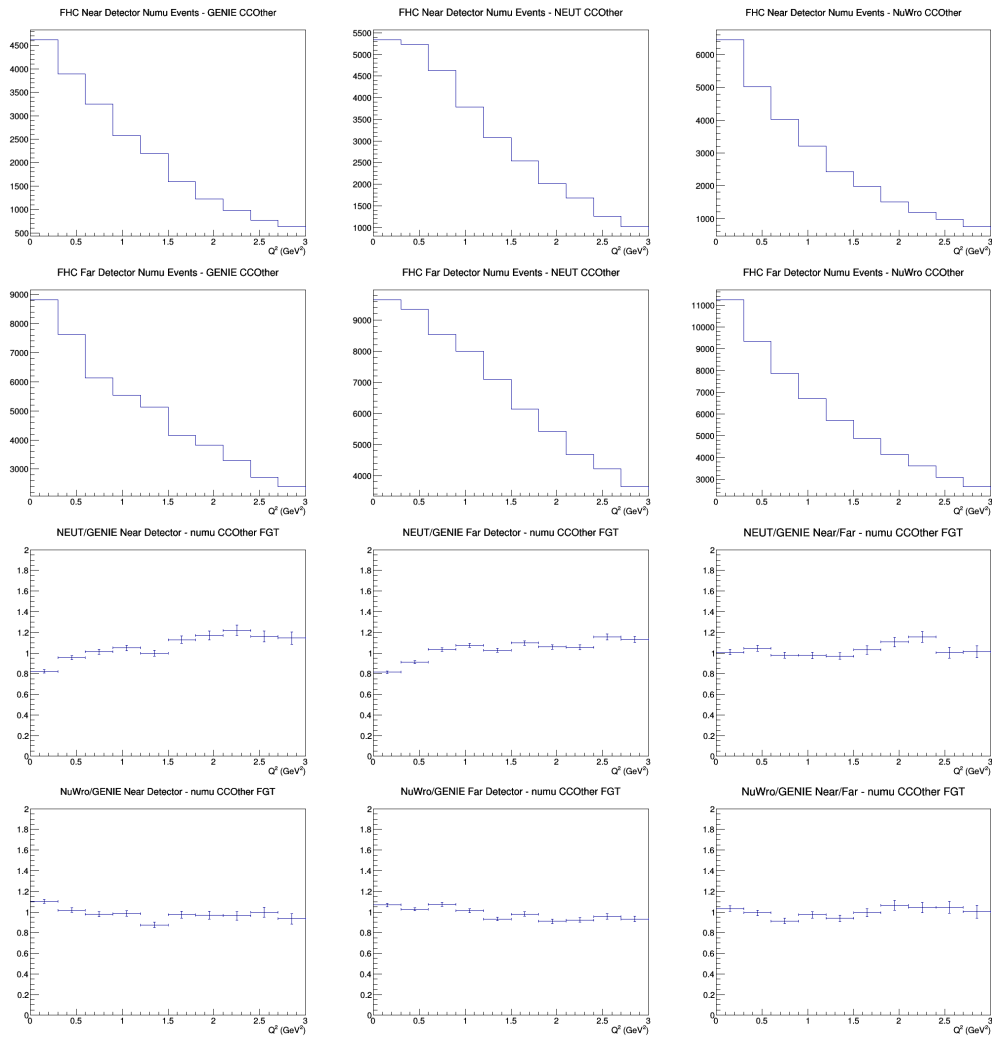
D.32 numubar CC1Pi GAr efficiencies



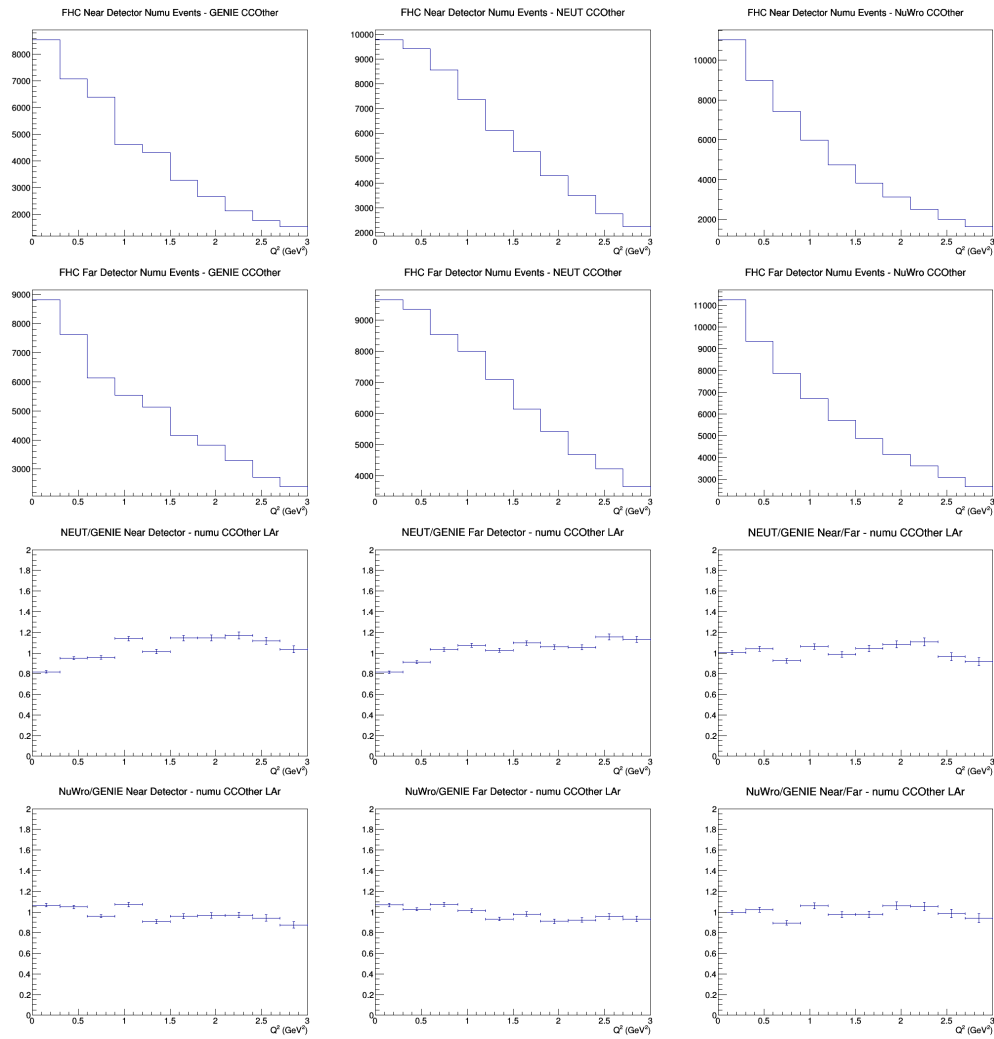
D.33 numu CCOther no efficiencies



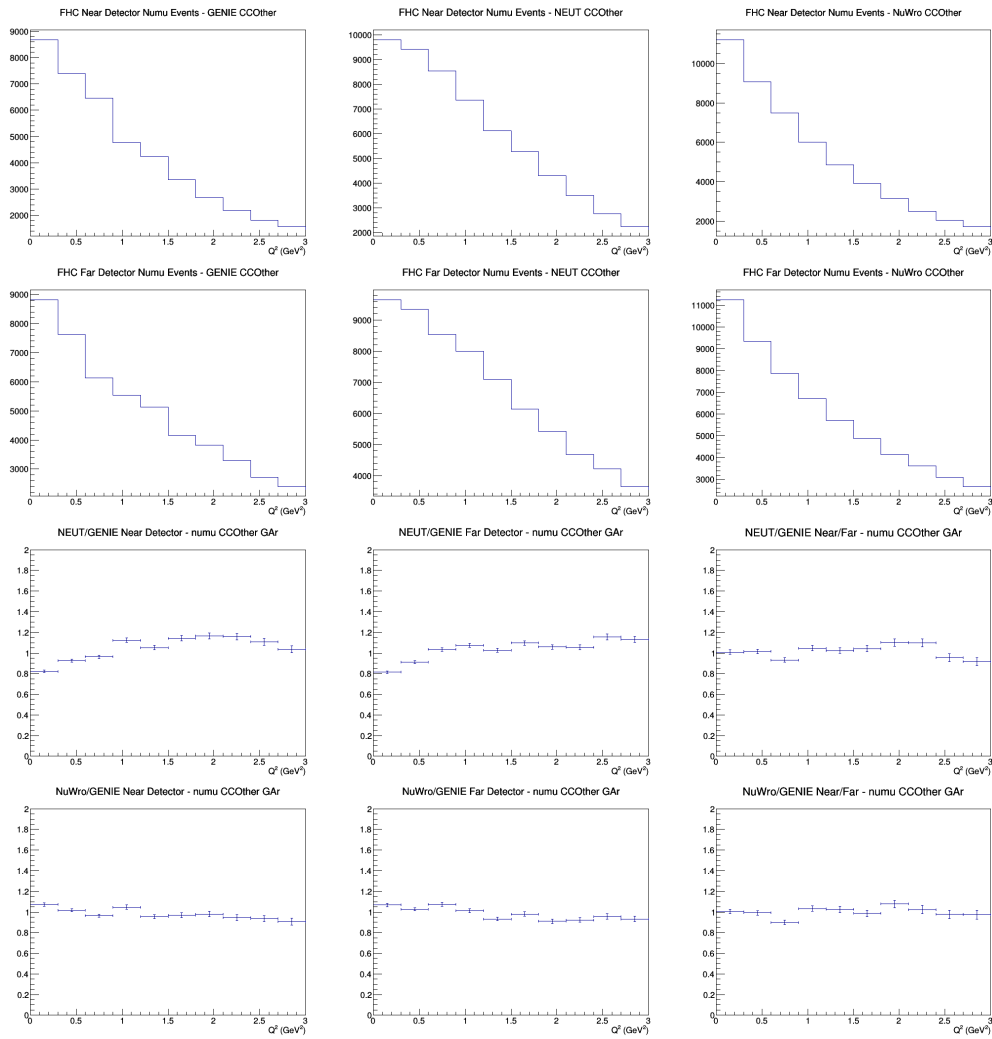
D.34 numu CCOther FGT efficiencies



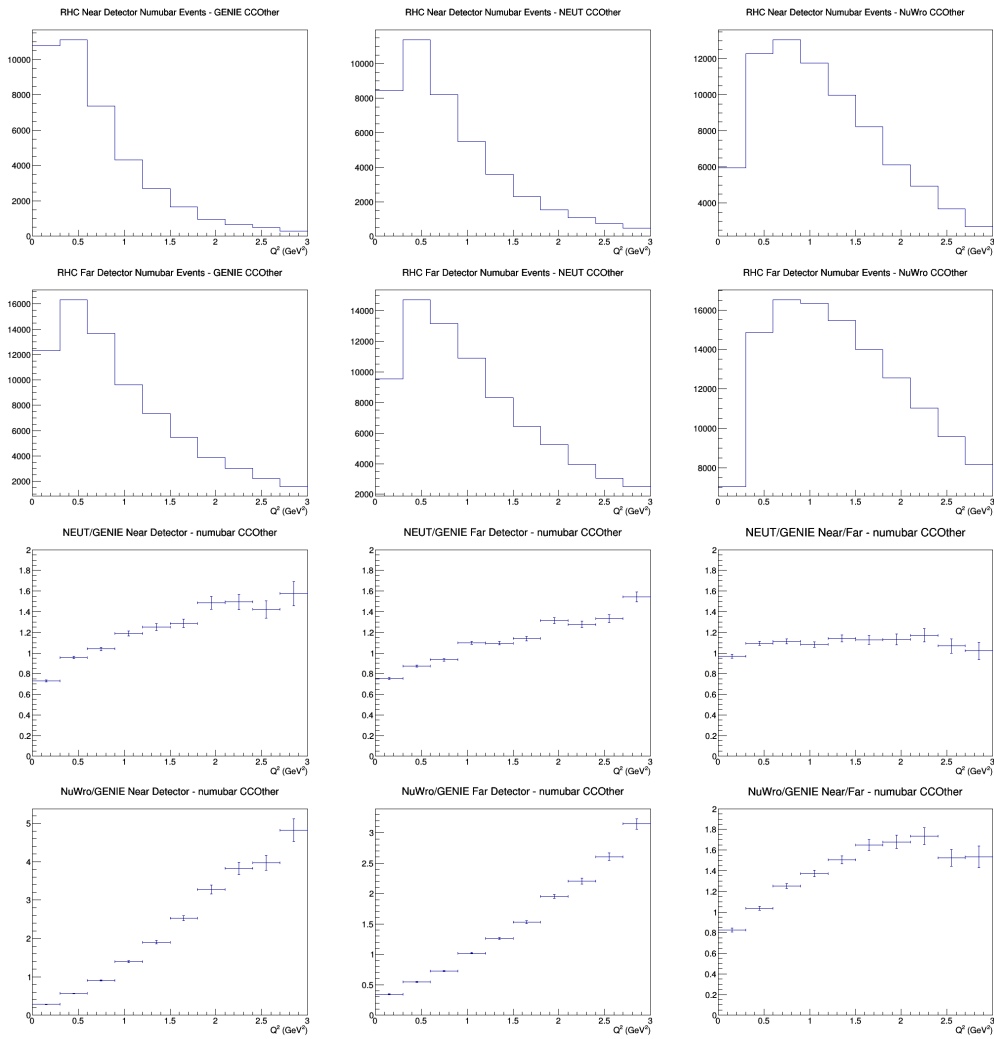
D.35 numu CCOther LAr efficiencies



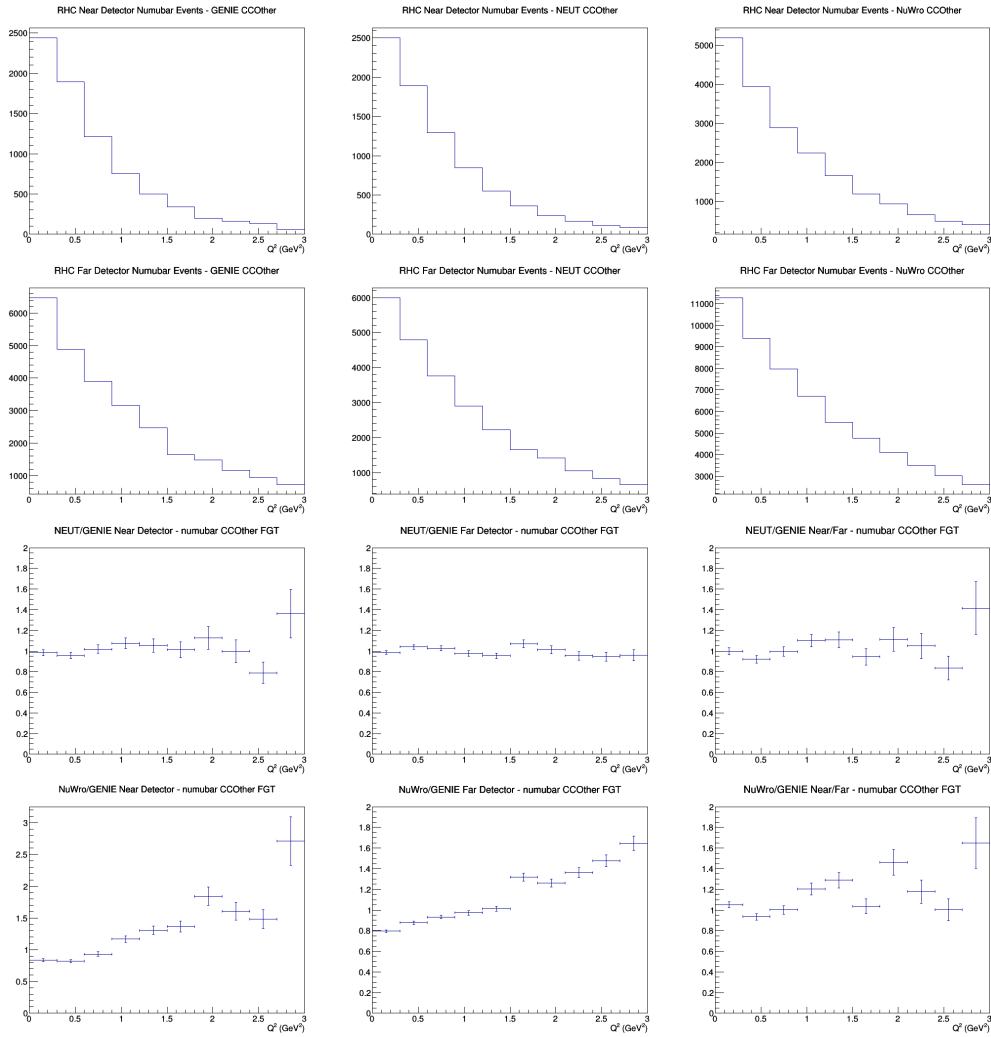
D.36 numu CCOther GAr efficiencies



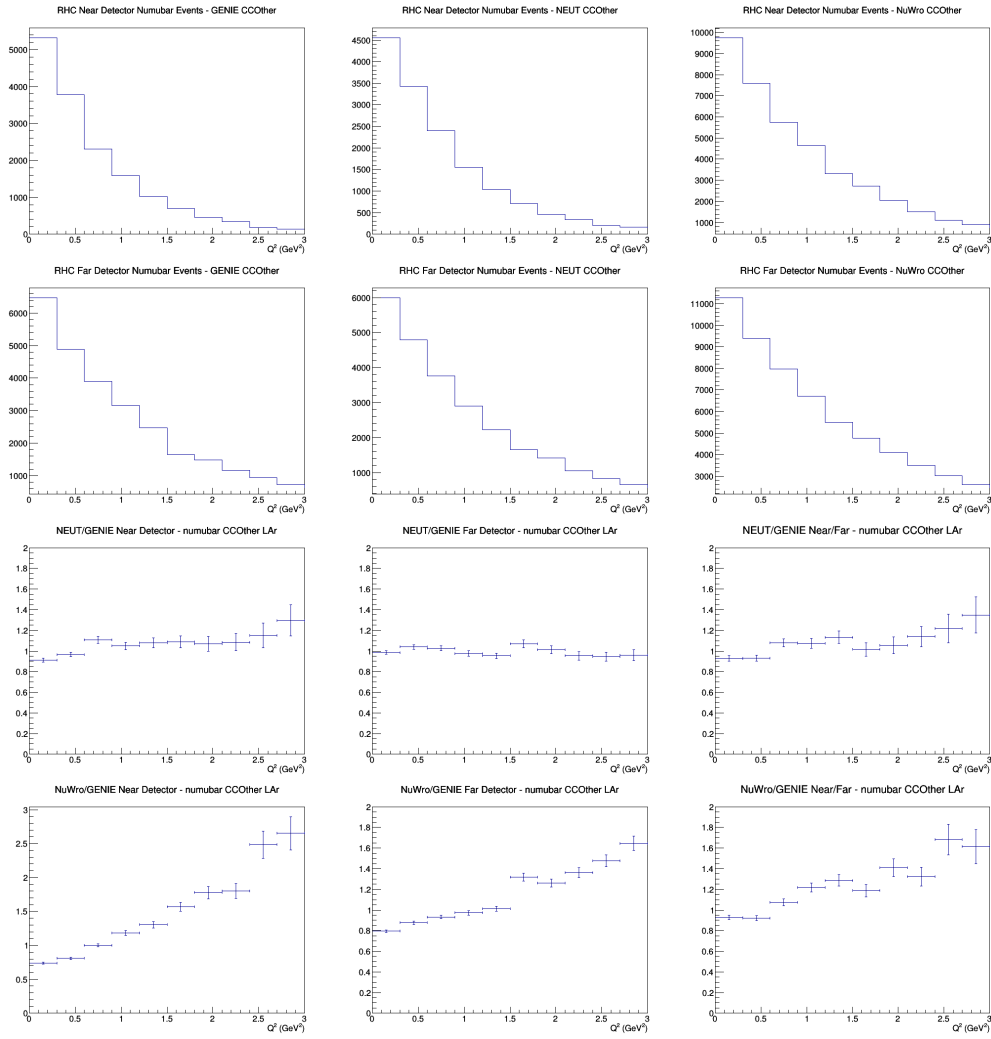
D.37 numubar CCOther no efficiencies



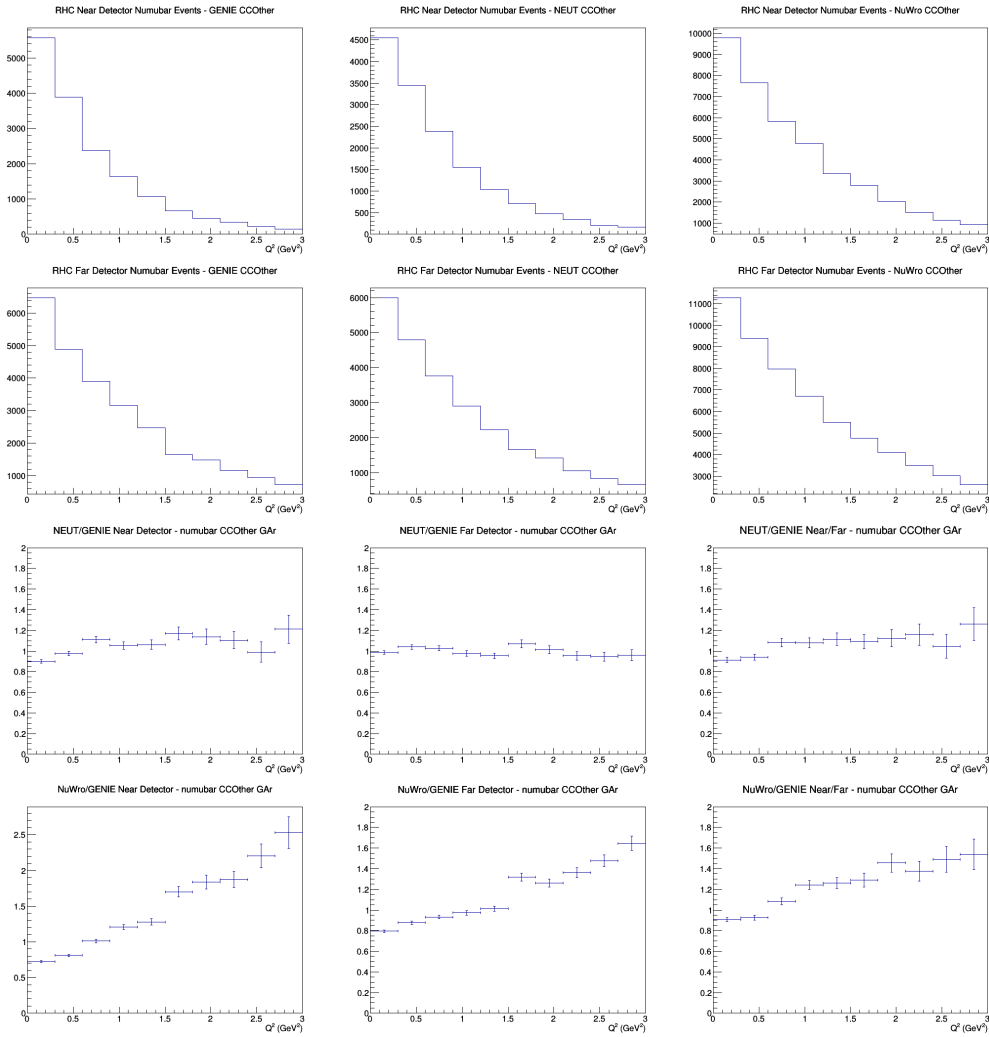
D.38 numubar CCOther FGT efficiencies



D.39 numubar CCOther LAr efficiencies



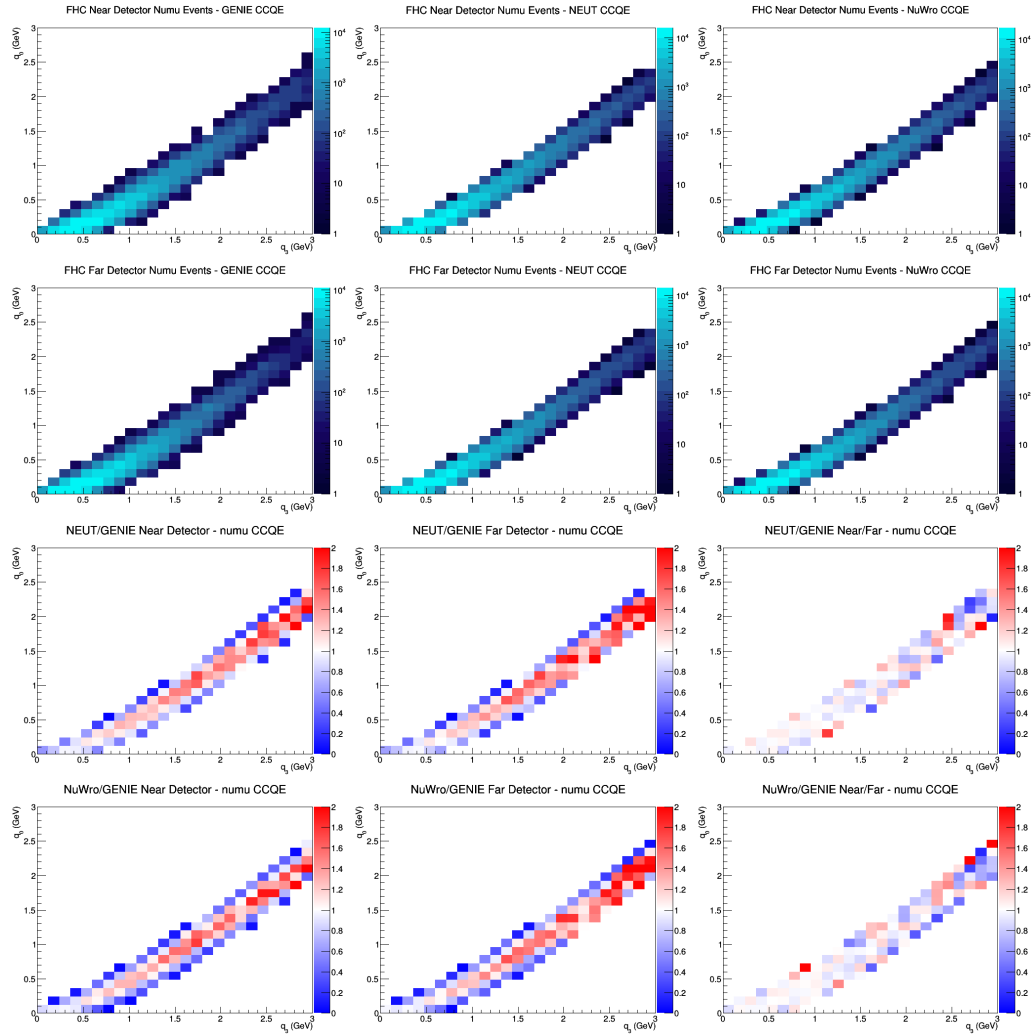
D.40 numubar CCOther GAr efficiencies



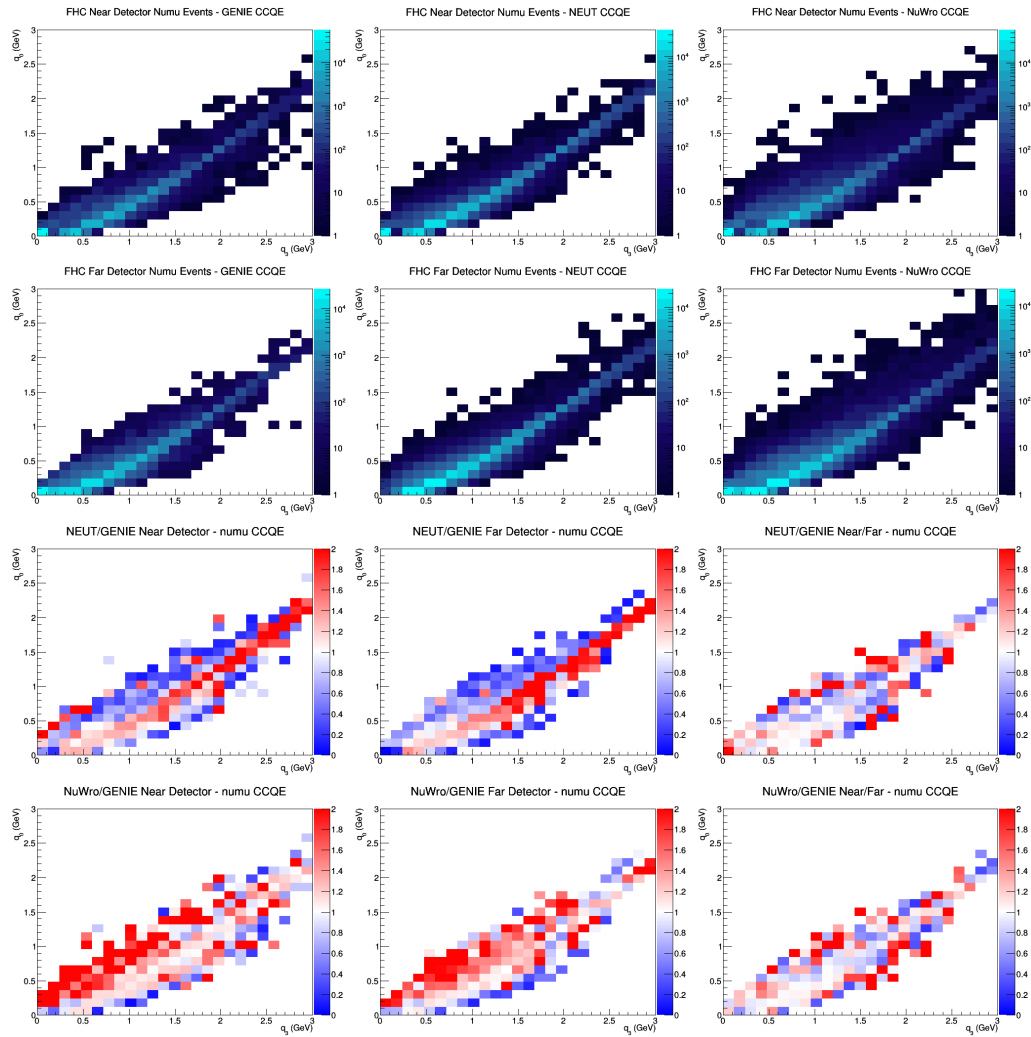
E q_0 vs. q_3 Plots

This appendix includes all the plots not show in Section 4.2. For full description of the files, please make reference to that section. The plots will be put in the same order as before.

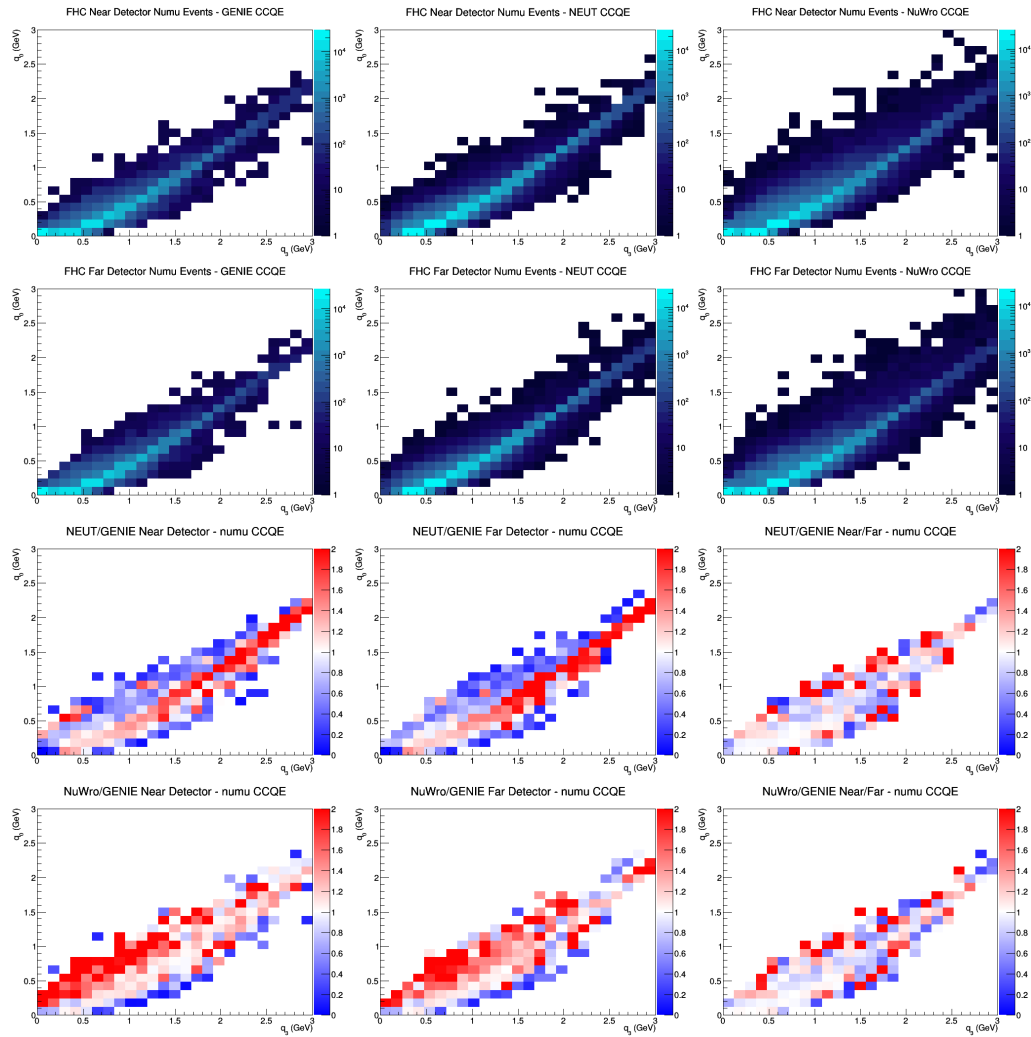
E.1 numu CCQE no efficiencies



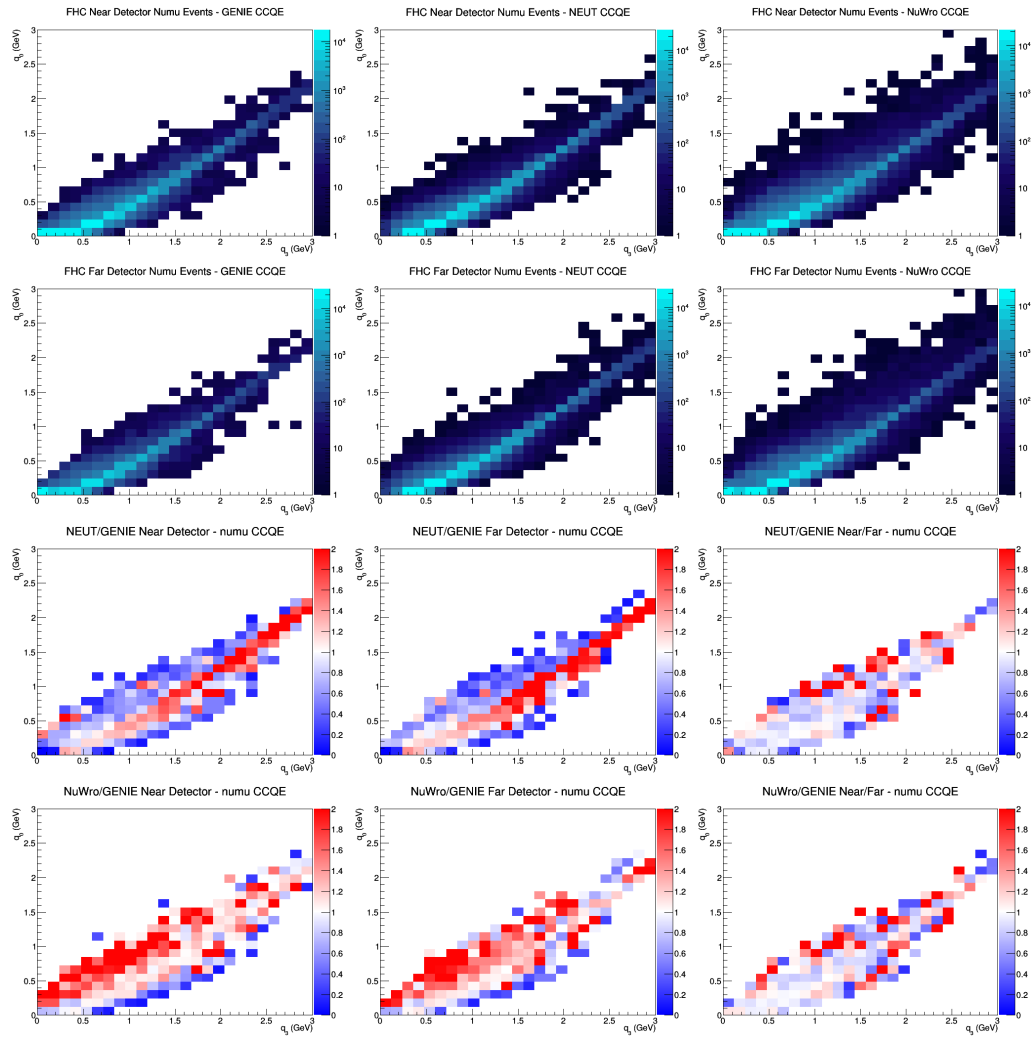
E.2 numu CCQE FGT efficiencies



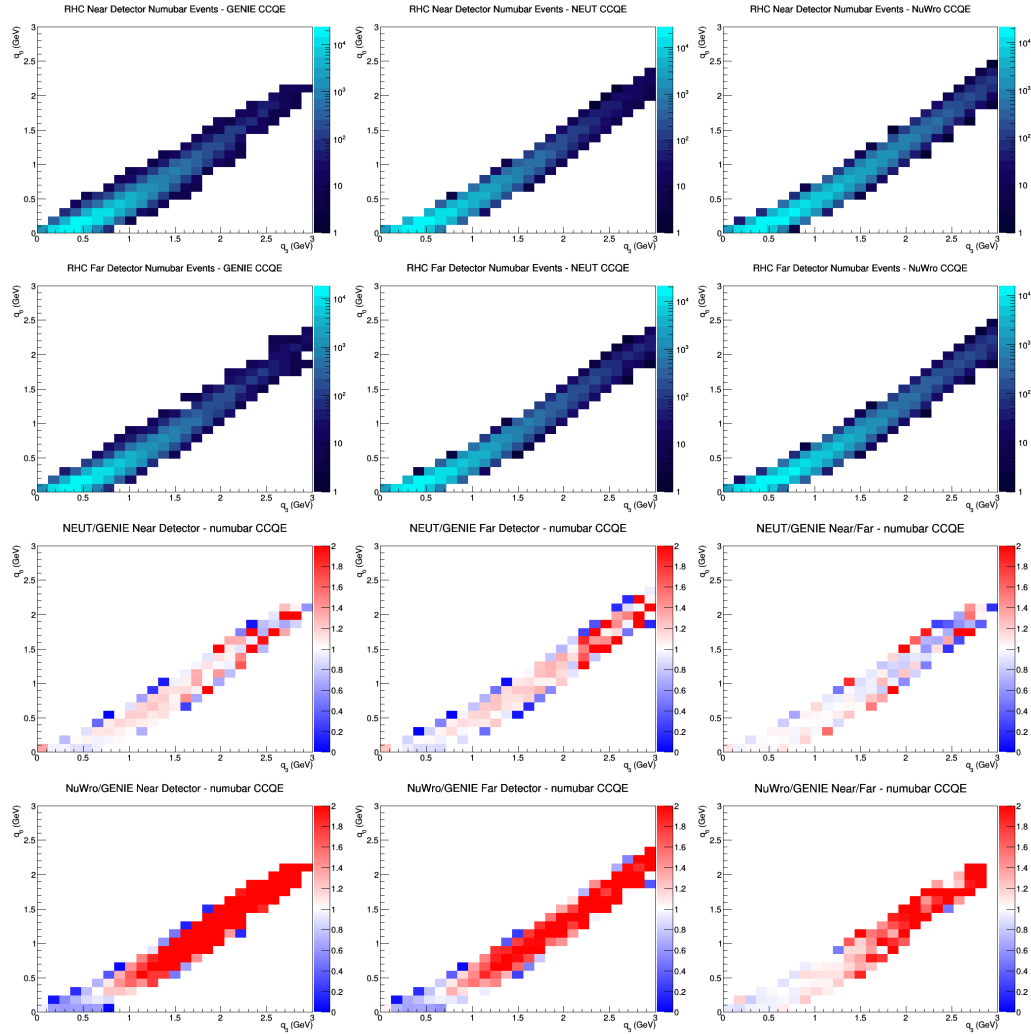
E.3 numu CCQE LAr efficiencies



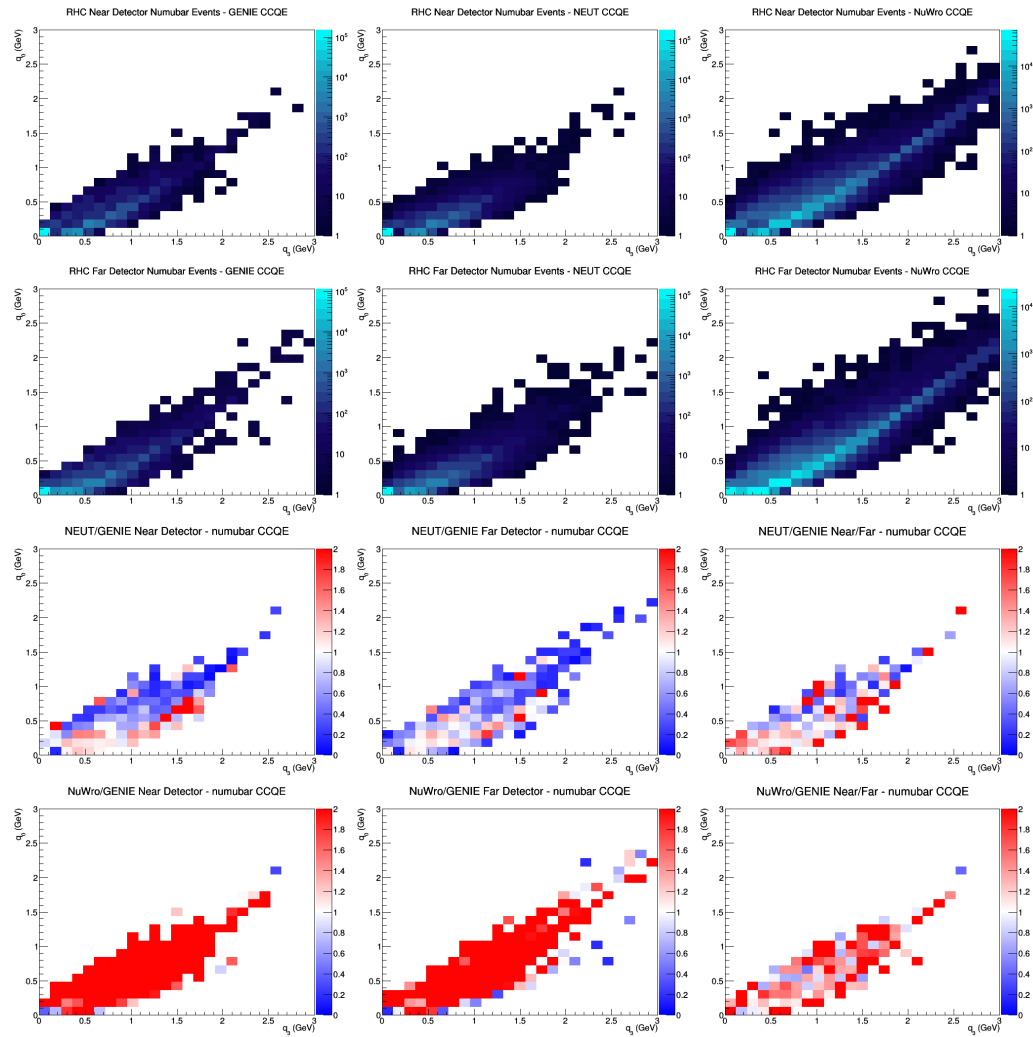
E.4 numu CCQE GAr efficiencies



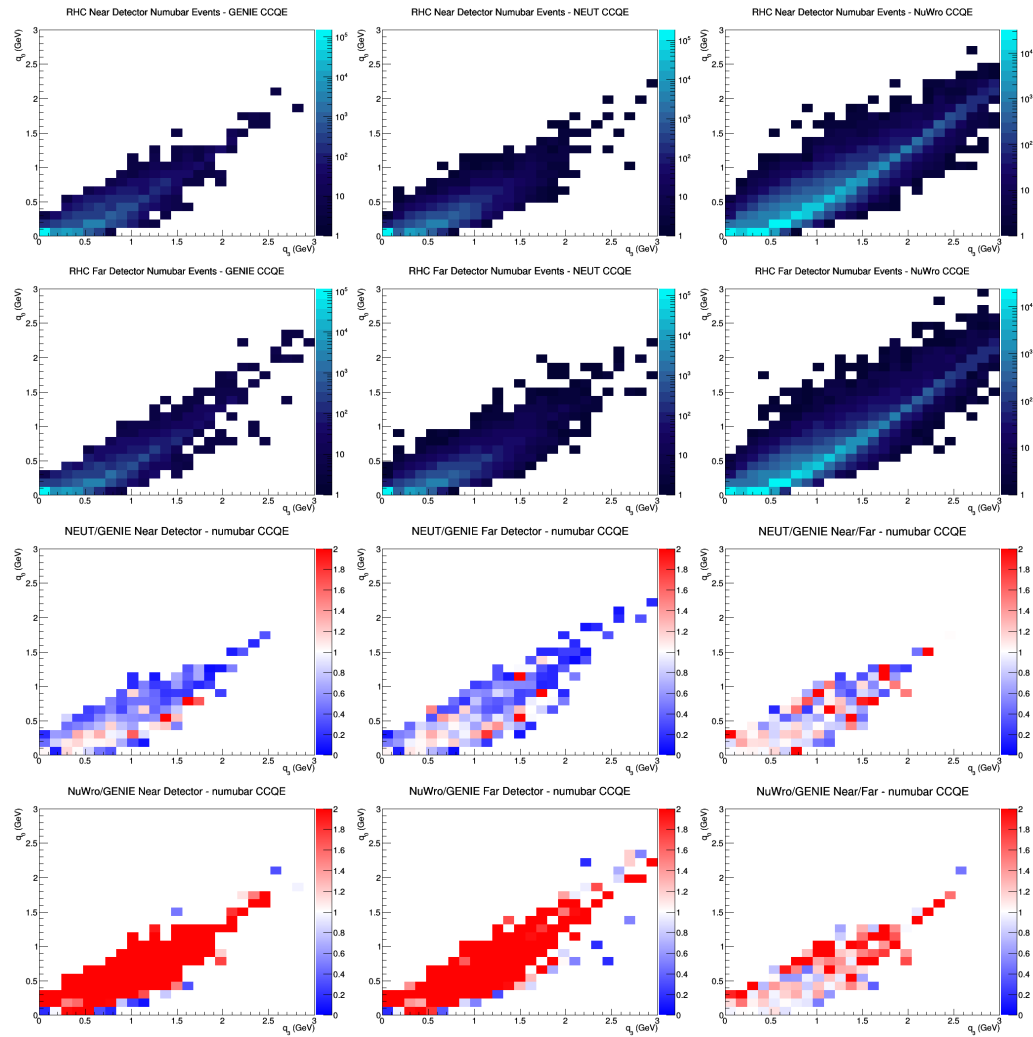
E.5 numubar CCQE no efficiencies



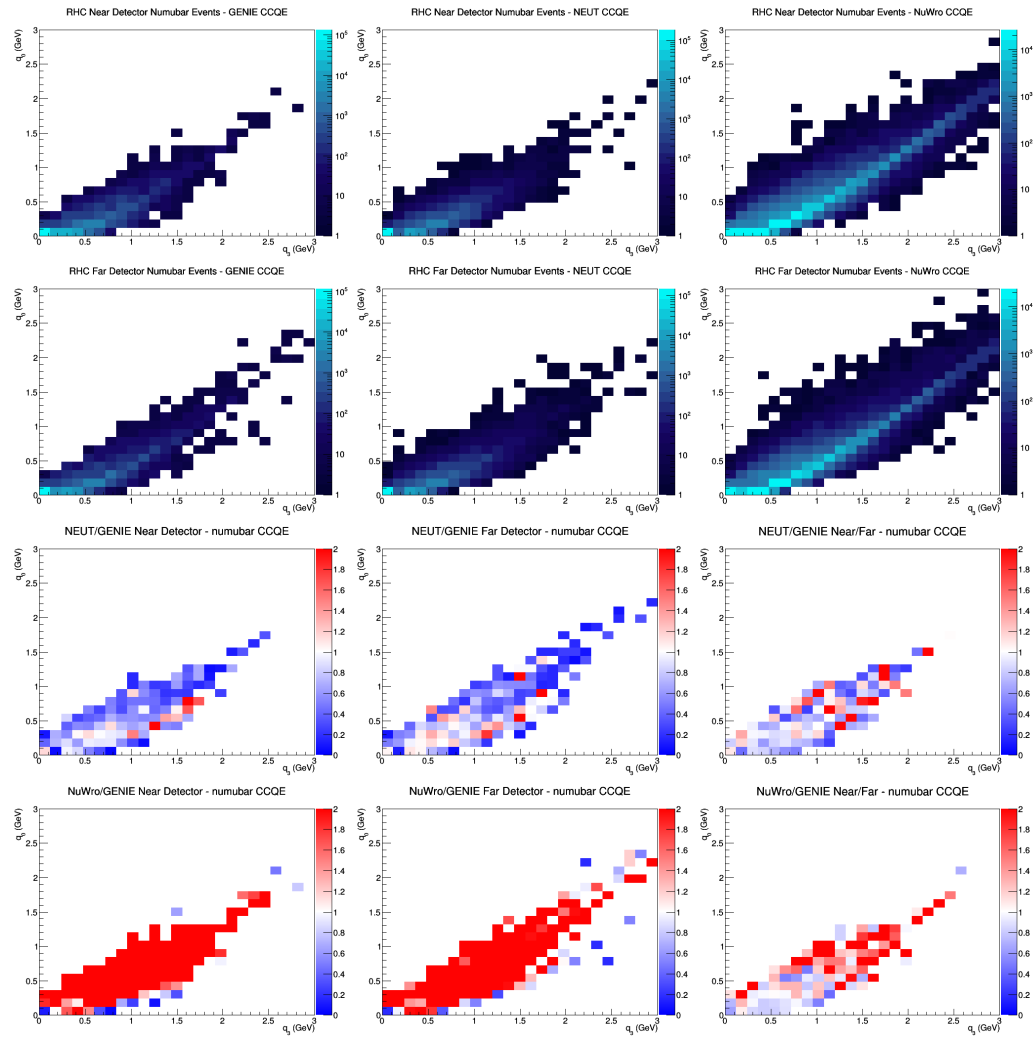
E.6 numubar CCQE FGT efficiencies



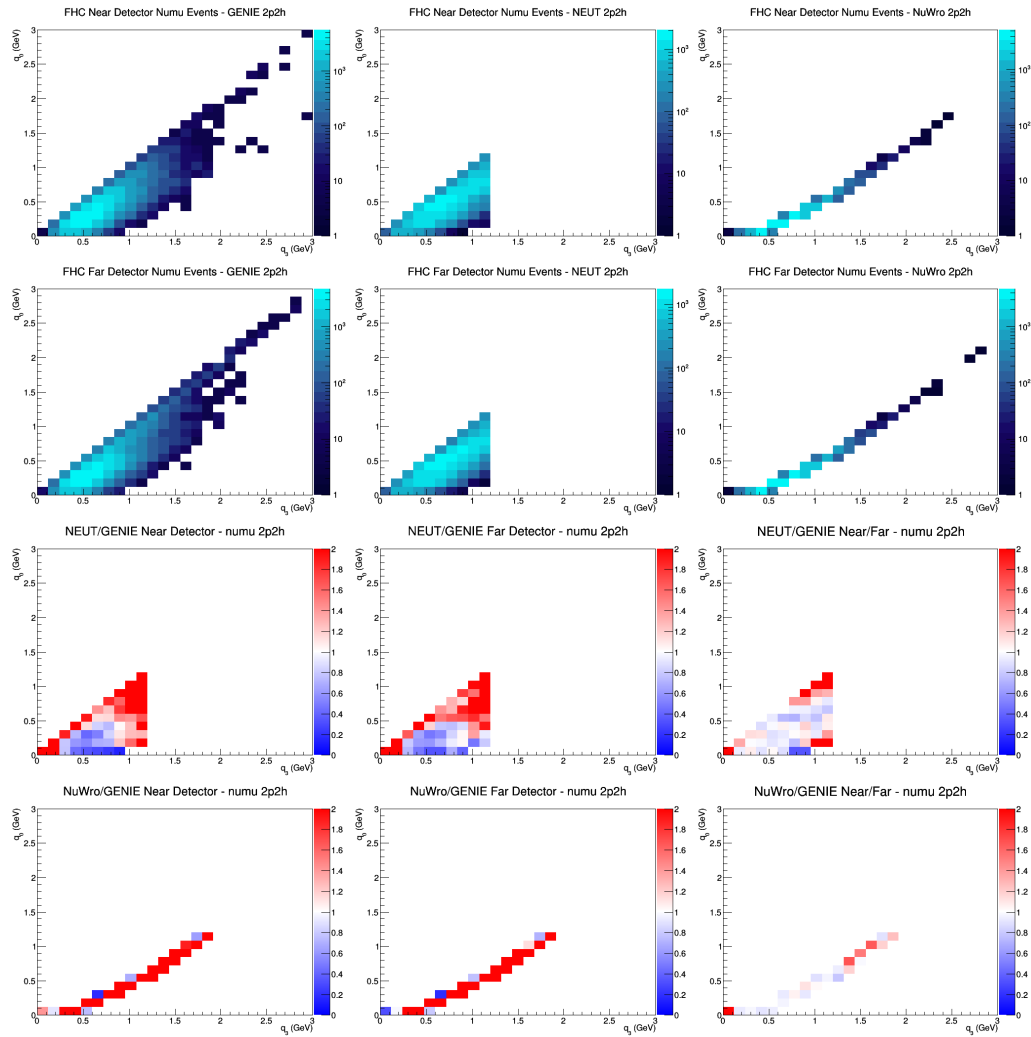
E.7 numubar CCQE LAr efficiencies



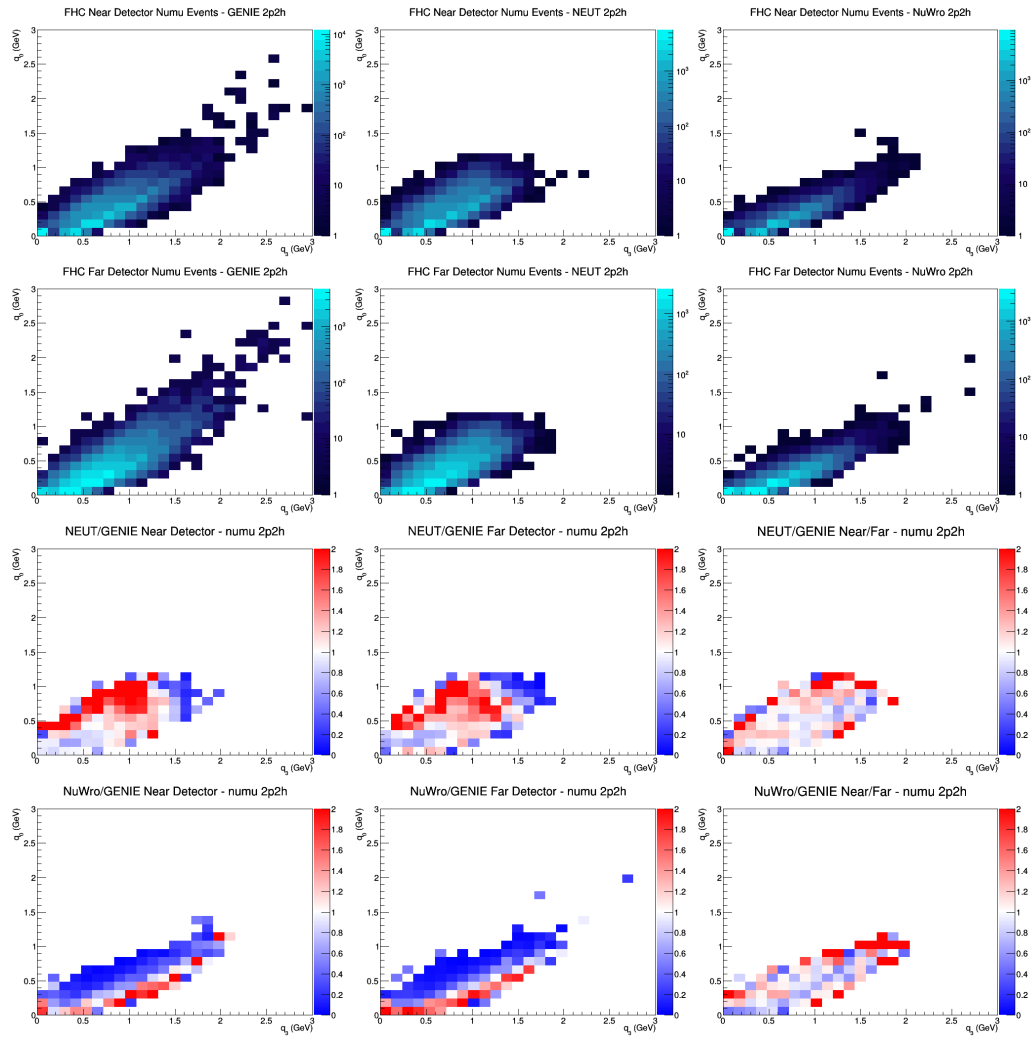
E.8 numubar CCQE GAr efficiencies



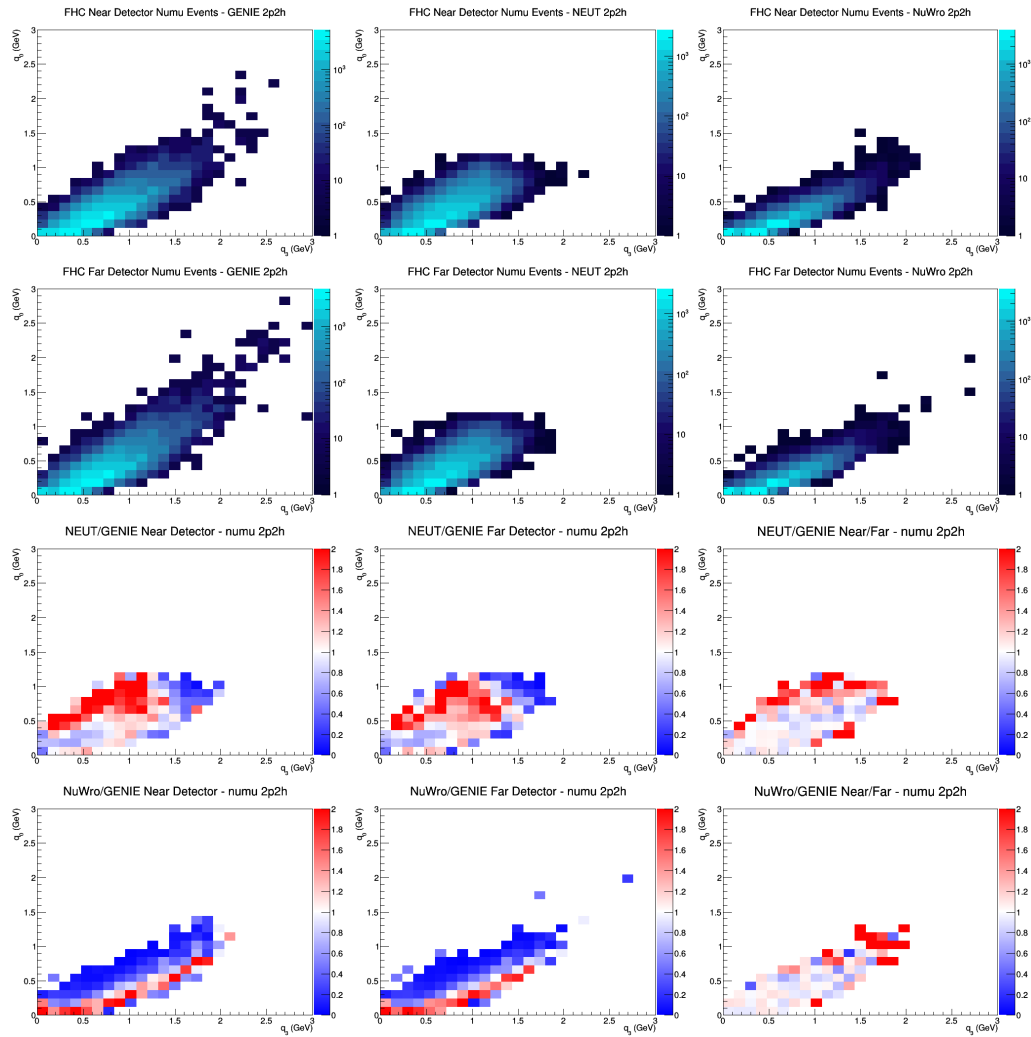
E.9 numu 2p2h no efficiencies



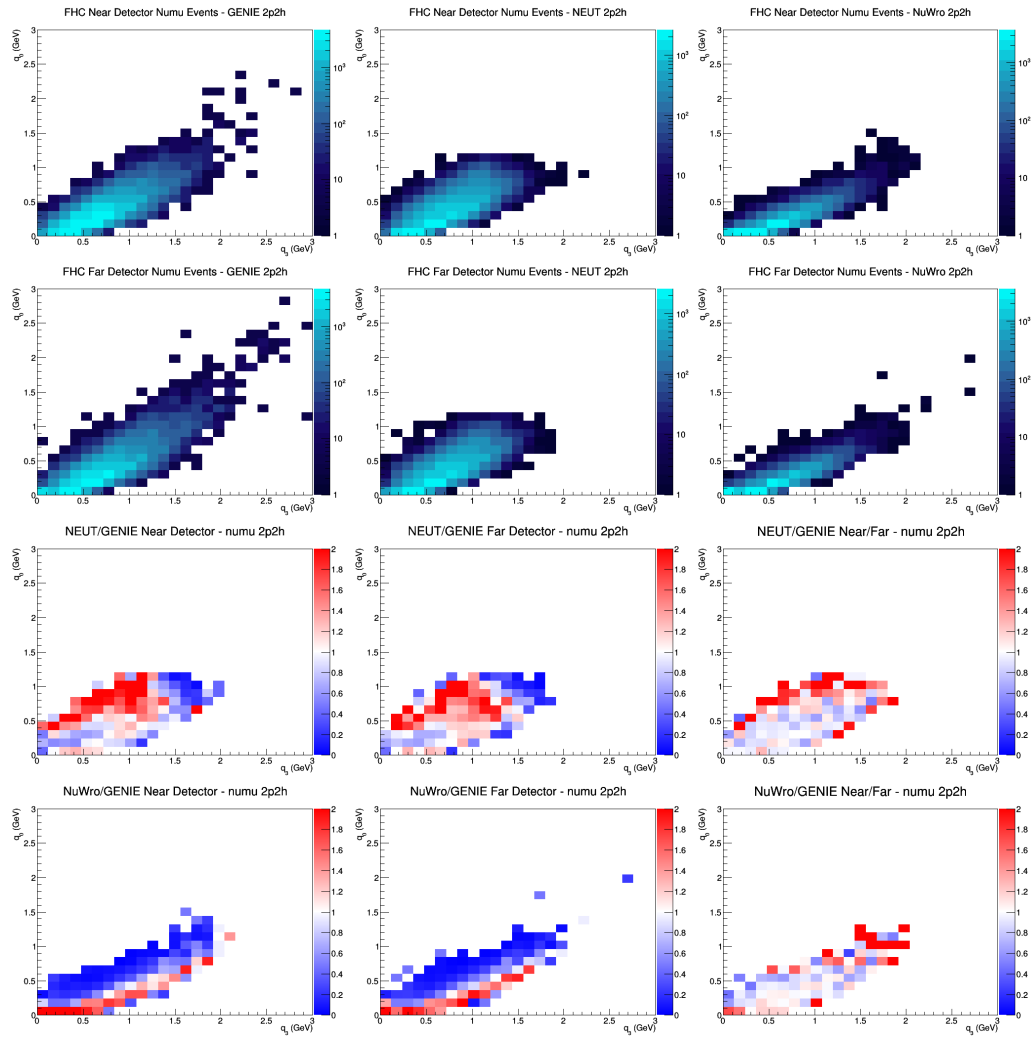
E.10 numu 2p2h FGT efficiencies



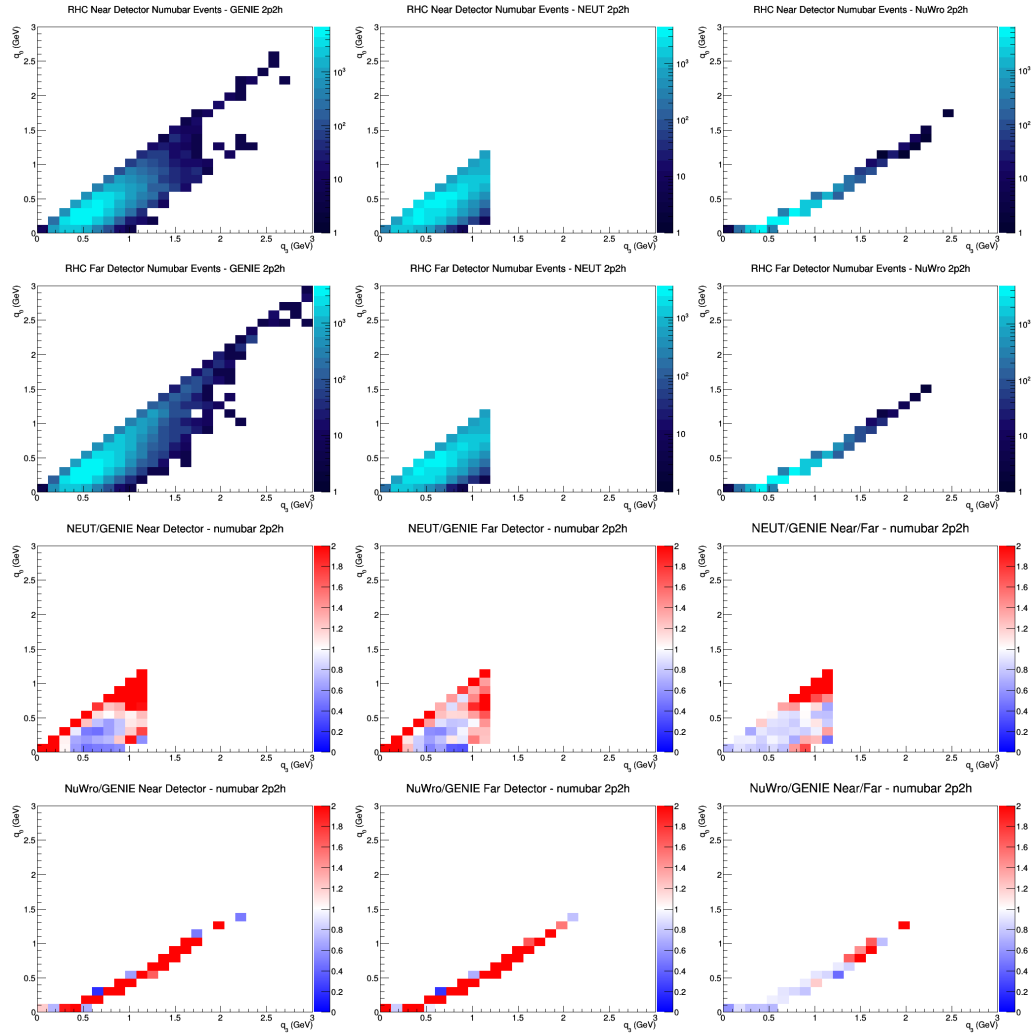
E.11 numu 2p2h LAr efficiencies



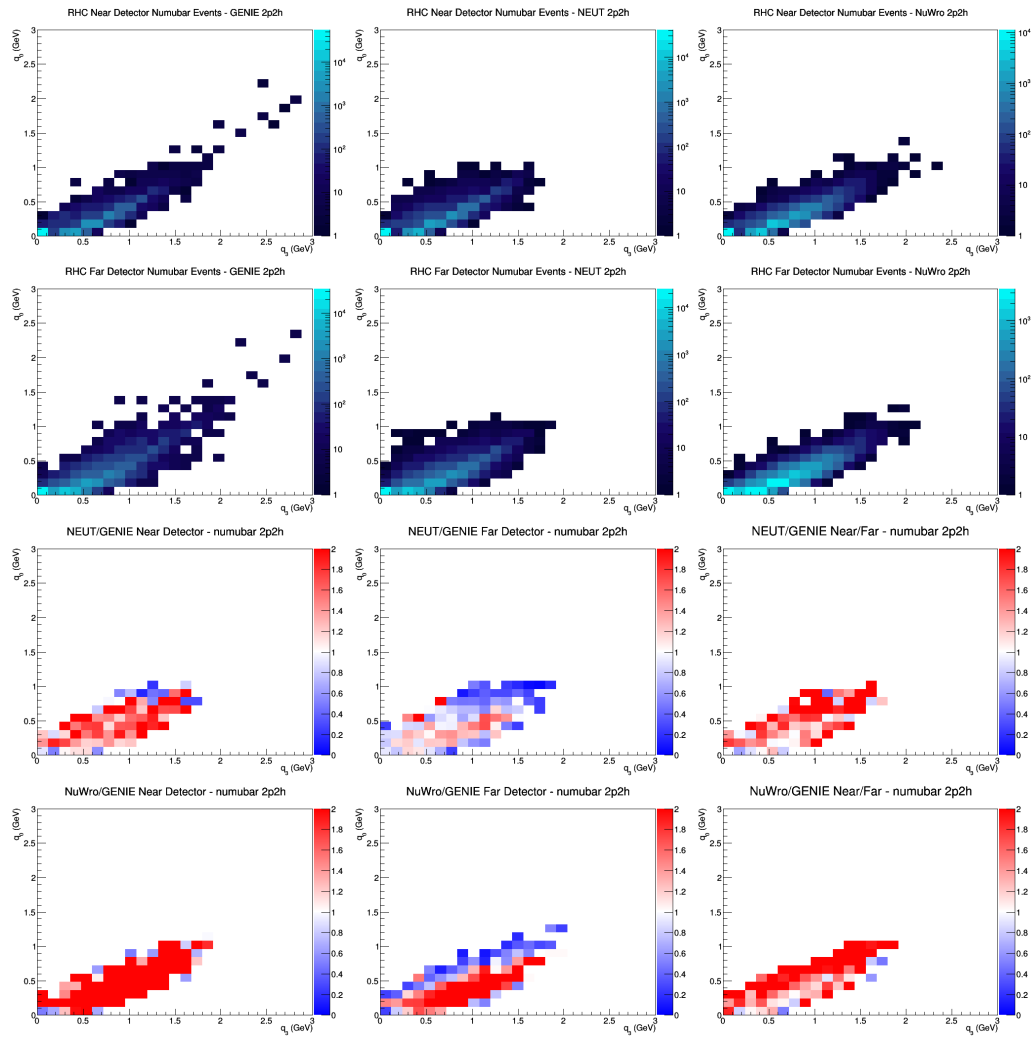
E.12 numu 2p2h GAr efficiencies



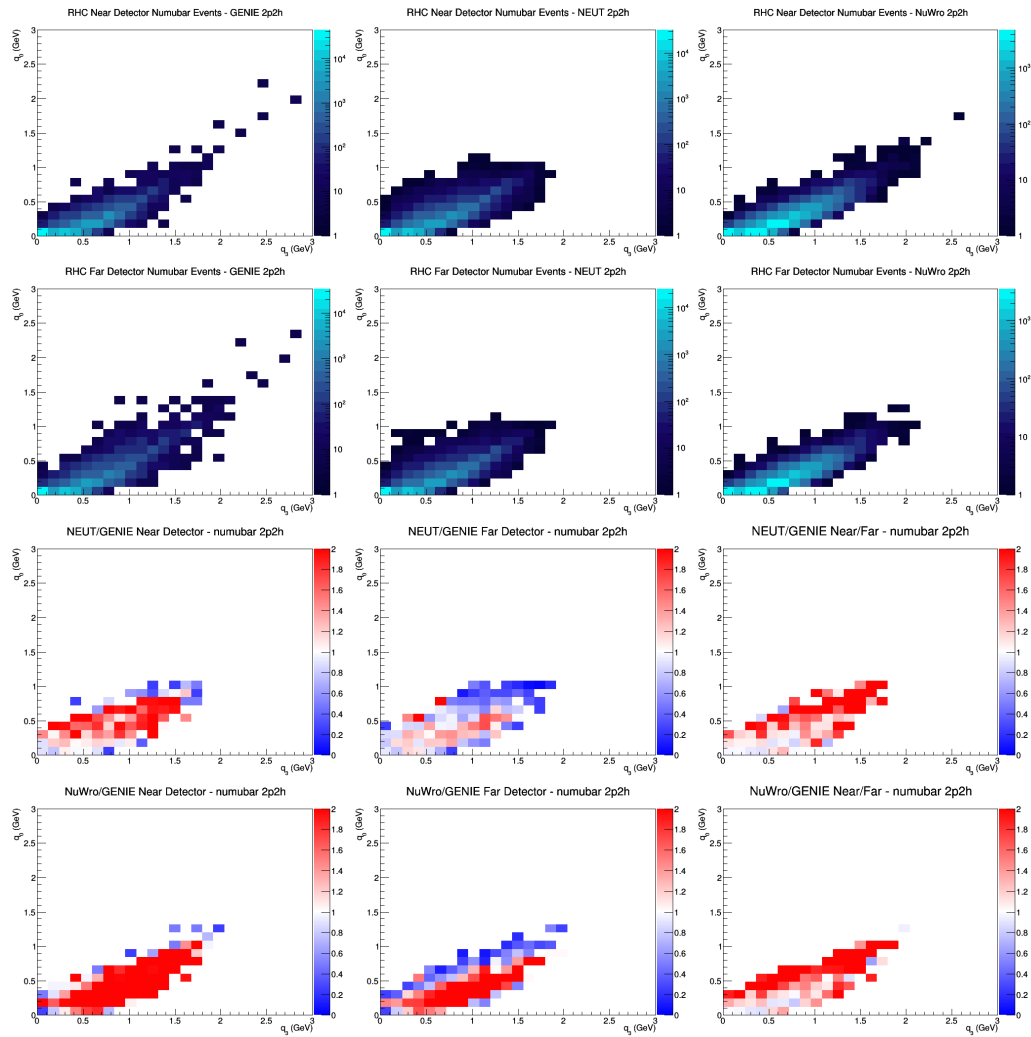
E.13 numubar 2p2h no efficiencies



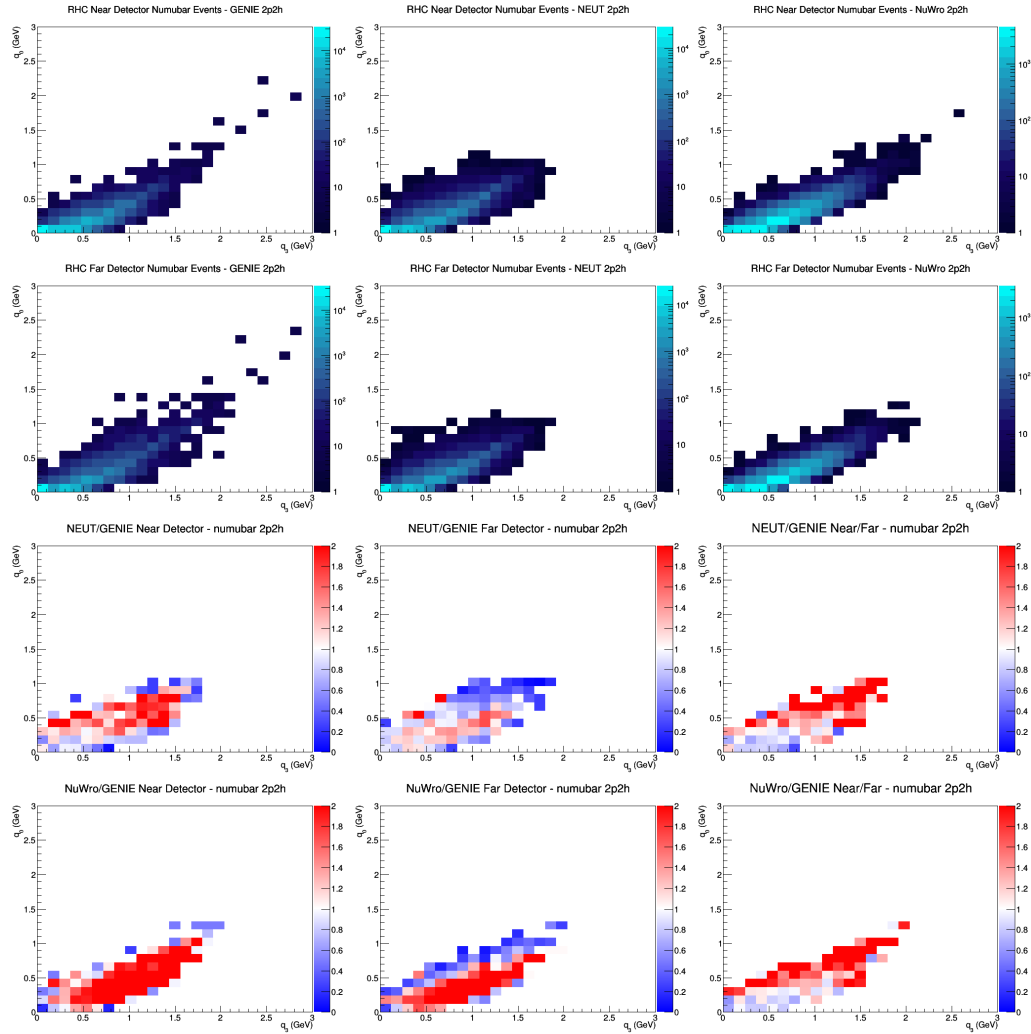
E.14 numubar 2p2h FGT efficiencies



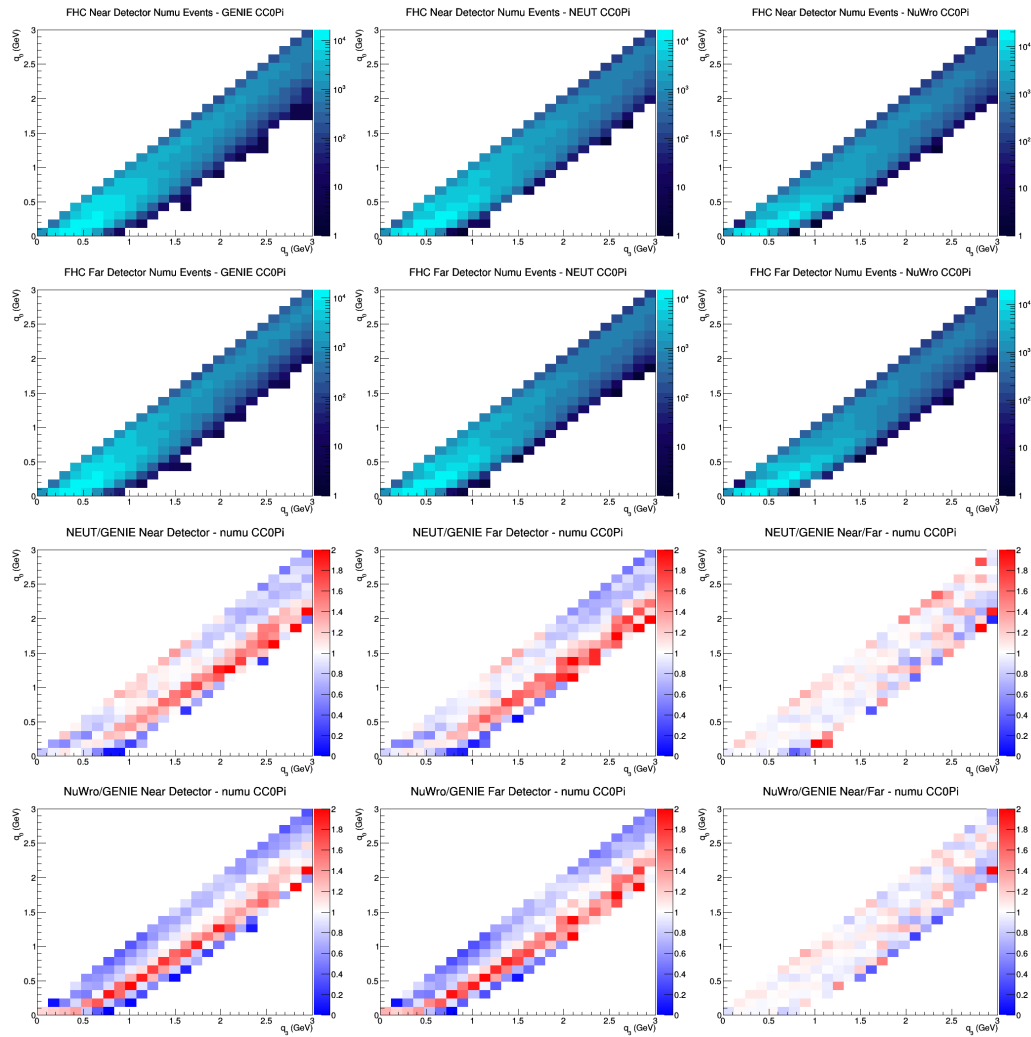
E.15 numubar 2p2h LAr efficiencies



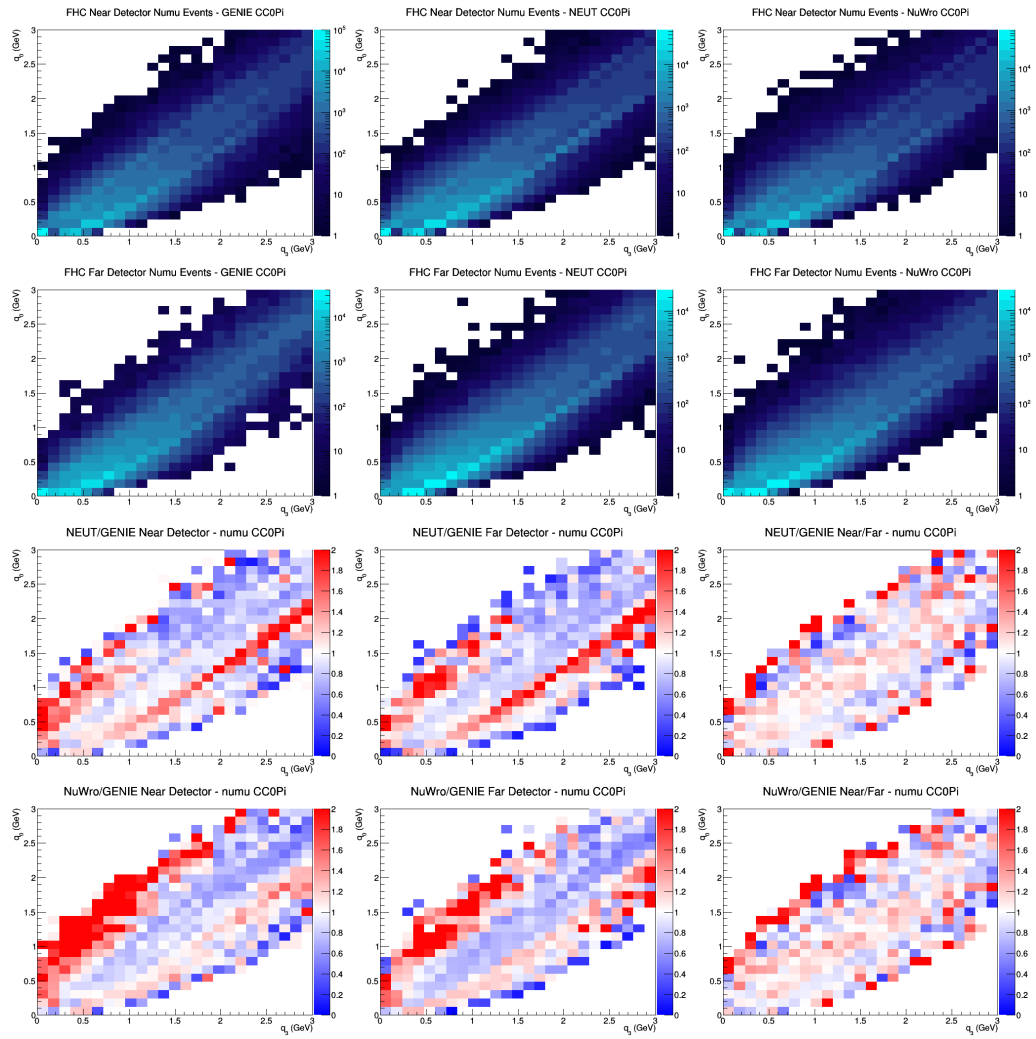
E.16 numubar 2p2h GAr efficiencies



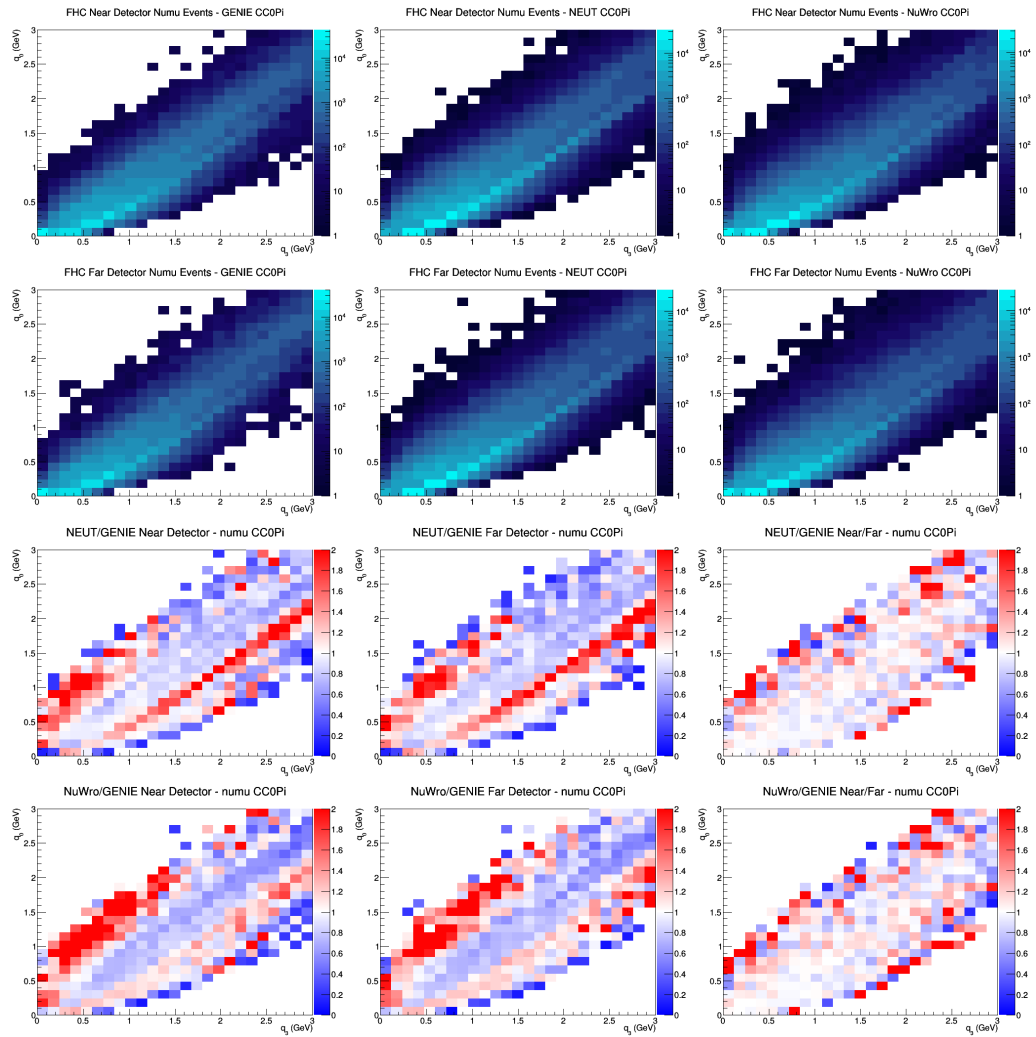
E.17 numu CC0Pi no efficiencies



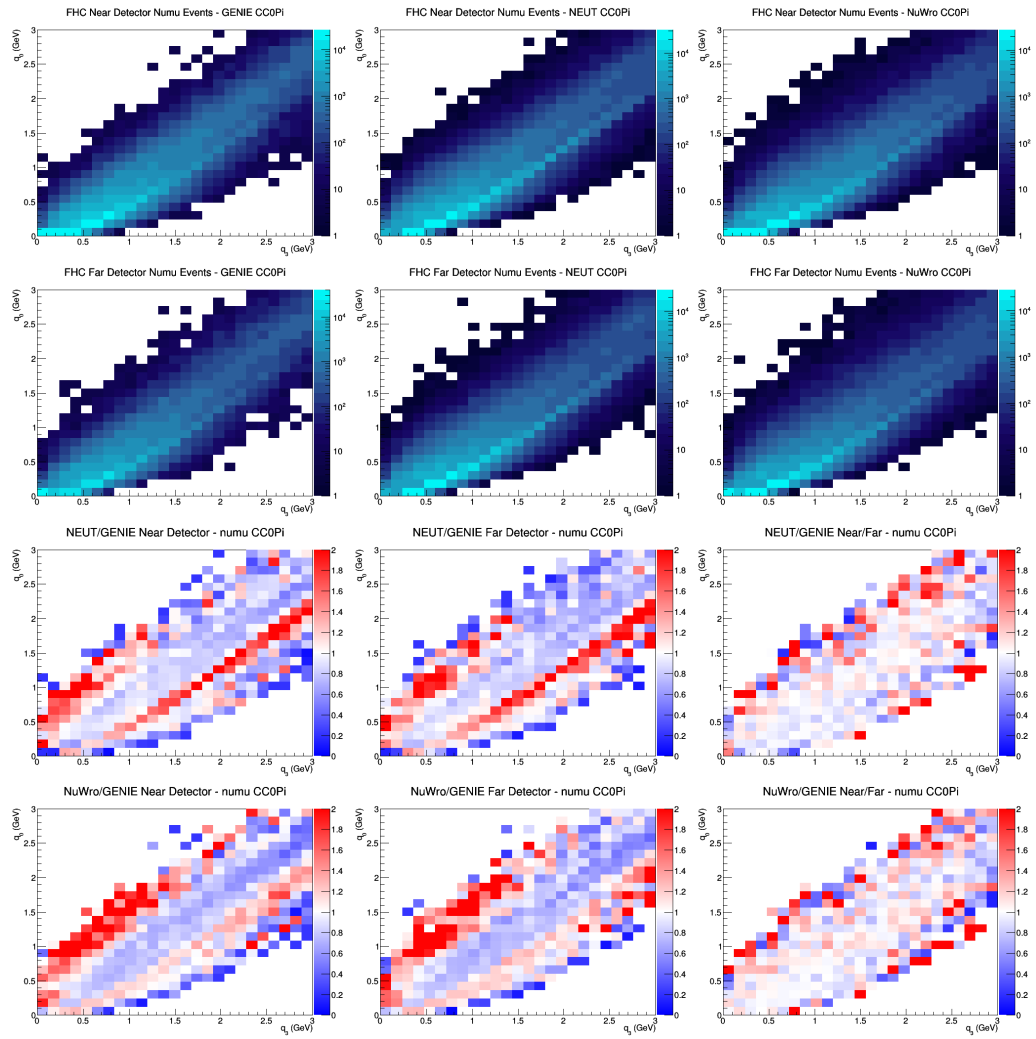
E.18 numu CC0Pi FGT efficiencies



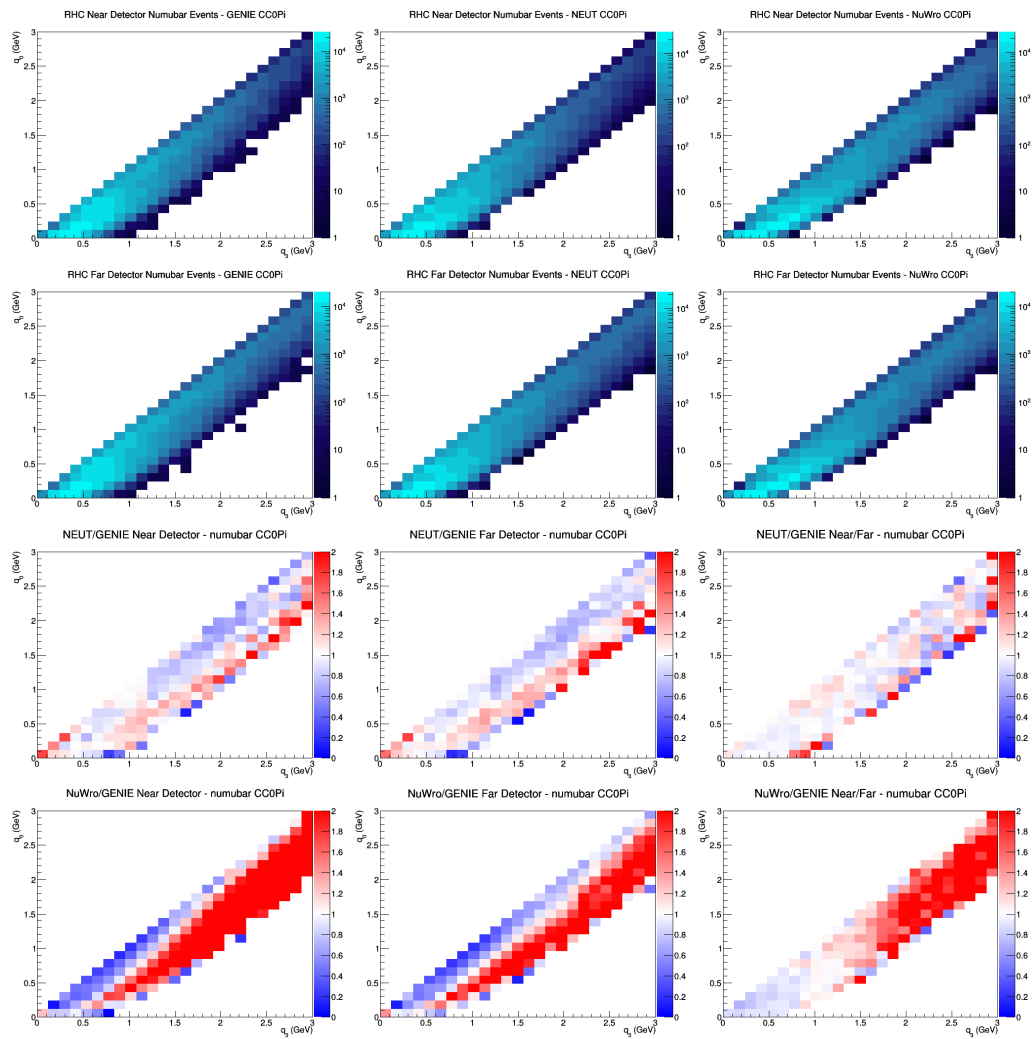
E.19 numu CC0Pi LAr efficiencies



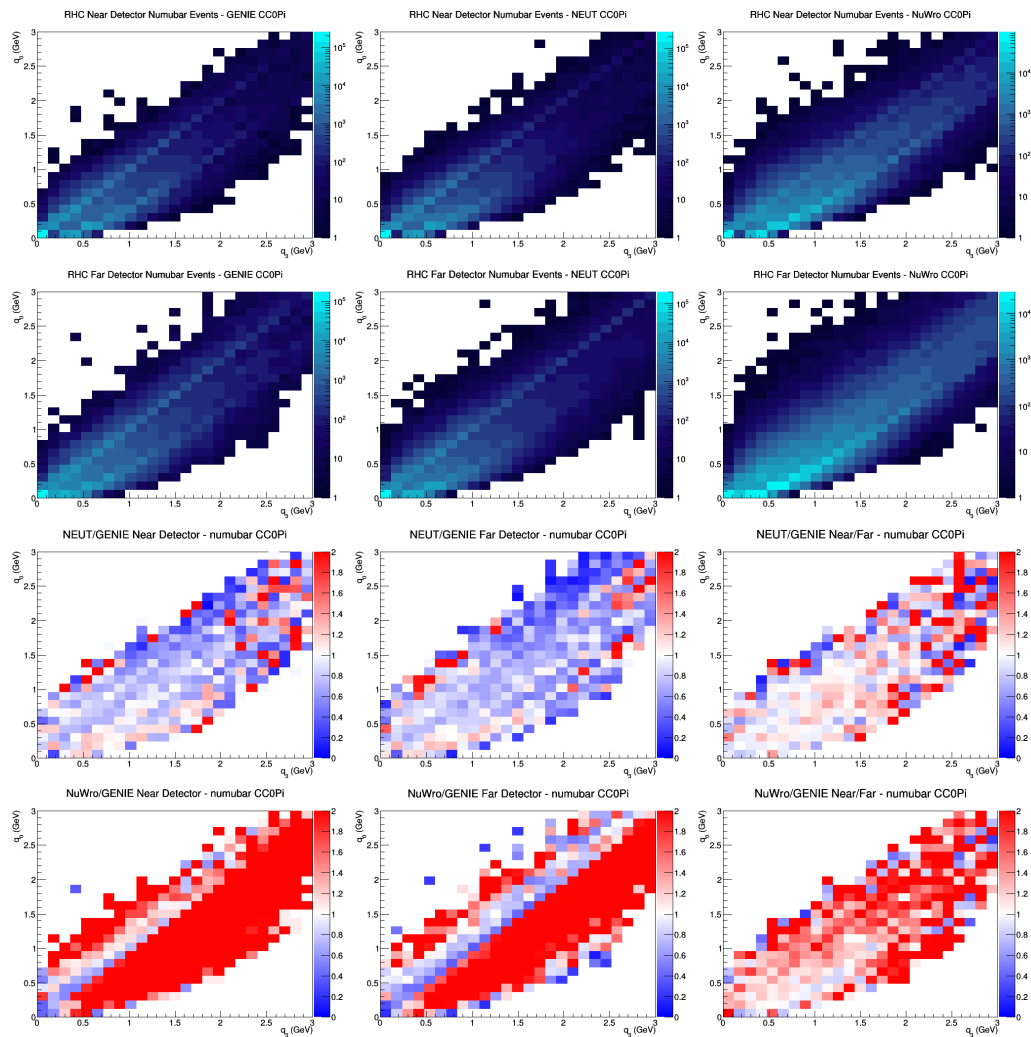
E.20 numu CC0Pi GAr efficiencies



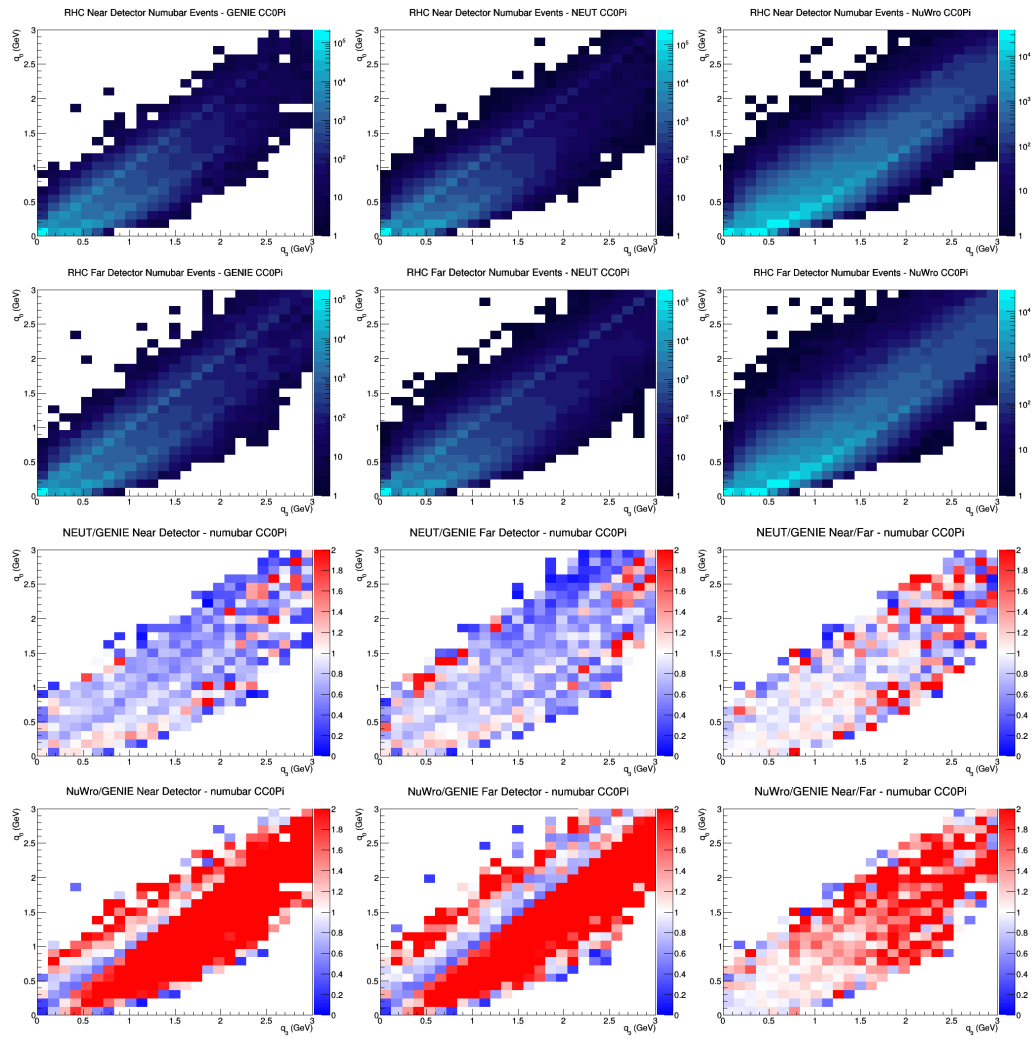
E.21 numubar CC0Pi no efficiencies



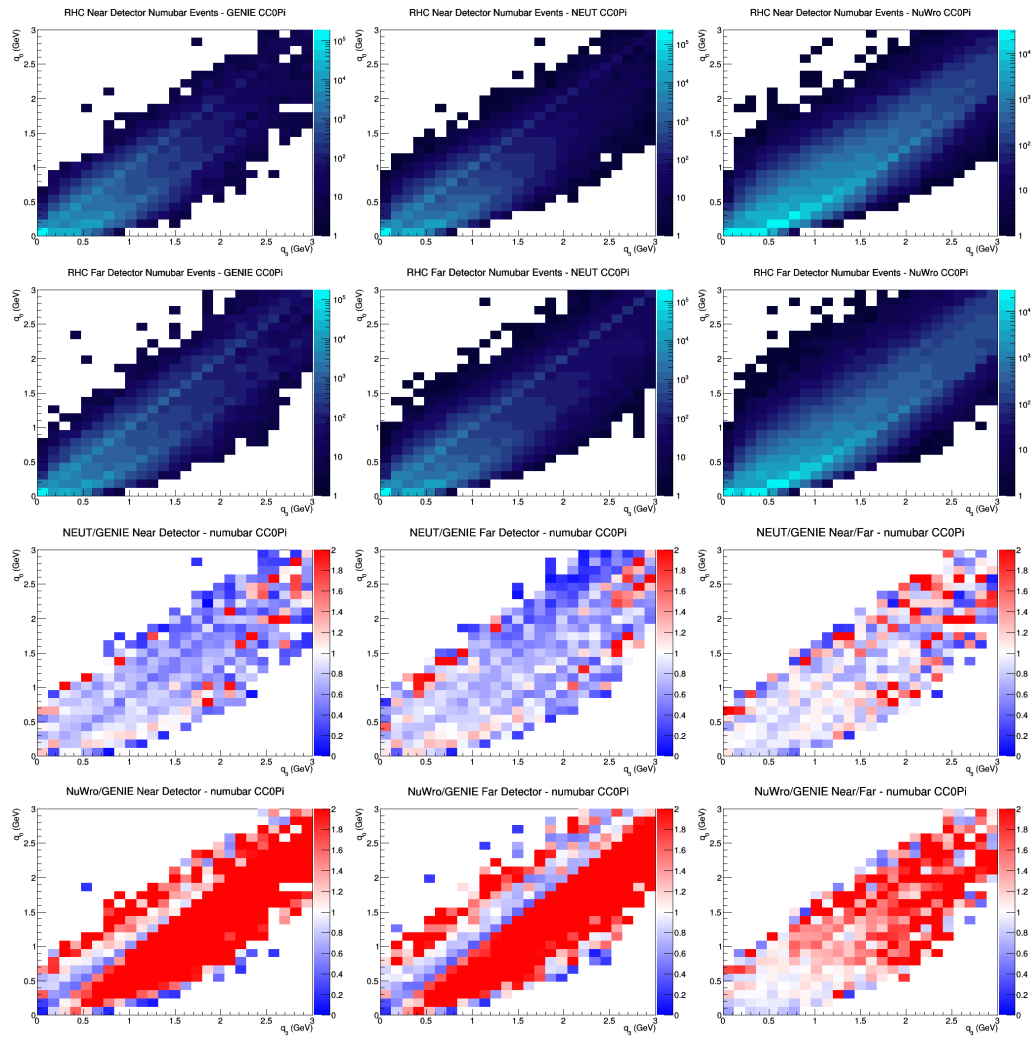
E.22 numubar CC0Pi FGT efficiencies



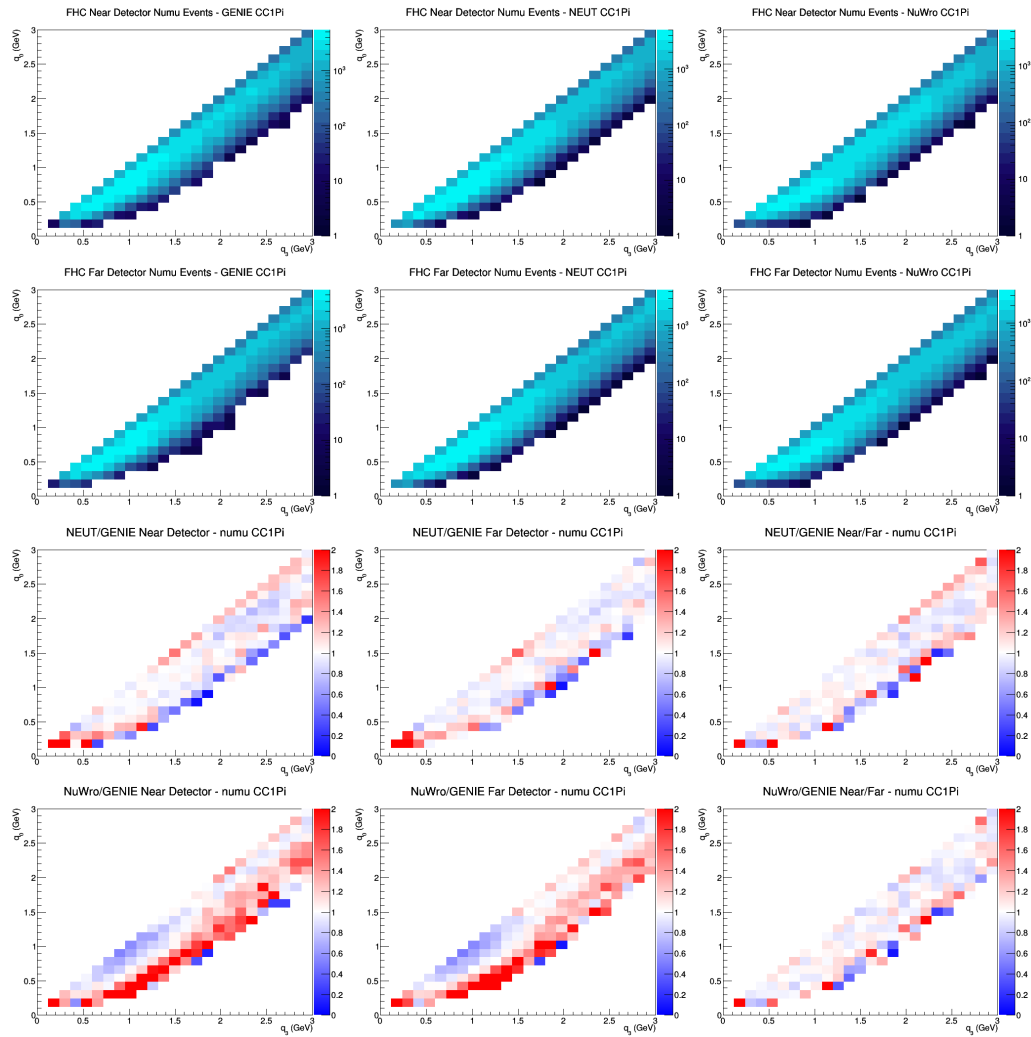
E.23 numubar CC0Pi LAr efficiencies



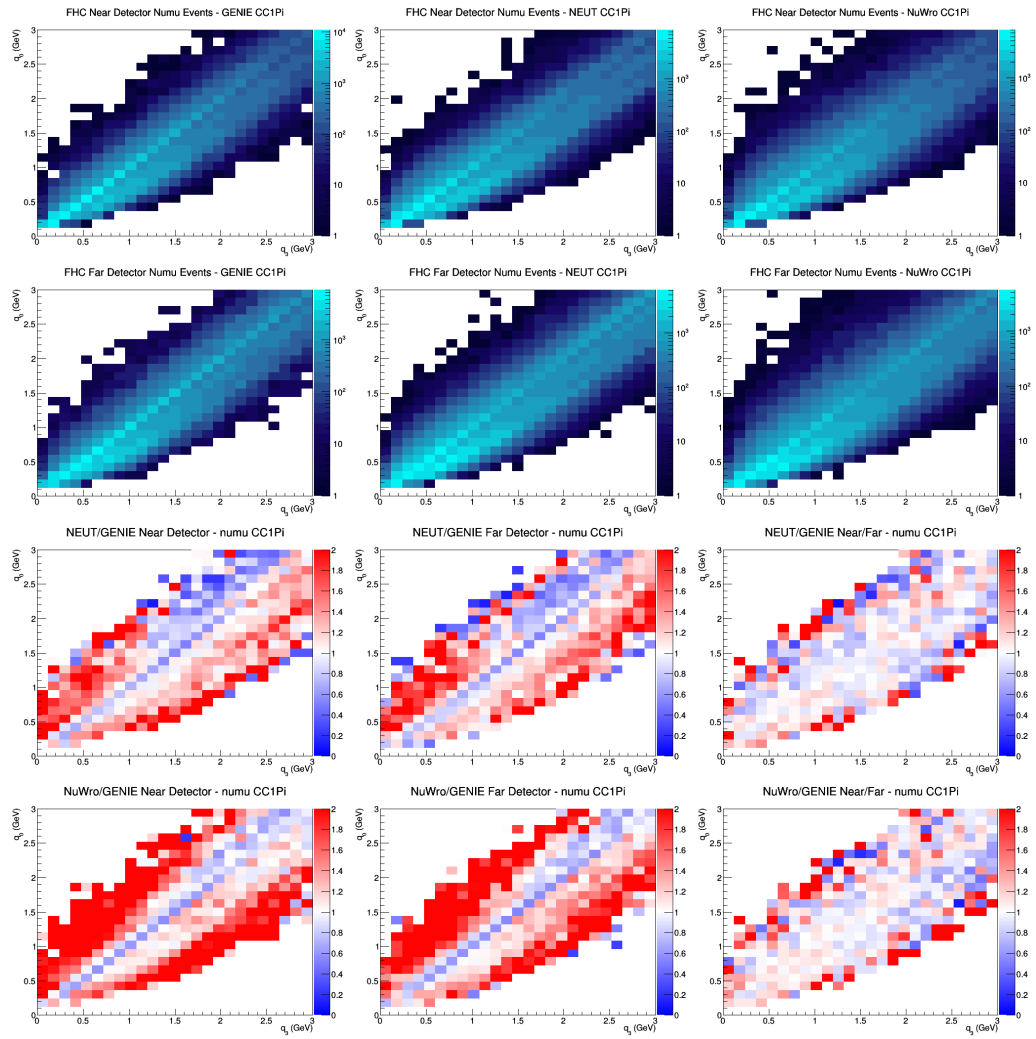
E.24 numubar CC0Pi GAr efficiencies



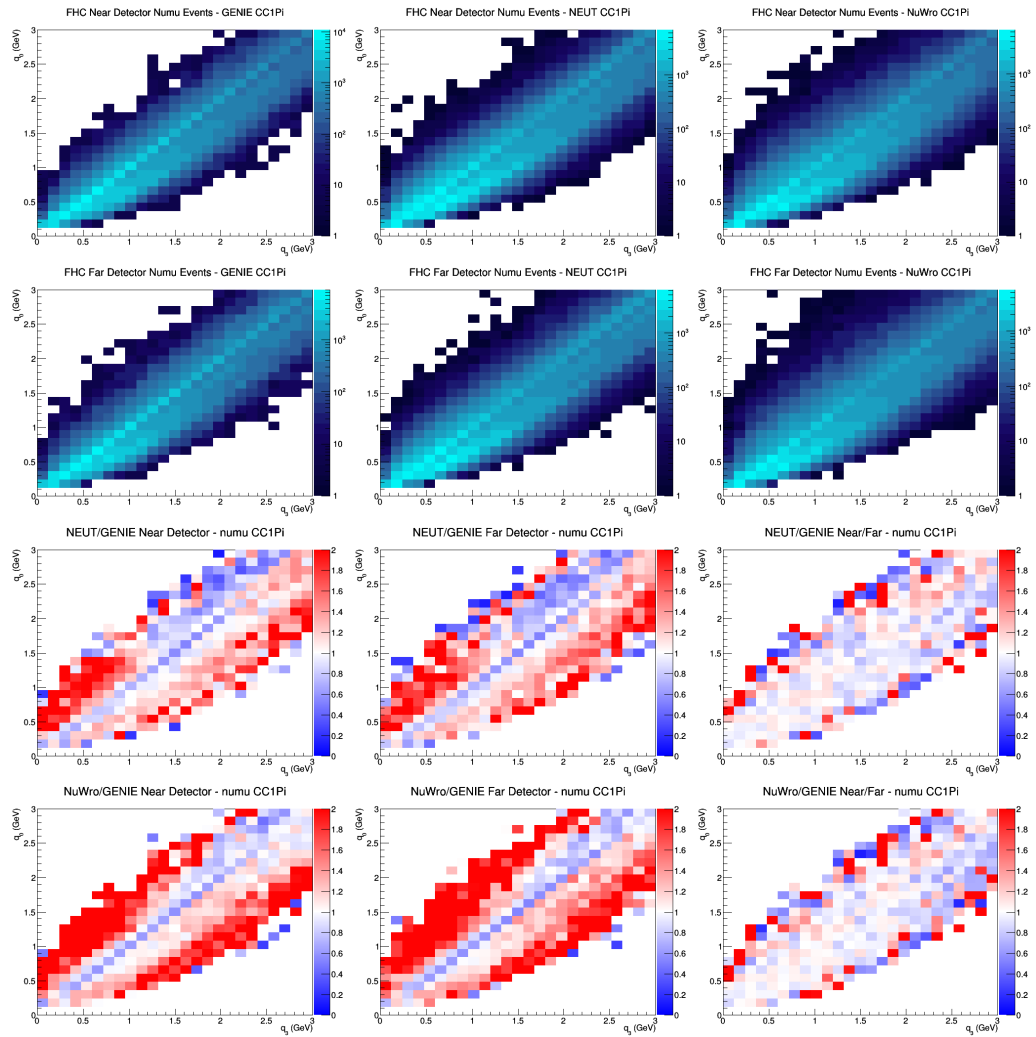
E.25 numu CC1Pi no efficiencies



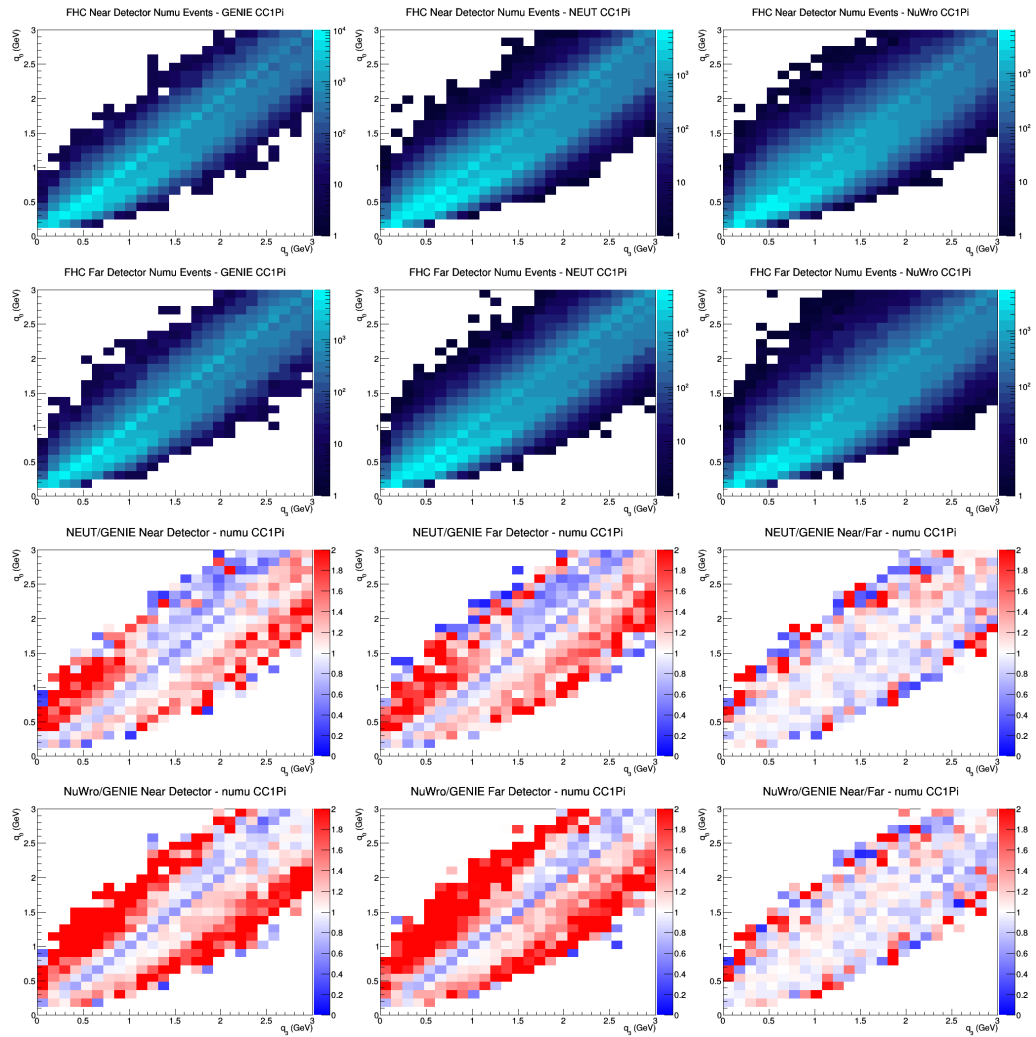
E.26 numu CC1Pi FGT efficiencies



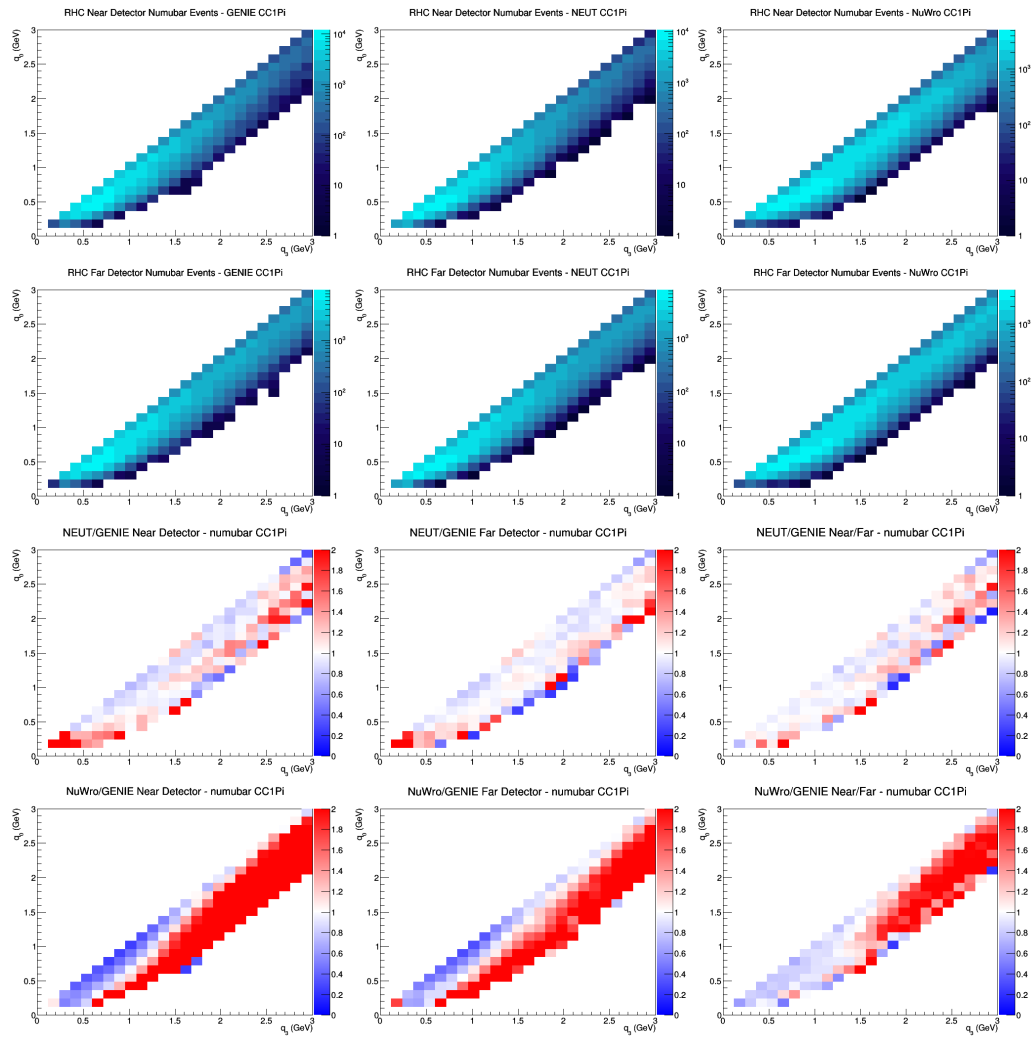
E.27 numu CC1Pi LAr efficiencies



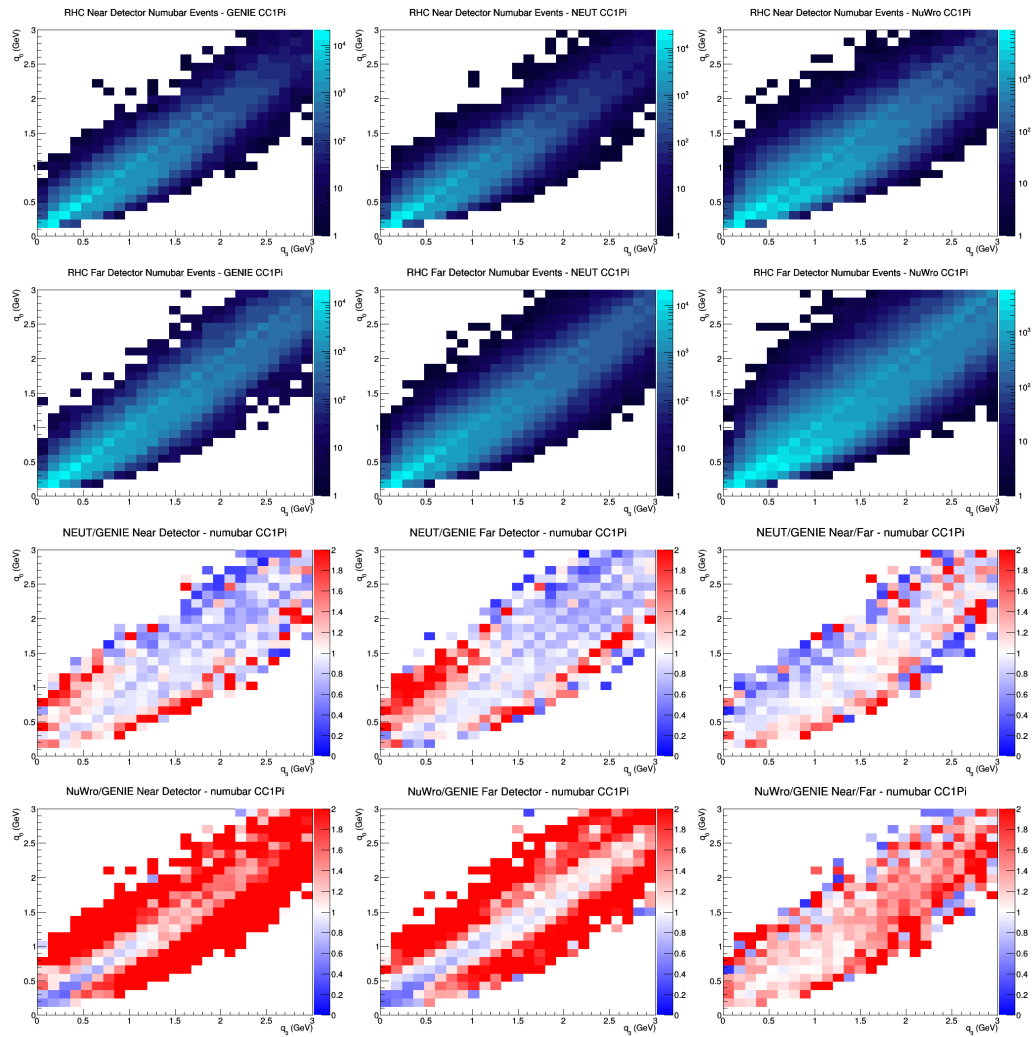
E.28 numu CC1Pi GAr efficiencies



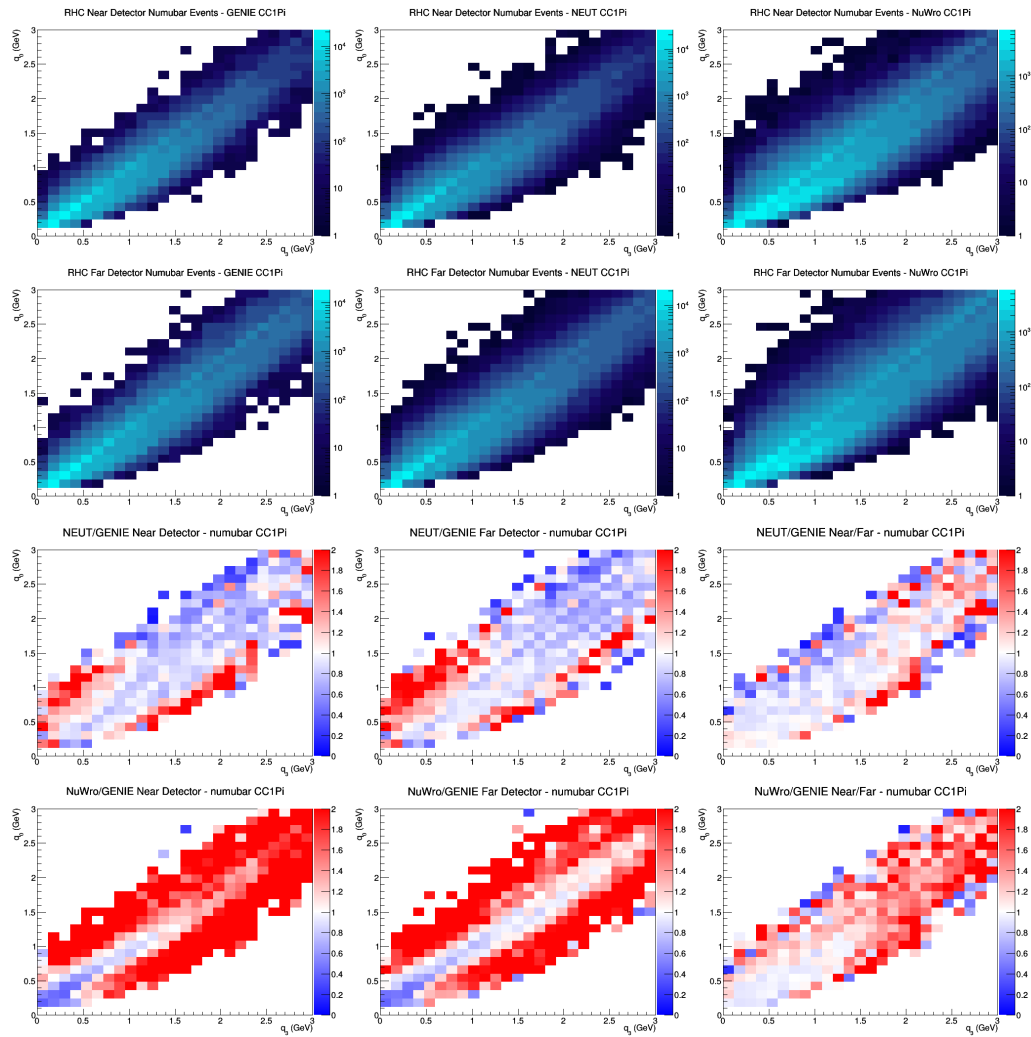
E.29 numubar CC1Pi no efficiencies



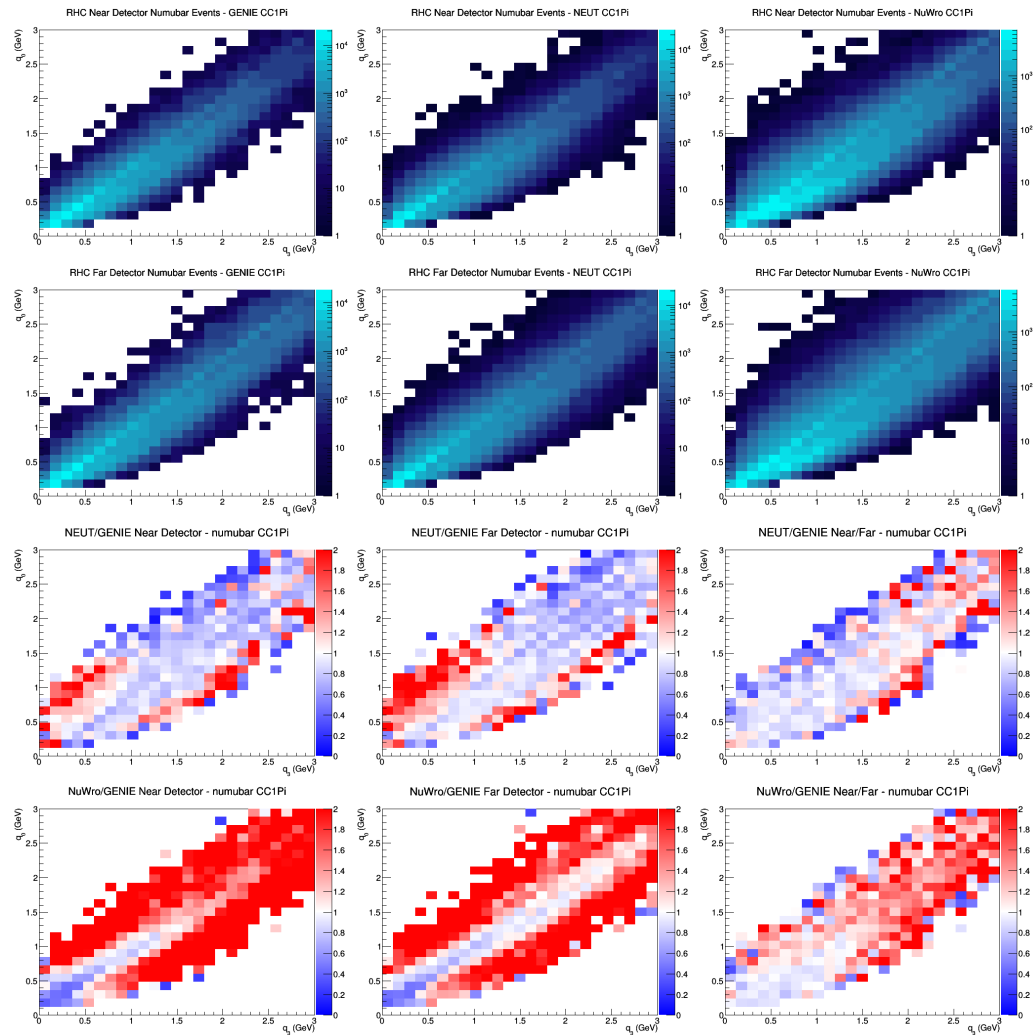
E.30 numubar CC1Pi FGT efficiencies



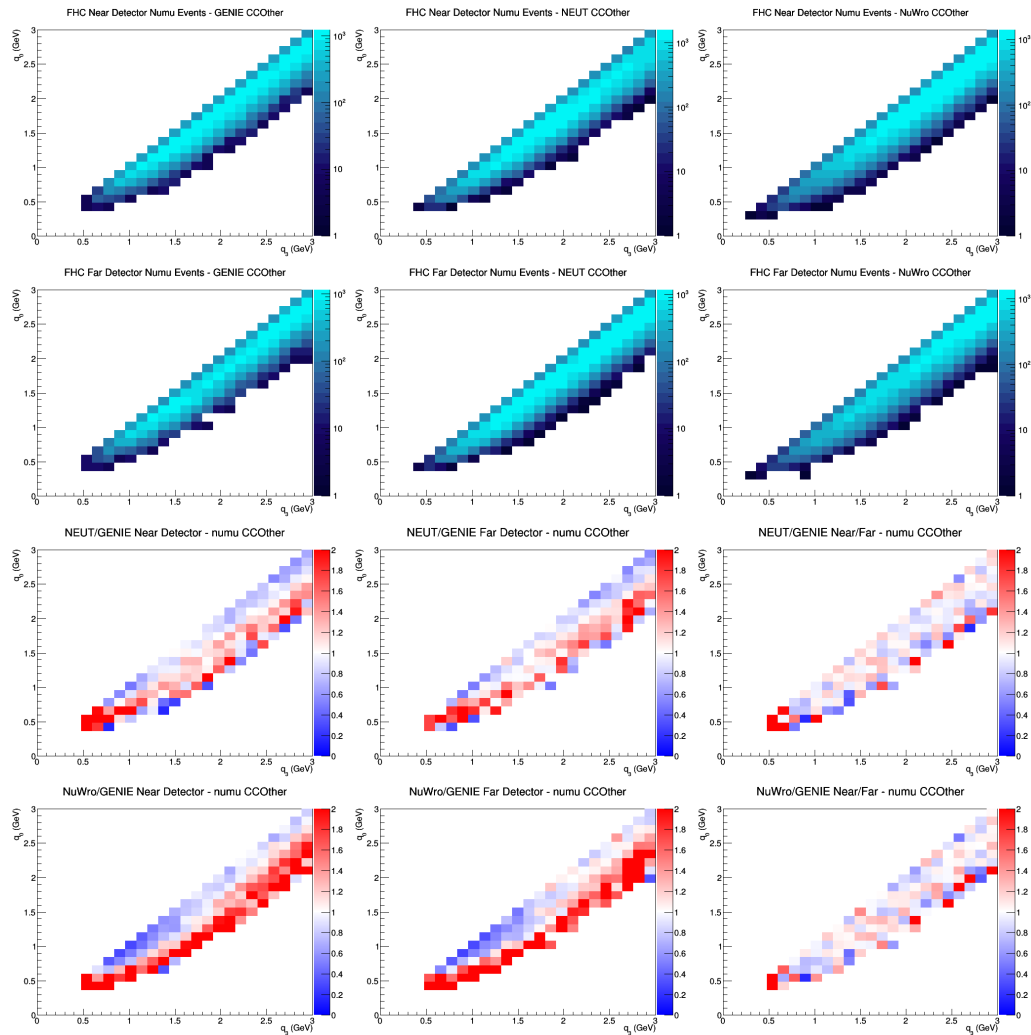
E.31 numubar CC1Pi LAr efficiencies



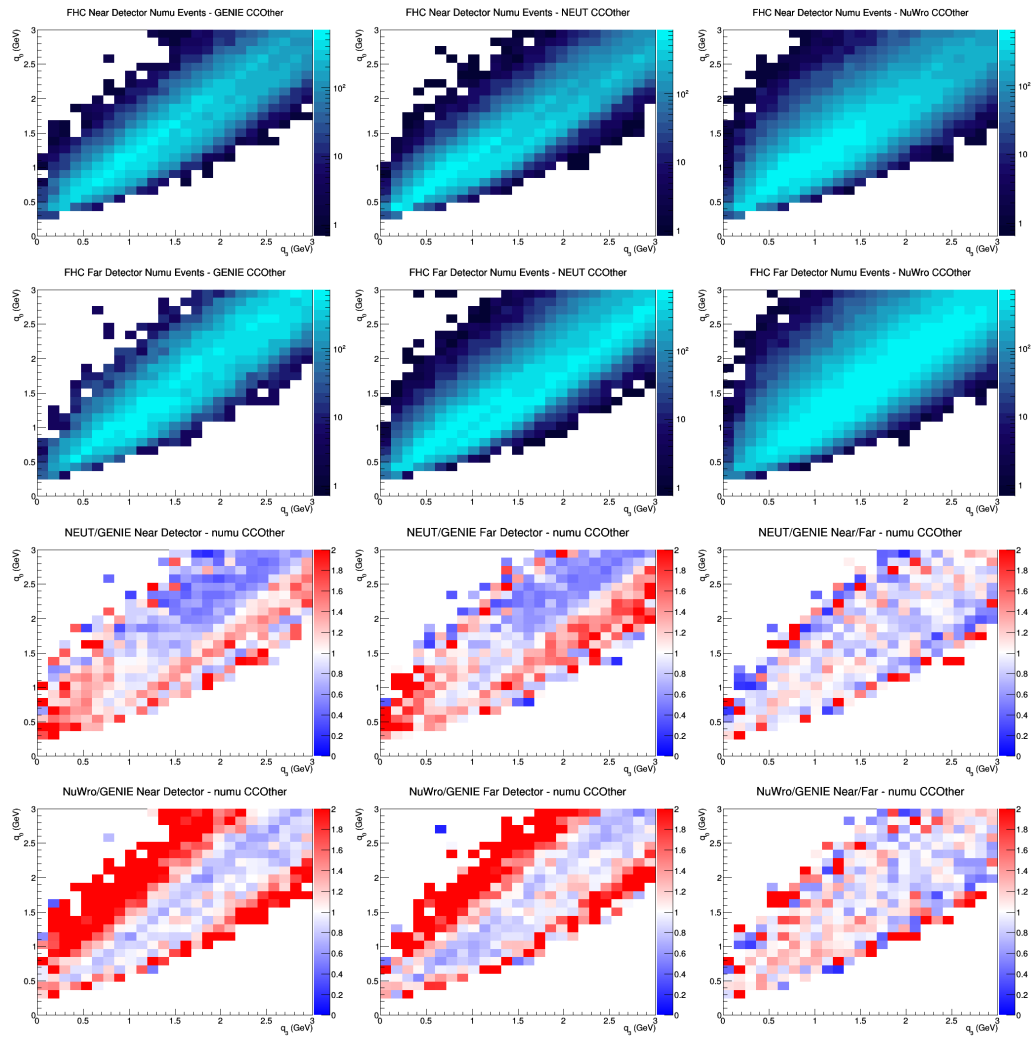
E.32 numubar CC1Pi GAr efficiencies



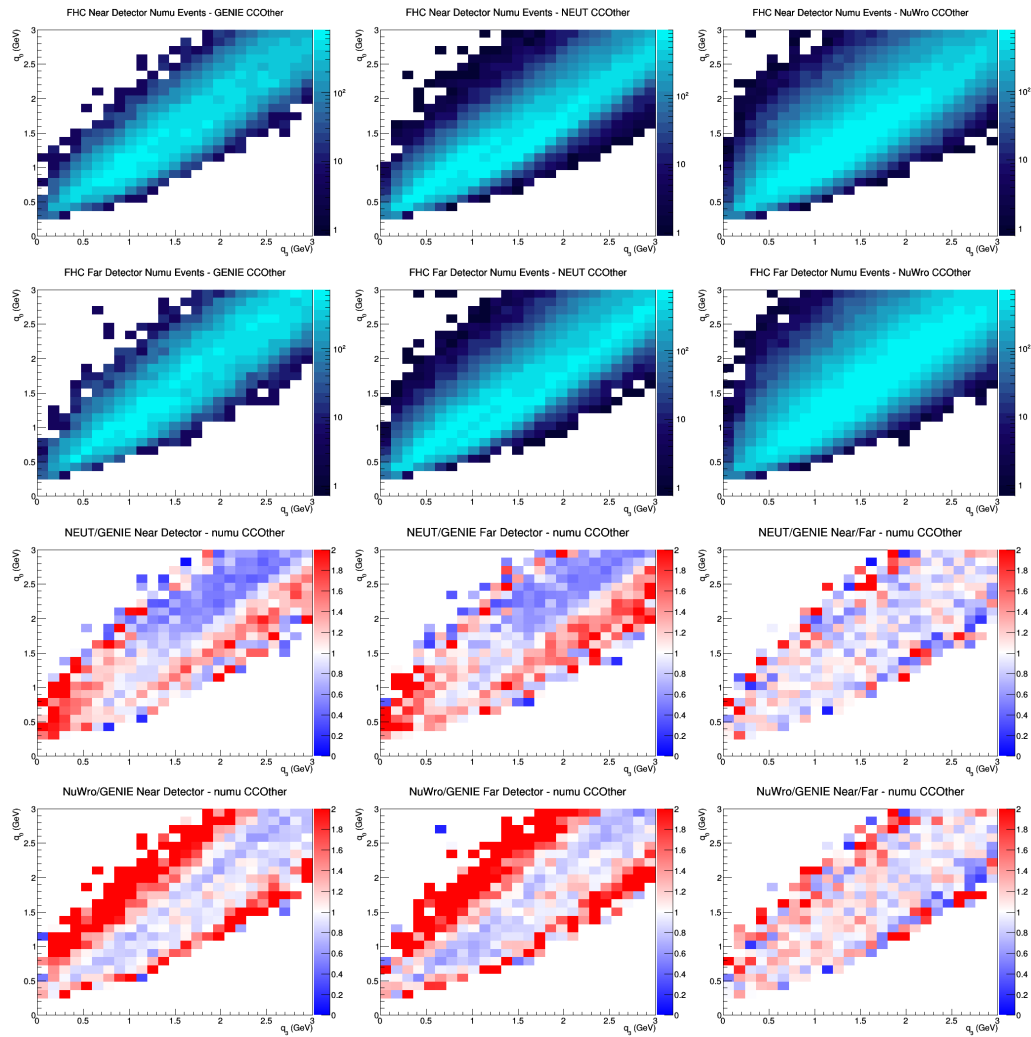
E.33 numu CCOther no efficiencies



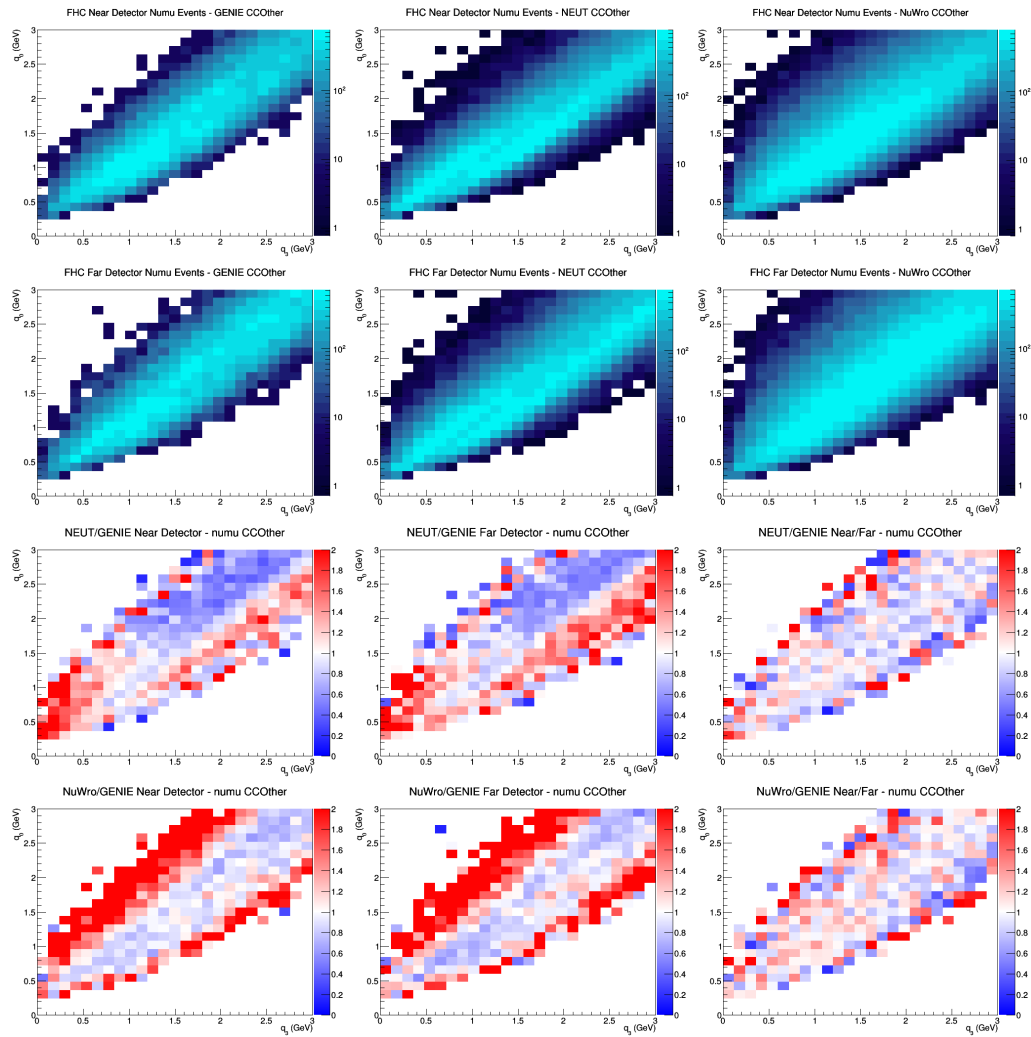
E.34 numu CCOther FGT efficiencies



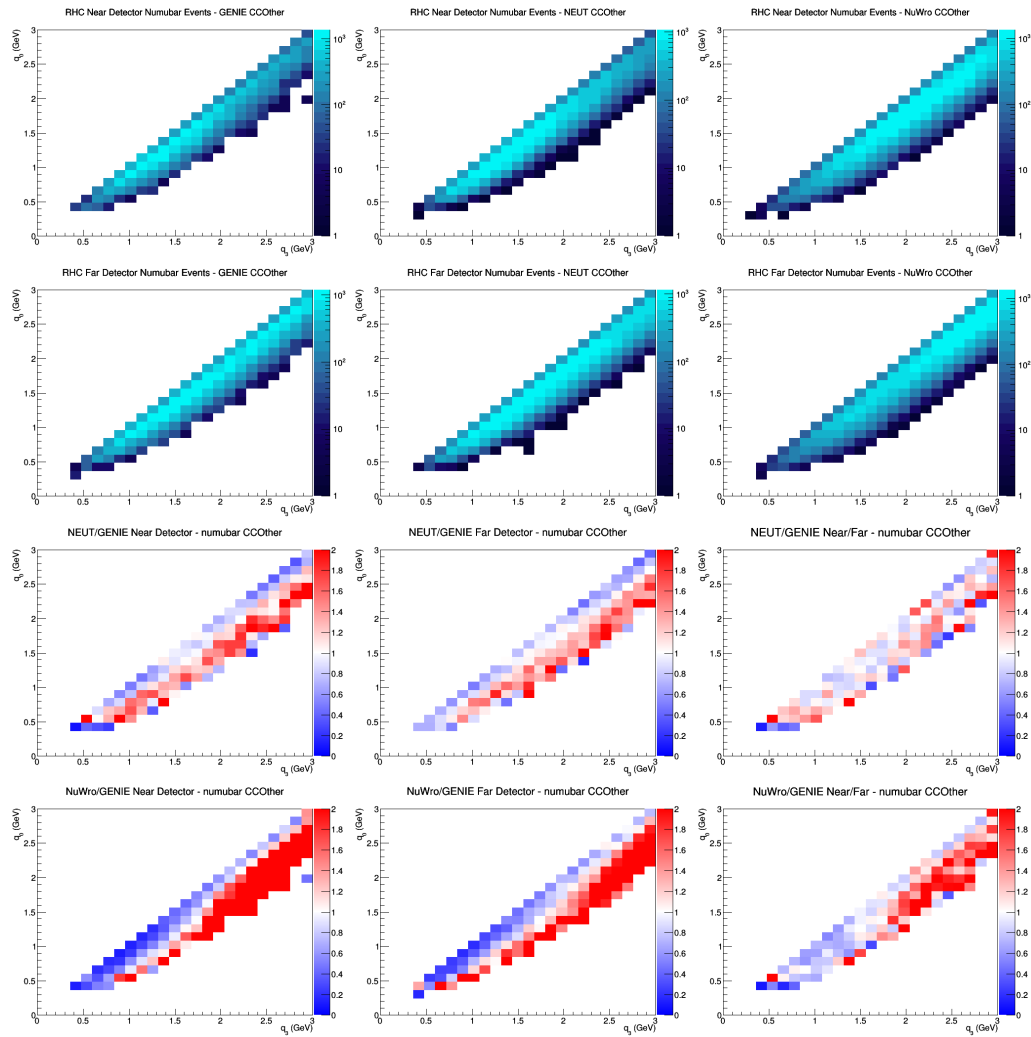
E.35 numu CCOther LAr efficiencies



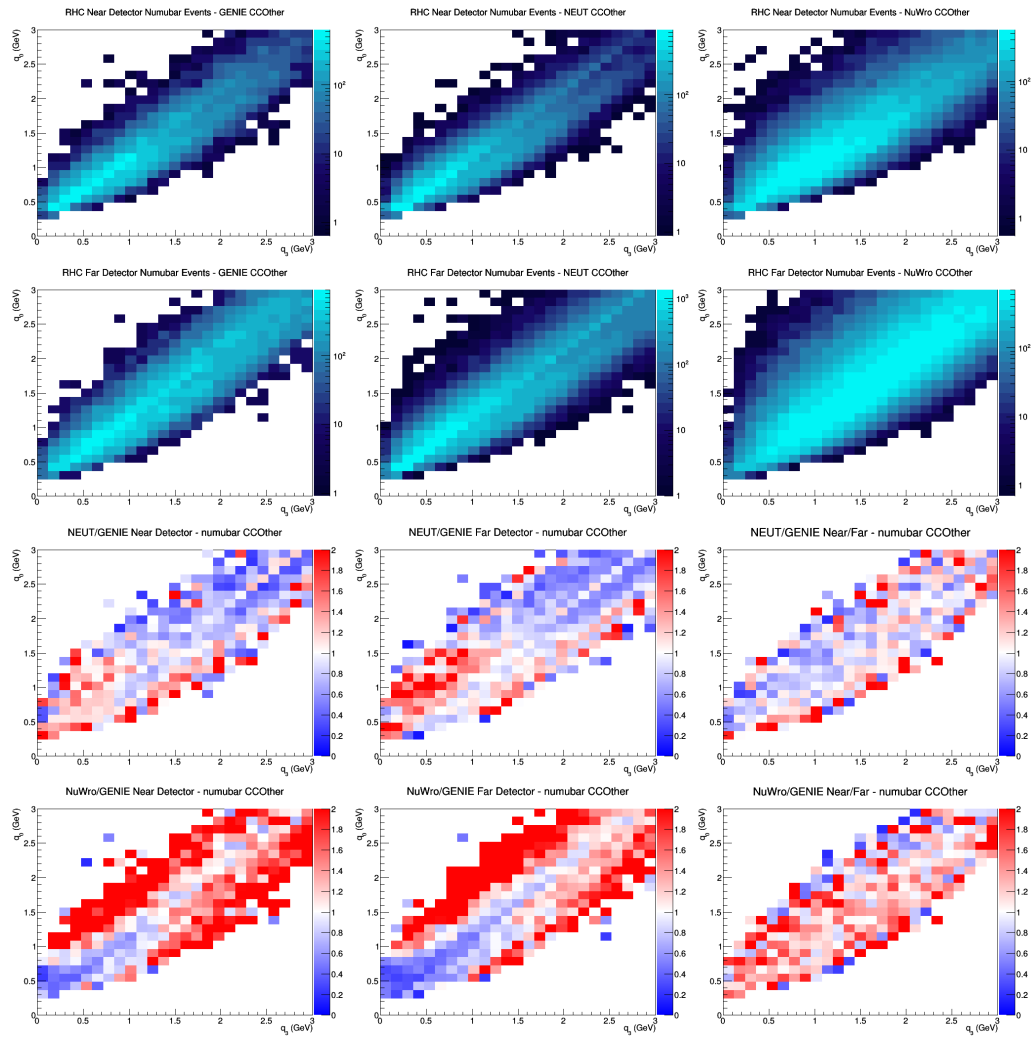
E.36 numu CCOther GAr efficiencies



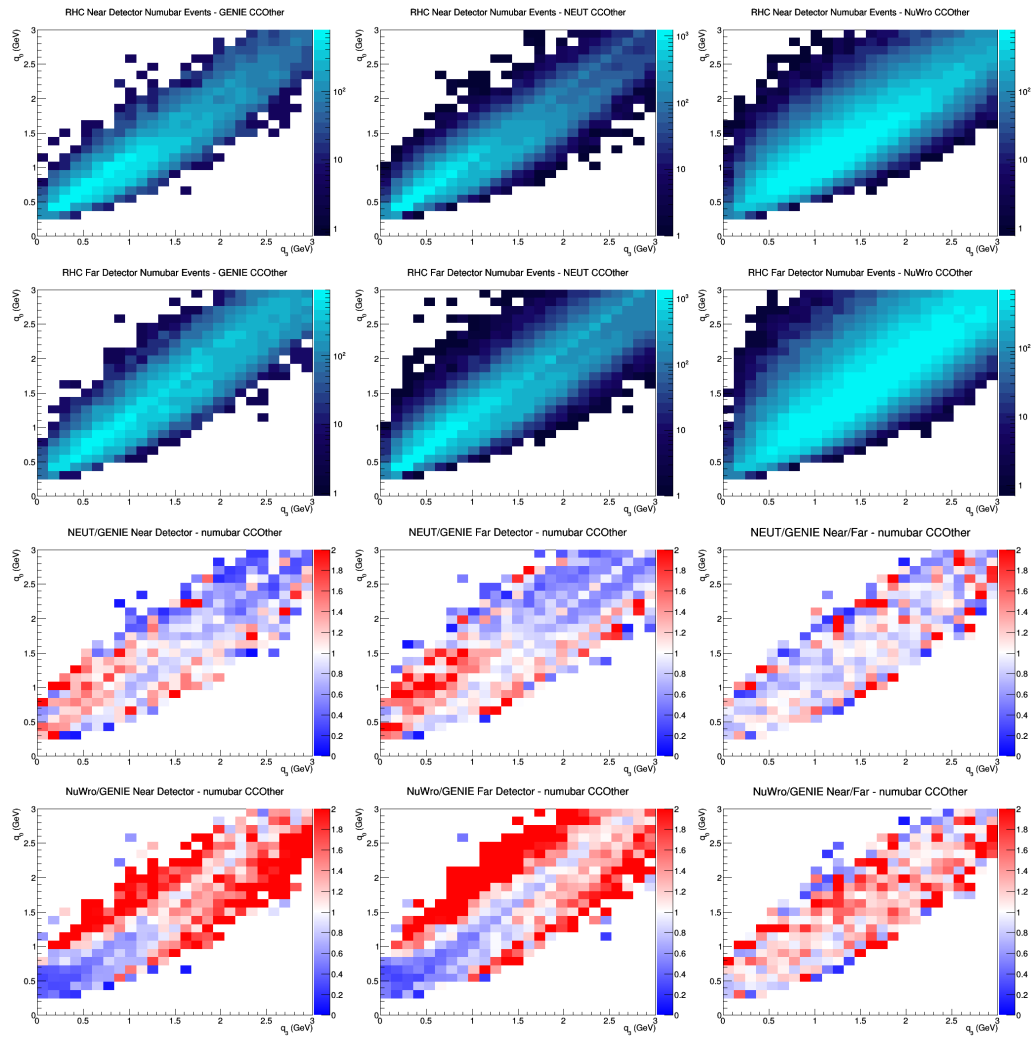
E.37 numubar CCOther no efficiencies



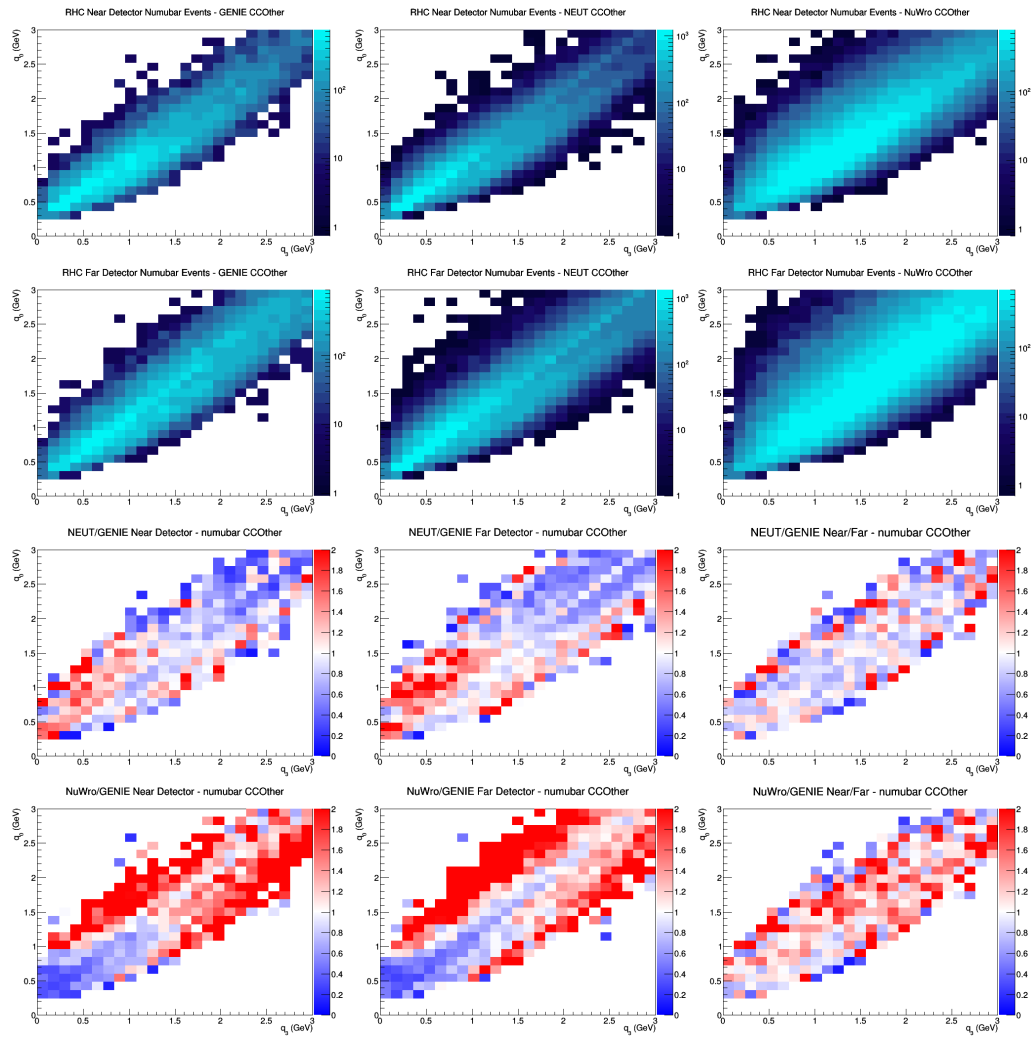
E.38 numubar CCOther FGT efficiencies



E.39 numubar CCOther LAr efficiencies



E.40 numubar CCOther GAr efficiencies



References

- [1] The DUNE Collaboration *Long-Baseline Neutrino Facility (LBNF) and Deep Underground Neutrino Experiment (DUNE) Conceptual Design Report Volume 1: The LBNF and DUNE Projects* arXiv:1601.05471v1
- [2] Maury Goodman *The Deep Underground Neutrino Experiment* Advances in High Energy Physics, vol. 2015, Article ID 256351, 9 pages, 2015. doi:10.1155/2015/256351
- [3] Andreopoulos, C. et al. *The GENIE Neutrino Monte Carlo Generator.* Nucl.Instrum.Meth. A614 (2010) 87-104 arXiv:0905.2517 [hep-ph] FERMILAB-PUB-09-418-CD
- [4] Hayato, Yoshinari *A neutrino interaction simulation program library NEUT.* Acta Phys.Polon. B40 (2009) 2477-2489
- [5] T. Golan, J.T. Sobczyk, J. Zmuda *NuWro: the Wroclaw Monte Carlo Generator of Neutrino Interactions.* Nuclear Physics B - Proceedings Supplements 229 (2012) 499
- [6] P. Stowell, C. Wret, C. Wilkinson, L. Pickering, S. Cartwright, Y. Hayato, K. Mahn, K.S. McFarland, J. Sobczyk, R. Terri, L. Thompson, M.O. Wascko, Y. Uchida *NUISANCE: a neutrino cross-section generator tuning and comparison framework* arXiv:1612:07393v2
- [7] Andreopoulos, et al. *VALOR DUNE Joint Oscillation and Systematics Constraint Fit*